JOHANNES GUTENBERG UNIVERSITÄT MAINZ

Polymer Functionalized Nanoparticles and Smart Polymersomes for Medical Applications

Dissertation zur Erlangung des Grades
„Doktor rerum naturalium (Dr. rer. nat.)“

der Fachbereiche
Chemie, Pharmazie und Geowissenschaften
der Johannes Gutenberg Universität Mainz

vorgelegt von

Redouane Krini

geboren in Mainz

Mainz 2017

This work was conducted unter supervision of [redacted] from April 2014 until March 2017 at the Johannes Gutenberg University Mainz.

Decan

1. Correspondent:

2. Correspondent:

Oral examination:

Declaration

Hereby I assure, that I compose the submitted dissertation on my own and did not use any other aid - except the indicated sources. Literally used sources are marked appropriate the acclaimed regulations for scientific working (lege artis). This dissertation is not submitted elsewhere or was used as examination purpose.

Mainz, March the 29th, 2017

Redouane Krini

To quest for knowledge is a duty for every muslim, man and women. Therefore quest for knowledge, where it is to find, and ask from all of whose, who own it.

Quest for knowledge from the bassinet until the bier.

He who travels in the search of knowledge, to him God shows the way of Paradise.

Some hadith from prophet Muhammad (s.a.s)

Acknowledgement

Abstract

Chapter 1-3 is about the design, modification and synthesis of new materials based on a core/shell/shell system (CdSe@ZnS@SiO_2, CdZnS@ZnS@SiO_2). During the process the nanoparticles undergo a reaction with silica sources which are different in their chain length and equipped with different functional groups. This enables their use in the lithography process in which highly luminescent 2D/3D patterning structures were obtained in the direction of designing promising candidates for metamaterials. Furthermore they were attached to a gold nanowire and energy transfer phenomena (e.g. SERS) were investigated and correlated to the chain length and polarity of the functional groups. In the direction of bioimaging the QDs were incorporated into polymeric micelles for tracking these hybrid materials in the process of cell uptake.

In chapter 4-7 the objective was the development of new drug carrier systems based on amphiphilic blockcopolymers (smart polymersomes) containing pH labile as well as redox sensitive units for the efficient drug delivery and facilitated cargo release over external stimuli. Particles formed by pH stimuli responsive polymers could encapsulate hydrophilic as well as hydrophobic drugs in encapsulation efficiencies of up to 50% and 90%, respectively, and redox sensitive particles hydrophilic cargos with 42%, making them attractive especially in the direction of using synergetic effects over codelivery. Besides active targeting (folic acid, mannose) the particles were loaded with different drugs like siRNA and TNF-α in which TNF-α could be temporally encapsulated safe. Injected subcutaneous it was found a stable local depot effect of over more than 72 h without significant loss of particle intensity at the injected side and no systemic redistribution as proved by *ex vivo* analysis.

Zusammenfassung

Kapitel 1-3 behandelt das Design, die Modifizierung und Synthese von neuartigen Materialien basierend auf einer Kern/Schale/Schale Struktur (CdSe@ZnS@SiO_2, CdZnS@ZnS@SiO_2). Während des Prozesses reagieren die Nanopartikel mit verschiedenen Silizium-Precursor, welche sich in ihrer Kettenlänge und funktionellen Gruppe unterscheiden. Dies ermöglicht die Einbindung dieser Partikel in den Lithografie Prozess wobei stark fluoreszierende 2D/3D Strukturen erhalten wurden im Hinblick auf die Generierung von vielversprechenden Kandidaten für Metamaterialien. Weiterhin wurden diese Partikel an einer Goldoberfläche aufgebracht und Energie Transfer Phänomene (z.B. SERS) untersucht und mit der Kettenlänge und Polarität der funktionellen Gruppen korreliert. Im Bereich des Bioimagings wurden die QDs in Polymer-Mizellen eingebunden und der Prozess der Zellaufnahme untersucht.

In Kapitel 4-7 war die Hauptaufgabe die Entwicklung von neuartigen smarten Trägersystemen basierend auf einem amphiphilen Blockcopolymer (smarte Polymersome) für den effizienten Wirkstofftransport und der erleichterten Freisetzung über externe Stimuli. Hierbei wurden sowohl pH als auch redox labile Einheiten in das amphiphile Blockcopolymer eingebunden um die Freisetzung des eingeschlossenen Wirkstoffs zu erleichtern. Die pH sensitiven Partikel konnten sowohl hydrophile als auch hydrophobe Cargos einschließen mit einer Einschlusseffizienz von bis zu 50% bzw. 90%, und die redox sensitiven hydrophile Cargos mit 42%, was diese Systeme besonders attraktiv macht, im Hinblick auf die Ausnutzung eines synergetischen Effektes über Codelivery. Neben dem aktiven Targeting (Folsäure, Mannose) wurden die Partikel mit verschiedenen Wirkstoffen beladen, wie siRNA und TNF-α. Für toxisches TNF-α konnte eine sichere temporäre Verkapselung gezeigt werden. In einer subkutanen Applikation konnte ein stabiler lokaler Depoteffekt von über 72 h erreicht werden ohne einer Abnahme an Intensität am Injektionsort oder einer systemischen Umverteilung, gezeigt durch *ex vivo* Untersuchungen.

Contents

Introduction into material science

Nanocrystals

In the year 1982, Prof. Louis Brus from Columbia University made the observation that the band gap (E_{gap}) of a semiconductor particle experimental was a function of size. Even if at that early stage this observation was a curiosity, it was at the same time a first class research problem. He also saw that the results obtained from this basic research are relevant to the industry (e.g. transistor materials). The semiconductor nanoparticles are of an increasing importance in the fundamental studies[1–6] and in a wide range of technological applications such as light emitting devices,[7–10] lasers[11–13] or fluorescent labels.[14–16] Due to their small sizes and the resulting quantum confined nature of their energy levels they possess very unusual and extraordinary optical and electronic properties. [17–20] As smaller the nanoparticles get as higher the volume to surface ratio. This ratio can be modified through a surface modification step with various organic capping agents. Such capping agents increase the colloidal stability of the particles and they introduce the possibility for chemical reactions on the surface.[21,22] Nevertheless, there is not a complete coverage of the organic capping agents on the surface and so dangling bonds remain.[23] To overcome this various methods and techniques were developed to shield the surface with an inorganic shell (e.g. ZnS) and so to obtain completely passivated nanoparticles.[24, 25] QDs are of huge interest in the area of optoelectronics and medicine.[26-28] Due to their quantum size effect (QSE), the resulting electronic and optical properties makes them very attractive for the use and manipulation of defined structures for certain applications. It is possible to change the size of the nanoparticles which leads to changes in their spectral absorption and fluorescence behaviour. Nanoparticles consist of 100-10000 atoms, meaning they can be characterized as a transition state between a macrocrystal and a molecule or a single atom.[29,30] These kinds of nanocrystals are in a quasi zero dimensional (0D) solid state structure.[31] QDs are not a point such as they are defined in a mathematical point of view. Rather, they are three times confined in space dimension. In reference to the volume of a crystal the space dimension is three dimensional (3D) with no

confinement in space dimension and so there exist a 3D mobility. When one applies a first confinement in space dimension the resulting two dimensional (2D) system with 2-D mobility can be referred to as a quantum film. After the second confinement in space dimension is applied the resulting one dimensional (1D) system with 1D mobility can be referred to as a quantum wire, which is based e.g. on the metal gold, and is also synthesized in this work in order to investigate the phenomena of energy transfer by attaching surface modified quantum dots on its surface to influence the photon flux. Finally, with the last and third space confinement the resulting 0D system can be referred to as the quantum dot which is often a semiconductor, such as Indium gallium arsenide (InGaAs) or CdSe, which changes their emission maxima depending on their sizes.[32] A confinement in one space dimension is happening when the expansion of the charge carrier is limited in the order of the de-Broglie wavelength which is given in the following equation where the plank constant (h), the kinetic energy (E_{kin}) and the impulse (p) of the considered particle is given.

$$\lambda = \frac{h}{p} = \frac{1.22\ \mathrm{nm}}{\sqrt{\frac{E_{Kin}}{eV}}} \quad \{1\}$$

Such quantum dots have a finite dimension of a few nanometers, consist of a few thousand atoms, and as mentioned earlier the dimensions of the quantum dots are smaller than the de-Broglie wavelength of the embedded electrons and holes. The charge carriers can only overcome the confinement when they can leave to the surrounded volume material, which can be accomplished by a higher energy difference.[32, 33] The following figure 1 is a schematic depiction of the confinement of the charge carrier and the resulting density states ($D(E)$) for a volume material (3D), a quantum film (2D), a quantum wire (1D) and a quantum dot (0D).

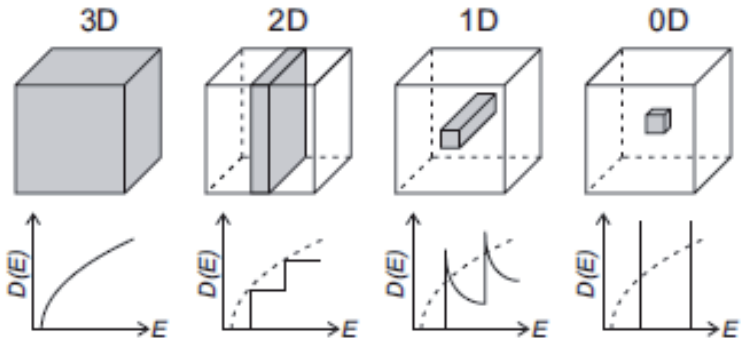

Figure 1: Applying of confinements in space dimension and resulting density states adopted from Ref.[32]

With decreasing the size and applying up to three confinements in one dimension the resulting quantum dots have interesting optical properties which change with the shape and form of the particle.[18] However, this also means that such systems are showing up along the borders of conventional semiconductor technology, as semiconductor structures change their properties by going smaller and smaller in size.[30] Nevertheless nanocrystals synthesized in solutions are reproducible and it is possible to manipulate them. One important example of such nanocrystals is CdSe, which is also used in this work through modification of their surface and investigation of properties resulting from their sizes. Besides CdSe, which is a heavy metal containing nanocrystals, there are newly synthesized quantum dots, which are heavy metal free e.g. Indium phosphide (InP).[34] Much investigation has been focused in that direction as the toxicity of InP is less compared to that of CdSe.[35–37] Additionally, it plays a crucial role in applications for human life, or in the area of bioimaging.[38, 39] Through synthesis it is possible to control and change the size of these nanocrystals from 1.5-10 nm with a narrow particle size distribution. It is also possible to synthesize them in macroscopic amounts, much in the same way that the company Nanoco Technologies does.[40, 41] There they developed a range of restricted heavy metal free QDs referred to as cadium free QDs (CFQDs), which also show bright emissions in the visible and the near infra-red region of the spectrum. With an overcoat of another material it is possible to enhance the quantum yield, as well as the fluorescence. With certain ligands attaching the nanoparticles one can dissolve

them in various solvents for further processing and for introduction into certain reactions. Also, the quantum dots can undergo a reaction with themselves when the attached ligands change on account of a ligand exchange, in which the ligands have a suitable functional end group which can connect two quantum dots to each other. This kind of quantum dot molecule can couple to dye molecules or proteins for use in the bio imaging area.[30] So, besides the intrinsic QSE, which will be discussed in detail later on, the surface plays a crucial role. For example, in a CdSe nanocrystal, which is 4 nm in diameter, almost 70 % of all atoms are on the surface and are no longer in a regular lattice arrangement. The volume V of one nanoparticle is given with equation (2), where the radius r for the nanoparticles is given and when one assumes a perfect spherical shape.[42]

$$V_{Sphere} = \frac{4\pi}{3} r^3 \quad \{2\}$$

To calculate the number of atoms on the surface of one nanoparticle it is first necessary to calculate how many atoms are in said nanoparticle. This can be accomplished by the following equation given with (3) which take into account the density ρ(CdSe) of the nanoparticles, the N_{atom}/NP and the Avogadro constant (N_A).

$$N_{Atom/NP} = V_{NP} \frac{\rho_{CdSe}}{M_{CdSe}} N_A \quad \{3\}$$

For the surface area, one must first consider the edge length of a cube which is given by $\sqrt[3]{V}$. This means that each of the six faces of the cube has an individual surface area that is the square of this given as $\sqrt[3]{V}^2$. In total, the resulting equation for the total surface area of the cube is

$$surface = 6\sqrt[3]{V} \quad \{4\}$$

Now it is possible to estimate how many atoms are on the surface by simply calculating the ratio between the atoms on the surface and the atoms in a nanoparticle. The resulting values are summarized in table 1.

Table 1: Diameter correlating with number of atoms on the surface.

Diameter / nm	N	% on the surface
4	605	70
6	2043	47
8	2843	35
10	9459	28
12	16345	23

Relatively small particles contain thus quasi only surface while relatively bigger particles have basically solid state properties. The smaller the particles are getting, the bigger the surface is becoming. A huge surface is desirable in applications as a catalyst while smaller surfaces are desirable for optical properties and it will be discussed further on how the surface is related to the optical properties of a material. Once one plots the diameter against the percentage of atoms on the surface it can be seen that there is at first a small increase in the percentage of atoms on the surface with a decrease in surface size. After a certain point there is a bigger increase in the percentage of atoms on the surface, which has an exponential character. This is shown in figure 2.

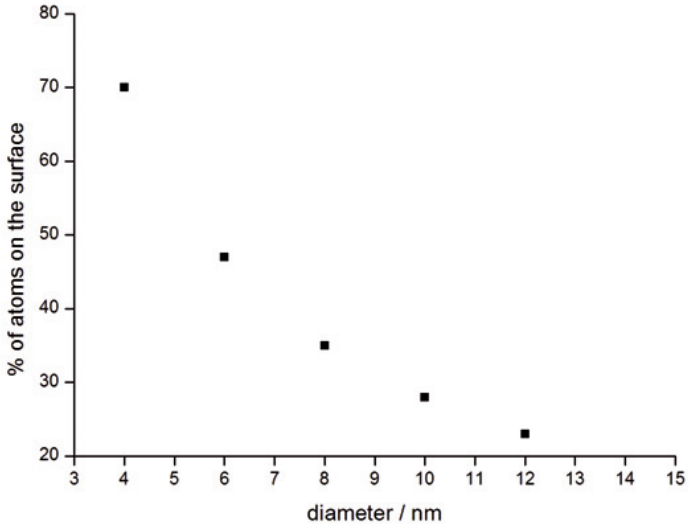

Figure 2: Percentage of atoms on the surface plotted against the different diameter of CdSe nanocrystals.

Quantum size confinement

In the year 1981, it was first observed that in the case of nanocrystalline CuCl the E_{gap} increased, while the particle size decreased.[43] This effect can be observed by the naked eye for nanocrystals that have a E_{gap} ranging from 1.8 to 3.1 eV, which is the spectrum of visible light. For example in the case of CdS the band gap increases from 2.5 eV to 4 eV with a decrease in size.[44] In figure 3, there is given a row of colloidal CdSe nanoparticles that have the same chemical composition, but due to their difference in size and resulting difference in band gaps they emit light in different wavelengths, which can be seen in the different colors obtained.[45]

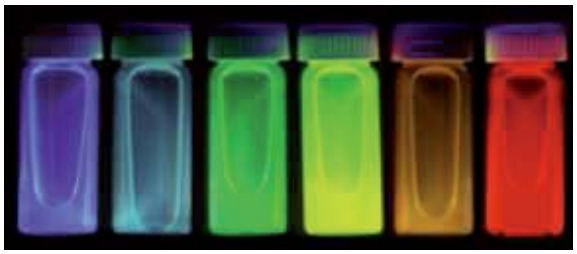

Figure 3: CdSe nanocrystals in different size and different emitting colors under UV light adopted from Ref.[46]

This phenomena is called quantum size effect (QSE). When an absorption of an electron from the valence band to the conduction band occurs due to excitation, two charge carriers are formed: the electron in the conduction band, and the hole, which has a subtend charge, that is left behind in the valence band. However these charge carriers are located in a finite area and have an electrostatic attraction to each other: this is called – the coulomb interdependency. The electron (*e*) and hole (*h*) pair is called exciton and is similar in structure to the Hydrogen atom: – one positive charge (proton) and one negative charge (electron). So, it is possible to describe the exciton in similar terms to the hydrogen atom with a quantum mechanical approach. This being said, the binding energy for the exciton is different as there is a smaller effective mass, which results in a bigger radius. The binding energy for the hydrogen atom in the ground state is 13.51 eV and its radius is 5.3 nm. For example, with CdS the binding energy from the exciton is only 0.05 eV and its radius is 2.5 nm.[47] There are in general two types of exciton, the Wannnier-Mott (named after Nevill Francis

Mott und Gregory Hugh Wannier) and the Frenkel (named after Jakow Iljitsch Frenkel).[48, 49] In case of the Wannier-Mott-exciton there are weak bonded electron-hole pairs with a big radius, which often are found in semiconductors. So, it is a phenomenological description of a border case for large distances. The binding energy can be calculated through the model of the hydrogen atom.[50] Furthermore, it is important to consider the dielectric constant of the medium in which the exciton is moving. After substituting the reduced mass of the electron-proton-system, with the reduced mass of the effective mass $1/\mu = 1/m_e * +1/m_h*$ from the electron-hole-pair in the solid the resulting equation, which also includes the Rydberg constant (R_H) with 13.6 eV, is given in {5}:

$$E_n = -\frac{\mu R_H}{m_e \varepsilon_r^2 n^2} = -\frac{R_\chi}{n^2} \quad \{5\}$$

The radius of the exciton is with the radius of the Hydrogen atom a_B shown in (1.1.6):

$$r_n = \frac{m_e}{\mu} \varepsilon_r n^2 a_B = n^2 a_\chi \quad \{6\}$$

On the other hand, the Frenkel excitons describes the opposite approximation in which electron and hole are located at one lattice point. They are strongly bound excitons with a small radius, which is in the same dimension as the lattice distance of the material. The energy of the interaction is in general the overlap of the wave functions from the electron and the hole. Through the small circumference it can not be assumed that the exciton is moving through homogenous material. Now it is important to consider the environment of the electron and the hole. Therefore, the equation derived for the Wannier excitons for calculating the binding energies cannot be used here. Frenkel excitons are observed when a high exciton binding energy is obtained. Experimental obtained values for these strong bonded excitons are from 10 meV up to 1 eV in organic semiconductors.[50, 51] The pure thermal excitation at room temperature is not enough to separate electron and hole. They are kept at a small distance (size dimension of 1 nm). The radius of an electron-hole-pair is very important for the resulting properties of the nanoparticles. When absorption occurs

in a noncrystalline material where the dimension is bigger or smaller than the Bohr radius of the exciton then it must have a higher kinetic energy. Then, if in a quantum dot the distance between the electron and the hole is smaller than the Bohr radius of the exciton, the charges cannot be separated more than the size of the particle. It results in a space confinement for the excitons and as the quantum mechanics assume, the distance has to be at least as big as the Bohr radius. However, in the quantum dots this is not possible to do, so it compensates with a higher energy. The needed energy results in a bigger E_{gap}. Therefore, the energy level is influenced by the size. This effect gets stronger when the dimension of the particle gets smaller. That means that the band gap Egap increases with decreasing of the particle size, which is shown schematically in the figure 4. The start of the light absorption is shifting to smaller wavelength, and higher energy, respectively.[47, 52, 53] The quantum size effect can be measured and also calculated through different approaches, which will be discussed later on.

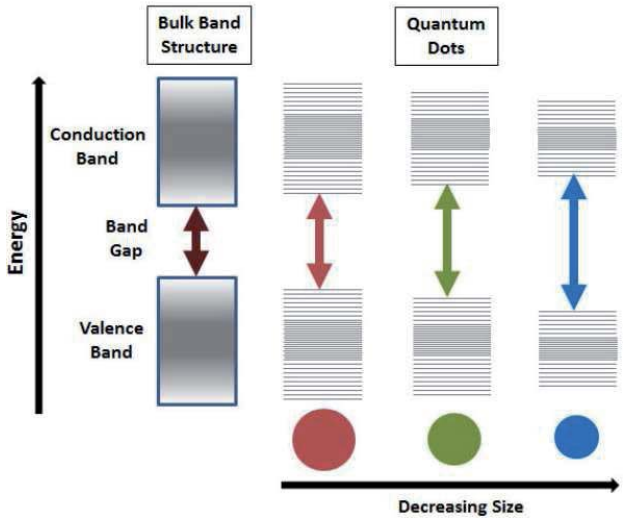

Figure 4: Quantum size confinement and resulting bandgaps Egap depending on nanoparticle size adopted from Ref.[54]

In one atom there are many discrete energy levels in regards to the electrons. An analogue situation is to find in molecules and clusters.[30] On the one hand, for infinite expanded macro crystals there are energy bands with a continuous distribution of energy levels. However, in the case of semiconductors there is an E_{gap}, which occurs between the valence band (VB) and the conduction band (CB). Between these extremes there is an intermediate position, which is realized for nanocrystalline

materials. They still have a quasicontinuous distribution of the levels in the band middles, but at the edge of the bands there are discrete energy levels. The reason for this discretion is the 3 dimensional space confinement - the QSE.

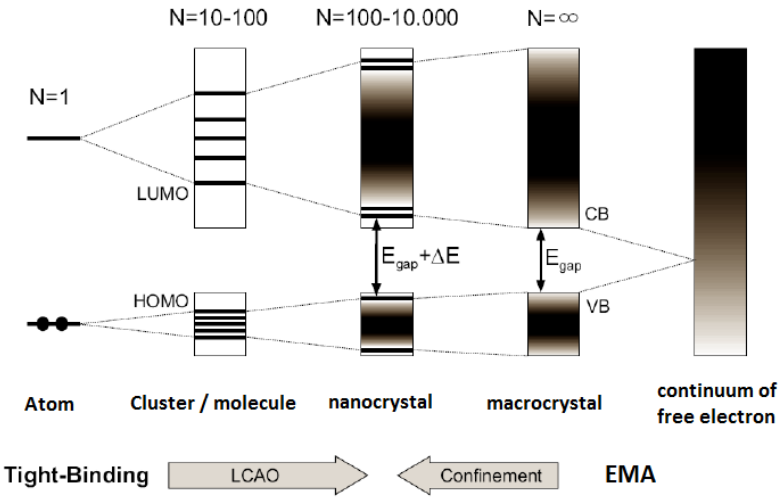

Figure 5: Nanocrystals as the transition state between molecules and macrocrystals adopted from Ref.[30] (redrawed and modified).

As a result of the QSE there are differences in the absorption spectra. While atoms have sharp absorption edges the macrocrystals have a less structured absorption spectra because there are many allowed transitions. However nanocrystals have discrete transitions near the absorption edge. Due to this discretion the absorption edge is shifting from E_{gap} to E_{gap}+dE to the higher energetic area.

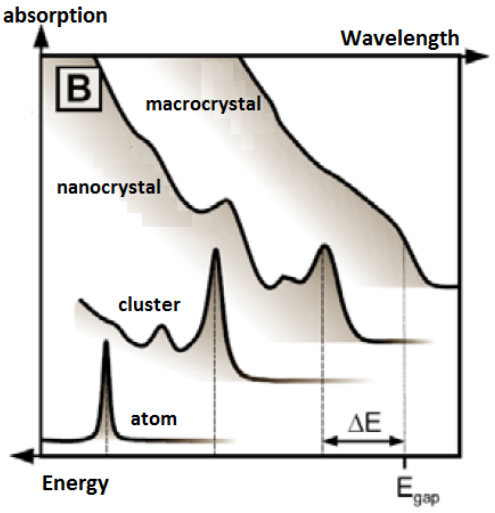

Figure 6: Typical absorption spectra of atoms, molecules, nanocrystals and macrocrystals adopted from Ref.[30] (redrawed and modified).

Growth of nanocrystals

To successfully synthesize nanocrystals it is necessary to use organic ligands, which stabilize the growth of the nanocrystals at the high temperature at which the precursors react together. Most syntheses are carried out at temperatures around 150-350 °C. As organic ligands there are various different compounds used e.g. long chain amine, phosphon acid, carboxylacids or thiol compounds, depending on the resulting desired size and shape of the nanocrystals.[66, 67] La Mer and coworkers studied the nucleation and growth process in sulfur sols. From that they developed a theory that explains the mechanism for the formation of nanocrystals from a homogenous medium.[66–68] In a LaMer diagram the concentration against time is plotted, in which a distinction is made between three parts. The following figure in 7 shows a LaMer diagram:

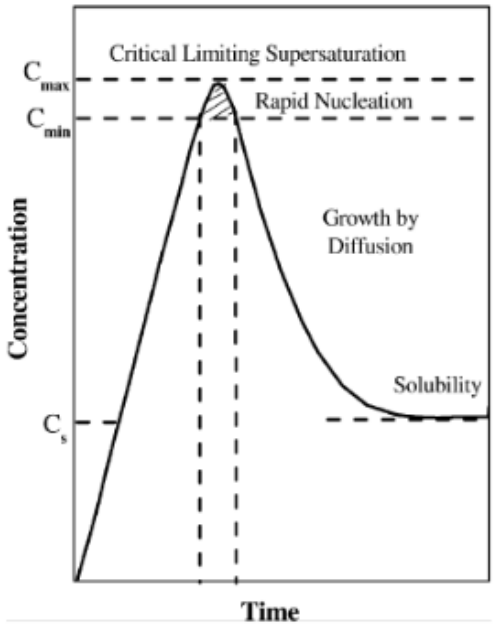

Figure 7: LaMer diagram adopted from Ref.[67]

In the first part there is a fast increase in the monomer concentration and after reaching the minimum critical concentration the rapid nucleation starts and continues until the maximum critical concentration (critical limiting supersaturation) is reached. This is referred to in the second part, in which the monomer concentration decreases after it was increased before. After the monomer concentration falls below the minimum critical concentration, the nucleation stops and the growth of the

nanocrystals occurs until there are no monomers left. This is referred to in the third part. As it can be seen in the diagram, a high rate of nucleation during a short period of time and a fast rate of subsequent growth after the nucleation step, which reduces the concentration rapidly, are requirements for monodispersity. Furthermore, the growth of the nanocrystals should have a slow rate compared to the nucleation rate. In order to influence the shape, size and monodispersity during the carried out synthesis the nucleation step and the growth step should be separated and controlled. For high monodispersity it is desired then to have a very short nucleation step, and in the case of the nanocrystal size it is controlled by a different growth time. That would explain the size, but still not the shape. For the shape explanation there are thermodynamic models that illustrate that the surface energy of each surface burnishing facet plays an crucial role.[69] For example, in a hexagonal-phase CdSe nanocrystal it is terminated mainly by 100, 001 and 001 facets.[70, 71] Furthermore, the 100 and 001 facets have only one dangling bond while the 001 facet form three dangling bonds. So the 001-facets are referred to as the most chemically active and have a high surface burnishing facet energy.[72] Monomers are more likely to attach on surfaces with higher energy so, in the case of CdSe, growth occurs through the c-axis. Furthermore, the crystal growth rate is exponentially correlated to the surface energy, which predicts the influence of the facet energys based on the shape of the nanocrystals.[73] Since it is desired for each system to undergo the reaction that leads to a low energy state, the one that is most thermodynamically stable, one should consider also the activation energy, which is important for the formation of the thermodynamic product. However, if the activation energy is not high enough then the kinetic product will be formed which in this case is more preferred. This can be accomplished by setting a high reaction temperature, with sonnication or also through a high mechanical activation step. The reactivity of a given crystalline facet can be increased by introducing of certain ligands that can attach to its surface. For example, it was found that for the asymmetric growth of a CdS shell on a CdSe core it is necessary to have a large excess of the sulfur precursor, which interacts with the growth active site of CdSe, which is the 001 facet.[72] When changing the ligands, changes in shape also occur. This can be explained with the fact that organic molecules attaching the surface reduces the surface energy, and that with different

ligands there are different resulting surface energies [55, 69] The ligands are surround the core to protect them for oxidation and to stabilize them. This can also be done with a shell around the core, which is discussed in the next section.

Core-shell system

As mentioned earlier it is necessary to saturate the traps on the surface, which can be accomplished through an excess of tight binding ligands equipped with various functional groups or an epitaxial growth of another material which is discussed in this section. Core shell materials are built up with a core and another material around the core which acts like a shell. In the following figure 8 there is an example given containing CdS as the core and ZnSe as the surrounding shell.

Figure 8: CdS@ZnSe core shell system adopted from Ref.[7]

To saturate the traps with an epitaxial growth of another semiconductor material on a nanocrystal core and to enhance the quantum yield and the stability, it is important to know the levels of the valence band and conduction band relative to each other. There are two types of core shell, which are named type I and type II.[58, 75] In type I core shell systems the material used for the shell has a higher band gap than that of the core material. After excitation with a certain energy and generating an exciton through absorption the two charge carrier, negative charged electron and positive charged hole, are located in the core. Through that the potential barrier, which separates the charges from the surface and from the existing traps on the outside of the shell, is built up. So, it is possible to enhance the quantum yield of these materials when applying this procedure because less charge carriers can get lost due to the traps and the probability of recombination is increased. Traps are electron- or hole deficit positions, which are built more favorably on the surface due to structural

faults. Even if the core was surrounded with ligands it would not be possible to saturate all existing traps, which is the reason why an additional potential barrier leads to a higher photostability. Examples of that kind of type are CdS@ZnS and InP@ZnS,[34–37] which is a heavy metal free compound and is of huge interest in the research of bio imaging and applications.[38, 39, 76–78] One more example for the type I material is CdSe@CdS synthesized in 2003 successfully from Peng et al.[79] This CdSe@CdS system is often described as a type I system, even in that it is known that the difference in the conduction band of CdS is too low as it is possible to locate the electron in the core.[80] Further investigations were carried out in the case of CdSe@CdS nanorods.[81] The result is a delocalization of the electron over the complete core shell system. Therefore, this kind of type is referred to type I-1/2[77] and can also be called a quasi type II system.[82] There is a red shift occurring due to the non localization of both charge carriers. More examples for type I-1/2 are ZnSe@CdSe, CdTe@CdSe and PbSe@CdSe.[78, 82, 83]

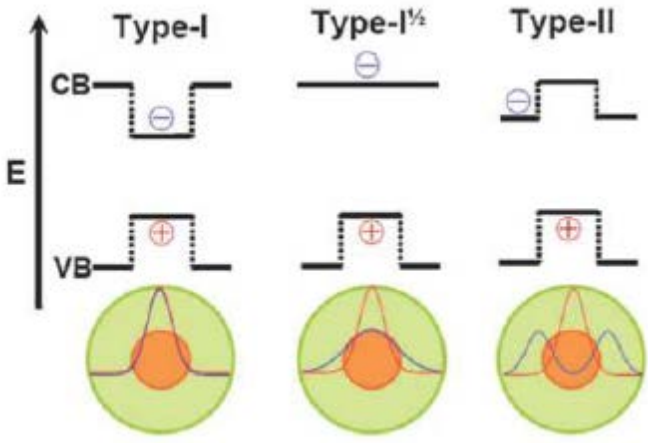

Figure 9: Different types of core-shell system adopted from Ref.[78]

In the other case, for type II core shell systems, the conduction band of the shell material is lying under the conduction band of the core material. That means that the generating positive charge carrier, the hole, is located in the core while the correspondent negative charge carrier, the electron, has a high probability of being found in the shell material. This charge separation is called a heterogen transition. The generated exciton is recombining at the interface of the core material and shell material which results in a fluorescence of lower energy and higher wavelength of

both materials, respectively.[82] This red shift is stronger as the shell thickness increases. Through this spatial separation the recombination is choked and the resulting quantum yield is low. This also explains why the fluorescence lifetime for type II systems are higher than for type I systems.[74, 84, 85] An example of that kind of material is CdS@ZnSe.[58] In order to build up shell material around the core material it is important that the lattice parameters are not that different. So, in this example it is good to use CdSe as a core material and ZnS for the shell material, as the band gap of ZnS is much higher than that of CdSe. This means that the generated exciton is located in the core, which as was discussed before, enhances the quantum yield and photostability. Both semiconductor materials are crystallizing in the zinc blend structure, but the difference in the lattice constant is still big with 12 % (6.05 Å for CdSe, 5.42 Å for ZnS).[6] To overcome this it is possible to build up more shell system by using a CdS shell as the interception surface between CdSe and ZnS, in which the CdS shell has a lattice constant of 5.83 Å and is therefore between that of CdSe and ZnS. Although the lattice mismatch between CdSe and CdS is comparable to the mismatch between CdSe and ZnS only by 3.9 %.[6] The following figure in 10 shows the energetic level of the valence and conduction band of each material, the lattice mismatch at the intersection border between each material, and the graphical core-shell-shell system.

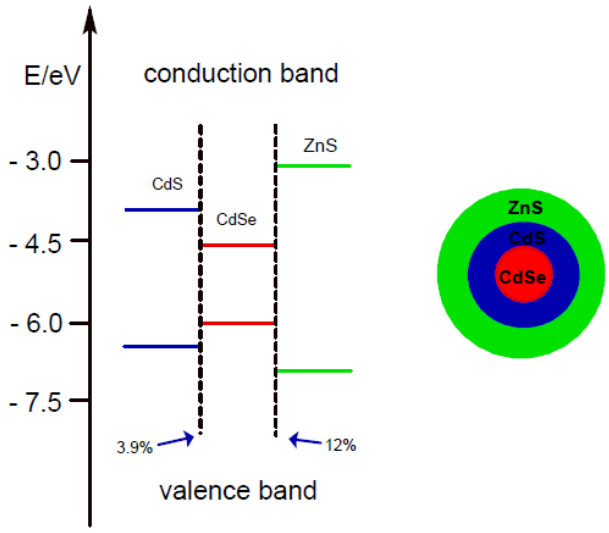

Figure 10: Core/shell/shell system and its lattice mismatch adopted from Ref.[6] (redrawed).

The following figure 11 gives the energetic levels of the certain valence and the conduction band of the commonly used material for both: as core material and also as
shell material.

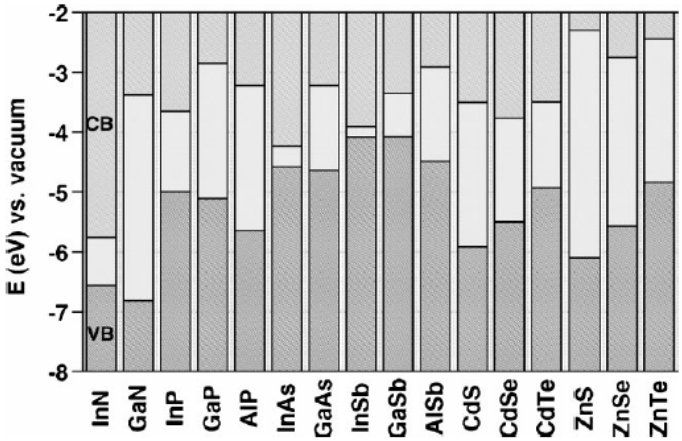

Figure 11: VB and CB and resulting Egap for different III-V and II-VI semiconductor adopted from Ref.[86]

The first realized multi shell system was done by Mews, Basche et al. (University Mainz, Germany) in 2005 on the system of CdSe-core CdS@CdZnS@ZnS multi shell nanocrystals.[6] It should also be said at this point that during the reviewing process of the paper an other paper on a similar topic was published by Talapin et al.[87] The product of such syntheses are stable nanoparticles with high quantum yields, up to 80 %,[88] the enhanced photo stability against photo oxidation, and also lower toxicity. The growth of defect free CdSe@ZnS nanoparticles is limited by 2-3 monolayers.[6, 77, 89, 90] Furthermore, the growth conditions are crucial for the epitaxial growth and can be crystalline, amorph or tensed up growth.

Optical lithography

The optical lithography is based on the two photon absorption process (TPA) [91, 92]. As the name let assume there is happening a simultaneous absorption of two photons which can have the same or different energy but in the sum the energy of those two photons is the same as the energy difference between the excited state and the ground state when absorption is occurring from the ground state. It is a third order

and a nonlinear optical process due to the dependency of the absorption on the square of the light intensity.[107] In the following figure 12 the simplified Jablonski scheme for the single and two-photon processes are given.[93] With a laser equipped with a monochromatic laser beam of a wavelength of 400 nm it is possible to accomplish an excitation from the ground state to the first electronic excited state which is shown with the blue arrow in (a). But it is also possible to do that with a laser which has the double wavelength and so half of the energy, namely 800 nm. The difference now is that this time two photons have to be absorbed simultaneous to accomplish an excitation. This is showed with two red arrows in (b). This physical phenomena was described in the 1930th from Maria Goeppert-Mayer but not until the 1930th Denk and Strickler used that concept for the microscopy.[94]

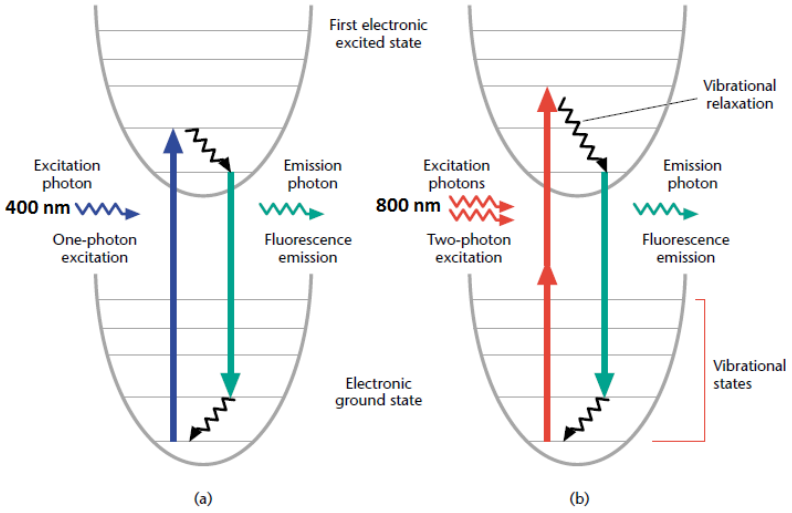

Figure 12: Jablonski diagram for single and two-photon absorption adopted from Ref.[93] (modified).

Nevertheless, the probability for TPA is compared to the one photon absorption (OPA) very low.[91] That is one reason why it is not possible to measure this phenomena with UV-VIS due to the need of high photon flow density. When high photon flow density is achieved then enough molecules can be excited from their ground state to excited states and it is possible to measure a fluorescence. So for observing the phenomena of the TPA it is needed to have high light intensities which are realized nowadays with pulsed titan-sapphire laser. With their ability of being pulsed and with high repetition rate the resulting energies are about 100 kW in

which each pulse has a FWHM of smaller than 200 fs. Furthermore the focusing of the light plays an important role. Only in the focus of the microscope objective noteworthy TPA is happening.[91] This is used in the process of optical lithography. It requires a photoresist which consist of a base resin (like ormocer or SU-8), a light sensitive material – a photoinitiator like a spirofluorene based TPA dye[95]. It is based usually on organic molecules which absorbs the exposed light to form high reactive species e.g. radicals which can initiate a further reaction and polymerization. Furthermore, the fluorescence peak of the TPA dye based on spirofluorene and used as the photosensitizer does not coincide with the fluorescence of e.g. the quantum dots. Then there has to be besides a substrate on which its surface the optical writing should be done a photomask with the desired structure. The photomask consist of areas with light blocking metal layer usually chromium is used for that and depending on which type of resist it is used, either a positive or a negative one, the areas which were exposed to the light or covered due the light blocking metal layer are removed. Furthermore it is possible when using a solvent to control the viscosity of the resist as it is important for the resulting layer thickness. So the goal of the optical lithography process is to write a structure on a substrate. This can be accomplished by using a monochromatic light source and a photomask which is put on the surface. A resist is put on the surface of the substrate and the photomask is put over the resist. Then they get exposed to light while the areas under the light blocking metal layer are not get exposed. But on the area where the light is not getting blocked a chemical reaction is happening. After the exposure the resulting resist on the substrate is developed in the developer step. That means that with in the case of the positive resist the developer liquid removes only the chemical changed structures which were exposed to light before. In the case of a negative resist then only the areas are removed which were under the light blocking metal layer. After drying the desired structure - given through the design of the photomask - is written on the resist. It is also possible to transfer the structure on the substrate when etching the substrate in the interspace of the resist. Furthermore it is possible to dope the area in the interspace or to grow up a layer of a metal in these spots. When the resist is then completely removed the structure of the photomask will be on the substrate or in the substrate.[91] This process is schematically shown in the figure 13.

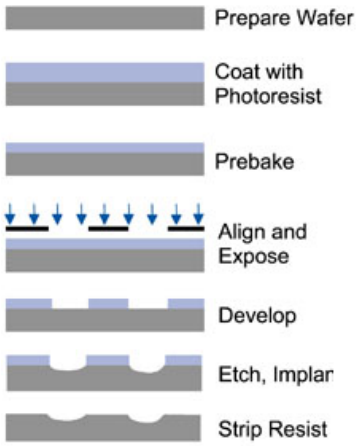

Figure 13: Shematically process of Lithography adopted from Ref.[96]

Ormocer (organically modified ceramics) - a preparation of new sol-gel based materials as an inorganic-organic hybrid polymer - were reported in the 1980´s from two independent groups. In the earlier stage Wilkes referred it to CERAMERs[91, 97] while Schmidt from the Fraunhof institute in Germany named the material ORMOSILs (organic modified silicates).[98, 99] There is made a difference between inorganic-organic polymers like ormocer where the stiffen backbone consist of an inorganic material while the side groups have an organic nature.[100] In contrary organic-inorganic polymers do have an organic backbone and inorganic side groups. Ormocer is used in wide range like in the optical devices,[101, 102] as functional coatings,[103–105] as filling material in dentistry[106] and as cell growth templates.[107] For patterning of 2D and 3D quantum dot structure it is used the commercial available Ormocomp which is trademark of the Fraunhofer institute in Germany.[108] Another resin which is widely used is SU-8 which is a multifunctional epoxy derivate of a Bis-phenol-A novolac which is negative photoresist for optical lithography.[109] The number 8 indicates the epoxy groups which a single molecule contains regarding the average.[91] It is suitable for thick layer applications.[110-112] It can be dissolved in various organic solvents like propylene glycol methyl ether acetate (PGMEA) or gamma-butyrolacton.[112] Furthermore, it has low optical absorption in the near UV spectral range and due the aromatic functionality and highly cross linked matrix which makes it very stiff and so the resulting glass transition temperature of cured SU-8 is to find at 240 °C.[113, 114] As SU-8 is chemically relatively stable and resistant against the most acids and solvents it is difficult to remove the cross-linked SU-8. Nevertheless it

was done by using laser techniques and highly reactive radical plasma.[91, 115, 116] As for this reason given above the used resin in this study was focused on Ormocomp instead of SU-8.

The two photon lithography (TPL) is a fast prototyping method that photo induces chemical reactions in a patternable medium and allows the direct writing of microstructures.[107] Femtosecond (fs) lasers with a high repetition rates induce very specific chemical changes at the focal spot of the laser within a photoactive medium. So the two-photon sensitivity is the key for initiating chemical changes during microfabrication. For this reason, the patternable medium should contain a two-photon absorbing (TPA) material acting as a photosensitizer or a photoinitiator. The spatial selectivity of the chemical process arises from the inverse dependence of two photon absorption on the intensity of the laser beam.[91] In figure 14 there is the setup given for the patterning. With the piezoelectric (PZT) stage it is possible to change the movement of patterning in each dimension in a desired step. The 80 fs pulsed Ti-Sapphire laser with a monochromatic wavelength of 780 nm is guided through an optical shutter to the lens and then to the resin (in this case it is SU-8). The immersion oil protect the lens. With changing the coordination in each dimension it can be written a structure which is modeled before in a program.

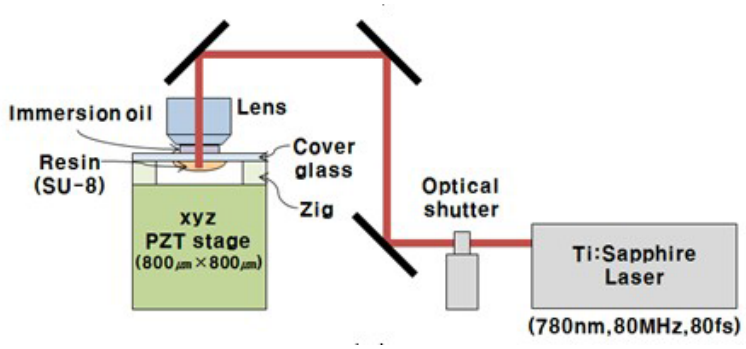

Figure 14: Experimental setup for the patterning process adopted from Ref.[117]

When using the quantum dots and mixing them with a resin the procedure is the same. The UV light is coming with a monochromatic wavelength inside the lens which is focused on the substrate and the resin. There are again on a XYZ PZT instrument for scanning in the desired coordinates of the resulting 3 D structure.

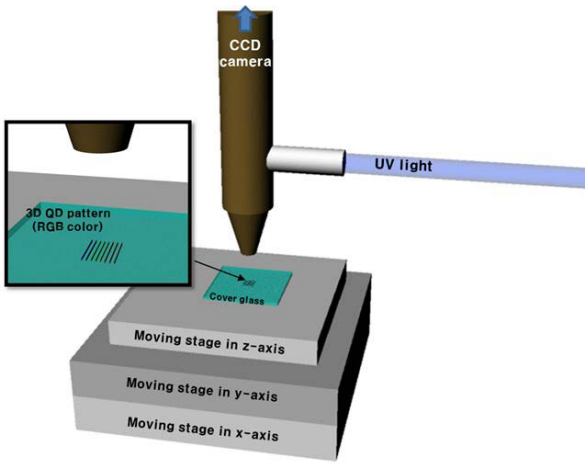

Figure 15: Patterning through desired scanning area adopted from Ref.[118]

Energy transfer predicted by Förster (FRET)

An important application of the FRET mechanism can be found in nature in the photosynthesis.[122] Here, the energy from the sunlight has to reach the center, in which the reactions are formed and for which the energy is needed. Photons from the sunlight get absorbed and through a fluorescence resonant energy transfer it is possible to transfer the energy to the reaction place where the energy is needed. Furthermore, FRET is an interesting mechanism to study in biomimetic solar cell dyes.[123] Here, it is possible to collect light in a way similar to photosynthesis and to enhance the efficiency when compared to conventional solar cells. Also, in the area of medicine it is possible to create a spectroscopic spacer based on this kind of mechanism, in which in vitro and in vivo distances can be measured. For example, in the case of a peptide chain it is possible to equip both ends with an acceptor and a donor. While the peptide chain is changing its conformation, the energy transfer and the distance between the acceptor and donor is changing too; therefore, one can gain information about the conformation of the peptide chain e.g. during a specific process. Furthermore, the FRET mechanism can be used in organic light emitting diodes (OLEDs) and organic solar cells: a subject that has recently become a big research topic. This is especially true when the FRET mechanism is considered in combination with other energy transfer processes like the triplet-triplet-annihilation[124] or the Dexter transfer, [125] in which it is possible to develop up-

conversion systems, and in which the energy of two single photons can be combined. As discussed before there are various possible ways for an excited electron to undergo a relaxation process before reaching its electronic ground state. Besides the fluorescence and radiationless processes there is another process for decreasing the population in the ground vibrational state of the first singlet state $S_{1,0}$ which is called the energy transfer after Foerster. One requirement for accomplishing that specific process is that there has to be besides a fluorescence donator molecule, a suitable acceptor molecule. The processes referred to as FRET are given in a reaction equation {7}, in which A stands for the acceptor, D for the donator molecule.[126]

$$D^*(S_{1,0}) + A(S_{0,0}) \rightarrow D(S_{0,i}) + A^*(S_{1,j}) \quad \{7\}$$

The following figure 16 gives the scheme of the possible processes that may happen, in which krl is the rate constant of the radiationless transitions, k_{abs} is the absorption, k_{fl} is the fluorescence and k_t is the energy transfer.

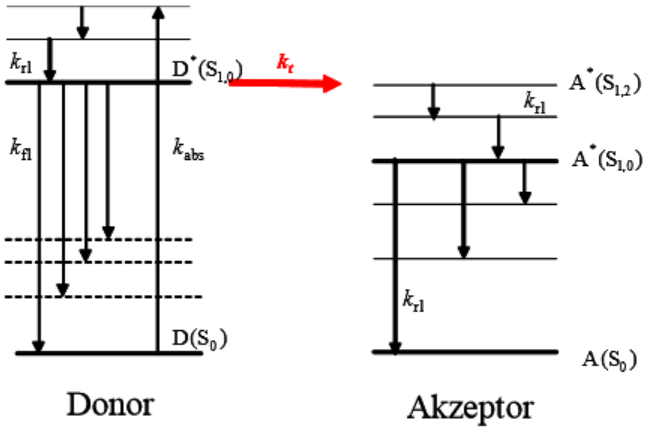

Figure 16: Fluorescence resonant energy transfer predicted by Förster adopted from Ref.[126]

It is furthermore assumed that the vibrational relaxation is occurring much faster than the energy transfer, which can be seen as fulfilled and so simplifies the theoretical dealing. That means that an energy transfer between a donor and acceptor always occurs from the vibrational ground state of the first singlet state $D(S_{1,0})$ of the donor molecule D. After the energy transfer a relaxation process occurs very fast to

the vibrational ground state of the first singlet state of the acceptor molecule $A(S_{1,0})$.[30] The rate constant k_t of the energy transfer can be written as shown in equation {8}, in which t_D is the fluorescence lifetime of the donor in the absence of the acceptor, R_0 is the Förster radius and r is the distance between donor and acceptor.

$$k_t = \frac{1}{\tau_D}\left(\frac{R_0}{r}\right)^6 \qquad \{8\}$$

The Förster radius is given with

$$R_0 = \left(\frac{\kappa^2 * \varphi_D * 9000 * \ln 10}{n^4 * 128 * \pi^6 * N_A}\int_0^\infty \frac{\Psi^D_{norm} * \varepsilon_A}{\tilde{\nu}^3 * \tilde{\nu}}\, d\tilde{\nu}\right)^{\frac{1}{6}} \qquad \{9\}$$

where φ_D is the quantum yield of the donor, κ^2 is the orientation factor that gives the one another orientation of the transition dipole moments μ^D and μ^A which should particularly be parallel or collinear. n is the refractive index of the solvent, ε_A the absorption coefficient of the acceptor and Ψ^D_{norm} is the normalized fluorescence spectra of the donor, which is given with the followed equation in {10}.

$$\Psi^D_{norm} = \Psi^D * \left(\int_0^\infty \Psi^D d\tilde{\nu}\right)^{-1} \qquad \{10\}$$

For a successful energy transfer from the donor to the acceptor there should be an overlap between the emission spectra of the donor and the absorption spectra of the acceptor. Another important value to calculate is the energy transfer efficiency E which defines the ratio of excited donor molecules that undergo a successful energy transfer with an acceptor molecule and so are unable to emit a fluorescence photon themselves. It is given:

$$E = \frac{k_t}{\tau_D^{-1} + k_t} = \frac{R_0^6}{R_0^6 + r^6} \qquad \{11\}$$

When it is r = R_0 then the energy transfer efficiency becomes E = 0,5. So the definition of the Förster radius is the distance between the donor and the acceptor molecule when the energy transfer efficiency becomes 50%.[126]

Surface plasmon resonance (SPR)

Surface plasmons (SPs) are coherent oscillations of free electrons at the boundaries between metal and dielectric which are often categorized into three classes: surface plasmon, particle plasmon (PP) and volume plasmons (VP).[127] Surface plasmons are surface waves (evanescent waves). Hereby, the longitudinal electronic vibrations are excited parallel to the surface of the metal. The direction of propagation is along the surface, whereas the intensity is decreasing exponentially with the length of propagation. The decrease is resulting from intensity loss in the metal. The resulting strength is in the area above the metallic surface increased. The following figure shows schematically the surface plasmon at the interface of the metal and the isolator.[128]

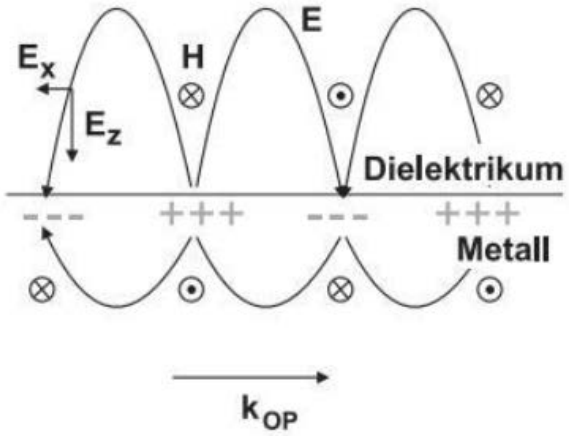

Figure 17: Surface plasmon at the interface of the metal and isolator adopted from Ref.[128]

The electric field which is connected with the electron density oscillation has one component which is vertical to the wave vector k_{OP}. Also the magnetic field *H* do has a component vertical to k_{OP}. That means, that an excitation with light is possible. Particle plasmon is a second kind of plasmon. They are also called located surface

plasmon or Mie-plasmon. A plasma is a full or partial ionized gas which is neutral to in the sum. When an electromagnetic wave is exposed to a metal - which is build up through the model of an electron gas - the electrons are getting excited to vibrate resulting in a harmonic oscillator. This vibration is called plasma vibration whereas it is allocate with a quasiparticle. What for a photon an electromagnetic wave constitute, it is for a plasmon the vibration in the electron gas of metals. In figure 18 there is given a volume plasmon in a plasma consisting of free charge carriers - e.g. quasi-free electrons in a metal.[42, 128]

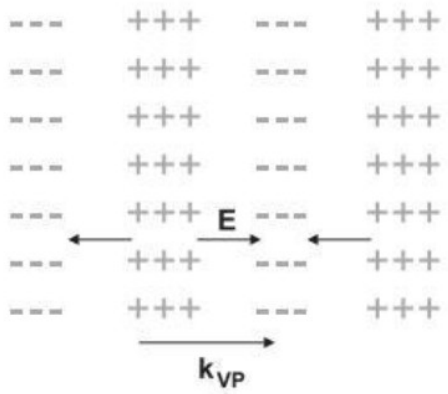

Figure 18: Volume plasmon consisting of free charge carriers adopted from Ref.[128]

The difference between a surface plasmon and a volume plasmon is that for the volume plasmon an excitation with light is not possible. Furthermore, the difference between a surface plasmon and a particle plasmon is that for the particle plasmon light absorption and emission is possible due to the conservation of momentum and of energy.[128]

Surface enhanced Raman spectroscopy (SERS)

SERS is a surface sensitive technique which enables to observe an enhancement of the Raman scattering when nanoparticles are adsorbed on metal electrodes, colloidal metal particles or rough metal surfaces. As a metal it is used silver (Ag), cupper (Cu) and gold (Au) which is also used in the carried out investigations. The mechanism which leads to an enhancement of about 1010 to 1011 is not clearly elucidated.[129-131] There are suggested two possible mechanism which can sub divide in two categories.

The first one is the theory of an electromagnetic effect and the second one is the theory of the chemical shifting. The first theory assume that due to exposure to certain wavelength the electrons of the metal get excited. Due to this excitation the metal particles become polarized and it comes to an adjustment of strong dipoles. Surrounding these metal particles there is a strong electric field resulting which interact with the investigated sample. That means that the interaction between the incident light and the sample is getting enhanced by the metal particles resulting in an increase of the intensity of the Raman scattering. In the second theory (chemical shifting) the chemical enhancement can occur due to charge carrier transport or formation of a bond between the metal particles and the sample. These leads to a change in the polarizability and therefore can enhance the intensity of the Raman scattering.[129, 131-134]

Chapter 1: Surface modified Quantum Dots for the application into the two photon initiated lithography process

The work described in this chapter was carried out in cooperation with Hannam University in Daejeon, South Korea, in the framework of the International Training Research Group (IRTG 1404). Hereby, the task was to design quantum dots with different emitting wavelengths and two different spacers as surface ligands. These ligands can be used to encapsulate the QDs with a silica shell to obtain more robustness and stability in the end. Furthermore their surfaces were functionalized with certain photopolymerizable groups to use them for the lithography process to obtain highly luminescent 2D/3D patterning structures in the direction of designing promising candidates for metamaterials. The patterning processes were conducted by the Korean cooperation partners at Hannam University and KAIST.

Photosensitive Functionalized Surface-Modified Quantum Dots for Polymeric Structures via Two-Photon-Initiated Polymerization Technique

Redouane Krini, Cheol Woo Ha, Prem Prabhakaran, Hicham El Mard, Dong-Yol Yang, Rudolf Zentel,* Kwang-Sup Lee*

Macromol. Rapid Commun., DOI: 10.1002/marc.201500045

In this paper, the surface modification of CdSe- and CdZnS-based quantum dots (QDs) with a functional silica shell is reported. Functionalized silica shells are prepared by two routes: either by ligand exchange and a modified Stöber process or by a miniemulsion process with amphiphilic poly(oxyethylene)nonylphenylether also know as Igepal CO-520 (IG) as oligomeric amphiphile and modified silica precursors. The polymerizable groups on the functionalized silica shell allow covalent bonding to a polymer matrix and prevent demixing during polymerization and crosslinking. This allows the homogeneous incorporation of QDs in a

crosslinked polymer matrix. This paper furthermore demonstrates that the resulting QDs, which are i) shielded with a proper silica shell and ii) functionalized with crosslinkable groups, can be used in two-photon-initiated polymerization processes in combination with different photoresists to obtain highly luminescent 3D structures. The resulting luminescent structures are attractive candidates for photonics and metamaterials research.

Photonic nanomaterials such as photonic crystals (PCs) and metamaterials are gaining increased attention due to their special optical properties. [P1–P5] Photonic materials act as wavelength selective mirrors. In addition, they allow it to localize light in defects (tiny voids, lines, or planes inside the PC, which do not have its periodic structure) and to guide it—lossless—around sharp corners [P6] or to modify the spontaneous emission of light sources incorporated into the PC, such as organic dyes, rare earth ions, or semiconductor quantum dots (QDs). [P7] Artificial opals, prepared by self-assembly, offer the advantage to prepare large scale (several cm^2) 3D PCs with reasonable effort. [P8] Metamaterials—on the other side—are claimed to allow the preparation of materials with negative refractive index. [P4] To obtain such materials, it is necessary i) to generally structure the material at the nanoscale; ii) to vary, especially, the refractive index of high index materials spatially and iii) to introduce chromophores at desired places in space. Classical methods to obtain a patterned refractive index (e.g., in PCs) are the crystallization of monodisperse colloids (artificial opals) [P8, P9] and the etching of silicon. [P10] Two-photon lithography (TPL) has the advantage here as that it allows a free design of 2D and 3D structures. [P11, P12] However, to make TPL attractive for the preparation of metamaterials and photonic materials, it is not sufficient to pattern classical resists (SU-8, ORMOCER [Fraunhofer Institute, Munich, Germany] or others) as it needs patterned high refractive index materials and the incorporation of good chromophores. Both requirements could be achieved by the incorporation of QDs into the resin. However, this requires their passivation against the conditions of TPL (photochemically created cationic species and radicals) and the incorporation of various organic groups for compatibility and crosslinking of the QDs with the matrix of the resin. For the chemical passivation of the QDs and their functionalization, a second silica shell—in

addition to the ZnS shell—is desirable. For compatibilization with the crosslinked polymer matrix the introduction of functional groups is necessary, which prevent segregation of the QDs during polymerization. But the topic of incorporating QDs into a polymer network is hardly unexplored. [P13] Generally various methods and techniques were developed to shield the surface of QDs with an inorganic shell (e.g., ZnS) to obtain passivated nanoparticles. [P14, P15] For chemical passivation, a second silica shell (SiO_2) can be grown around the ZnS layer of the QDs. This silica shell makes the QDs less toxic and more resistant against to undesired oxidation. Thus, the resulting silica-coated nanoparticles have a big interest in the optoelectronics. [P16–P18] There are generally two approaches to cover the nanoparticles with a silica shell and to introduce various organic end groups. Both require, at first, the attachment of hydroxyl groups on the sulfidic nanoparticles. The first one is a modified sol–gel based Stöber process, [P16] which builds a silica shell starting from hydroxyl groups introduced via a ligand exchange. It has been used successfully to cover metallic particles, semiconductor nanoparticles, [18] insulators,[P19–P21] and organic dyes. [P22–P24] The second approach for the introduction of a silica shell uses a microemulsion process. [P25] Generally, it should be possible to embed such QDs in a
resin to create polymeric fluorescent 2D or 3D patterns via TPL, if their surface is modifi ed with polymerizable end groups. In this contribution we present such surface modified QDs compatible with polymer resins. We describe i) the synthesis and surface modification of QDs as luminescent high refractive index materials; ii) their incorporation into certain resins (ORMOCER or SU-8); and iii) their patterning via the TPL technique to obtain fluorescent 2D/3D polymeric structures with different emission colors.

1.1 Experimental Section

All chemicals were purchased from Sigma-Aldrich, Acros Organics, Alfa Aesar, Microchem, or Fluka and used without further purifi cation unless noted otherwise.

1.2 Synthesis of Core–Shell QDs

Blue emitting CdZnS@ZnS capped with oleic acid (OA), green-, orange-, and red-emitting CdSe@ZnS-OA were synthesized according to the procedure in refs. [P26–P28]

with a slight experimental modification for the orange emitting QDs. Here, the temperature was kept at 295 °C for the QDs formation.

1.3 Formation of the Functional Silica Shell

The silica shell was either introduced by a two-stage process (ligand exchange and addition of the silica precursor afterwards) or in a one-stage microemulsion process.

1.3.1 Ligand Exchange Modification of QDs with 11-Mercapto-1-Undecanol (MUD) (Figure 1.1, Upper Line)

The ligand exchange with MUD and the formation of the silica shell with 3-(trimethoxysilyl)propyl methacrylate (T-MMA) as the silica precursor was carried out as follows: 20 mg of OA capped CdSe@ZnS were given in a reaction vessel together with 400 mg of MUD and it was diluted with 30 mL of chloroform and 30 mL of ethanol. The mixture was then sonicated for 2 h. Then 60 mL of chloroform was added to precipitate the MUD functionalized nanoparticles. After centrifugation the resulting nanoparticles were dispersed in dimethyl sulfoxide.

1.3.2 QDs Encapsulation into Silica Shell via Functional Silica Precursors

For the silica encapsulation, 5 mg of CdSe@ZnS-MUD was used and diluted with 3 mL of dry dimethyl spectroscopy (DMSO). Then 100 µL of T-MMA was added and stirred for 10 h at 50 °C under continuous nitrogen flow. The core–shell QDs with a functionalized silica shell with photosensitive end groups were precipitated by adding an excess of chloroform followed by centrifugation. The precipitates were washed with ethanol and chloroform to remove excess ligands.

1.3.3 The Surface Modification of QDs with Functional and Photosensitive Groups via Microemulsion System (Figure 1.1, Lower Line)

The experimental procedures leading to the QDs is presented in the supporting Information.

1.4 Instrumentation

The UV–vis spectra were taken on a Shimadzu UV-3600 UV–vis–NIR spectrometer. The fluorescence experiments were conducted on a LS-55 spectrofluorophotometer (Perkin Elmer, Waltham, MA, USA). Transmission electron microscopy (TEM) and energy dispersive X-ray spectroscopy (EDXS) investigations were carried out on a G2T-20S instrument (Tecnai, Hills-boro, OR, USA). The arrays of triangular helical spring structure were fabricated by using the two-photon stereolithography process. For the two-photon absorption process, a mode-locked Ti sapphire laser was used as the laser source. The laser has a wavelength of 780 nm, 80 MHz in repetition and an ultra-short pulse width of 100 fs. An optical shutter for controlling the on/off state of the laser beam was operated. The laser beam was fi xed and tightly focused by a high-numerical-aperture objective lens (N.A. 1.3 × 100 with immersion oil). The cover glass

with photocurable resin was moved along the 3D laser scanning data by using the x, y, z piezoelectric stages with a resolution of 0.1 nm. The fabrication process was monitored using a high magnification charge-coupled device camera. For patterning the polymeric lattice structures, ORMOCER, 0.4 wt% of Michler's ketone as a co-initiator, and 0.1 wt% of a phenylenev-inylene-based two-photon absorbing dye 4,4′-((1E,1′E)-(2-((2-ethylhexyl)oxy)-5-methoxy-1,4-phenylene)bis(ethene-2,1-iyl))bis(N,N-diphenylaniline) (EMPA) (details and structure will be reported elsewhere since this material has not been published yet) were used as a two-photon sensitizer. For the metamaterial structures, SU-8 2035, 0.5 wt% of the photoacid generator triarylsulfonium hexafluoroantimonate and 0.1 wt% of EMPA were used. The Fourier transform IR (FTIR) spectroscopy were taken on a Bruker IFS 88 and on a Jasco FTIR 4100. The scanning electron microscope (SEM) images were carried out on a S-4800 (Hitachi) field-emission SEM. To display the obtained fluorescent polymeric structures, a LSM 710 confocal micro-scope (Zeiss) was used.

1.5 Results and discussion

1.5.1 Synthesis and Characterization of Photoreactive QDs

Starting point of the synthesis of the photo-processable quantum dots (QDs) were 3 CdSe and 1 CdZnS based QDs of different size and a ZnS shell for stabilization. To coat them with the second silica shell and to introduce functional organic groups two

processes were applied (Fig. 1.1). The first one relies on a ligand exchange of oleic acid versus MUD and a subsequent condensation of the silica precursor (Fig. 1.1, upper row) according to the scheme of Lee et al. [26] (See Experimental Part). The second process is a microemulsion process (see SI), which leads to the simultaneous formation of layered structures of the amphiphilic IG (Fig. 1.1, lower row) on the QD and the silica shell formation. In both cases the silica precursors react with each other (shell formation) and get bound to the QD via the hydroxyl groups of MUD and IG. The formation of the silica shell offers thereby the possibility to incorporate functional groups like methacrylate or olefin groups by proper choice of the silica precursor. In this way the functional QDs for photo-patterning like **QD 1-4** (Fig. 1.1 and 1.2) were obtained. They are based on the ligand exchange route. Comparable QDs made by the micro-emulsion route are presented in the Supporting Information (SI) section.

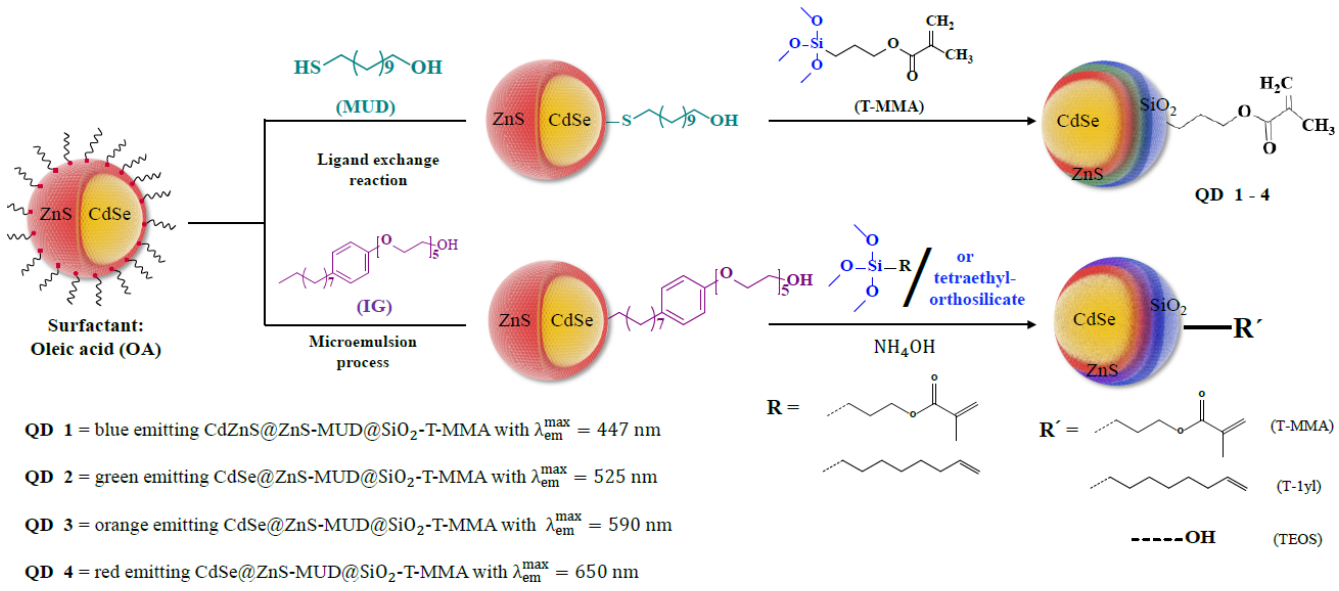

Figure 1.1: Silica encapsulating and modification of CdSe QDs with functional and photosensitive groups like methacrylates or olefins adopted.

The successful shell formation can be detected by FTIR (strong band around 1020 cm^{-1} in Fig. 1.2 (b), which belongs to the Si-O vibration of the silica shell. EDXS measurements confirm the presence of Si (SI Fig. 5). The introduction of the functional photosensitive methylmethacrylate groups via the functional silica precursor can be detected for **QD 2** in the FTIR spectrum (for **QD 1**, **QD 3** and **QD 4**

see SI Figs. 2-4) - as there is a strong band for the carbonyl groups at 1718 cm^{-1} and a weaker band around 1651 cm^{-1} typical for the unsaturated ester structure. The TEM images for **QD 1** in Fig. 1.2 (c) and (d) - for **QD 2** and **QD 4** see SI Fig. 6 and 7 - show the nanoparticles before the ligand exchange with MUD and after the surface modification and functionalization with polymerizable and photosensitive groups.

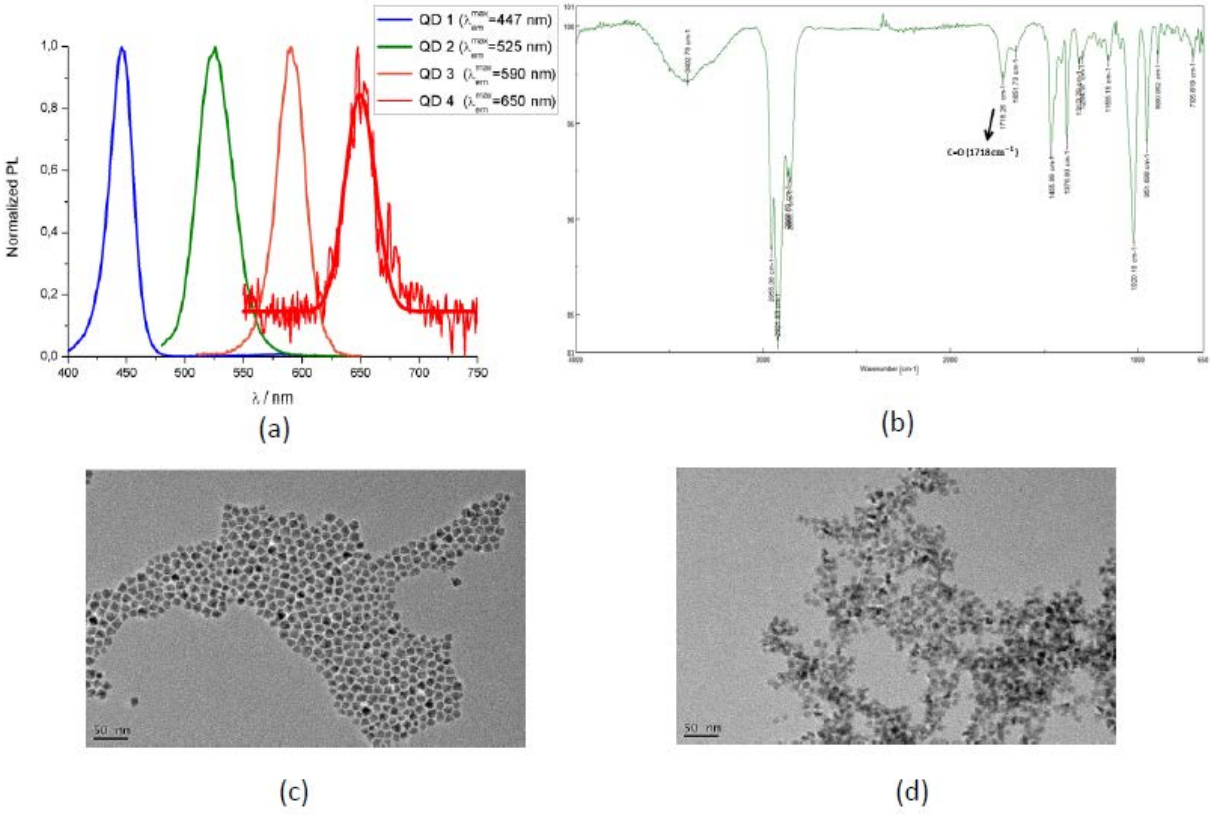

Figure 1.2: PL maxima of **QD 1-4** (a), FTIR of green emitting CdZnS@ZnS-MUD@SiO_2-T-MMA **(QD 2)** (b), TEM image of blue emitting CdZnS@ZnS capped with OA (c) and after silica shell formation CdZnS@ZnS-MUD@ SiO_2-T-MMA **(QD 1)** (d).

Also the microemulsion process (see SI) allows the formation of a functional silica shell (functional polymerizable and photosensitive end groups) around the QDs. The silica shell around the QDs shows up again in the FTIR in Fig. 1.3 (a) at a wavenumber of 1120 cm^{-1} (the strong band belonging to the Si-O vibration). For the T-MMA particles (Fig. 1, lower line) the carbonyl group (C=O) of the methylmethacrylates can be detected too at a wavenumber of 1680 cm^{-1}. The green emitting modified nanoparticles shown in Fig. 2.3 (b) have a PL maximum λ_{max} = 551 nm. In the HR-TEM images also the lattice constant can be seen. It is around 0.35 nm.

The size average of the particles was found to be 9 nm (Fig. 2.3 c, d), which leads after substraction of the core size of the unmodified nanoparticles (4 nm for CdSe@ZnS-OA, see SI Fig. 6 (a)) to a silica shell thickness of 2,5 nm.

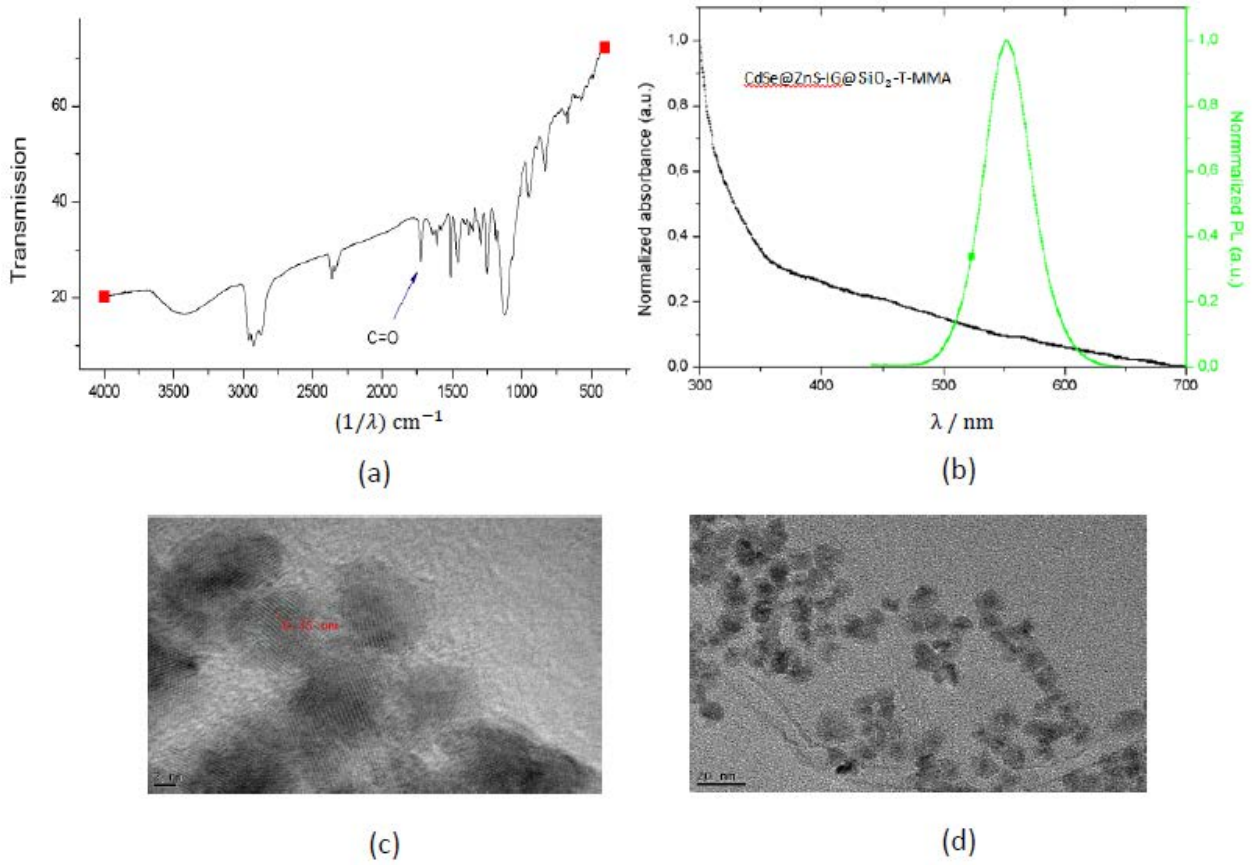

Figure 1.3: TEM image of CdSe@ZnS-IG@ SiO_2-T-MMA.

In this context it is interesting to mention some other consequences of the formation of a silica shell. Using TEOS as silica precursor a silica shell rich in Si-OH groups, or with negative charges after deprotonation is obtained. Thus the CdSe QDs get water soluble and it becomes possible to transfer the surface modified nanoparticles from organic solvents into water (see SI Fig. 8). At this point it should, however, be stressed, that this gets only possible for the TEOS modified nanoparticles. For the QDs modified with the other silica sources (methylmethacrylate and olefine end groups) this was not possible and the QDs are still soluble in organic solvents. This is important to ensure the solubility in organic solvents and the compatibility with ORMOCER® and SU-8 for the TPL technique.

In addition there is a slight red shift of the fluorescence of the CdSe core, at first, after the passivation with the inorganic ZnS shell and secondly after the silica shell formation (see SI Fig. 16) as to be expected. At last it gets possible to crosslink the QDs modified with methylmethacrylate groups on the surface with a radical initiator. Thereby, the QDs react with each other and form a crosslinked network as schematically shown in SI Fig. 15).

1.5.2 Patterning by the TPL technique

Based on the knowledge, that the photosensitive end groups can be successfully polymerized, the surface modified QDs with the polymerizable end groups were introduced into the TPL technique to obtaining 2D and 3D fluorescent network structures. To accomplish this they were mixed with either ORMOCER®, which is a trademark of the Fraunhofer Institute in Germany or SU-8 which is based on an epoxy structure.[28,29] Here, the QDs take part in the polymerization of the resin initiated by two photon laser pulses to form the desired network structure. For this purpose **QD 1-4** were used (for other QDs see SI) to build up the structures presented in figure 1.4 and 2.5.

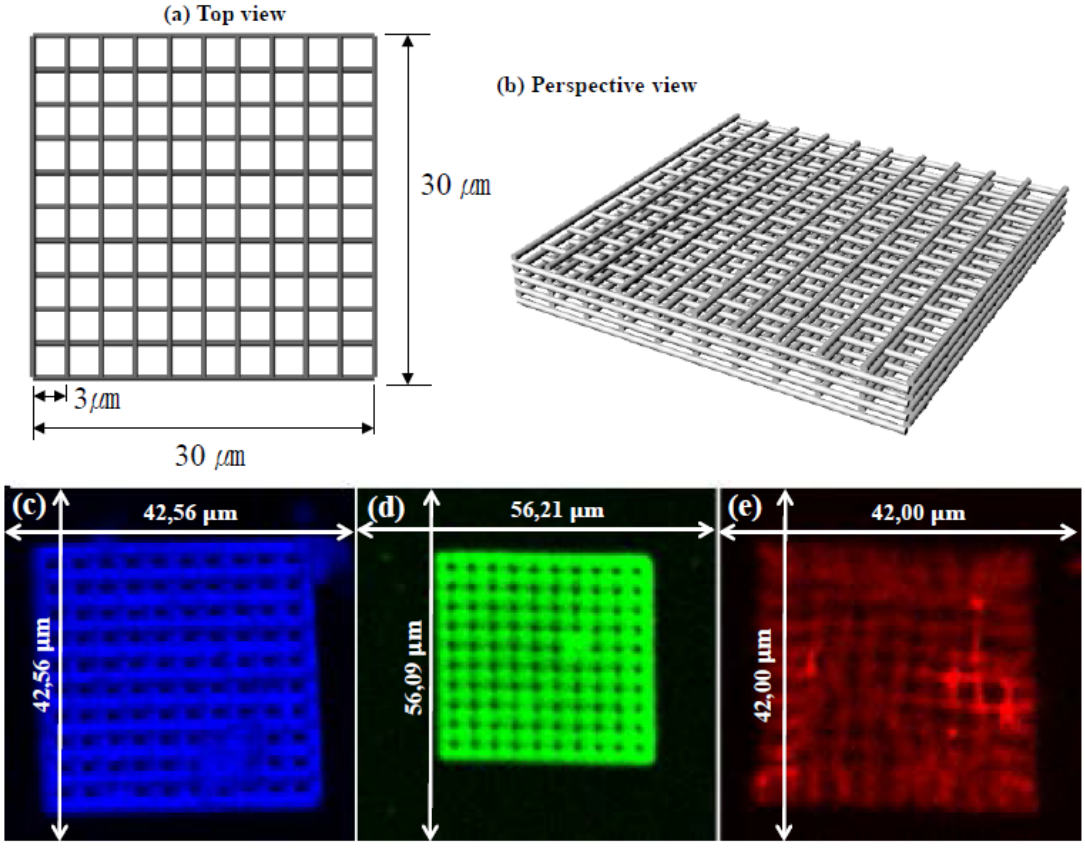

Figure 1.4: Top view (a) and prespective view (b) and the obtained fluorescent confocal images (c-e) of the lattice materials of polymerized structures via TPIP.

The 3D lattice pattern (Fig. 1.4) obtained with the TPIP technique show the successful incorporation and polymerization of the different surface modified QDs with the resin ORMOCER® at a laser working condition of 120 mW. The photosensitive methylmethacrylate end groups on the surface of the nanoparticles shell undergo a polymerization with the resin to form the stable lattice pattern. It was carried out here for the blue, green and red emitting QD 1, QD 2 and QD 4 as demonstrated in the confocal images (Fig. 2.4). In addition it was possible to fabricate a 3D polymeric metamaterial structure consisting of triangular helices using a cationic photoresist (SU-8) at a laser working condition of 70 mW containing the blue, green and red-QDs mixed in (Fig. 1.5). The base of the structure is 65 µm in width and the side of an individual triangle in the helical structure is 7 µm.

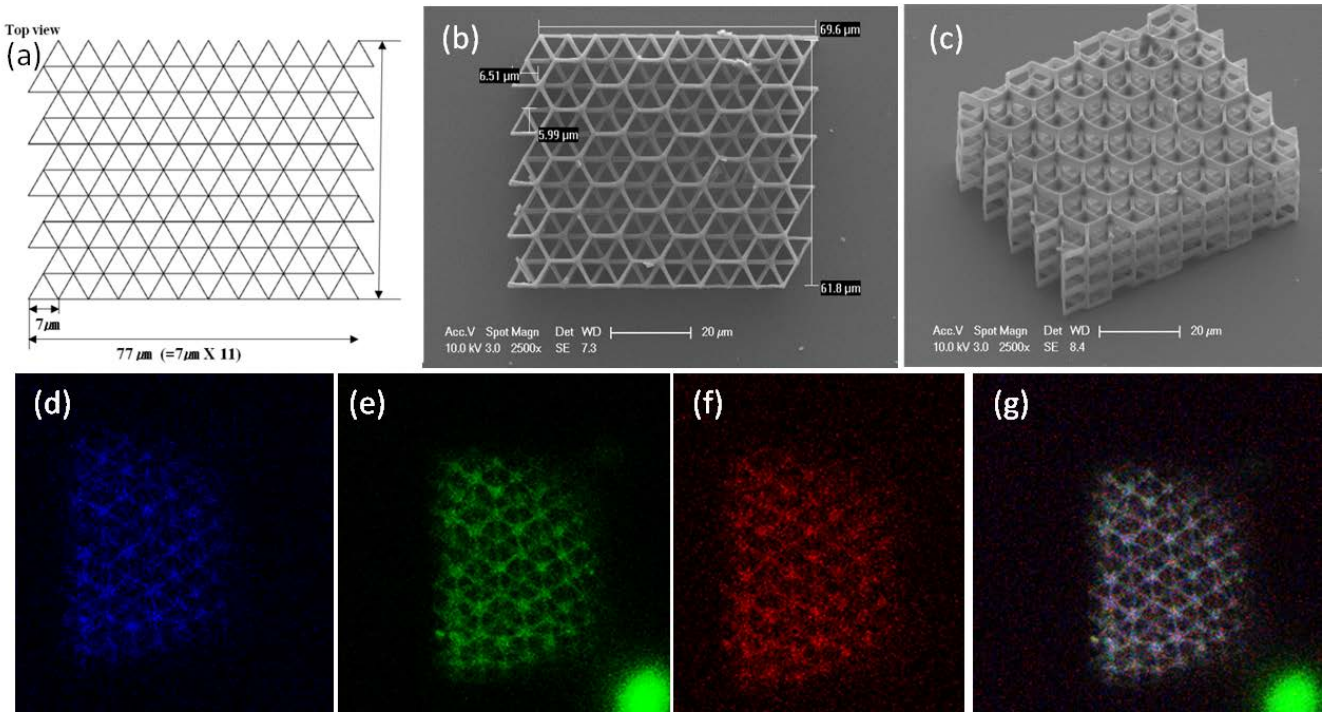

Figure 1.5: (a) Top view of the the metamaterial structure comprising triangular helices, the base of the triagle is 7 µm and the edge length of the helix array is 77 µm, the helix has a pitch of 6 µm. The helix array comrises 11 arrays in x-direction and 10 arrays in y-direction. (b) & (c) SEM images of the triangular helix array. (d) - (f) The blue, green and red fluorescence shown by the microstructure imaged by confocal microscopy at Z = 7 µm (g). The combined effect of blue, green and red fluorescence.

Figure 1.5 shows the confocal microscopy image of the triangular helical structures at an excitation wavelength of 375 nm. The blue fluorescence of the microstructure (d) was imaged using selective fluorescence filters in the wavelength range 465-510 nm. The green (e) and red (f) fluorescence images of the metamaterial structure was made using selective fluorescence filters in the wavelength ranges 560-610 nm and 650-710 nm respectively. For obtaining the white fluorescence resulting from the combination of the blue, green and red fluorescence all the filters were used simultaneously (g). Further different patterns obtained from TPIP process with photosensitive equipped QDs can be found in the in figure SI 17.

Conclusions

This paper demonstrates that QDs shielded with (i) the proper silica shell and (ii) functionalized with crosslinkable groups can be used in TPIP processes to obtain highly luminescent 3D structures. The necessary silica shells can be prepared by two routes, whereas the functional organic groups (methacrylates or olefins) can be incorporated into the silica shell by the use of modified silica precursors. The resulting luminescent materials are attractive as photonic materials or as meta-materials. Independent of the successful patterning this work demonstrates also the incorporation of nanoparticles with a high refractive index into a polymer network structure. This is a promising strategy to obtain high refractive index hybrid systems.[P5] Such high refractive index of polymers (HRIP) attracted a huge attention because of their potential applications concerning advanced optoelectronics fabrications like the formation of micro-lenses

Bibliography

[P1] E. Yablonovitch, *Phys. Rev. Lett.*, **1987**, *58*, 2059.

[P2] S. John, *Phys. Rev. Lett.* **1987**, *58*, 2086.

[P3] R.B. Wehrspohn, H.-S. Kitzerow and K. Busch, *Nanophotonic Materials: Photonic Crystals, Plasmonics and Metamaterials*, Wiley-VCH Verlag GmbH, Weinheim, **2008**.

[P4] J. B. Pendry, *Phys. Rev. Lett.*, **2000**, *85*, 3966.

[P5] J.-G. Liu, M. Ueda**,** *J. Mater. Chem.***, 2009**, ***19***, 8907-8919.

[P6] A. Birner, R.B. Wehrspohn, U. Gösele, K. Busch, *Adv. Mater.* **2001**, *13*, 377.

[P7] F. Fleischhaker, R. Zentel, *Chem. Mater.*, **2005**, *17*, 1346 – 1351.

[P8] B. Lange, F. Fleischhaker, R. Zentel, *Macromol. Rapid Commun.*, **2007**, *28*, 1291 - 1311

[P9] P. Jiang, G. N. Ostojic, D. M. Mittleman, V. L. Colvin, *Adv. Mater.,* **2001**, *13*, 389.

[P10] T. Meier, P. Thomas, S. W. Koch, *Coherent Semiconductor, Optics: From Basic Concepts to Nanostructure Applications*, Springer, Berlin, **2007**.

[P11] Chris Mack, *Fundamental Principles of Optical Lithography: The Science of Microfabrication*, John Wiley & Sons, London, **2007**.

[P12] R.L. Clough, *Nucl. Instr. and Meth. In Phys. Res., B* 2001, *185*, 8-33.

[P13] A.R. Kortan, R. Hull, R.L. Opila, M.G. Bawendi, M.L. Steigerwald, P.J. Carroll, L.E. Brus, *J. Am. Chem. Soc.*, **1990**, *112*, 1327-1332.

[P14] A. Mews, A. Eychmueller, M. Giersig, D. Schooss, H. Weller, *J. Phys. Chem.*, **1994**, *98*, 934-941.

[P15] W. Stoeber, A. Fink, E. Bohn, *J. Colloid Interface Sci.*, **1968**, *26*, 63-69.

[P16] A. Schroedter, H. Weller, R. Eritja, W.E. Form, J.M. Wessels, *Nano Lett.*, **2002**, *2*, 1363-1367.

[P17] T. Nann, P. Mulvaney, *Angew. Chem. Int: Ed.*, **2004**, *43*, 5393-5396.

[P18] Michiel JA de Dood, Basjan Berkhout, Carlos M van Kats, Albert Polman, Alfons van Blaaderen, *Chem. Mater.*, **2002**, *14 (7)*, 2849–2853.

[P19] Kobayashi Y, Misawa K, Takeda M, Kobayashi M, Satake M, Kawazoe Y, Ohuchi N, Kasuya A, and Konno M., *Colloids and Surfaces,* **2004**, *251*, 197-201.

[P20] Kobayashi Y, Misawa K, Kobayashi M, Takeda M, Konno M, Satake M, Kawazoe Y, Ohuchi N, and Kasuya A., *Colloids and Surfaces*, **2004**, *242*, 47-52.

[P21] R. Nyffenegger, C. Quellet, J. Ricka, *J. of Colloid and Interface Science*, **1993**, *159*, 150-157.

[P22] Ow, H., D.R. Larson, M. Srivastava, B.A. Baird, W. W. Webb, and U. Wiesner, *Nano Letters,* **2005**, **5** (1) , 113-117.

[P23] M. Ohobosheane, S. Santra, P. Zhang, W. H. Tan, *Analyst*, **2001**, *126*, 1274-1278.

[P24] M. Darbandi, R. Thomann, T. Nann, *Chem. Mater.*, **2005**, *17*, 5720-5725.

[P25] K.K. Jang, P. Prabhakaran, D. Chandran, J.J. Park, K.S. Lee, *Optical Material Express*, **2012**, *2*, 519-525.

[P26] P. Prabhakaran, W.J. Kim, K.S. Lee, P.N. Prasad, *Optical Material Express*, **2012**, *2*, 578-593.

[P27] W.K. Bae, K. Char, H. Hur, S. Lee, *Chem. Mater.*, 2008, *20*, 531-539.

[P28] S. Tuomikoski and S. Franssila, *Sensors and Actuators A: Physical*, **2005**, *120 (2)*, 408–415.

[P29] S. Aura, V. Jokinen, M. Laitinen, T. Sajavaara, S. Franssila, *J. Micromechanics and Microengineering*, **2011**, *21*, 125003.

Supporting Information (SI)

for Macromol. Rapid Commun., DOI: 10.1002/marc.201500045

Photosensitive Functionalized Surface-Modified Quantum Dots for Polymeric Structures via Two-Photon-Initiated Polymerization Technique

Redouane Krini, Cheol Woo Ha, Prem Prabhakaran, Hicham El Mard, Dong-Yol Yang, Rudolf Zentel,* Kwang-Sup Lee*

The surface modification of quantum dots (QDs) with functional and photosensitive groups via the microemulsion system:

The silica encapsulating with the oligomeric detergent Igepal CO-520 (an alkylated phenol etherified with PEG and abbreviated **IG**) via microemulsion system was carried out as follows. Briefly, 5 mg of green-emitting CdSe@ZnS-OA was dissolved in 15 mL chloroform and declared as the stock solution. Then 500 μL of the stock solution was added to 10 mL of cyclohexane. Then 1.5 mL of IG was added followed by 150 μL of a silica source. A total of three different silica sources were used with different chain lengths and polarity. The first one was tetraethylorthosilane (TEOS), which has functional ethoxy groups but no carbon chain. The second one is trimethoxy(7-octen-1-yl)silane (T-1yl) and has a long alkyl chain with eight carbon atoms, including a photosensitive end group, which is a double carbon bond. For the third and last one, T–MMA with a short chain length and a polymerizable methylmethacrylate end group was used. Then it was stirred for 40 minutes to form a stable microemulsion system with a high stirring rate of 1300 rpm. Finally, 50 μL of NH_4OH (25 wt %) as the catalyst was added and the resulting microemulsion system was stirred for 30 h. Then the resulting nanoparticles equipped with photosensitive and functional end groups were isolated by acetone and were centrifuged. To remove excess surfactant and none reacted molecules, it was washed in the following step with ethanol. The

resulting nanoparticles were declared to CdSe@ZnS-IG@SiO_2-*FG* in which *FG* stands for the functional groups obtained from the different silica sources, such as the photosensitive double bonds.

Analysis studies of compounds QDs 1–4

FT-IR measurements for the modified nanoparticles CdSe(CdZnS)@ZnS-MUD@$Si0_2$-FG were carried out and compared with the unmodified quantum dots (QDs). Oleic acid capped QDs have characteristic strong signals around 1555 cm^{-1}. This corresponds to the antisymmetric ν(CO) stretching vibration bands of carboxylate. Also, there is no signal for a carboxylic group, which would be at a wavenumber around 1700 cm^{-1}. There are also two strong bands at 2922 and 2850 cm^{-1} (Figure SI 1). These bands correspond to the ν(CH) vibrations of CH_2 groups. After silica encapsulating, a new band appears for all modified QDs around 1020 cm^{-1}, which corresponds to the Si-O vibrations of the silica shell (Figures SI 2–4).

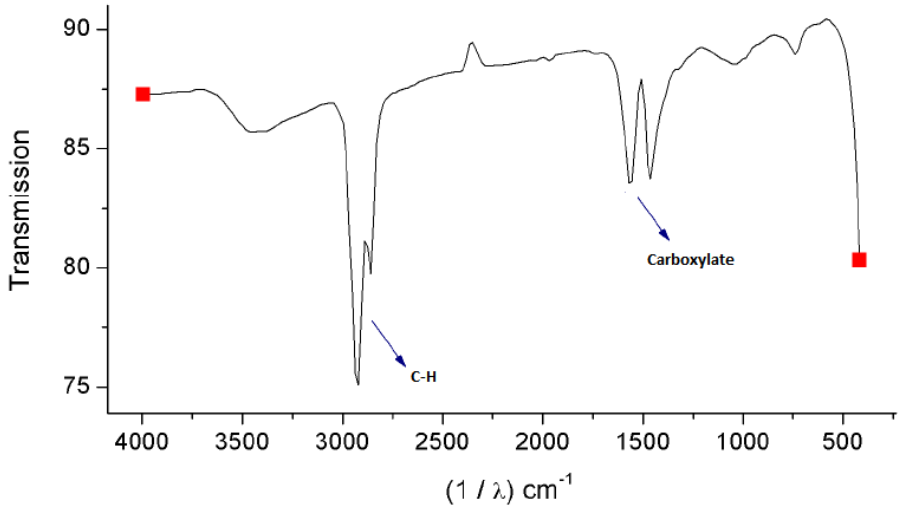

Figure SI 1: CdSe@ZnS capped with oleic acid.

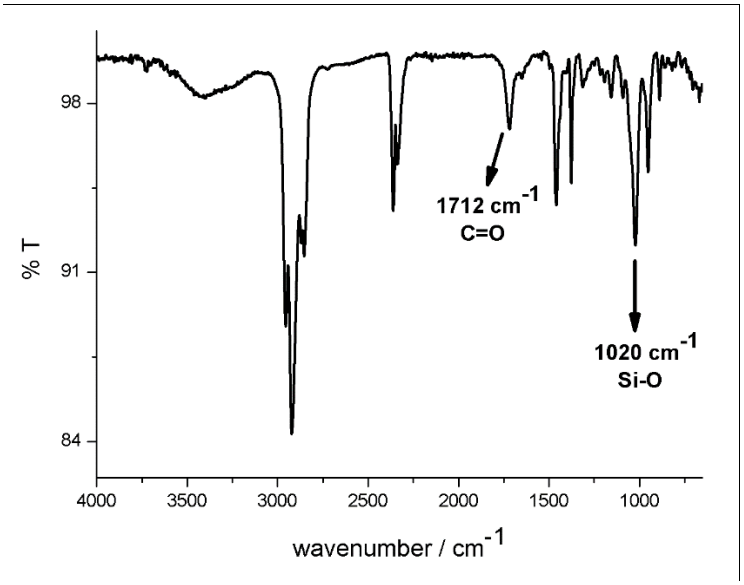

Figure SI 2: FT-IR of blue-emitting CdZnS@ZnS-MUD@ SiO_2-T-MMA (QD 1).

IR (KBr): ν = 2953 (s), 2918 (vs), 2850 (m), 1712 (m; C=O), 1644 (w; CH2=CH2), 1455 (m), 1020 (vs; Si-O) cm^{-1}

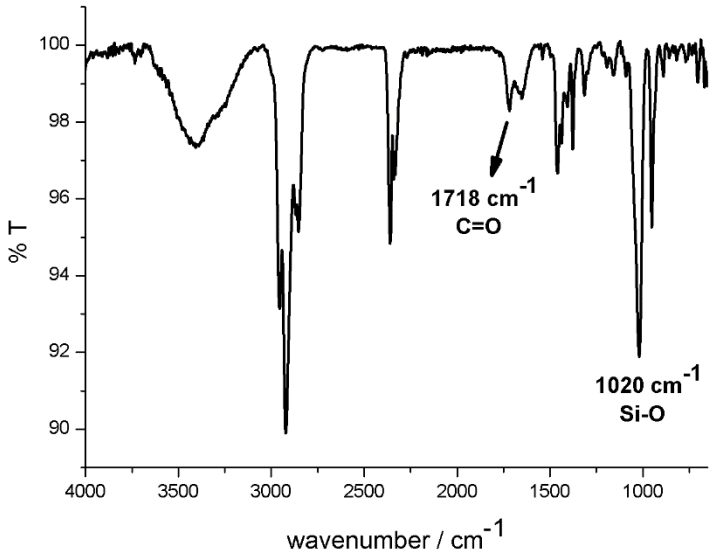

Figure SI 3: FT-IR of orange-emitting CdZnS@ZnS-MUD@ SiO_2-T-MMA (**QD 3**).

IR (KBr): ν = 2955 (s), 2918 (vs), 2852 (m), 1718 (m; C=O), 1651 (w; CH2=CH2), 1455 (w), 1020 (vs; Si-O) cm^{-1}

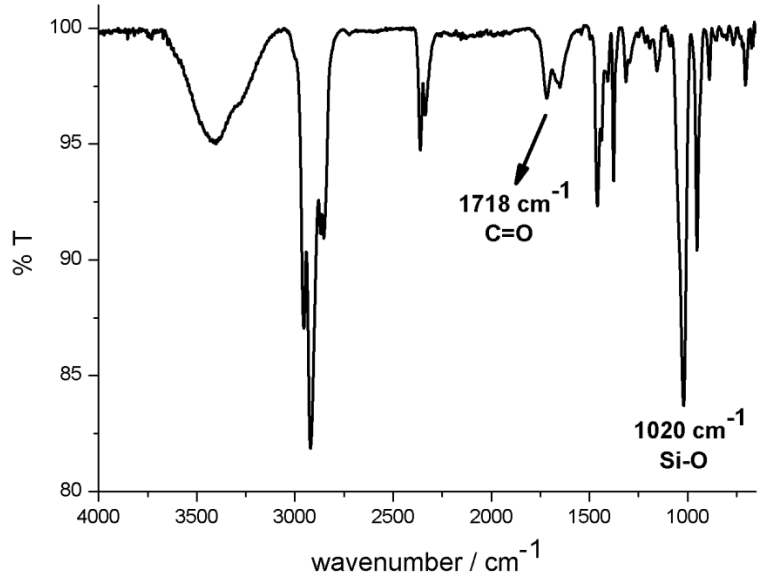

Figure SI 4: FTIR of red-emitting CdZnS@ZnS-MUD@ SiO_2-T-MMA (**QD 4**).

IR (KBr): ν = 2953 (s), 2921 (vs), 2850 (m), 1718 (m; C=O), 1651 (w; CH2=CH2), 1458 (m), 1020 (vs; Si-O) cm^{-1}

Blue emitting CdZnS@ZnS-OA and CdZnS@ZnS-MUD@ SiO_2-T-MMA (QD 1)

Also, for the modified QDs, an EDX analysis was carried out (Figure SI 5). Here, also copper (Cu) and carbon (C) appear, which belong to the used round-carbon-coated copper transmission electron microscopy (TEM) grid. Furthermore, it can be seen that Si is presented.

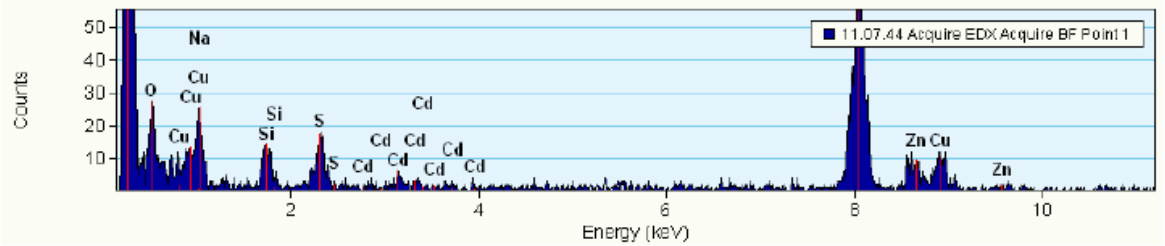

Figure SI 5: EDX of blue-emitting CdZnS@ZnS-MUD@ SiO_2-T-MMA.

Green-emitting CdSe@ZnS-OA and CdSe@ZnS-MUD@SiO_2-T-MMA (QD 2)

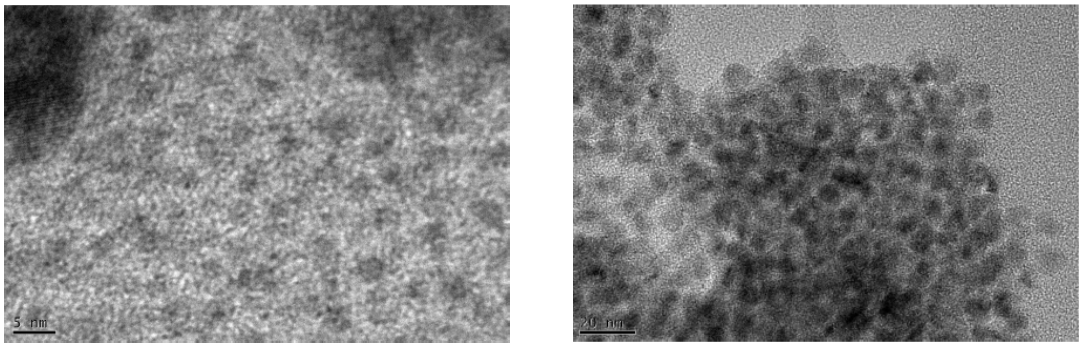

(a) (b)

Figure SI 6: (a) TEM image of green-emitting CdSe@ZnS capped with OA. (b) Green-emitting CdSe@ZnS-MUD@ SiO_2-T-MMA.

Red emitting CdSeZnS-OA and CdSe@ZnS-MUD@ SiO_2-T-MMA (QD 4)

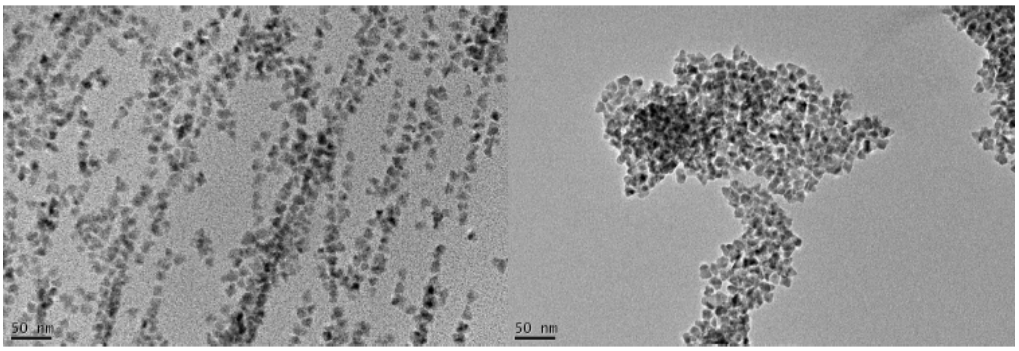

(a) (b)

Figure SI 7: (a) TEM image of red-emitting CdSe@ZnS capped with OA. (b) Red-emitting CdSe@ZnS-MUD@ SiO_2-T-MMA.

Analysis data of CdSe@ZnS-IG@ SiO_2-TEOS:

After the incorporation of the QDs into a silica shell, the obtained nanoparticles could be easily transferred to the water system due to the existing stable passivating silica shell in the case of the used silica source TEOS (left in Figure SI 8). Without the silica shell the QDs could be dispersed only in chloroform (right in Figure SI 8).

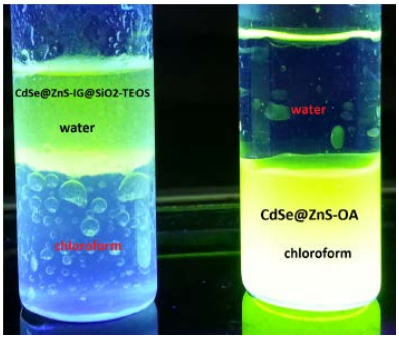

Figure SI 8: CdSe@ZnS-OA (right) and CdSe@ZnS-IG@$Si0_2$-TEOS (left) dispersed in water/chloroform.

In the FT-IR in Figure SI 9, of CdSe@ZnS-IG@ $Si0_2$ −TEOS, the OH group at wavenumbers higher than 3000 cm^{-1} can be seen. Furthermore, there is a broad stretching band existing from 1000 to 1200 cm^{-1}, which is an overlapping of the Si–O stretching band and the stretching band of IG.

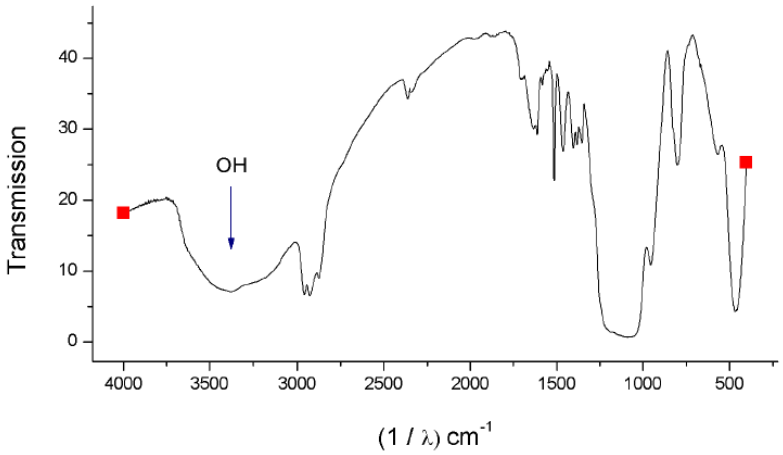

SI Figure 9: FT-IR CdSe@ZnS-IG@$Si0_2$-TEOS.

Also, UV-vis and PL measurements were carried out, which is presented in Figure SI 10.

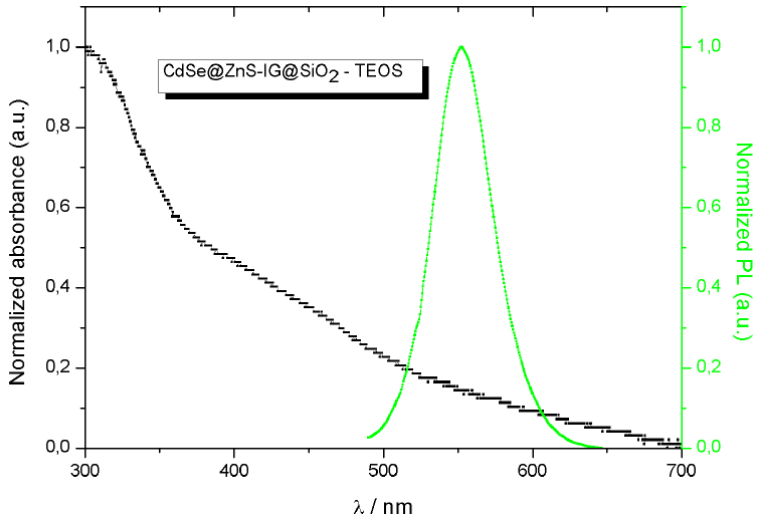

Figure SI 10: TEM image of CdSe@ZnS-IG@ $Si0_2$-TEOS.

It can be seen in the TEM image in Figure SI 11, with higher resolution, that there is an overlapping of the silica shells, which seems to be aggregated and sharing one surrounded silica shell, which also coalesces.

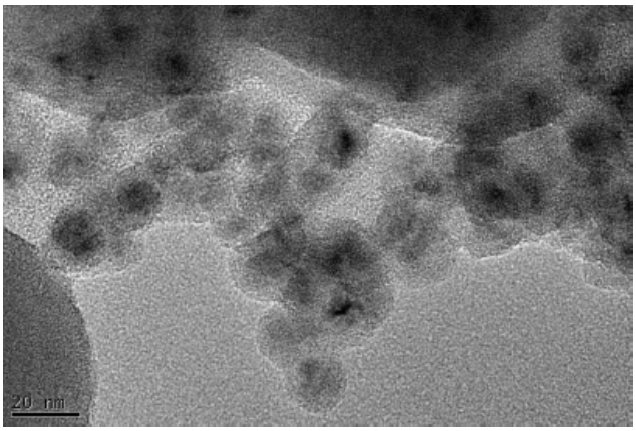

Figure SI 11: TEM image of CdSe@ZnS-IG@ $Si0_2$-TEOS.

Analysis data for CdSe@ZnS-IG@SiO_2-T-1yl

Figure SI 12 shows the FT-IR spectra of CdSe@ZnS-IG@ $Si0_2$-T-1yl. There are no other functional groups—besides the carbon double bond—in the structure that could be observed.

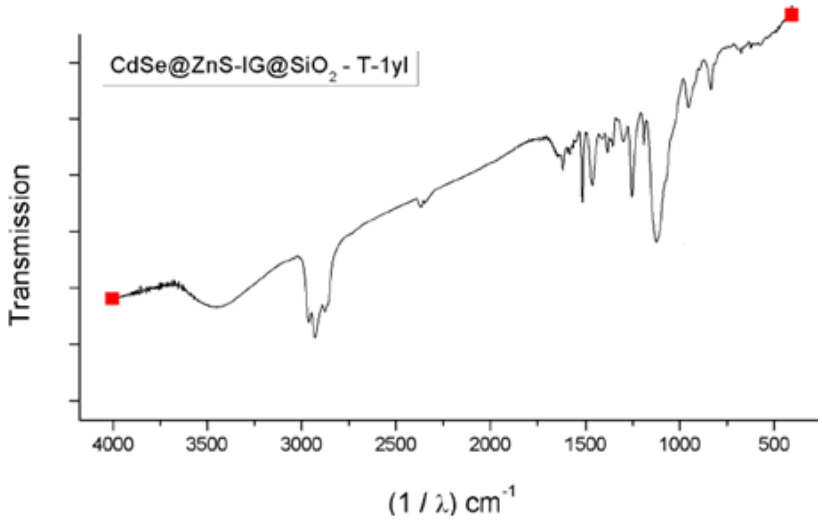

Figure SI 12: FT-IR of CdSe@ZnS-IG@$Si0_2$-T-1yl.

In the TEM image for CdSe@ZnS-IG@$Si0_2$-T-1yl in Figure SI 13, the successful silica incorporation can be observed. The diameter is almost the same as for the other surface modified nanoparticles, as the only change is the resulting chain length on its surfaces equipped with a photosensitive group. The nanoparticles have a tendency to glow to each other, but it is still possible to see the shape of them, although there are many areas in which a higher aggregation is happening.

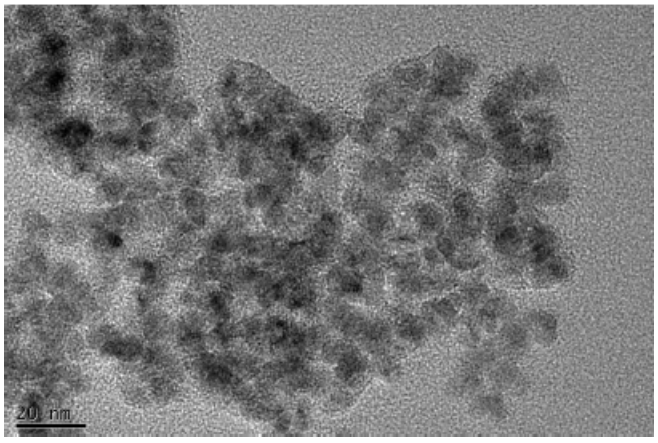

Figure SI 13: TEM image of CdSe@ZnS-IG@ $Si0_2$-T-1yl.

Also, UV-vis and PL analysis for CdSe@ZnS-IG@ $Si0_2$-T-1yl was carried out as shown in Figure SI 14.

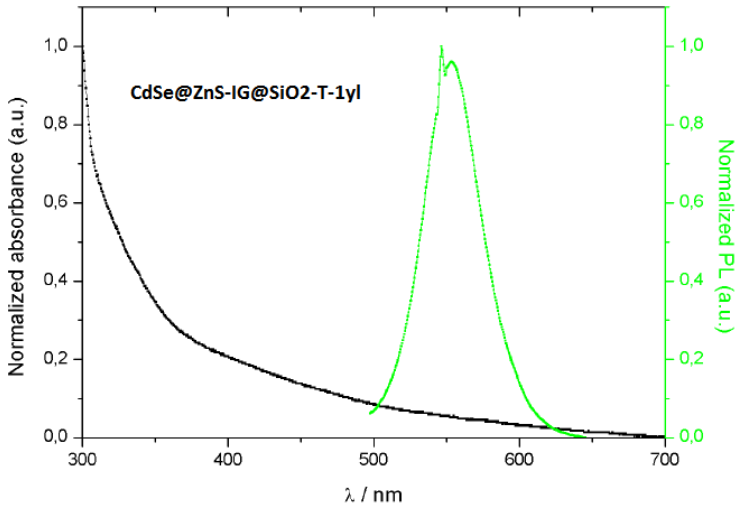

Figure SI 14: UV-vis and PL of CdSe@ZnS-IG@ SiO_2-T-1yl.

<u>Analysis data for CdSe@ZnS-IG@SiO_2-FG:</u>

The PL maximum for each compound (with different functional groups (FG)) were plotted together and it was found that the red shift, which occurs after the silica encapsulating, is stronger for longer and less polar silica sources relative to the used starting material CdSe@ZnS-OA.

Table SI 1: PL and red shift of CdSe@ZnS-IG@ SiO_2-FG.

Compound	$\boldsymbol{\lambda_{em}^{max}}$ **/ nm**	**PL FWHM/nm**	**Red shift/ nm**
CdSe@ZnS-OA	550.8	50	0
CdSe@ZnS-IG@SiO_2-TEOS	553.5	49	2.7
CdSe@ZnS-IG@SiO_2-T-MMA	554.1	48	3.2

CdSe@ZnS-IG@SiO_2-T-1yl	555.2	51	4.4

Polymerization of functionalized QDs with photosensitive methylmethacrylate groups:

With the photosensitive end groups, it is possible to let the nanoparticles undergo a polymerization between each other initiated by a radical initiator like azoisobutyronitrile (AIBN). So, it was investigated the effects coming up when one polymerizes the carbon double bond resulting due to the introduction of the silica source T–MMA. A scheme of the polymerization reaction is given in Figure SI 15 (upper row). The methylmethacrylate layer showed a slight red shift in the PL and a polymerized structure in the TEM images (Figure SI 15 lower row). In the TEM images, it can be seen that after the polymerization there is a densely packed structure as the nanoparticles are building a strong network between each other. In the case before the polymerization, the nanoparticles are randomly distributed and no clear order was found.

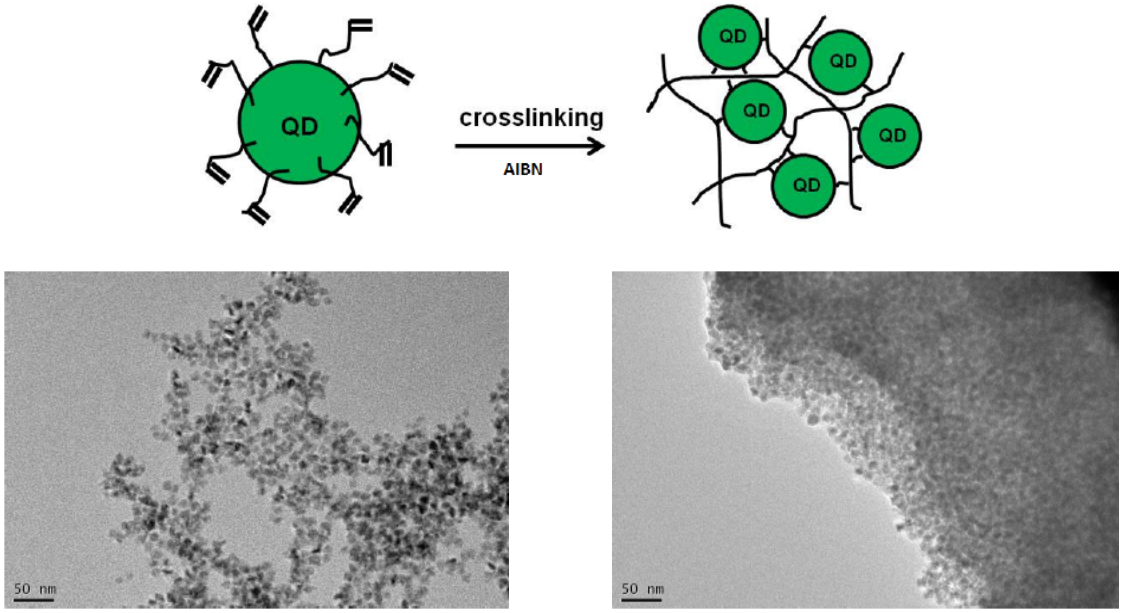

(a) **(b)**

SI Figure 15: Polymerization reaction scheme (upper part) and TEM images of (a) CdSe@ZnS-MUD@SiO2-T-MMA before polymerization and (b) CdSe@ZnS-MUD@SiO2-T-MMA-PM after polymerization.

Also, the diameter of the spherical shaped nanoparticles did not change as the reaction is only happening between the carbon double bonds and between the nanoparticles to each other. There is a slight red shift occurring in the PL due to the polymerization. Also the PL studies showed that there is a slight red shift occurring after each successfully grown shell relative to the CdSe@ZnS-OA nanoparticles, and it is possible to find a linear dependency of the emission maxima to the number of shells (see Figure SI 16 and Table SI 2). The first shell is based on silica and was introduced through a silica source. The second shell is the methylmethacrylate layer, which was built up through the polymerization of the functional groups.

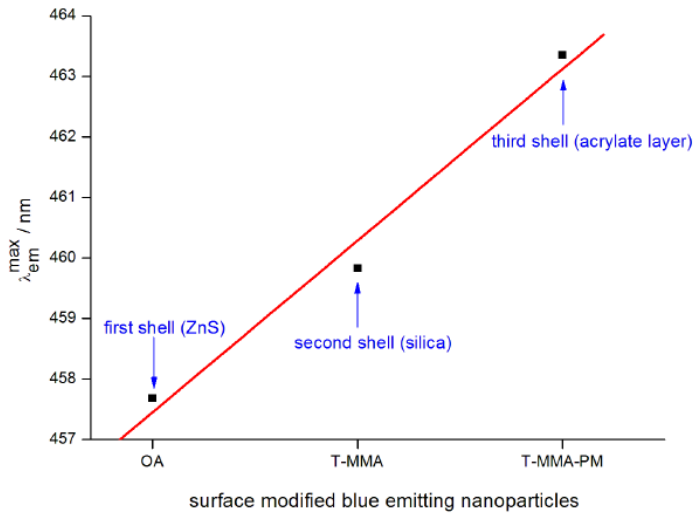

Figure SI 16: Behavior between PL maxima and shell modification.

Table SI 2: PL data maxima before and after polymerization.

Compound	$\boldsymbol{\lambda_{em}^{max}}$ **/ nm**
CdZnS@ZnS-OA	457.7
CdZnS@ZnS-MUD@ $Si0_2$-T-MMA	459.8
CdZnS@ZnS-MUD@ $Si0_2$-T-MMA-PM	463.4

Patterning via two-photon-initiated polymerizations:

To obtain 2D or 3D structures with incorporated QDs there has to be requirements to achieve. On the one hand, the QDs should have photopatternable groups, which can react with the resin that also have polymerizable groups. On the other hand, the resin and QD mixture has to be compatible. With the use of a two-photon absorption dye, it is then possible to create the desired polymeric structures via TPIP. The introduction of the green-emitting surface modified QD with IG as the spacer and a photosensitive group, CdSe@ZnS-IG@ $Si0_2$-T-1yl, was able to create a five-letter word "KAIST" (Figure SI 17). Due to the functionalization strategy, the QDs have greater compatibility to the photoresist. Here it was used as the resin ORMOCER® at a laser working condition of 200 mW.

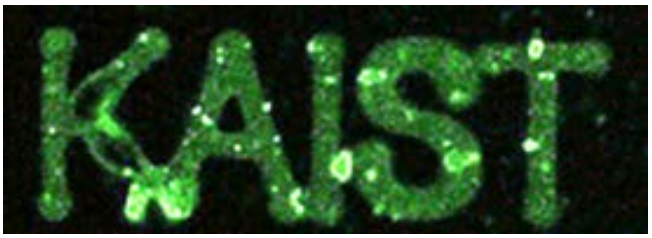

Figure SI 17: "KAIST" pattern with green-emitting CdSe@ZnS-IG@ $Si0_2$-T-1yl and ormocer.

<u>Incorporation of QDs with and without functional groups in the shell into a crosslinked polymer film</u>

<u>General process for incorporating nanoparticles into a polymer matrix</u>

For polymerization of either methylmethacrylate functionalized orange emitting quantum dots (QDs) or unmodified ones into a polymer matrix, they were mixed with butyl-methacrylate, 1% hexanedioldiacrylate and a photoinitiator (Diphenyl(2,4,6-trimethylbenzoyl)phosphine oxide). Then the mixture was exposed to an UV lamp (LOT LSE340 / 850.27B / 25 kV) to initiate the polymerization for 1 hour. For the imaging a fluorescence microscope (Olympus TH4-200) with an

excitation wavelength of 550 nm and a selective filter in the wavelength ranges of 560-620 nm was used.

CdSe@ZnS-IG@SiO_2-TEOS (unfunctionalized QDs)

In the case of quantum dots, which posses a silica shell, but are not equipped with photopolymerizable end groups (like methacrylate groups) aggregates are formed due to segregation from the polymer gel.

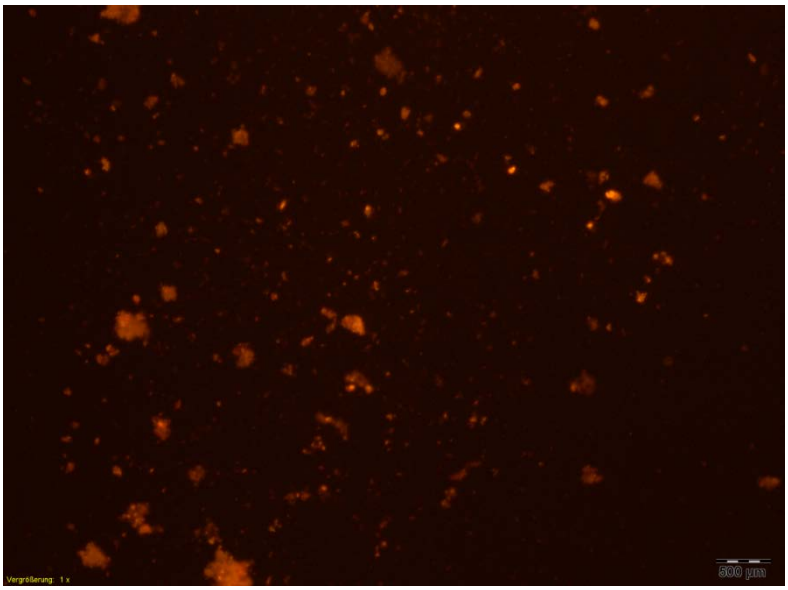

Figure SI 18: CdSe@ZnS-IG@SiO_2-TEOS into a polymer matrix.

CdSe@ZnS-IG@SiO_2-T-MMA (functionalized nanoparticles derived from the miniemulsion process)

But when there are polymerizable groups on the quantum dots it is possible to obtain a homogenous fluorescent film as the modified quantum dots get covalently linked to the polymer matrix.

Figure SI 19: CdSe@ZnS-IG@SiO_2-T-MMA into a polymer matrix.

Dynamic light scattering measurements (DLS):

Dynamic light scattering (DLS) was performed at 293.15 K in n-dodecane and 298.15 K in DMSO utilizing a He-Ne laser (Uniphase, 22 mW, λ = 632.8 nm), an ALV-SP86 goniometer equipped with an ALV High QE APD Avalanche photodiode fiber optical detection system an ALV3000 correlator. All measurements of the intensity correlation functions were recorded in linear tau-mode with tau=13 µs and 100 µs per channel for n-dodecane and DMSO respectively using 320 decay channels, a delay time of 1 ms and additional 280 baseline channels for experimental normalization. Temperature was controlled by a Lauda RKS6C Ultrathermostat within 0.1°C. All solutions were filtered by passing through Acrodisc GHP syringe Filters 200 nm. (PALL) and 2 mL of solution directly transferred into cylindrical suprasil light scattering cells of 2 cm diameter (Hellma Mülheim, Germany). All measurements were performed at 30° scattering angle (low angle limit), correction of sizes larger than 20 nm by angular dependent measurement and extrapolation to zero angle was omitted due to low concentration and weak signals at larger angles respectively. Diffusion coefficients were determined from intensity autocorrelation functions after Siegert transformation ($g_1(t)$=sqrt(abs(($g_2(t)$-A)/A))*sign($g_2(t)$)) with A the experimentally measured baseline) by a non-linear fitting (Simplex algorithm) of the

field autocorrelation function by applying a biexponential fit function $g_1(t)=A_1 \cdot \exp(-t/\tau_1)+A_2 \cdot \exp(-t/\tau_2)$ and average values were calculated following $g_{av}=(A_1/\tau_1+A_2/\tau_2)/(A_1+A_2))$ and $1/\tau = D \cdot q^2$ with A_i amplitude, t time, τ correlation decay time, D diffusion coefficient and q experimental scattering vector. The fit quality was evaluated by analyzing the residuum and only accepted in case of^statistically distributed deviations. Hydrodynamic radii were calculated from average diffusion coefficients by applying the Stokes-Einstein equation. Dynamic light scattering is carried out for the orange emitting Quantum Dots capped with oleic acid. Here it is shown that it was found a monodispersity with a hydrodynamic radius of 5.9 nm.

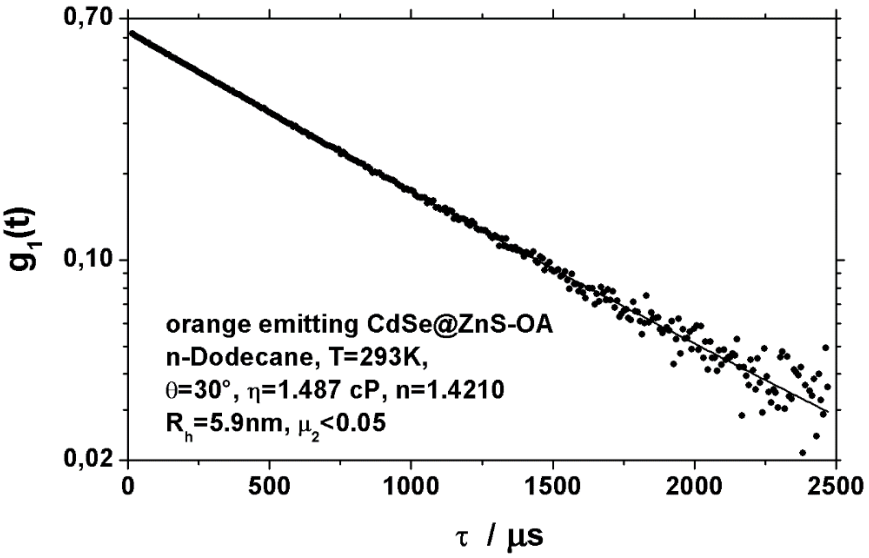

Figure SI 20: Orange emitting CdSe@ZnS capped with oleic acid.

In the case of the modified nanoparticles with a silica shell equipped with photosensitive groups the dynamic light scattering showed a bimodal distribution in which the smaller nanoparticles have a hydrodynamic radius of 19 nm and the bigger particles (aggregates) have a hydrodynamic radius of 100 nm. There is a percentage given of 30 % and 70 % for smaller and bigger one.

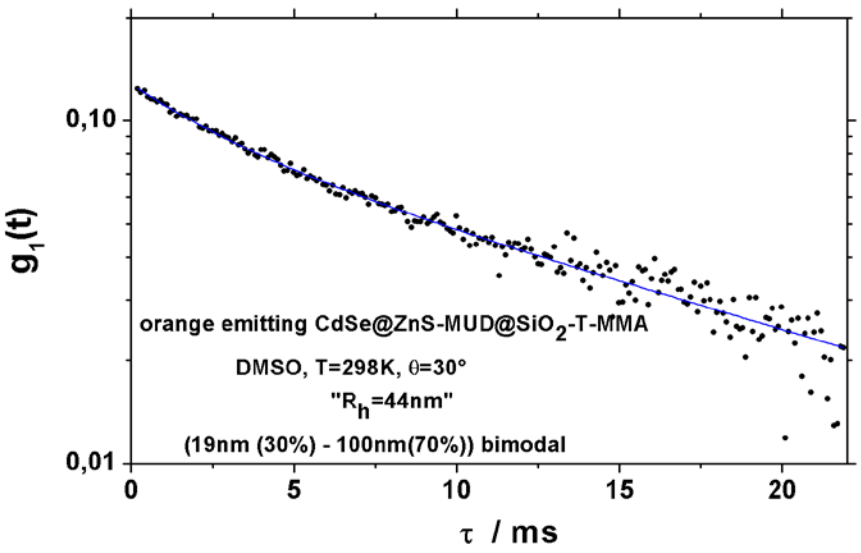

Figure SI 21: Orange emitting CdSe@ZnS-MUD@SiO_2-T-MMA.

Fluorescence correlation spectroscopy (FCS):

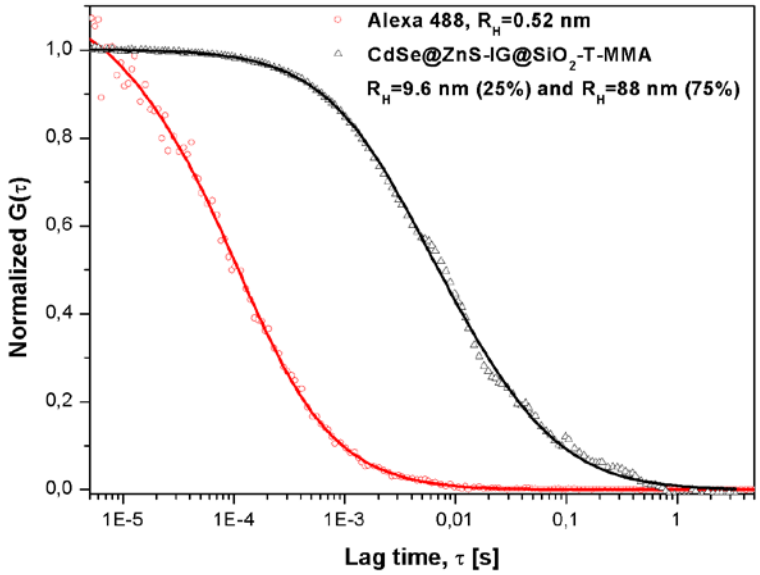

Figure SI 22: Normalized FCS autocorrelation curve (black triangles) measured in DMSO dispersion of the modified QDs obtained from the miniemulsion procedure. The autocorrelation curve measured in DMSO solution of Alexa 488 (red circles) is also shown for comparison. The solid lines represent the corresponding fits.

As the surface modified QDs show strong fluorescence, their size and aggregation behavior in DMSO dispersions were characterized by fluorescence correlation spectroscopy.[1] The experiments were performed on a commercial setup (Zeiss,

Germany) consisting of the module ConfoCor 2 and an inverted microscope model Axiovert 200 with a Zeiss Plan-Neofluar 40×/0.9 multi immersion objective using glycerol as immersion liquid. The excitation was done by the 488 nm line of an argon laser and the collected fluorescence was filtered through a LP505 long pass emission filter before reaching the detector, an avalanche photodiode that enables single-photon counting. Eight-well polystyrene-chambered coverglass (Laboratory-Tek, Nalge Nunc International) was used as a sample cell. For each solution, a series of 10 measurements with a total duration of 5 min were performed. The confocal observation volume was calibrated using a reference dye with a known diffusion coefficient i.e. Alexa Fluor 488. [2] The measured autocorrelation curve was fitted with two component model function [1] (Figure SI 22) in order to account for the large fraction of aggregates presented in the dispersion. From the fit, average hydrodynamic radii of 9.6 nm for the quantum dots and 88 nm for the aggregates were estimated. The corresponding fractions were 25% and 75% respectively. The later values, however, should be considered with care, because FCS strongly overestimates the fraction of the larger and brighter aggregates. [SI1, SI2]

[SI1] K. Koynov, H.J. Butt, *Current Opinion in Colloid & Interface Science*, **2012**, *17*, 377-387.

[SI2] Zdenek P, Schwille P, *Biophysical Journal,* **2008**, *94*, 1437–1448.

Chapter 2: Investigation of energy transfer phenomena between surface modified QDs and Au NW

This part of the work was carried out in cooperation with Hannam University in Daejeon, South Korea, in the framework of the International Research Training Group (IRTG 1404). Quantum dots were surface functionalized with different silica sources and attached to a gold nanowire. Thereby energy transfer phenomena were observed with an interesting reverse correlation between the chain length and the polarity of the resulting nanoparticles.

Semiconductor nanoaprticles are of an increasing importance in the fundamental studies [Q1] and in a wide range of technological applications such as light emitting devices [Q2], lasers [Q3] or fluorescent labels [Q4]. Due to their small sizes and the resulting quantum confined nature of their energy levels they possess very unusual and extraordinary optical and electronic properties [Q5]. The smaller the nanoparticles gets the higher its surface to volume ratio. This means concrete that the smaller the particle the higher the percentage of atoms on the surface which can be modified through a surface modification step with various organic capping agents. Such capping agents like oleic acid increase the colloidal stability of the particles and they introduce the possibility for chemical reactions on the surface. [Q6] Nevertheless, the capping agents do not completely cover the surface of the nanoparticles, many dangling bonds remain on the surface. [Q7] One of the most efficient solutions to this problem was to grow an inorganic shell consisting of ZnS to shield the surface and to obtain completely passivated nanoparticles. [Q8] For the different second shell it was used a layer based on silica. As a result of this choice, it gets possible to introduce different molecules with defined end groups on the surface of the resulting quantum dots which can be modified further in other reactions. The silica coated quantum dots have a big interest in optoelectronics[Q9], making them through passiviation of its shell, less toxic and more resistant against undesired oxidation, furthermore, it is optically inert and in a relative way chemically inert. [Q1] Metal nanostructures with high positive redox potential like gold exhibit local surface plasmon resonance

(LSPR) phenomena which are intensively studied in the fields of plasmonics, photonics and biosensing. [Q11] This happens due to the collective oscillation of electrons on the surface of a metal stimulated by incident light. [Q12] The physical properties are determined by the shape and dimension which can be modified throughout the synthetic procedure. [Q13] One can obtain a PL enhancement due to energy and or charge transfer effect which is appendant to LSPR when hybridizing e.g. luminescent QDs with metal nanostructures. [Q14] Surface modification of QDs govern the charge and chemical tendencies of their surface and act as a handle to obtain a rich variety of QD based hybrid nanostructures. Coupling QDs with organic or inorganic nanomaterials can give rise to various energy and charge transfer effects which are widely relevant in optoelectronics, plasmonics and biosensor research. [Q15] Previous investigation on Au and QD nanocomposites have found potential application in detection of small molecule analytes like Pb^{2+} or Trinitrotoluene (TNT), and also biomacromolecular analytes like preoteases, human immunoglobulin (IgG) as well as DNA. [Q16]

Here, there are presented new surface modification strategies for QDs to investigate their interaction with a gold nanowire (GNW) under photoexcitation. Therefore materials based on a core/shell/shell sytem were used. Starting from synthezised oleic acid stabilized core/shell systems (CdSe@ZnS-OA) the new materials were build up – step by step – by attachment of a relatively short spacer, 11-mercapto-1-undecanol (MUD), onto the surface of the CdSe@ZnS nanoparticles. This enables the nanoparticles to undergo a reaction with silica sources which are different in their chain length (CL) and have different fuctional groups (FG). Thus it is possible to grow a spherical silica shell around their surfaces. Depending on the used silica sources the resulting silica shell modified nanoparticles are functionalized with certain end groups that enables their use in various processes, like the lithography process or in the field of bioimaging. Furthermore, these surface modified nanoparticles were attached to a GNW in order to investigate some energy transfer phenomena and to correlate the achieved data to the chain length and polarity of these surface modified nanoparticles.

As mentioned before, to introduce a silica shell, certain end groups which can couple with the silica source is needed first. With the introduction of MUD through a ligand exchange procedure by replacing the capping agent oleic acid there are now alcohol groups which can undergo a further reaction. The free OH groups on the surface of CdSe@ZnS-MUD can react with the silica source to form a silica shell. The silica shell is formed by the build up of a network of Si-O bonds. The following figure 2.1 shows the general reaction procedure in which **R** stands for the modified chain lengths of the used silica sources.

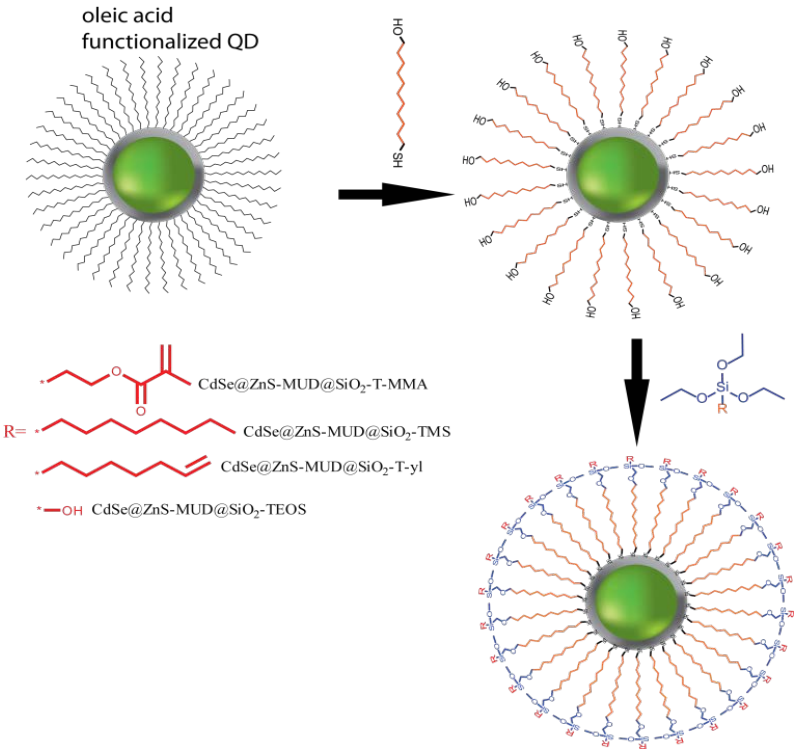

Figure 2.1: Reaction pathway for the surface modified nanoparticles through different silica sources.

The first shell around CdSe is consisting of the semiconductor material ZnS which stabilizes the surface and gives a shielding against photooxidation, the progressive destruction on the surface of the nanoparticles as well as an enhanced stability against chemical and physical stress. The ZnS shell can be surface coated with a tight shell of MUD, which offer hydroxyl groups for the build-up of a further silica shell (Figure 2.1). So MUD is acting like a spacer between the first shell (ZnS) and the second shell (SiO_2). So it is possible to substitute and modify the chain length and polarity of the silica sources e.g. R=OH (high polar) to a silica source which has a

longer alkyl chain R=C_9H_{19} (less polar) or functional groups, or both, and to investigate the influences of those surface modifications, respectively. To accomplish that, 4 different silica sources were used. The first one is Trimethylorthosililane (TEOS) which has as its functional group an OH group but no carbon chain. The second one is Trimethoxy(octyl)silane (TMS) and has a long alkyl chain with nine carbon atom and its silica group but no functional group at the other end, the third one is Trimethoxy(7-octen-1-yl)silane (T-1yl) and has a long alkyl chain with eight carbon atoms, including a polymerizable double bond as its end group. For the fourth and last one, 3-(trimethoxysilyl)propylmethacrylate (T-MMA) with a short chain length and a polymerizable methylmethacrylate end group was used. So as the resulting chain length on the surface of the nanoparticles increases as bigger the particles becomes, respectively. So the size should be increasing in the following order from smaller to bigger: CdSe@ZnS-MUD@SiO_2-TEOS < CdSe@ZnS-MUD@SiO_2-T-MMA < CdSe@ZnS-MUD@SiO_2-T-1yl < CdSe@ZnS-MUD@SiO_2-TMS. Depending on the used silica source it is possible to introduce certain functional groups and chain lengths. The TEM images of the surface modified nanoparticles attached to gold nanowire can be seen in the following figure 2.2. It shows the quantum dots are attached in high densities to the GNW surface. There is also evidence for aggregation of QDs near the GNW surface.

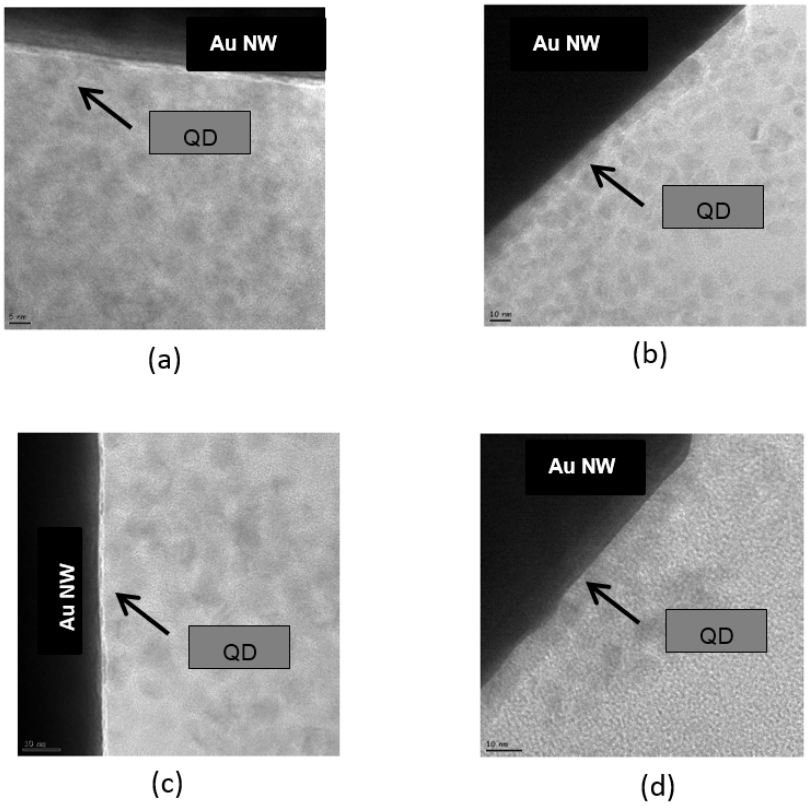

Figure 2.2: TEM images of functionalized QDs attached to the surface of a GNW.

The attachment in (b) also exhibit similar environment to the previous case. They are present in large quantities near the surface of GNW. For the surface modified nanoparticles obtained from the synthesis with the longest alkyl chain – accomplished by introduction of the silica source TMS, CdSe@ZnS-MUD@SiO_2-TMS the TEM image shows in (c) a film in the periphery of the GNW accompanied by aggregated QDs. The PL of the GNW-QDs nanocomposites were investigated with laser confocal microscope photoluminescence (LCM PL) measurements. Measurements were made on both – the surface modified QDs themselves and their corresponding nanocomposites with GNW. The details of LCM PL setup are discussed elsewhere. [Q17]

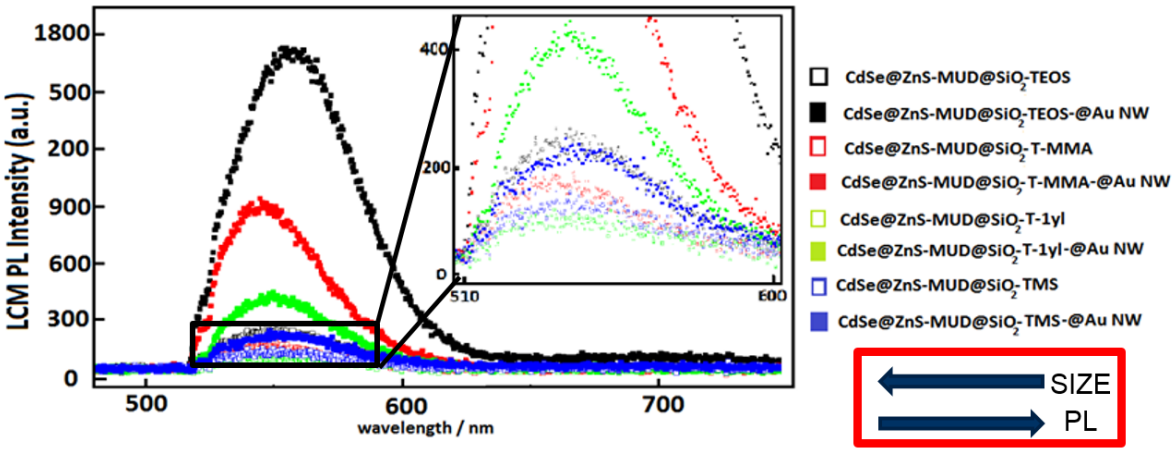

Figure 2.3: LCM PL of surface modified QDs themselves and corresponding nanocomposites.

From the LCM-PL measurements it was obvious that the spacer length on the QD surface had a strong influence on the observed PL enhancement. The black curve corresponding to CdSe@ZnS-MUD@SiO_2-TEOS@Au-NW, the silica source with the shortest spacer, gives the biggest enhancement. On the contrary the blue curve corresponding to CdSe@ZnS-MUD@SiO_2-TMS@Au-NW, the silica source with the longest spacer, gives the lowest enhancement. Between these two extremes there are the green (CdSe@ZnS-MUD@SiO_2-T-1yl@Au-NW) and the red curves (CdSe@ZnS-MUD@SiO_2-T-MMA@Au-NW). For the green curve the nanoparticles do have the second longest chain length and so the resulting enhancement due to the attachment to the Au NW is the second smallest. The red curve does have a mediate chain length on the surface which lies between the longest chain length (TMA) and the smalles one (TEOS). So the resulting enhancement is also between these extremes but still bigger than in the case of the second longest chain length (T-1yl).

Conclusion

It was possible to show a clear trend between the PL enhancement and the spacer chain length on the QDs, with shorter chains leading to higher enhancement due to the surface plasmon resonance (SPR) of the GNW in which the resulting PL intensity is sensitive to the distance between the GNW and QDs. The field enhancement of

GNW influences the photon flux of the QDs when they are at an adequate distance to each other leading to an enhanced PL. Besides that, the radiative recombination rates are increased by a high electromagnetic field induced by the SPR. [Q18] Apart from chain length there may be other factors influencing the interaction between the GNW surface and QDs like polarity. As the surface of the GNW is hydrophilic it can be suggest that for more hydrophilic nanoparticles the attachment should be more favourable. The trends observed in these experiments would also favour a polarity based discussion. As the TEOS modified QDs are the most polar of the systems investigated they can be expected to interact to a greater extent with the GNWs. The biggest observed in CdSe@ZnS-MUD@SiO_2-TEOS@Au-NW does point towards higher energy transfer phenomena which could be correlated to improved attachment and stronger interaction. In comparison, the nanoparticles surface modified with TMS have the lowest polarity, it was found to show the smallest PL enhancement. However the true confirmation of a polarity based explanation would only be conclusive with an investigation involving polar groups with different spacer lengths. At this stage the PL enhancement does suggest that the energetic interactions between the GNWs and the QDs change with the spacer length.

Synthesis

All chemicals were purchased from Sigma Aldrich, Acros Organics, Alfa Aesa or Fluka and used without further purification if not noted otherwise. Cadmium(II)oxide (0.4 mmol), zinc acetate (0.5 mmol), 5,5 mL oleic acid and 20 mL 1-octadecene were given together in a 250 mL reaction vessel and the mixture was heated up to 150 °C with a controlled temperature program. At this temperature it was degased for 30 min with nitrogen. Then it was further heated to a temperature of 310 °C. the reaction mixture turned colorless due to solved cadmium(II)oleate and zinc(II)oleate. To this mixture it was added a prepared solution of Se (0.4 mmol) and S (2.3 mmol) in 1 mL of 1-octadecene. It was given for the growth of the nanoparticles

a timeframe of 6 min at 310 °C and then it was cooled up to room temperature. The obtained nanoparticles were centrifugated at 4300 rpm for 20 min and solved and stored in hexane until further processing. Then 50 mg of the pre synthesized CdSe@ZnS-OA were given together with 500 mg MUD in a 250 mL reaction vessel and diluted with 60 mL of an equal volume mixture between ethanol and chloroform. The mixture was then given in a sonication bath for 3 h to process the reaction. Then 40 mL chloroform was added and the precipitated functionalised nanoparticles were purified by centrifugation (4300 rpm, 20 min). The obtained nanoparticles were solved in DMSO and stored until further processing. To make silica shell containing nanoparticles 20 mg of MUD capped CdSe@ZnS were put in four different vials and each one was diluted with 5 mL of dry DMSO as wel as 100 µL of one silica source (in total 4). The mixture was stirred for 6 h at 50 °C under continuous nitrogen flow. Core shell QDs with functionalized silica shells were precipitated by adding 40 mL of chloroform followed by centrifugation (3500 rpm / 20 min). The precipitates were washed with ethanol and choloroform to remoce excess ligands. The gold nanowire were synthesized galvanostically based on Al_2O_3 nanoporous template which has a diameter of 200 nm and a thickness of 60 µm (Whatman International, Ltd)[Q11]. Then for the growth of the Au NWs, a current density of 2.0 mA/cm^2 and a voltage of -1.20 (±0.05) V was applied to the electrode for 2 h using the Orotemp gold plating solution. Sequentially, after dissolving the Al_2O_3 template using the HF solution vertically arranged Au NWs were obtained. Finally, both, Au NWs and QDs, were homogeneously dispersed in the toluene solution and stirred for 24 h at 40 °C to attach the silica modified QDs to the surface of Au NWs.

Bibliography

[Q1] Brus, L. E., *J. Chem. Phys.*, **1986**, *90*, 2555-2560.

[Q2] Colvin, V. L.; Schlamp, M. C.; Alivisatos, A, P., *Nature*, **1994**, *370*, 354-357

[Q3] Klimov, V. I.; Mikhailovsky, A. A.; Xu, S.; Malko, A.; Hollingsworth, J. A.; Leatherdale, C. A.; Bawendi, M. G., *Science*, **2000**, *290*, 314-317.

[Q4] Bruchez, M.; Moronne, M.; Gin, P.; Weiss, S.; Alivasatos, A. P., *Science*, **1998**, *281*, 2013-2016.

[Q5] Murray, C. B.; Norris, D. J.; Bawendi, M. G., *J. Am. Chem. Soc.*, **1993**, *115*, 8706-8715.

[Q6] Wang, Y. A.; Li, J. J.; chen, H.; Peng, X., *J. Am. Chem. Soc.*, **2002**, *124*, 2293-2298.

[Q7] Katari, J. E. B.; Colvin, V. L.; Alivasatos, A. P., *J. Phys. Chem.*, **1994**, *98*, 4109-4117.

[Q8] Mews, A.; Eyschmüller, A.; Giersig, M.; Schooss, D.; Weller, H., *J. Phys. Chem.*, **1994**, *98*, 934-941.

[Q9] Nann, T.; Mulvaney P., *Angew. Chem. Int. Ed.*, **2004**, *43*, 5393-5396.

[Q10] Darbandi, M.; Thomann, R.; Nann, T., *Chem. Mater.*, **2005**, *17*, 5720-5725.

[Q11] Park, S. H.; Park, D. H.; Hong, Y. K.; Lee, S. H., Kim, D.-C.; Dhakal, K. P.; Joo, J.; Kim, J., *J. of Raman Spectrosc.*, **2012**, *43*, 965-970.

[Q12] Langhammer, C.; Yuan, Z.; Zoric, I.; Kasemo, B.; *Nano Lett.*, **2006**, *6*, 833.

[Q13] Mock, J. J.; Barbic, M.; Smith, D. R.; Schultz, D. A.; Schultz, S.; *J. Phys. Chem.*, **2002**, *116*, 6755.

[Q14] Stefani, F. D.; Vasilev, K.; Bocchio, N.; Stoyanova N.; Kreiter, M.; *Phys. Rev. Lett.*, **2005**, *94*, 023005.

[Q15] Anikeeva, P. O.; Madigan, C. F.; Halpert, J. E.; Bawendi, M. G.; Bulovic, V., *Phys. Rev. B*, **2008**, *78*, 085434.

[Q16] Choi, Y.; Cho, Y.; Kim, M.; Grailhe, R.; Song, R., *Anal. Chem.*, **2012**, *84*, 8595.

[Q17] Fournier, J.; Neauport, J.; Grua, P.; Fargin, E.; Jubera, V.; Talaga, D.; Jouannigot, S., *Optics Express.*, **2010**, *18*, 21559.

[Q18] Jung, D.-R.; Nahm, C.; Nam, S.; Kim, J. I.; Park, B., *Mater. Research Bulletin*, **2012**, *47*, 453-457.

Chapter 3: Incorporation of QDs into polymeric vesicles (hybrid systems)

Oligonucleotides like short, double stranded RNA (siRNA) or plasmid DNA (pDNA) promise high potential in gene therapy – for pharmaceutical application, however, adequate drug carriers are required. Among various concepts nanosized hydrogel particles may serve as novel transport media drugs like siRNA.[L1] In this context fluorophores with QDs as electron dense materials get very attractive. In

combination of confocal laser microscope and cryoTEM it gets possible to freeze the cell activity which makes it possible to track the nanoparticles with the QDs inside of the carrier systems to make them visible on nanoscale. With labeled siRNA colocalisation of the vesicles and the drug could be obtained.

In this chapter, a concept of synthesizing polymeric cationic nanohydrogels incorporated with orange emitting QDs (CdSe@ZnS-OA) was developed, which offers a promising strategy to complex and transport drugs like siRNA into cells and to track the particles via CryoTEM to image the time depending interaction . For this purpose, amphiphilic reactive ester blockcopolymers were synthesized by Dr. Lutz Nuhn[L1] via RAFT polymerization of pentafluorophenylmethacrylate (PFPMA) as reactive ester monomer together with tri(ethyleneglycol)methylethermethacrylate (MEO_3MA). Furthermore lipoic acid was converted to reactive ester– pentafluorophenyl lipoic acid – and the QDs stabilized with OA were given in a ligand exchange reaction in a sonication bath to obtain QDs functionalized with pentafluorophenyl lipoic acid in which the sulfur bond is attached to the ZnS shell of CdSe@ZnS. In polar aprotic solvents a self assembly of the blockcopolymer (PFPMA)-*b*-(MEO_3MA) could be observed leading to the formation of nm sized polymer aggregates and with the functionalized QDs with their fluorophob ligands they migrate into the inner of the aggregates using the fluorophobic effect. The resulting superstructures were used to convert the reactive precursor block copolymers with amine containing crosslinker molecules into covalently stabilized hydrogelparticles with covalently bounded and incorporated QDs.

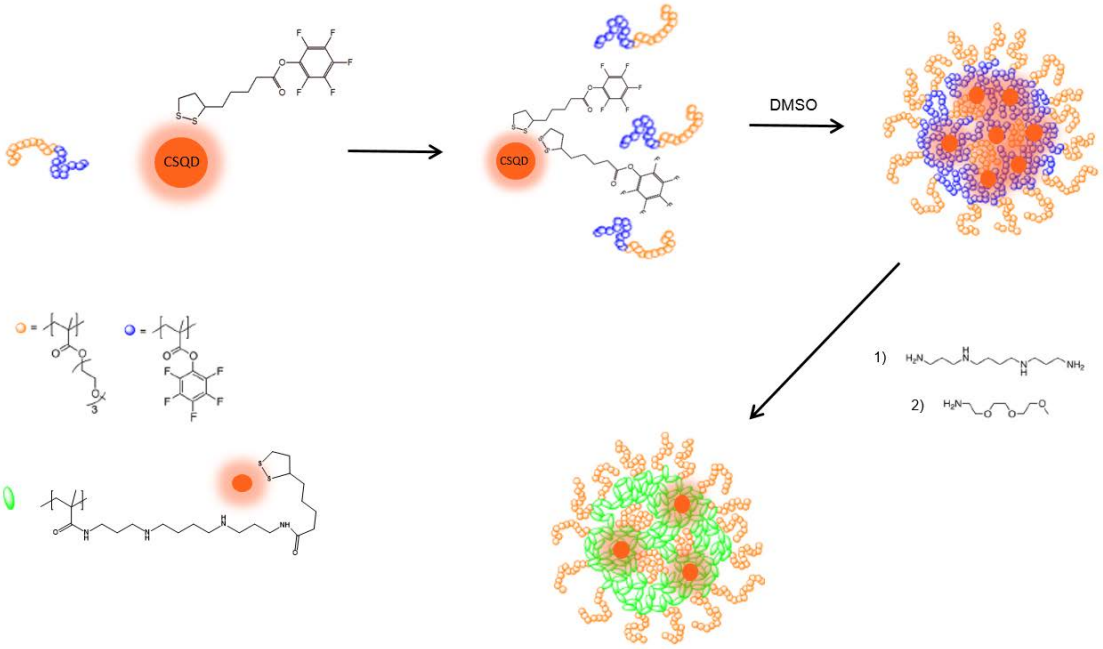

Figure 3.1: Reaction procedure for incorporation of QDs into nanohydrogels (QD-NH) adopted and modified from Ref[L1].

This method offers a new possibility to synthesize precise nanohydrogels of different size starting from various block copolymers with simultaneous incorporation of hydrophobic compounds. Moreover, *via* reactive ester approach further functionalities could be attached to the nanoparticle, *e.g.* fluorescent dyes, which allowed distinct tracking of the hydrogels during complexation with siRNA or cell uptake experiments. Looking ahead, these novel cationic nanohydrogel particles incorporated with hydrophobic or hydrophilic compounds may serve as a new platform for proper drug delivery systems and deeper understanding of interactions between cells and polymeric structures.

Proof of concept

Before conducting the synthesis for the polymeric nanogels incorporated with the covalently bonded functionalized QDs it was conducted preexperiments to prove the successfull functionalization of QDs.

Lipoic acid reacted with pentafluorophenylactetate to obtain pentafluorophenyl lipoic acid (PFP-LA) which has an intact sulfur-sulfur bond. This has a higher affinity to the ZnS shell of CdSe@ZnS-OA and can be attached to the surface and displace the weaker attached oleic acid. As the QDs are good fluorophores they can be tracked through the whole synthesis under UV light where they emit orange light. After sonication the QDs functionalized with pentafluorophenyl lipoic acid are soluble in chloroform but not in water, as the whole compound has a hydrophobic nature.

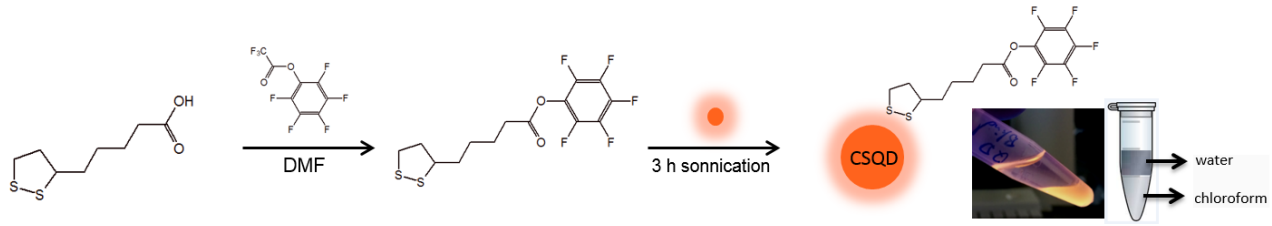

Figure 3.2: Synthetic route for funtionalizing of QDs with lipoic acid (PFP-LA).

After aminolysis with a PEG amine (1 kDa / 5 kDa) the resulting product can be dispersed in water and not in chloroform anymore, as now the QDs are of hydrophilic nature. Alternatively the aminolysis with a long alkyl chain amine result in solubility in hexane. These preexperiments with low molecular weight polymers and small molecules demonstrate a successfull functionalization of QDs and the ability to tune the polarity and the solubility in certain solvents.

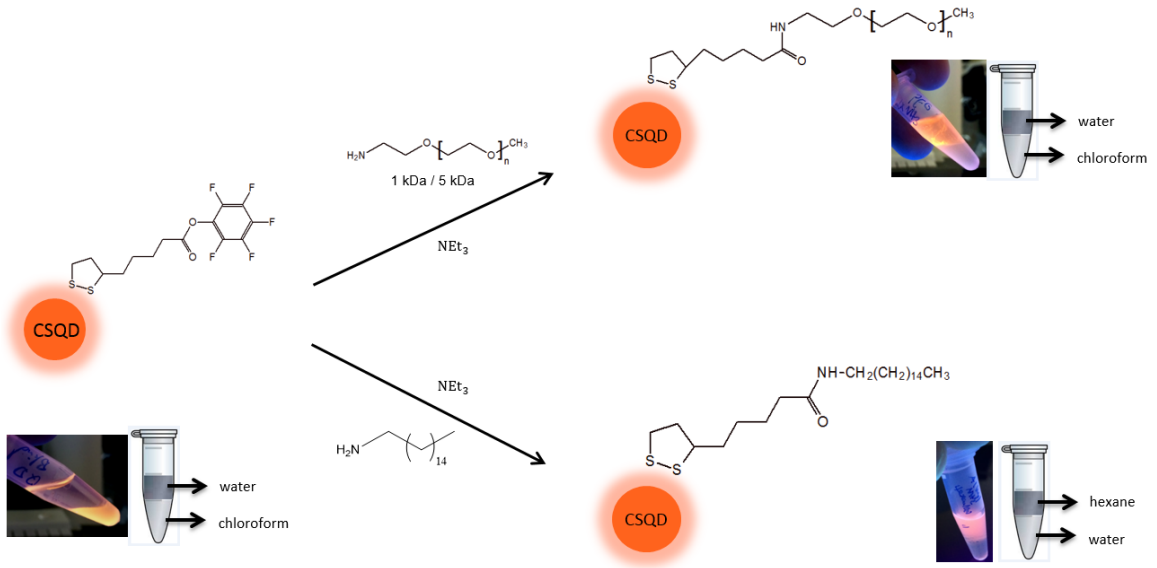

Figure 3.3: Aminolysis of lipoic acid - PFP QDs with different amines and obtained solubility in different solvents.

Furthermore it was possible to functionalize QDs with polymers with high molecular weights. For this purpose I used a polymer synthesized by [redacted] poly(hydroxypropylamin) (pHPMA) with a molecular weight of 7,5 kDa in which the chain amine is protected by BOC protection group (Fig. 3.4). After deprotection the resulting free accessable amine group can be used to undergo a reaction with the pentafluorophenyl lipoic acid under aminolysis to decorate the surface of QDs with the hydrophilic polymer pHPMA.

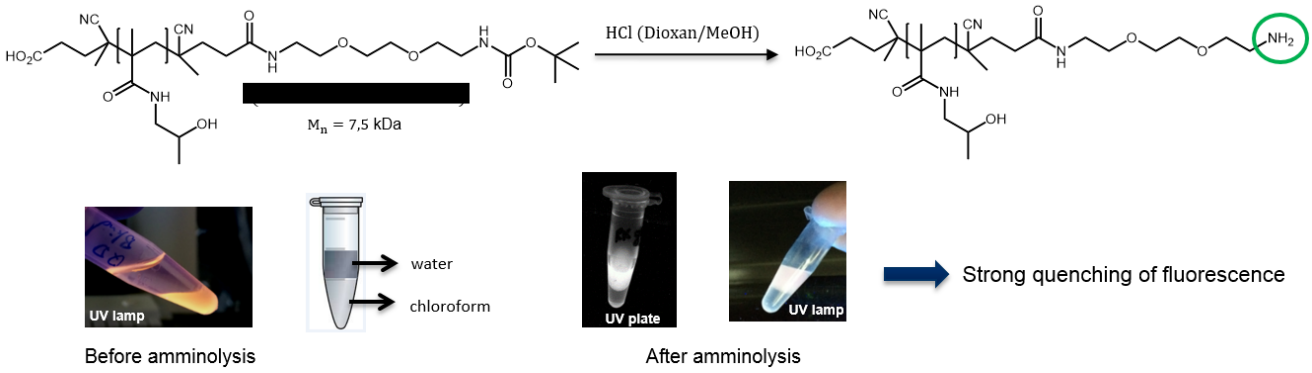

Figure 3.4: Aminolysis of PFP-LA with deprotected pHPMA polymer and obtained fluorescence intensity and solubility.

Before aminolysis the QDs functionalized with pentafluorophenyl lipoic acid are soluble in chloroform but not in water due to their hydrophobic nature. After deprotection and accessable of free amine group and after aminolysis the resulting particles can be found in the water phase as the QDs now are of hydrophilic nature due to the pHPMA shell. Nevertheless, the fluorescence is quenched very strongly but under UV plate (high UV intensity) it can be seen that only the water phase shows the characteristic emission. The loss of the strong fluorescence might have various reasons which can include progressive destruction of the surface of the QDs and a low conversion of the ligands. However, it could be shown that CdSe@ZnS-PFP-LA-pHPMA can be obtained and the intension for modification can be successfully be demonstrated within this framework of experiment. Also a conversion via aminolysis could be confirmed with polymers with relatively high molecular weight of 32 kDa, namely polysarcosine p(Sar-NH_2). The amine functionalized polysarcosine was synthesized from [redacted] and was provided for this experiment. It can be seen before the aminolysis there is a very

strong emission under UV light (PFP-LA in chloroform). Then triethylamine and p(Sar-NH_2) was given to the mixture and it was stirred at 60°C for 3 days under reaction control in ^{19}F-NMR (release of pentafluorophenol).

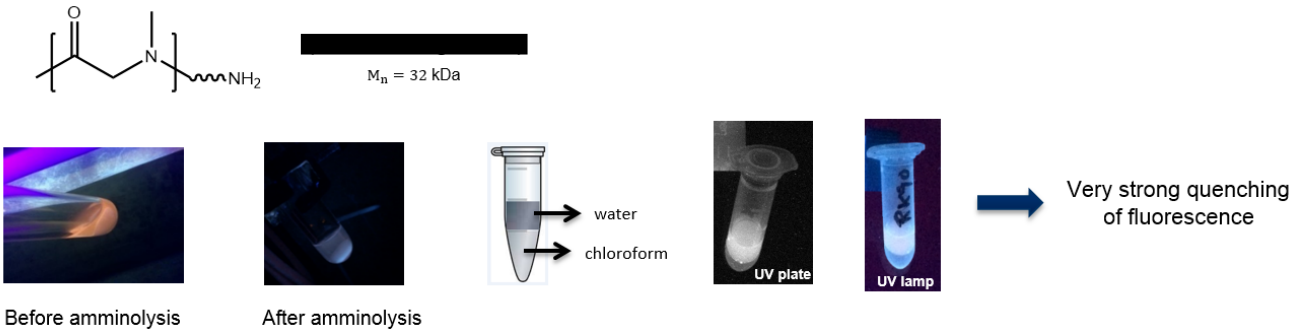

Figure 3.5: Aminolysis of lipoic acid – PFP with amine terminated p(Sar-NH_2) and obtained fluorescence intensity and solubility.

As the conversion was completed the reaction mixture was irradiated with UV light and it was found that the fluorescence is quenched strongly and the characteristic emission color is not remained. After dialysis and lyophilisation, a dispersion in a water/chloroform mixture showed that the functionalized QDs with p(Sar) are in the water phase as expected due to their hydrophilic nature whereas the chloroform phase remains colorless.

In general, it could be shown that QDs in which the ligands are attached through a disulfide bond can be modified with the help of reactive ester chemistry. Here, small molecules, oligomers and high molecular weight polymers can be covalently bounded to the surface of the QDs by the PFP-LPA approach. As higher the molecular weight of the polymer as stronger is the resulting fluorecence quenching effect. Nevertheless, the intension here was to show a successful conversion and modification with hydrophilic polymers to disperse the resulting modified QDs in hydrophilic solvents which could be confirmed before going ahead to the main synthesis and project.

Hereby, the blockcopolymer $(PFPMA)_{46}$-*b*-$(MeO_3MA)_{15}$ was given together in a reaction vessel under Ar atmosphere with surface modified QDs with pentafluorophenyl lipoic aicd (CdSe@ZnS-PFP-LA) and were sonicated for 4 h in

DMSO. Under the use of the fluorophobic effect there is a preorganizing given between the fluorophobic part of the blockcopolymer and the one of the modified QDs.

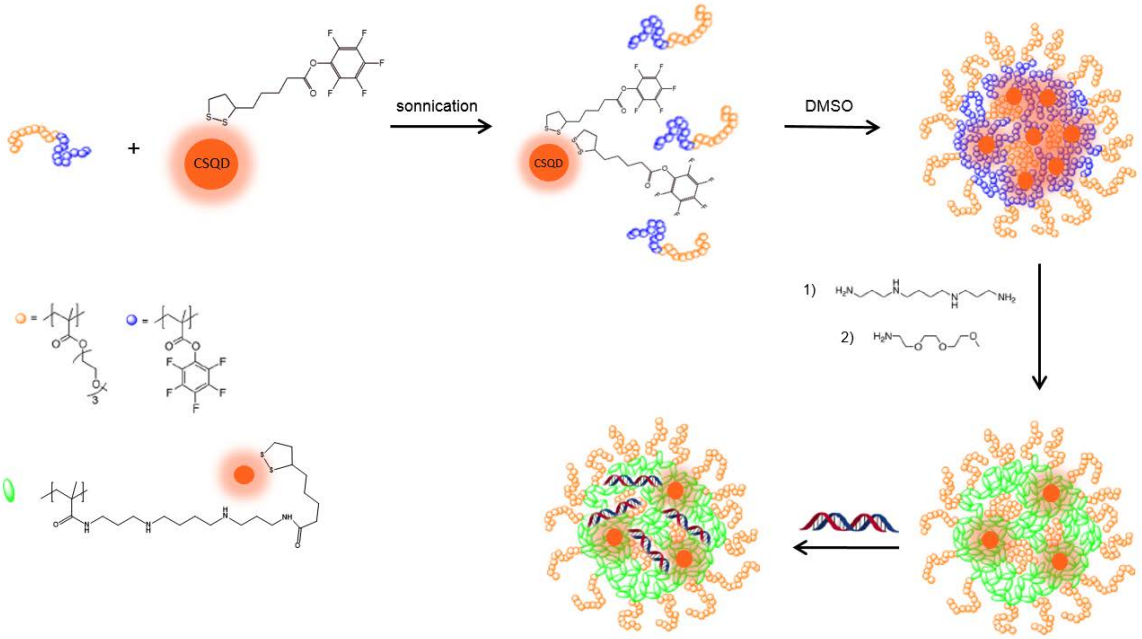

Figure 3.6: Reaction procedure for incorporation of QDs into nanohydrogels (QD-NH) and subsequent loading with negatively charged siRNA.

In DMSO, as a polar aprotic solvent, the blockcopolymer $(PFPMA)_{46}$-*b*-$(MeO_3MA)_{15}$ formes aggregates [L1] in which ideally the QDs are inside of the aggregates as the inner sphere has a hydrophobic nature. With spermine, an diamine, the modified QDs can be covalently bounded into the network structure of the aggregates. Reaction control was done over ^{19}F-NMR until full conversion was achieved (tracking of released pentafluorophenol). After 40 h at 60 °C there can be found released pentafluorophenol and after 90 h there is no pentafluorophenylester of the polymer remaining as indicated in the ^{19}F-NMR.

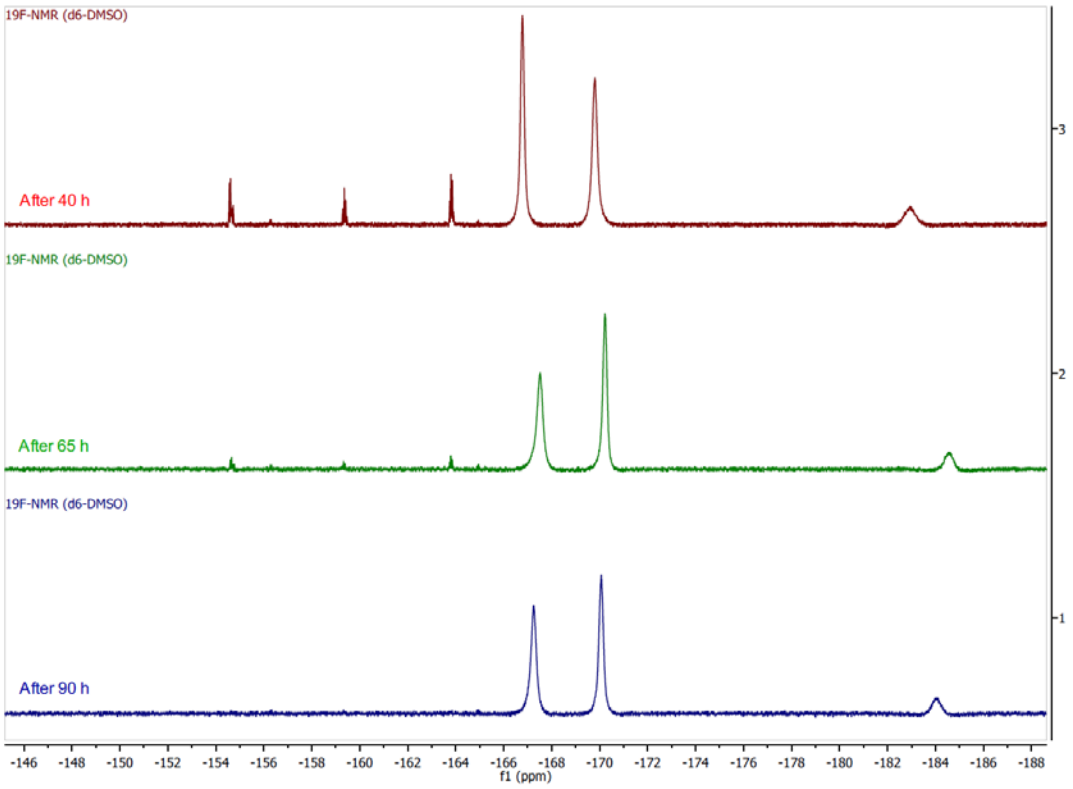

Figure 3.7: Tracking and control of conversion over released pentafluorophenol in ^{19}F-NMR.

To convert all reactive ester units – also those traces not detectable by ^{19}F-NMR and to reduce absolute toxicity – the reaction mixture was quenched with an excess of MEO-TEG. The next step was dialysis against Milli-Q water and lyophilisation to obtain slighly yellow voluminous powder. As the inner sphere is slightly positively charged it would be possible to incorporate by electrostatic interactions negatively charged siRNA. It was carried out an absorption spectra of the obtained QDs loaded nanogels compared to the naked QDs.

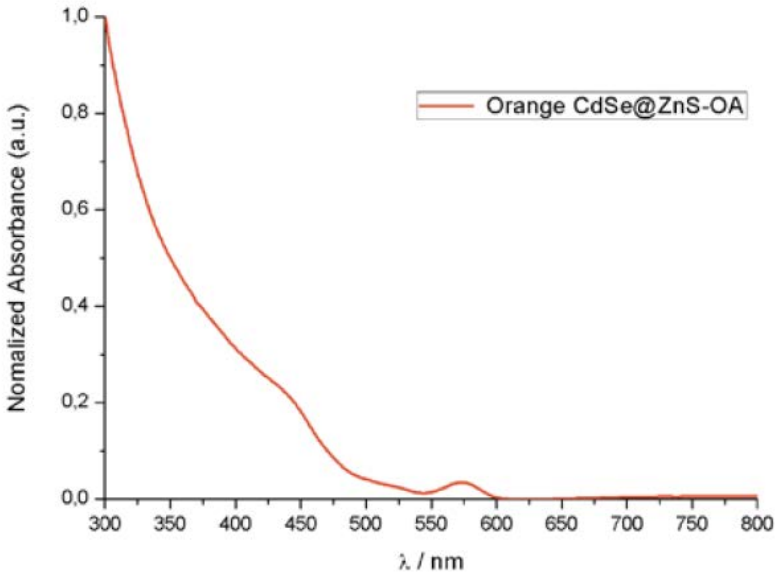

Figure 3.8: UV-vis of QDs functionalized with oleic acid.

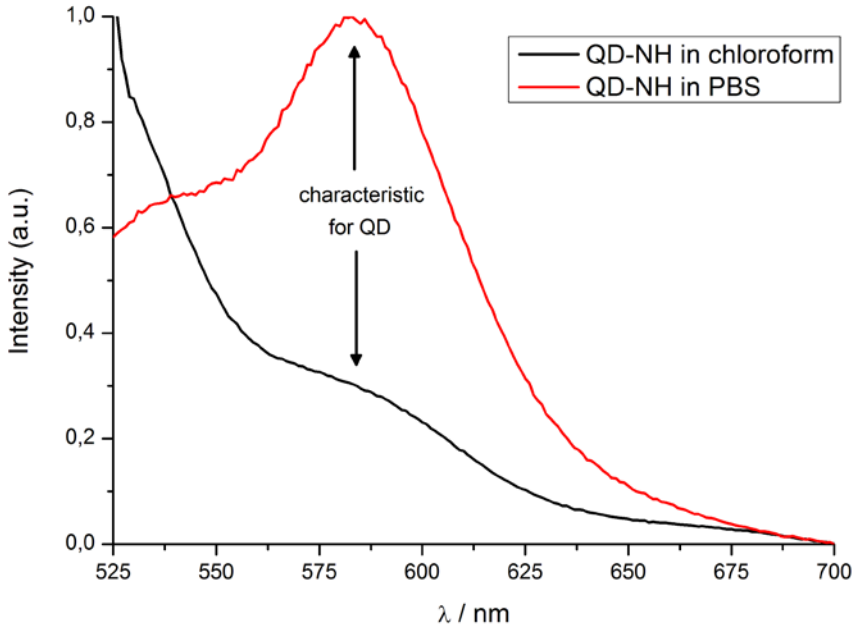

Figure 3.9: UV-vis of QDs incorporated nanohydrogels (QD-NH).

The characteristic absorption peak at $\lambda_{em}^{max} = 575$ nm for the QDs can be found, indicating a successfull incorporation of QDs into the polymeric micelles. Dispersed in different solvents the characteristic peak can still be tracked. As the blockcopolymer is not labeled with a dye but contains covalently bounded good fluorophores inside (QDs), FCS measurements were carried out in which a

hydrodynamic radius for the hybrid materials of R_H=47 nm was found even the correlation curve was not strong enough as the amount of QDs inside the micelles was either too low or the quenching effect was too strong. The QDs themselves have a R_H of 5.9 nm with a high monodispersity as obtained over dynamic light scattering measurements in n-dodecane. Also DLS of the hybrid materials revealed the expected size as determined before over FCS.

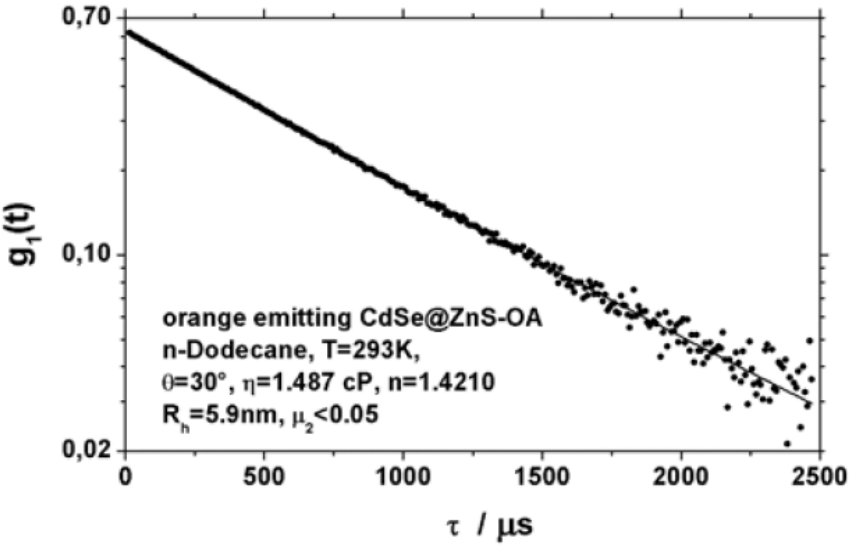

Figure 3.10: DLS measurement of oleic acid functionalized QDs in n-dodecane.

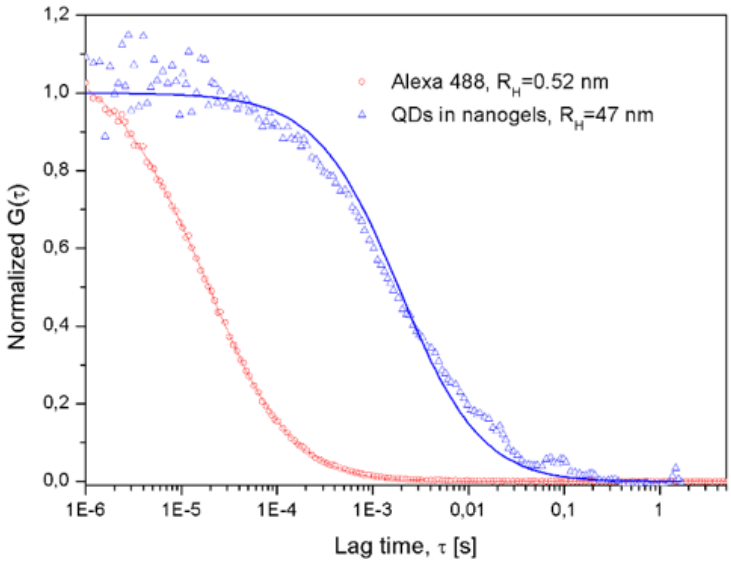

Figure 3.11: FCS measurement of QDs incorporated nanohydrogels (QD-NH) dispersed in PBS.

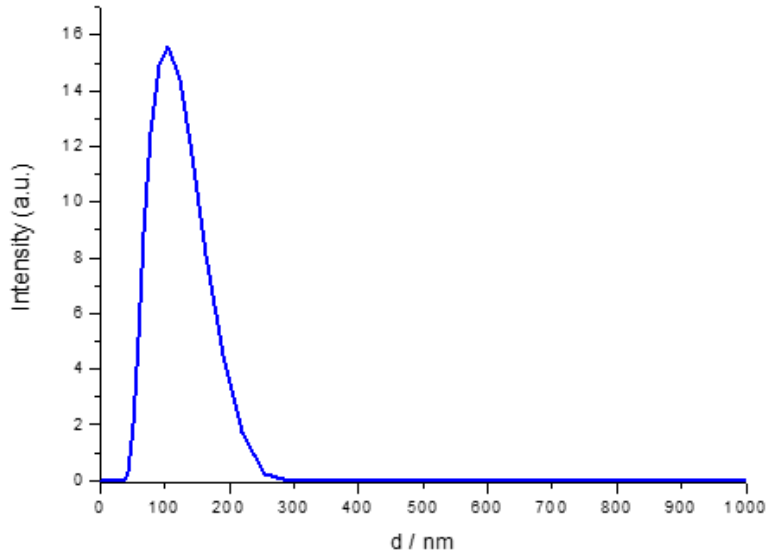

Figure 3.12: Zetaziser measurement of QDs incorporated nanohydrogels QD-NH dispersed in PBS.

This analysis gives a strong evidence that the nanohydrogels are containing QDs and furthermore the QDs are now water soluble, as the QDs before modification and incorporating into micelles were water unsoluble. The next step is to use the intrinsic electrodense properties of the QDs to picture these hybrid nanogels in Transmission Electron Microscope (TEM) and CryoTEM. In a combination setup of Confocal Laser Scanning Microscope (CLSM) and TEM one can detect the particles by optical microscopy due to the fluorescence of the QDs and also image them at the same time with high resolution TEM. In the following figure there is given the CLSM measurement on the left side and the TEM images on the right side for the investigated particles.

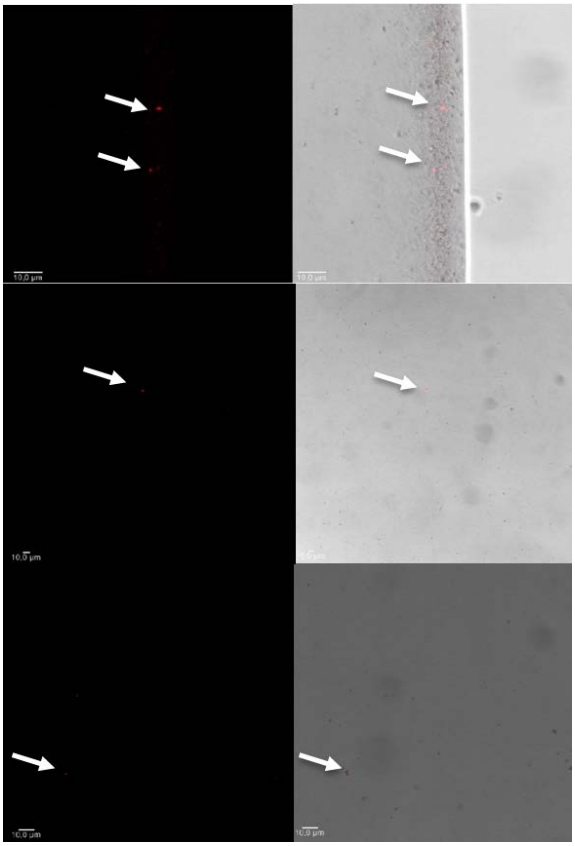

Figure 3.13: Confocal laser scanning microscope measurement of QDs incorporated nanohydrogels.

The arrows indicating the localization of said particles. On the left side there can be seen the CLSM fluorescenct measurement, while in the right the overlay with the transmitted light is given. The scale bar is 10 µm. Here, the fluorescence of the QDs could be successfully detect. Also the QDs seem to lie inside of an area of material with a higher contrast. The higher resolution TEM images of the hybrid nanohydrogels dispersed in PBS were conducted by Dr. Patricia Renz (MPI-P) and are shown in the following figure.

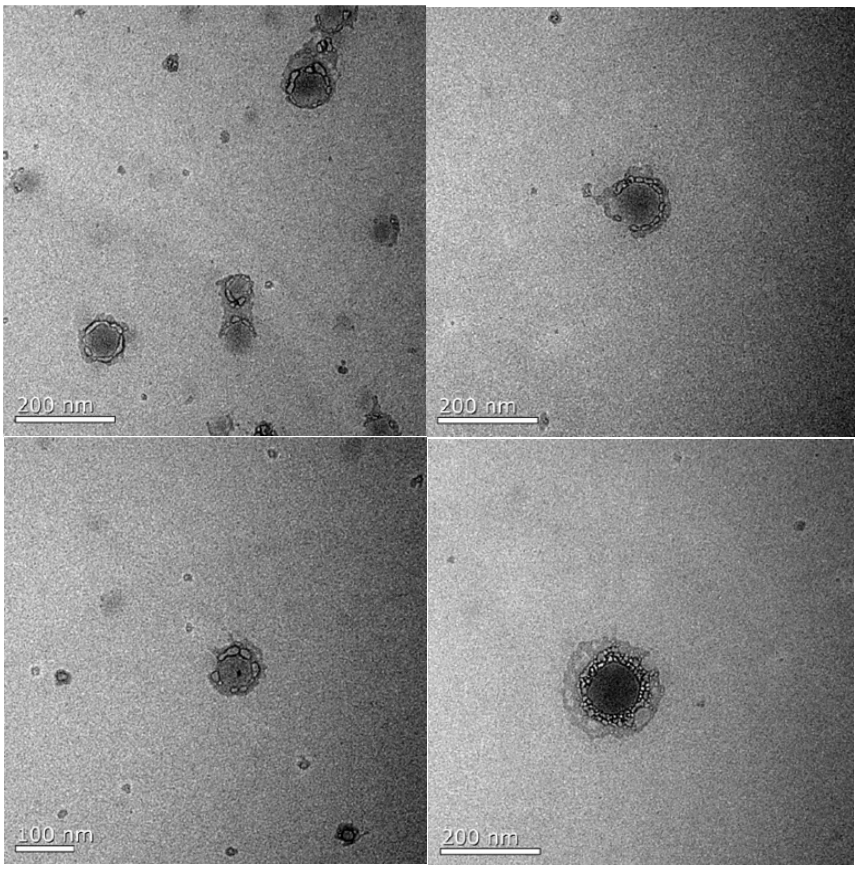

Figure 3.14: TEM measurement of QDs incorporated nanohydrogels from dispersion of PBS.

The size here found is the same as obtained before from FCS and DLS measurements. The revealed data are conform to the direct visible measurement method. The deposits on the edge of the particles came from drying effects as the dispersed QD-NH were dropped on the TEM grid and dried before measurement. The dark area indicates a material with a high electron density which can be referred to the QDs as the blockcopolymer does not appear such dark in TEM images. Nevertheless, EDX analysis did not reveal detection of existing QDs. Also the particles were dispersed in chloroform in which the expected size still could be found but the particles seem to be different in their composition. Only the edge of the round particle is with a dark contrast which indicates an electrondense material. Furthermore there are small aggregates but no clear trend can be observed besides the higher polydispersity of this system in the used solvent.

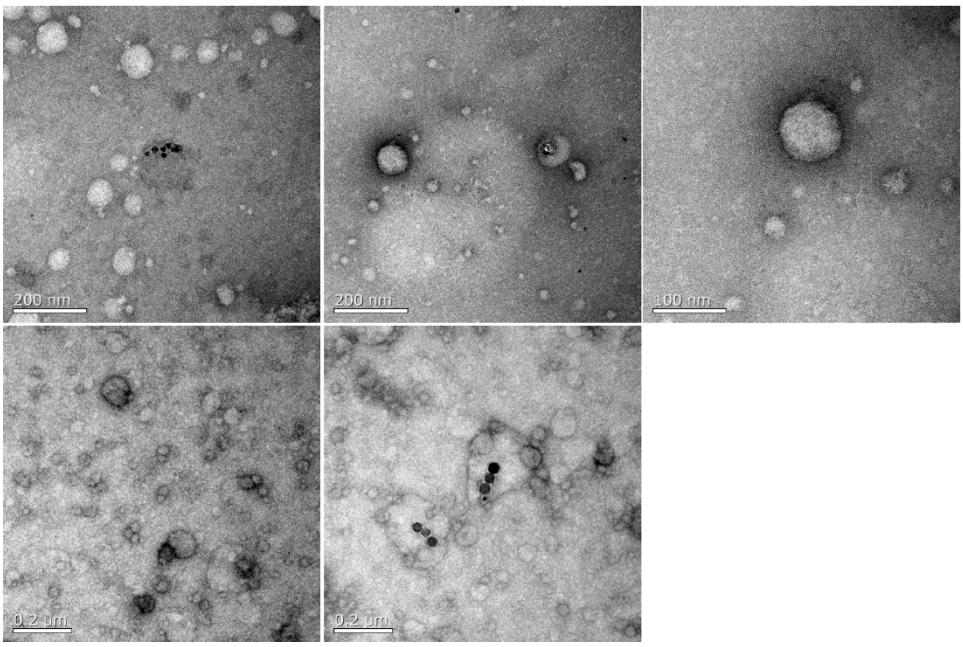

Figure 3.15: TEM measurement of QDs incorporated nanohydrogels from dispersion in chloroform.

In contrary to the expectations, with EDX no QDs could be detected and confirmed. As FCS and DLS measurements besides CLSM showed succesfull incorporated QDs the further thought was to increase the QDs amount for its easier tracking in EDX analysis. Furthermore, it has to be thought about the purification of the modified QDs. There are still free ligand molecules, free OA ligands, which can influence the conversion and incorporation of the QDs.

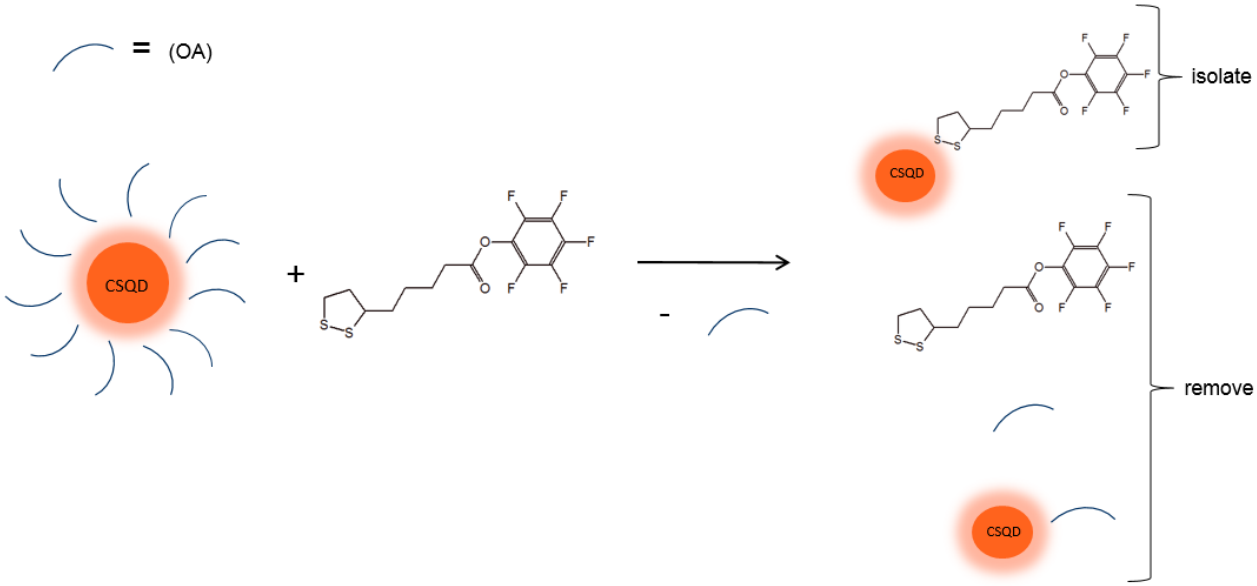

Figure 3.16: Shematically depiction of excess products which should be removed.

With a fluorinated silica column chromatography it was possible to wash the resulting modified mixture of QDs. The excess of free OA, PFP-LA and QD-OA could be eluate with chloroform while the QDs modified with PFP-LA (CdSe@ZnS-PFP-LA) remain on the fluorinated silica gel as the interaction resulting from a product of fluorophobic effect is strong enough to stay on the column. It was later extracted and used for a further trial of synthesis as described before. The obtained lyophylised QDs incorporated nanogels were measured again in TEM, FCS and DLS measurements. In the FCS measurements it was found again the expected size of R_H=50 nm.

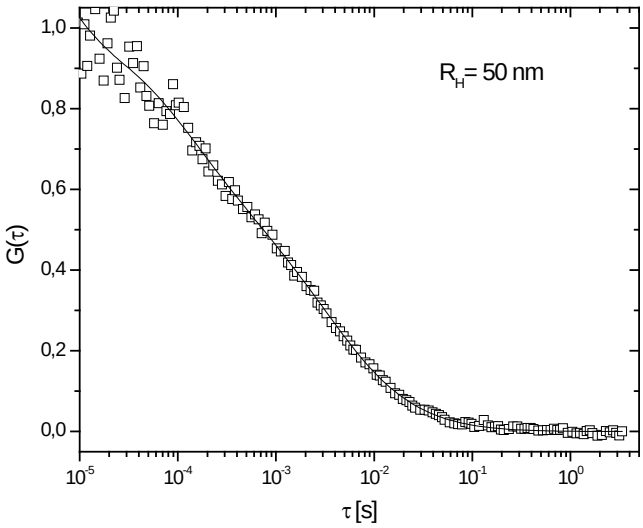

Figure 3.17: FCS measurement of QD-NH from dispersion in PBS.

TEM images were done with an embedded procedure using trehalose and uranyl acetate, ionic liquid and uranyl acetate, and ionic liquid with ferrocene conducted by Dr. Ingo Lieberwirth. The structure of the resulting particles is shematically given in the following figure.

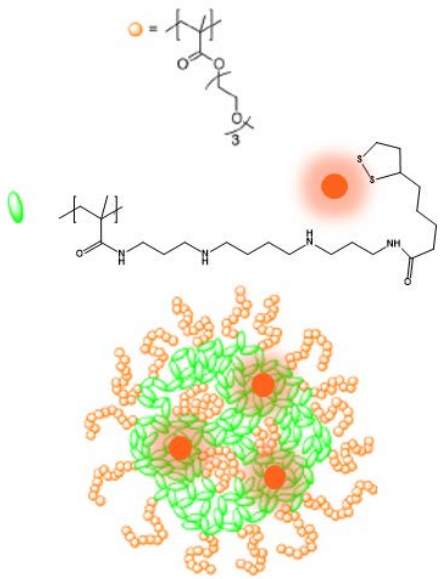

Figure 3.18: Schematic depiction of QD-NH.

Using the embedded procedure of trehalose and uranyl acetate the resulting nanoparticles seem to have a round shaped nature but the size is not conform to the results found in FCS and DLS measurements. Through the staining with uranyl acetate the particles get a high contrast. The visible particles obtained with this procedure are smaller in the hydrodynamic radius. Here against the expectations there were only 25 nm big in diameter.

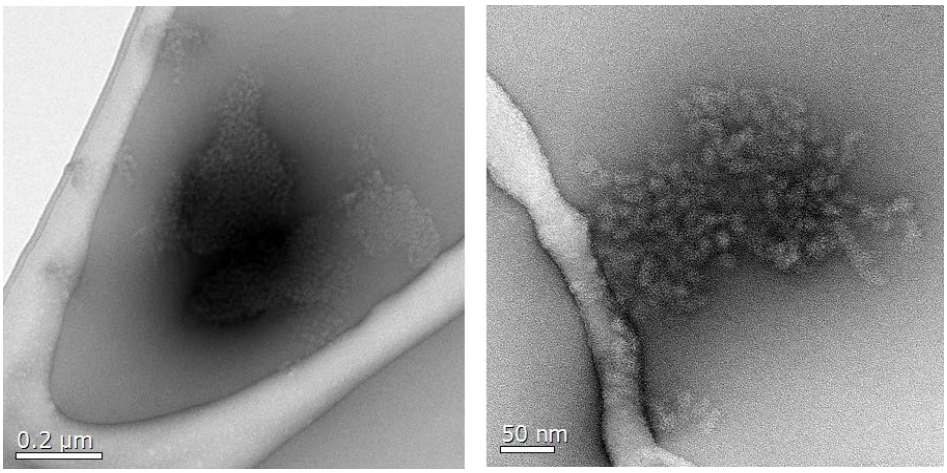

Figure 3.19: Cryo TEM of QDs incorporated nanohydrogels embedded in trehalose and uranyl acetate.

Also in the the case of embedded procedure with ionic liqid and uranyl acetate it can be found a high contrast in the TEM images with round shaped form but a polydisperse nature.

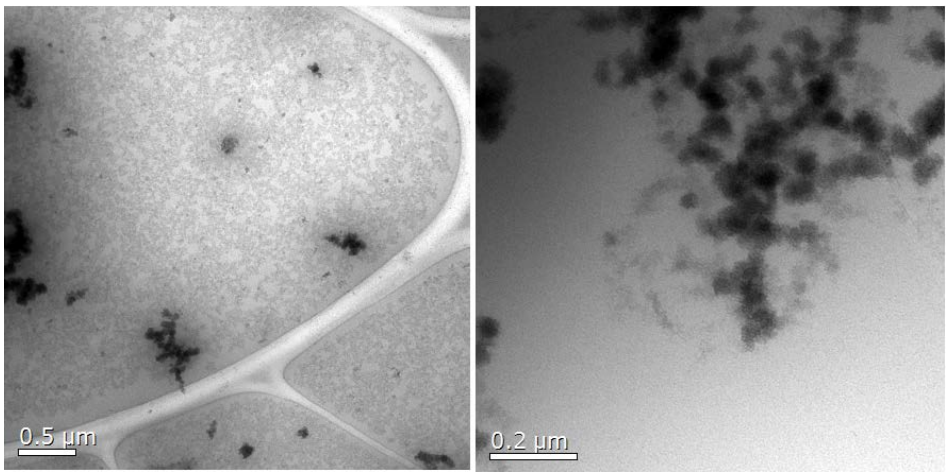

Figure 3.20: Cryo TEM of QDs incorporated nanohydrogels embedded in an ionic liquid and uranyl acetate.

Measurements of high TEM resolution reveal particles as they were expected to have the size found in preexperiments with FCS and DLS measurements for embedded structure with ionic liquid and ferrocene.

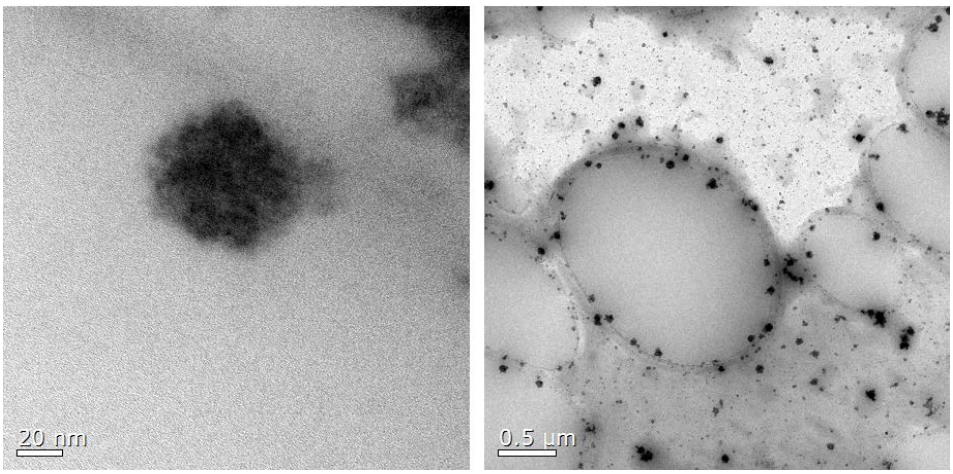

Figure 3.21: Cryo TEM of QDs incorporated nanohydrogels embedded in an ionic liquid and ferrocene.

The next step was a bio readout and a bio application in which the QDs incorporated nanogels were incubated on HeLa cells to investigate the uptake and to track the way and interaction of these particles. The time dependant imaging over 24 h of the

hybrid systems in interaction with HeLa cells are given in the following figure. It can be seen the size as proved before in FCS and DLS measurements and a strongly dark area which indicates elecrondense material.

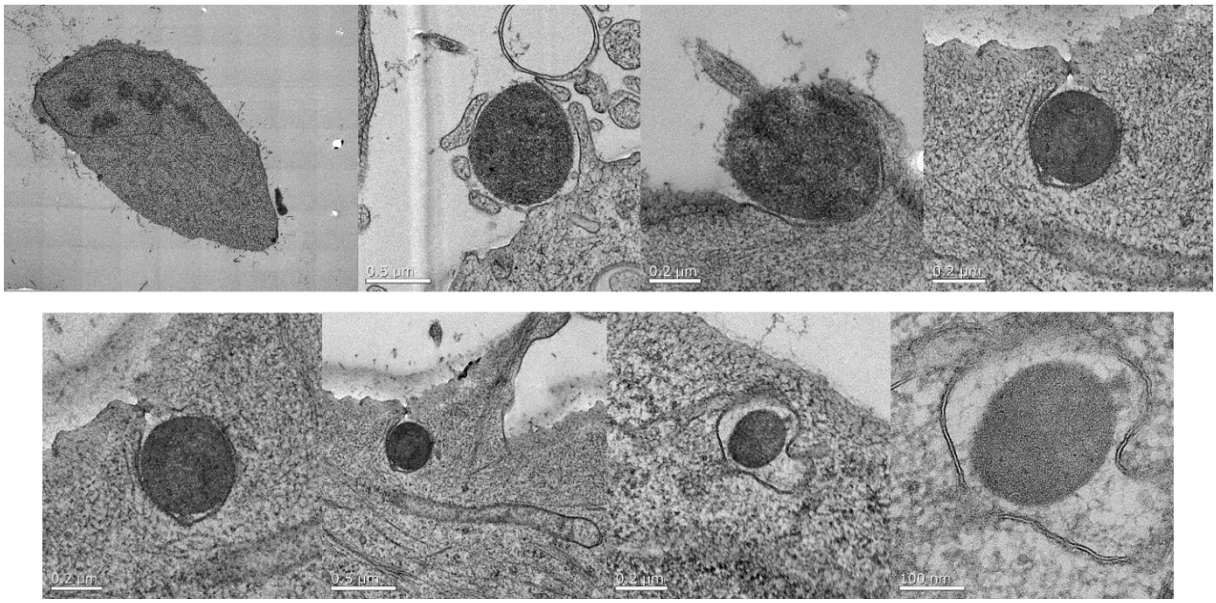

Figure 3.22: Cryo TEM of cell uptake in HeLa cells of QDs incorporated nanohydrogels.

There is a successful uptake happening. Nevertheless, EDX measurements did not prove the present of QDs give arise to question the dark area as it has to be a material with an electrondense property. The blockcopolymer does not have the ability to produce such a high contrast. One reason for the absence of QDs may be the concentration of QDs in the nanogels as through EDX only a small partial area or scanning point can be analysed. For this purpose it was conducted a further experiment with high concentration of QDs loaded nanogels (QD-NH) incubated with HeLa cells (50 times higher as before). Now, it was possible to detect high density of particles at the cell membrane as well as inside of the cell after cell uptake over pinocytose.

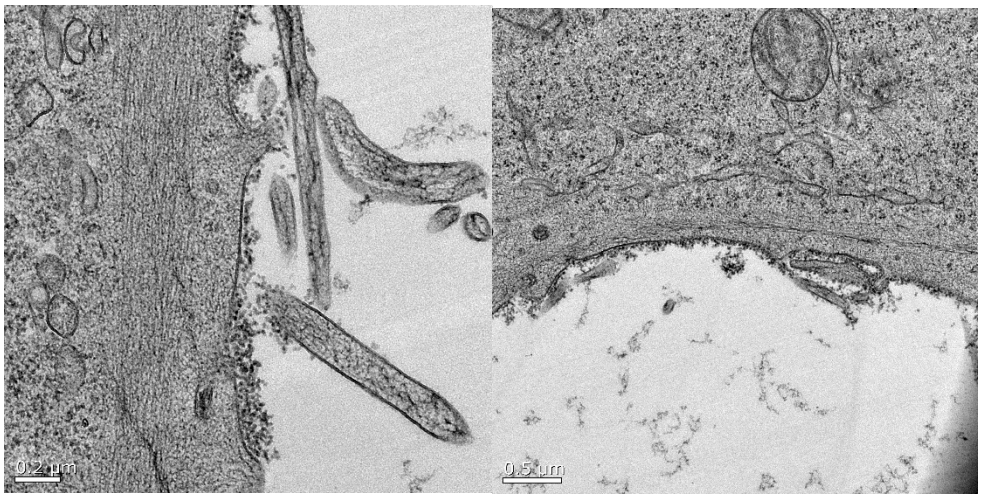

Figure 3.23: Cryo TEM of cell uptake in HeLa cells of QDs incorporated nanohydrogels (high concentration) - 1.

Furthermore, it can be seen clearly the uptake of high density of particles with slight aggregates into the cell while a high desity of particles still remain on the cell surface.

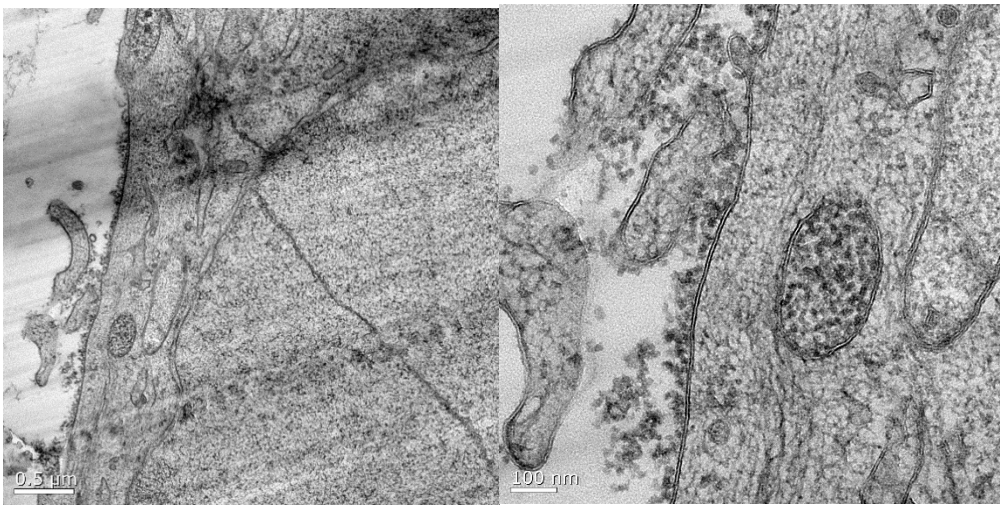

Figure 3.24: Cryo TEM of cell uptake in HeLa cells of QDs incorporated nanohydrogels (high concentration) - 2.

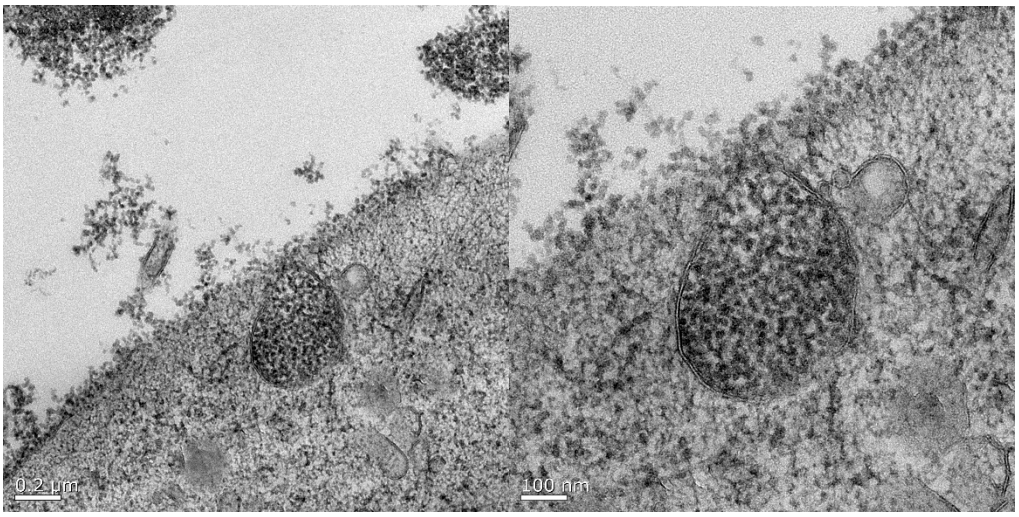

Figure 3.25: Cryo TEM of cell uptake in HeLa cells of QDs incorporated nanohydrogels (high concentration) - 3.

The Cryo-TEM images showed that some type of particles are taken up by the cell. But there was no indication that these are the QDs prepared.

Conclusion

It was able to functionalize oleic acid capped QDs based on CdSe@ZnS core shell system with pentafluorophenyl lipoic acid (PFP-LA). With the disulfide bond a ligand exchange with oleic acid can be accomplished to obtain the stronger attached PFP-LA on the surface of the QDs. The reactive ester was used to modify the surface with several amines via aminolysis. It could be detected and analysed via NMR and UV irradiation. These preexperiments showed the possibility to modify the surface of QDs to turn them from a hydrophobic to a hydrophilic nature and so make them soluble in aqueos solvents. The incorporation of the PFP-LA-QDs into cationic nanohydrogels revealed in FCS and DLS studies the desired product with covalently bounded QDs into the spherical micelles and in the expected size. Also TEM, CLSM and cell uptake studies showed the presence of these particles and successful cell uptake over macropinocytose. Although the QDs in the cell uptake Cryo TEM images could not be detected, the preexperiments conducted and prestudies with FCS and DLS techniques revealed that the QDs should be present and incorporated. The FCS measurement is a very sensitive method and even a very low amount of good fluorophore is needed for tracking. But in the visible technique as well as TEM, high amount of tracking compound is needed as one is limited by finding the localisation and position of the QDs for conducting the EDX measurements.

Bibliography

[L1] Nuhn, L.; Dissertation; Mainz; **2014**

Appendix I

Synthesis

CdSe@ZnS functionalised with oleic acid (CdSe@ZnS-OA):

Cadmium(II)oxide (0.4 mmol), zinc acetate (0.5 mmol), 5,5 mL oleic acid and 20 mL 1-octadecene were given together in a 250 mL reaction vessel and the mixture was heated up to 150 °C with a controlled temperature program. At this temperature it was degased for 30 min with nitrogen. Then it was further heated to a temperature of 310 °C. the reaction mixture turned colorless due to solved cadmium(II)oleate and zinc(II)oleate. To this mixture it was added a prepared solution of Se (0.4 mmol) and S (2.3 mmol) in 1 mL of 1-octadecene. It was given for the growth of the nanoparticles a timeframe of 6 min at 310 °C and then it was cooled up to room temperature. The obtained nanoparticles were centrifugated at 4300 rpm for 20 min and solved and stored in hexane until further processing.

CdSe@ZnS functionalized with 11-mercapto-1-undecanol (MUD):

50 mg of the pre synthesized CdSe@ZnS-OA were given together with 500 mg MUD in a 250 mL reaction vessel and diluted with 60 mL of an equal volume mixture between ethanol and chloroform. The mixture was then given in a sonication bath for 3 h to process the reaction. Then 40 mL chloroform was added and the precipitated functionalised nanoparticles were purified by centrifugation (4300 rpm, 20 min). The obtaied nanoparticles were solved in DMSO and stored until further processing.

Blue emitting CdZnS@ZnS-MUD@SiO_2-T-MMA:

1 mmol of CdO, 10 mmol of $Zn(ac)_2$ and 7 mL of OA were given in a reaction vessel and the mixture was heated to 150 °C under a continuously nitrogen flow. Then the temperature reached 150 °C it was kept for further 15 min before adding the next chemical compound. Then 15 mL of ODE was added and the temperature was raised up to 300 °C where a clear mixture is resulting which indicates the formation of the Cd oleate $Cd(OA)_2$ and zinc oleate $Zn(OA)_2$. At this temperature, 2 mmol of S

powder dissolved in 3 mL of 1-octadecene was quickly injected and the reaction temperature was raised up to 310 °C to support the growth of the CdZnS quantum dot cores. After 8 minutes at this temperature, 8 mmol of S powder dissolved in tributylphosphine (TBP) were given into the reaction vessel for the overcoating the existing CdZnS cores with a ZnS shell without any purification steps. The reaction was kept under these conditions for 30 min and was then cooled down to room temperature. With adding 20 mL of chloroform and 45 mL of acetone (done twice) the resulting overcoated nanoparticles could extracted and purified. After centrifugation at middle speed (3500 rpm) they were kept for drying to use for the next reaction. After drying 50 mg of the OA stabilized CdZnS@ZnS was given together in a vial with 500 mg of MUD and diluted with a mixture of ethanol (30 mL) and chloroform (30 mL) in a ratio of 1:1. Then sonication was done for 3 hours. After the sonication 230 mL of chloroform was added to participate the MUD attached nanoparticles. After centrifugation at middle speed (3000 rpm) the resulting nanoparticles were kept for drying. Then 20 mg of MUD capped CdZnS@ZnS were put in a vial and diluted with 5 mL of dry DMSO. Then 100 µL of T-MMA was added and the mixture was stirred for 6 hours at 50 °C under continuously nitrogen flow. After that 40 mL of chloroform were added to precipitate the nanocrystals and centrifuged. The resulting nanocrystals were washed with methanol and chloroform to remove excess ligands and compounds.

Red emitting CdSe@ZnS-MUD@SiO_2-T-MMA:

The experimental procedure was a one pot synthesis. 1 mmol of CdO, 2 mmol of $Zn(ac)_2$ and 5 mL of OA were heated to 150 °C under a continuously flow of nitrogen. When it reached the temperature of 150 °C 25 mL of 1-octadecene is given into the mixture in the reaction vessel. Then it was heated to 300 °C and 0.2 mmol of Se in 0.2 mL of Trioctylphosphine (TOP) was quickly injected. After 3 min it was injected 0.3 mL of 1-dodecanthiol and the reaction proceeded further for 20 min. After that 2 mmol of sulfur powder in 1.5 mL of TOP was added for the formation of the ZnS shell over a period of 10 min. Then the reaction mixture was cooled down to room temperature and with chloroform the resulting CdSe@ZnS-OA nanoparticles were precipitate and purified by centrifugation at middle speed (3500 rpm). After

isolating and drying, 50 mg of OA stabilized red emitting CdSe@ZnS were given together in a vial with 500 mg of MUD and diluted with a mixture of ethanol (30 mL) and chloroform (30 mL) in a ratio of 1:1. Then sonication is carried out for 3 hours. After the sonication 220 mL of chloroform were added to participate the MUD attached nanoparticles and after centrifugation at middle speed (3200 rpm) the resulting nanoparticles were kept for drying. Then 20 mg of MUD capped CdZnS@ZnS were put in a vial and diluted with 5 mL of dry DMSO. Then 100 µL of T-MMA was added and the mixture was stirred for 6 h at 50 °C under continuously nitrogen flow. After that 40 mL of chloroform were added to precipitate the nanocrystals and centrifugated. The resulting nanocrystals were washed with methanol and chloroform to remove excess ligands and compounds.

Synthesis of QDs incorporated cationic nanohydrogel particles:

The nanohydrogel particles presented in this work were synthesized followed: For a typical reaction, in a round bottom flask equipped with a stirbar $P(PFPMA)_{46}$-b-$(MEO_3MA)_{15}$ (40 mg; 26.15 µmol polymer or 12 µmol reactive ester) was dispersed in anhydrous DMSO (4 mL) under nitrogen atmosphere and QDs (4 mg) dispersed in 2 mL chloroform were added. The reaction mixture was set in a sonication bath for 4 h. The flask containing the reaction mixture was immersed in an oil bath at 55 °C under vigorously stirring and ^{19}F-NMR samples (0.1 mL dissolved in 0.5 mL DMSO-d_6) were taken at certain time points to determine complete reactive ester conversion. After 90 h no polymer bounded pentafluorophenol could be detected anymore. To remove further traces of it below the NMR detection limit, excess of non cross-linking methoxytriethyleneglycolamine (220 µL of a 0.1 g/mL solution in DMSO; 135 µmol) was added and the reaction mixture was stirred for additional 24 h at 55 °C. To remove small molecular byproducts, the reaction mixture was afterwards purified by dialysis against millipore water for 4 d (including frequent water exchange). In the dialysis membrane there was obtaining a precipitate which was filtered and subsequent the filtrate was lyophilized affording the desired product (15.0 mg, 64%) as an yellowish powder.

Bibliography

[1] Krini, R.; Diploma Work, **2014**.

[2] Brus, L. E., *J. Chem. Phys.*, **1986**, *90*, 2555–2560.

[3] Weller, H., *Angew. Chem.*, **1993**, *105*, 43–55.

[4] Peng, X.; Greenham, N. C.; Alivisatos, A. P., *Phys. ReV. B*, **1996**, *54*, 17628–17637.

[5] Empedocles, S.; Bawendi, M., *Acc. Chem. Res.*, **1999**, *32*, 389–396.

[6] Basche T.; Xie, R.; Mews, A., *J. Am. Chem. Soc.*, **2005**, *127*, 7480–7488.

[7] Alivisatos, A. P.; Colvin, V. L.; Schlamp, M. C., *A. P. Nature*, **1994**, *370*, 354–357.

[8] Coe, S.; Woo, W. K.; Bawendi, M.; Bulovic, V., *Nature*, **2002**, *420*, 800–803.

[9] Kazes M.; Kann S.; Banin U.; Tessler N. Medvedev V., *Science*, **2002**, *295*, 1506–1508.

[10] Talapin D. V.; Weller H.; Hikmet, R. A. M., *J. Appl. Phys.*, **2003**, *93*, 3509–3514

[11] Klimov, V. I.; Mikhailovsky A. A.; Xu, S.; Malko, A.; Hollingsworth, J. A.; Leatherdale, C. A.; Eisler, H.-J.; Bawendi, M.G.; *Science*, **2000**, *90,* 314–317.

[12] Finlayson, C. E.; Russell, D. M.; Ramsale, C. M.; Ginger, D. S.; Silva, C.; Greenham, N. C., *Adv. Funct. Mater.*, **2002,** *12*, 537–540.

[13] Kazes M.; Lewis, D. Y.; Ebenstein Y.; Mokari T.; Banin U., *Adv. Mater.*, **2002**, *14*, 317–321.

[14] Brunchez, M; Moronne M.; Gin, P.; Wiess, S.; Alivisatos, A. P., *Science*, 1998, *281*, 2013–2016.

[15] Chan, W. C. W.; Nie, S., *Science*, **1998**, *281*, 2016–2018.

[16] Clapp, A. R.; Medintz, I. L.; Mauro, J. M.; Fisher, B.R.; Bawendi, M. G.; Mattoussi, H., *J. Am. Chem. Soc.*, **2004**, *126*, 301–310.

[17] Murray, C. B.; Norris, D. J., Bawendi, M. G., *J. Am. Chem. Soc.*, **1993**, *115*, 8706.

[18] Peng, X.; Manna, L.; Yang, W.; Wickham, J.; Scher, E.; Kadavanich, A.; Alivisatos, A. P., *Nature*, **2000**, *404*, 59.

[19] Battaglia, D.; Li, J. J.; Wang, Y.; Peng, X., *Angew. Chem. Int. Ed.*, **2003**, *42,* 5035.

[20] Ye, X.; Zhuang, W.; Hu, Y.; Luo, X.; Zhao, C.; Huang, X, *Rare Metals*, **2009**, *28*, 107–111.

[21] Wang, Y. A.; Li, J. J.; Chen, H.; Peng, X., *J. Am. Chem. Soc.*, **2002**, *124*, 2293–2298.

[22] Aldana, J.; Wang, A.; Peng, X., *J. Am. Chem. Soc.*, **2001,** *123*, 8844–8850.

[23] Katari, J. E. B.; Colvin, V. L.; Alivisaos, A. P., *J. Phys. Chem.*, **1994,** *98*, 4109–4117.

[24] Kortan, A. R.; Hull, R.; Opila, R. L.; Bawendi, M. G.; Steigerwald, M. L.; Carroll, P. J.; Brus, L. E., *J. Am. Chem. Soc.*, **1990,** *112*, 1327–2332.

[25] Mews, A.; Eyschmuller, A.; Giersing, M.; Schooss D.; Weller, H., *J. Phys. Chem.*, **1994,** *98*, 934–941.

[26] Mansur, H. S.; Mansur, A. A. P.; Curti, E.; De Almeida, M. V., *J. Mater. Chem. B*, **2013,** *1*, 1696–1711.

[27] Derfus, A. M.; Chan, W. C. W.; Bhatia, S. N., *Nano Letters*, **2004,** *4*, 11–18.

[28] Hoshino, A.; Fujioka, K., Oku, T.; Suga, M.; Sasaki, Y. F.; Ohta, T.; Yasuhara, M.; Suzuki, K.; Yamamoto, K., *Nano Letters*, **2004,** *4*, 2163–2169.

[29] Ballou, B.; Lagerholm, B. C.; Ernst, L. A.; Bruchez, M. P.; Waggoner, A. S., *Bioconjugate Chem.*, **2004,** *15*, 79–86.

[30] Blachnik, N., *Praktikum Grundmodul*, Praktikum, 1–26, **2011**.

[31] Reed, M. A.; Randall, J. N.; Aggarwal, R. J.; Matyl, R. J.; Moore, T. M.; Wetsel, A. E., *Physical Review Letters*, **1988,** *60*, 535–537,.

[32] Weber A., Berlin-Germany, Dissertation, **2005.**

[33] Klingshirn, C. F., Springer-Verlag, Berlin, **1997**.

[34] Micic, O. I.; Curtis, C. J.; Jones, K. M.; Sprague, J. R.; Nozik, A. J., *J. Phys. Chem.*, **1994,** *98*, 4966–4969.

[35] Joung, S., Yoon, S.; Han, C.-S.; Kim, Y.; Jeong, S., *Nanoscale Research Letters*, **2012,** *7*, 93.

[36] Kim, K., Jeong, S.; Woo, J. Y.; Han, C.-S., *Nanotechnology*, **2012,** *23*, 065602.

[37] Gary, D. C.; Cossairt, B. M., *Chem. Mater.*, **2013,** *25*, 2463–2469.

[38] Bharali, D. J.; Lucey, D. W.; Jayakumar, H.; Pudavar, H. E.; Prasad, P. N., *J Am Chem Soc.*, **2005,** *32*, 11364–11371.

[39] Massadeh, S.; Xu, S.; Nann, T., *Proc. SPIE 7189*, *Colloidal Quantum Dots for Biomedical Applications IV*, **2009,** *718902*, 7189,.

[40] Nanoco, *Nanoco bought in reverse takeover*, **2010**, Manchester Evening News.

[41] Nanoco Group PLC, *Annual Report and Accounts*, **2011,** 1–68.

[42] Soennichsen, C., Kolb, U., *Übungen zur Biophysikalischen Chemie,* **2012**.

[43] Onushchenko, A. A.; Ekimox, A. I., *JETP Lett.*, **1981,** *34*, 345–349.

[44] Vossmeyer, T.; Katsikas, L.; Giersig, M.; Popovic, I. G.; Diesner, K.; Chemseddine, A.; Eyschmüller, A.; Wellter H., *J. Phys. Chem.*, **1994,** *98*, 7665–7673.

[45] Murray, C. B.; Norris, D.J.; Bawendi, M. G., *J. Am. Chem. Soc.*, **1993,** *115*, 8706–8715.

[46] Frankel, F., *Science*, **1998,** *280*, 1698–1700.

[47] Weller, H., *Angew. Chem. Int. Ed*. Eng., **1993,** *32*, 41–53.

[48] Engelsmann, A.; Yudson, V. I.; Relneker, P., *Phys. Rev. B*, **1998,** *57*, 1784–1790.

[49] Huong, N. Q.; Birman, J. L., *Phys. Rev. B*, **2000,** *61*, 13131–13136.

[50] Protiere, M.; Reiss P.; Li, L., *Photolumineszenz. II.*, **2011**, *Physikalisches Institut A*, RWTH Aachen.

[51] Fox, M.; *Optical Properties of Solids*, **2001**, *Oxford University Press*, Oxford Master Series in Physics.

[52] Bawendi, M. G.; Steigerwald, M. L.; Brus L. E., *Annu. Rev. Phys. Chem.*, **1990,** *41*, 477–496.

[53] Reimann, S. M.; Manninen M.; *Rev. Mod. Phys.*, **2002,** *74*, 1283–1342.

[54] Sigma Aldrich, *Materials Science*, **2014**, Quantum Dots.

[55] Jander, S., Dissertation, **2011,** Uni Hamburg,.

[56] Petzke F., *Rev. Mod. Phys.*, **2003,** 55.

[57] D. J. Norris, M. G. Bawendi, *Phys. Rev. B*, **1996,** *53*, 16338–16346.

[58] Niehaus, J.-S., Dissertation, **2012,** Uni Koblenz,.

[59] U.Woggon, *Springer Verlag*, **1997,** 136.

[60] Nirmal, M.; Norris, D. J.; Kuno, M.; Bawendi, M. G.; Efros, AI. L.; Rosen, M., *Phys. Rev. Lett.*, **1995,** *75,* 3728–3731.

[61] Bol, A. A.; Van Lingen, J. N. J.; Donega, C. M.; Meijerink, A., *Phys. Rev. Lett.*, **2003,** *90*, 257404.

[62] Kittel, C., *Oldenbourg Verlag*, **1999,** *12*.

[63] Gomez, D. E.; Califano, M.; Mulvaney P., *Phys. Chem. Chem. Phys.*, **2006,** *8*, 4989.

[64] Efros, A. L.; Rodina, A. V., *Phys. Rev. B*, **1993,** *47*, 10005.

[65] The free Encyclopedia on Wikipedia, **2013**, Quantum Yield.

[66] LaMer, V. K.; Dinegar, R. H., *J. Am.Chem. Soc.*, **1950,** *72*, 4847–4854.

[67] R. Viswanatha, R.; Sarma, D. D., *Wiley-VCH Verlag GmbH Co. KGaA*, **2007,** *4*, 141.

[68] LaMer V. K., *Ind. Eng.Chem.*, **1952,** *44*, 1270–1277.

[69] Yin, Y.; Alivisatos, P., *Nature*, **2005,** *437*, 664–670.

[70] Shiang, J. J.; Kadavanich, A. V.; Grubbs, R. K.; Alivasatos, A. P., *J. Phys. Chem.*, **1995,** *99*, 17417.

[71] Peng, Z. A.; Peng, X., *J. Am. Chem. Soc.*, **2001,** *123*, 1389–1395.

[72] Talapin, D. V.; Koeppe, R.; Götzinger, S.; Kornowski, A.; Lupton, J. M.; Rogach, A. L.; Benson, O.; Feldmann, J.; Weller, H., *Nano Letters*, **2003,** *3*, 1677–1681.

[73] Jun, Y.-W., Choi, J.-S.; Cheon, J., *Angewandte Chemie-International Edition*, **2006,** *45*, 3414–3439.

[74] Klimov, V. I.; Ivanov, S. A.; Nanda, J.; Achermann, M.; Bezel, I.; McGuire, J. A.; Piryatinski, A., *Nature*, **2007,** *447*, 441–446.

[75] Balet, L. P.; Ivanov, S. A.; Piryatinski, A.; Achermann, M.; Klimov, V. I., *Nano Letters*, **2004,** *4*, 1485–1488.

[76] Steckel, J. S.; Zimmer, J. P.; Coe-Sullican, S.; Stott, N. E.; Bulovic, V., Bawendi, M. G., *Angewandte Chemie-International Edition*, **2004,** *43*, 2154.

[77] Reiss, P.; Protiere, M.; Li, L., **2009,** *Small*, *5*, 154.

[78] Donega, C. de M., *Chemical Society Reviews*, **2011,** *40*, 1512.

[79] Li, J. J.; Wang, Y. A.; Guo, W.; Keay, J. C.; Mishima, T. D.; Johnson, M. B.; Peng, X., *J. Am. Chem. Soc.*, **2003,** *125*, 12567.

[80] Dabbousi, B. O.; Rodriguez-Viejo J., Mikulec F. V., Heine, J. R.; Mattoussi, H.; Ober, R.; Jensen, K. F.; Bawendi, M. G., *Journal of Physical Chemistry B*, **1997,** *101*, 9463.

[81] Eshet, H.; Grünwald, M.; Rabani, E., *Nano Lett.*, **2013,** *13*, 1485–1488.

[82] Ivanov, S. A.; Piryatinski, A.; Nanda, J.; Tretiak, S.; Zavadil, K. R.; Wallace, W. O.; Werder, D.; Klimov, v. I., *Journal of the American Chemical Society*, **2007,** *129*, 11708.

[83] Swart, I.; Sun, Z., Vanmaekelbergh, D.; Liljeroth, P., *Nano Letters*, **2010,** *10*, 1931-1935.

[84] Weller, H., *Advanced Materials*, **1993,** *5*, 88–95.

[85] Akiyama, K.; Suzuki, A.; Morikuni, H.; Tero-Kubota, S., *Journal of Physical Chemistry A*, **2003,** *107*, 1447–1451.

[86] Protiere M.; Reiss P.; Li L., *Wiley-VCH Verlag GmbH and Co. KGaA*, **2009,** Weinheim, *5*, 154–168.

[87] Talapin, D. V.; Mekis, I.; Götzinger, S.; Kornowski, A.; Benson, O.; Weller, H., *J. Phys. Chem. B*, **2004,** *108*, 18826–18831.

[88] Smith, A. M.; Mohs, A. M.; Nie, S., *Nature Nanotechnology*, **2009,** *4*, 56.

[89] Li, J. J, Wang Y. A.; Guo, W.; Keay J. C.; Mishima T. D.; Johnson, M. B.; Peng, X., *Journal of the American Chemical Society*, **2003,** *125*, 12567.

[90] Talapin, D. V.; Rogach, A. L.; Kornowski, A.; Haase, M.; Weller, H., *Nano Lett.*, **2001,** *1*, 207–211.

[91] Gericke, *Zweiphotonenmikroskopie*, **2013,** *Institut für Physikalische und Theoretische Chemie*, Grundlagen.

[92] Lee, K.-S., **2007***, J. Nonlinear Optic. Phys. Mat.*, *16*, 59.

[93] So, P., *Encyclopedia of life sciences*, **2002**, *1*, Macmillan Publishers Ltd, Nature Publishing Group.

[94] Denk, W.; Strickler, J. H.; Webb, W. W., *Science*, **1990**, *248*, 73–76.

[95] Park, S. H.; Lim, T. W.; Yang, S.-Y.; Kong, H. J.; Kim, R.-H.; Kim, K.-S.; Lee, K.-S., *Bull. Korean Chem. Soc.*, **2004***, 25*, 1119–1120.

[96] Mack, C. A., *SPIE Press,* **2006**.

[97] Huang, H.-H.; Orler, B.; Wilkes, G. L., *Polym. Bull.*, **1985,** *14*, 557–564.

[98] Schmidt, H., *Mater. Res. Soc. Symp. Proc.*, **1984,** *32*, 327–335.

[99] Schmidt, H., *J. Non-Cryst. Solids*, **1985,** *73*, 381–691.

[100] K.-H. Haas, K.-H.; Rose, K, *Rev. Adv. Mater. Sci.*, **2003,** *5*, 47–52.

[101] Houbertz, R.; Domann, G.; Cronauer, C.; Schmitt, A.; Martin, H.; Park, J.-U., Fröhlich, L.; Buestrich, R.; Popall, M.; Streppel, U.; Dannberg, P.; Wächter, C.; Bräuer, A., *Thin solid films*, **2003,** *442*, 194–200.

[102] Obi, S.; Gale, M. T.; Kuoni, A.; De Rooij, N., *Microelectron. Eng.*, **2004**, *73*, 157–160.

[103] Haas, K.-H.; Amberg-Schwab, S.; Rose, K., *Thin solid films*, **1999,** *351*, 198–203.

[104] Sainiemi, L.; Jokinen, V.; Shah, A.; Shpak, M.; Aura, S.; Suvanto, P.; Franssila, S., *Adv. Mater.*, **2011**, *23*, 122–126.

[105] Gombert, A.; Rose, K.; Heinzel, A.; Horbelt, W.; Zanke, C.; Bläsi, B.; Wittwer, V., *Sol. Energy Mater. Sol. Cells*, **1998,** *54*, 333–342.

[106] N. Moszner, N.; Salz, U., *Prog. Polymer. Sci.*, **2001**, *26*, 535–576.

[107] Schlie, S.; Ngezahayo, A.; Ovsianikov, A.; Fabian, T.; Kolb, H.-A., *J. Biomater. Appl.*, **2007**, *22*, 275–287.

[108] Gesellschaft für chemische Materialien spezieller Photoresistsysteme mbH, *Curable Hybrid Polymers for Micro Optics*, **2011**

[109] Shaw, J. M.; Gelome, J. D.; LaBianca, N. C.; Conley, W. E.; Holmes, S. J., *IBM J. Res. Develop.*, **1997**, *41*, 121–124.

[110] Lorenz, H.; Despont, M.; Fahrni, N.; LaBianca, N.; Renaud, P.; Vettiger, P., *J. Micromech. Microeng.*, **1997**, *7*, 121–124,.

[111] Conradie, E. H.; Moore, D. F., *J. Micromech. Microeng.*, **2002,** *12*, 368–374.

[112] Jang K. K.; Park J.-J.; Yang D.-Y.; Lee, K.-S., Prabhakaran P.; Son, Y., SPIE Newsroom, **2011**, Micro/Nano Lithography.

[113] Lorenz, H.; Despont, M.; Fahrni, N.; Brugger, J.; Vettiger, P.; Renaud, P., *Sens. Actuators, A: Phys.*, **1998**, *64*, 33–39.

[114] R. Feng, R.; Farris, R. J., *J. Micromech. Microeng.*, **2003**, *13*, 80–88.

[115] Cheong, F. C.; Varghese, B.; Sindhu, S.; Liu, C. M.; Valiyaveettil, S.; Bettiol, A. A.; van Kann, J. A.; Watt, F.; Chin, W. S.; Lim, C. T.; Sow, C. H., *Appl. Phys. A*, **2007**, *87*, 71–76.

[116] Engelke, R.; Mathuni, J.; Ahrens, G.; Gruetzner G.; Bednarzik, M; Schondelmaier, D.; Loechel, B., *Microsyst. Technol.*, **2007**, *14*, 1607–1612.

[117] Jeong, Y. J.; Lim, T. W.; Son, Y.; Yang, D.-Y.; Kong, H.-J.; Lee, K.-S., *Optics Express*, **2010,** *18*, 13745–13753.

[118] Ha, C. W., *Self Drawed*, **2013**, KAIST.

[119] Kwak, J.; Bae, W. K.; Lee, D.; Park, I.; Lim, J.; Park, M.; Cho, H.; Woo, H.; Yoon, D. Y.; Chr, K.; Lee, S.; Lee, C., *Chem. Mater.*, **2008**, *20*, 5307–5313.

[120] Paek, K.; Chung, S.; Cho, C.-H.; Kim, B. J., *Chem. Commun.*, **2011**, *47*, 10272–10274.

[122] Krini, R.; Kim, H.; Zentel R.; Chang, J. Y., *Poster on the polymer society of Korea - Pacific Polymer Conference*, **2011**, Poster.

[123] Clegg, R. M., *SPIE Press*, **2009**, *33*, 1–57.

[124] Lopez, L. B.; Thimsen, E. J.; Collins, A. M.; Blankenship, R. E.; Biswas, P., *Energy Environ. Sci.*, **2010**, *3*, 216–222.

[125] Clegg, R. M., *Phys. Rev. B*, **2000**, *62*, 10967–10977.

[126] Sun, Y.; Giebink, N. C.; Kanno, H.; Ma, B.; Thompson, M. E.; Forrest, S. R., *Nature*, **2006**, *440*, 908–912.

[127] Gerald Hinze, G., *Skript zur Physikalische Chemie*, **2011**, *Grundmodul*, 5.

[128] Chen, Y.; Ming, H., *Photonic Sensors*, **2012**, *2*, 37–49.

[129] Mendach, S.; M. Bröll, M., *Oberflächenplasmonen,* Fortgeschrittenen Praktikum Institut fuer Angewandte Physik Universität Hamburg, **2008**, 7–10.

[130] Chemgaaroo, *Chemgapedia*, **2013**, 3.

[131] Blackie, E. J.; Le Ru, E. C.; Etchegoin, P. G., *J. Am. Chem. Soc.*, **2009,** *131*, 14466–14472.

[132] Blackie, E. J.; Le Ru, E. C.; Etchegoin, P. G., *J. Phys. Chem. C*, **2007***, 111*, 13794–13803.

[133] Xu, X.; Li, H.; Hasan, D.; Ruoff, R. S.; Wang, A. X.; Fan, D. L., *Funct. Mater.*, **2013**, *23*, 4332–4338.

[134] Lombardi, J. R.; Birke, R. L.; Lu, T.; Xu, J., *Chem. Phys.*, **1986,** *84*, 4174.

Introduction into biomedical research area

Properties of amphiphilic polymers

In the last years the use of amphiphilic polymers in the area of nanomedicine gain more and more in importance.[B0,B1] For application in biomedical area there are many new polymer based formulations which are at this stage in clinical studies.[B2] This includes a broad variety of different systems as drug delivery systems as micelles, liposomes, polymersomes as well as polymer protein conjugate or conjugates of polymer and antibody.[B3]

For the self assembly of such superstructres as in the case of liposomes and polymersomes the properties of amphiphils are crucial. Amphiphil (greek. *amphi* „both“, *philos* „loving“) describes the chemical property of a compound which contains hydrophil as well as lipophil structures. Through the structure properties in a molecule it posseses polar and apolar compartments. Depending on the solvent they are soluble (solvophil) or not soluble (solvophob).[B4] This results in different interactions between polar and apolar compartments of the molecule with the solvent, in most cases water. This interaction depends strongly on the relative dimension of the different domains. Such molecules-either polymeric or of low molar mass-are surface active.[B5]

Such molecules arrange themselves in that way that the hydrophobic groups are shielded from water. For example they embed between the interface of air and water (segregation) leading to a local distrubance of hydrogen bonds. Thereby the surface ernergy of pure water is decreased.[B6] This is an essential effect which is used in e.g. wash active compounds.

When a certain concentration of amphiphilic molecules, as shown in figure 5, is reached a spontaneuos superstructure structure is formed the so called micelles. This concentration is substance specific and is referred to critical micelle concentration (CMC) meaning the concentration when micelles are formed.

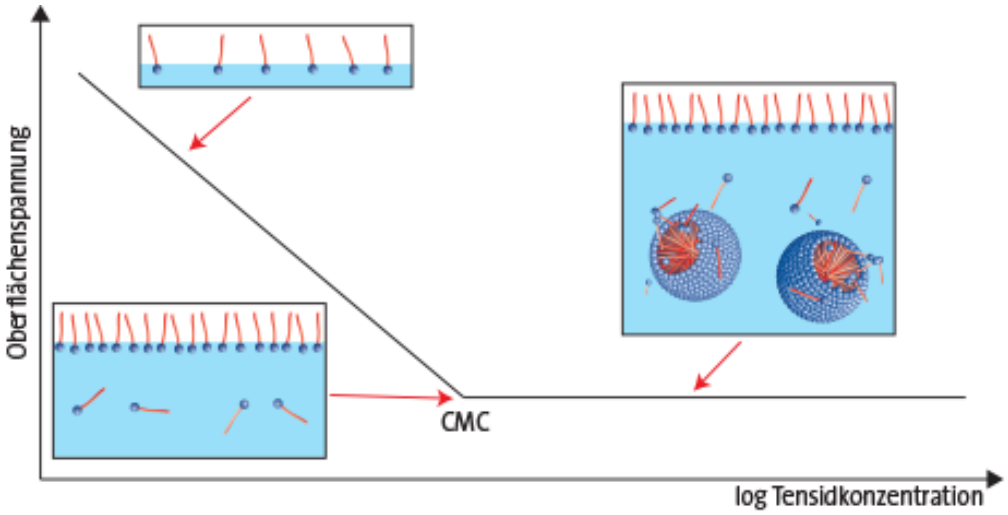

Figure 1: Surface energy dependent on surfactant concentration adopted from Ref[B1].

At this concentration the maximum solubility of tensides in an unimolecular form is reached. In the case of further addition of amphiphils the hydrophobic domains are orienting themselves in a way to avoid the contact with water.[B7]

After Kauzmann the water molecules cannot fom hydrogen bonds to the apolar compartment of the molecule (solvatisation). Therefore the water molecules are bonding each other stronger and form a higher ordered structure which leads to a reduction in entropy.[B8] With the aggregation of the hydrophob domains the interface to water is reduced whereby the ordered water film is also reduced. This is called as the hydrophobic effect.[B9] Micelles are only one aggregation form for self assembly of amphiphilic molecules. Dependent on molecular composition and other extern parameters like preparation method, concentration, temperature, pH value and ionic strength it can be achieved a broad range of different superstructures.[B10] For the experimental determination the shape of aggregation the ρ-ratio can be used. Thereby R_G is the radius of gyration which is determined by static light scattering (SLS) and R_H the hydrodynamic radius determined by dynamic light scattering (DLS).

$$\rho = \frac{R_G}{R_H} \qquad \{1\}$$

Table 1 shows the most important particle morphologies for the certain calculated ρ-ratios.[B11]

Table 1: ρ-ratio of common particle morphologies.

Topology	ρ-ratio
Homogenous sphere	0.775
Hollow sphere	1
Ellipse	0.775-1
Random polymer coil	1.505

In this work the synthesized amphiphilic blockcopolymers and obtained vesicles over duale centrifugation technique are the desired polymersomes with a hollow sphere which encloses an aqueuos interior with a ρ-ratio of 1.

Amphiphilic Polymers

As an interesting alternative to low molecular amphiphils there are synthesized over the years a broad range of various amphiphil polymers especially in the biomedical research field.[B12-B16] They can form in aqueos milieu similar aggregats as to that found for low molecular amphiphils.[B17] Due to the high molecular weight of the polymeric amphiphils they have a distinct higher mechanical and colloidal stability. [B18] Furthermore they can be vary in a broad range regarding the materials and architecture. In a simple way they are a blockcopolymer of type AB in which one block is build up by an hydrophilic material and other one from an hydrophobic. For linear polymers consisting of more than two blocks they can form complex structures like pfropfcopolymers, dendritic and star formed polymers as well as ring closed amphiphils. [B19-B21] To predict the expected aggregat structure it can be used analogous to the package parameter for low molecular weight amphiphils the volume ratio of amphiphilic block copolymers of the hydrophilic block or in commonly use the hydrophilic weight fraction f.[B22,B23] When increasing the ratio of the hydrophilic block different architectures are obtained as shown in the following figure.

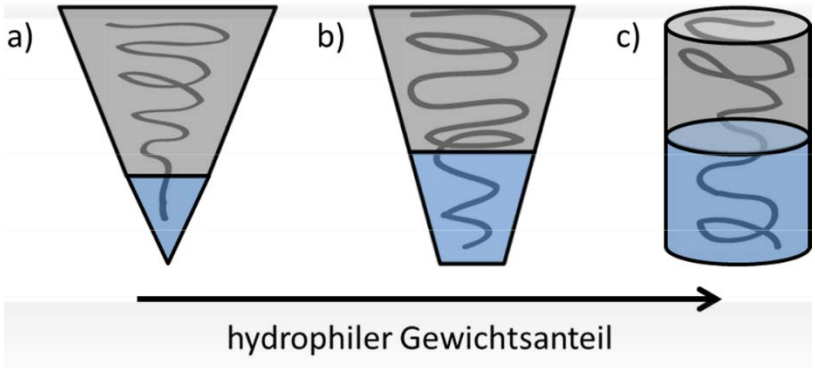

Figure 2: Structure of polymer molecules with different hydrophilic weight fraction f. In analogou way to lipids here with inreasing f there are formed a) micellar, b) cylindrycal and c) vesicular lamellar structures adopted from Ref[B0].

For blockcopolymers which are more in the direction of hydrophilic nature the architecture are micelles which is also kineticly favourised due to the simplification of this structure. That is the reason why even for polymers with a higher hydrophobic ratio forms micelles before turn over to opther complex aggregat structures.[B18] Besides cylindrical micelles in many cases there are form so called compound micelles for block copolymers.They consist of a simple core shell structure, so aggregates of inverse micelles with a low degree of order. They are stabilised colloidally to the outer sphere by hydrophilic chains. Due to the inverse order of the polymer chains it can be contain multiple aquesous domains with a polydispersity in the size distribution. [B24,B25] Furthermore it is possible that hydrophobic domains could be found on the particle surface (figure below).

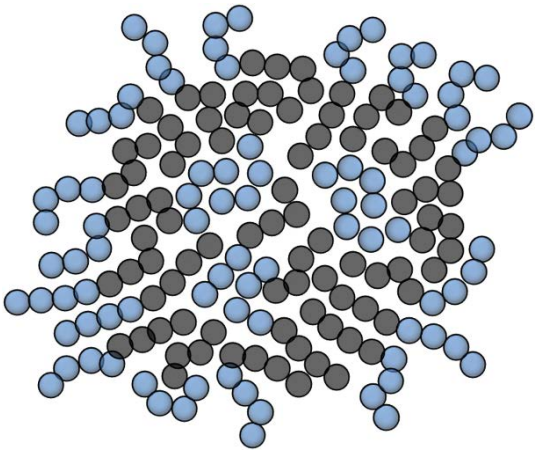

Figure 3: Depiction of a compound micelle adopted from Ref[B0].

Vesicles consisting of amphiphilic blockcopolymers are referred to polymersomes which are used in this work. During the process of self assembly there are three

essential factors for the free energy of the system with which the morphology can be regulate: aspect ratio of the solvophobe block, its surface energy to the ambient solvent as well as the repulsive interdependency between the solphophile chains which forms the corona.[B18,B26,B27] Polymer amphiphils have the advantage in contrast to low molecular weight species that the aggregat form can be regulate directly over the copolymer composition. A detailed observation is done by Zhang and Eisenberg based on the system polystyrol-*b*-polyacrylic acid.[B26] The surface energy and the interdependency between the hydrophilic chains are strong dependant by the experimental conditions. They can be regulate by the concentration of the amphiphil, the nature of the common solvent and the amount of the selective solvent.

Polymersomes

Polymersomes are vesicles which are build up of amphiphilic blockcopolymers. In most cases of these AB blockcopolymers it is a spherical closed double layer of polymer molecules. Their arrangement is structural in an analogous way to the liposomes which consist of low molecular amphiphiles e.g. phospholipids. Since their discovery in the year 1945[B27] liposomes are a matter of extensive studies. Due to their attractive biological properties they have in particular found as application in medical research. They are biocompatible and able to encapsulate and incorporate as a result of their aqueos interior and hydrophobic membrane hydrohilic as well as hydrophobic compounds. This leads to protection against external degradation conditions.[B28] Furthermore their pharmacologic relevant properties like size, charge and surface modification can be selective influenced by suitable choice of fabrication methods and the admixture of appropriate functionalized lipid derivates.[B28-B31] However, phospholipids exhibit due to their low molecular weights of the constituent building blocks several disadvantages. Hereby, the high exchange rate, low mechanical stability and relative high permeability of the lipid membrane as well as a fast elimination through cells of mononuclear phagozyte systems (MPS)[B32] play a crucial role. Since 70th there is driven extensive research at the synthesis of bilayer membranes which should overcome the natural disadvantages of

phospholipids. For this purpose Regen, Czech and Singh developed a new concept of polymerized vesicles.[B33] Central point here is the subsequent crosslinking of before formed vesicles via polymerizable functional groups. Through the use of such synthetic amphiphiles the advantages of vesicles should be maintained by cleary enhanced stability and circulation time. This concept was initially implement via a methacryl functionalized aliphatic ammonium compound. The so formed vesicles exhibit a clearly enhanced resistance against the degradation in the presence of ethanol.[B33] Later on further developments of this concept e.g. the use of crosslinkable cholesterin derivates[B34] which are good mixable with phospholipids were done. Besides polymer lipid conjugates were developed by sterical stabilization of lipid vesicles.[B35] This concept should shield sterically the lipid vesicles against the environmet leading to a reduction of the adsorption of proteines. Today it is in particular widespread in form of PEGylated lipid vesicles.[B36] A disadvantage in the use of polymer lipid conjugates is the fact that they can added only to an extent of 10 % due to sterical reasons. The physical properties of the vesicles are basicly defined by the used low molecular lipids.[B37]

oreover there is a tendency in segregation for most of the conjugates given. They dissociate from lipid membranes and form an own micelle.[B38] 1995 van Hest observed for the first time vesicles from amphiphilic polymers. He compared the morphology of dendritic poly(styrol)-dend-poly(propylenimin) polymers with different degree of polymerization and found that PS_{30}-*dendr*-$(NH_2)_8$ aggregates to vesicles in aqueous media.[B39] The first published vesicles based amphiphilic diblock polymers are from Zhang and Eisenberg in 1996.[B40] They form a doubled layer membrane after the example of lipid vesicles. They exhibit due to their significant high molecular weights and sterical stability through their hydrophilic corona a colloidal as well as a mechanical enhanced stability. Due to this properties the polymer vesicles are since that object of extensive research, especially as promising candidates for drug carrier systems as an alternative to the liposomes.

Polymersomes are a particular system consisting of amphiphilic block copolymers in contrary to the liposomes (greek. lipos „fat“) which consisitng of amphiphil lipids. As to see in figure 4 there is a bilayer formed. The hydrophilic areas are pointing into

the middle and into the outer phase while the membrane is build up from hydrophobic molecules. This makes it possible to encapsulate hydrophilic compounds into the aqueous interior as well as hydrophobic compounds into the membrane.

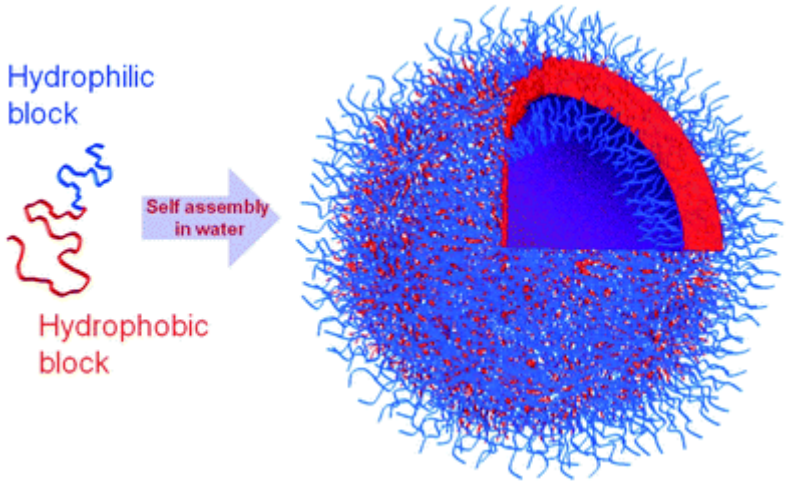

Figure 4: Schematically depiction of polymersomes adopted from Ref[B41].

In the direct comparision of these amphiphilic aggregates the polymersomes come with various advantages. Due to the thicker double layer membrane they have a higher stability compared to liposomes. This leads to a higher blood circulation time as they are more robust against the enzymatic degradation. Furthermore the thicker membrane layer and the choice for the size of the polymersomes have a higher encapsulation layer for hydrophobic compounds and a bigger aqueous interior for hydrophilic compounds. This enhances the encapsulation efficiency compared to liposomes.[B42] Due to the broad scope of different polymers there is a higher variability given in regard to desired properties. As shown schematically in figure 5 it is also possible to synthesize polymers with sensitive units which react on extern stimulis. Therefore pH labile groups can be incorporated which degrade at a desired pH value and leads to a change in conformation within the polymer structure enhancing the drug relase for the encapsulated compound.[B43,B44]

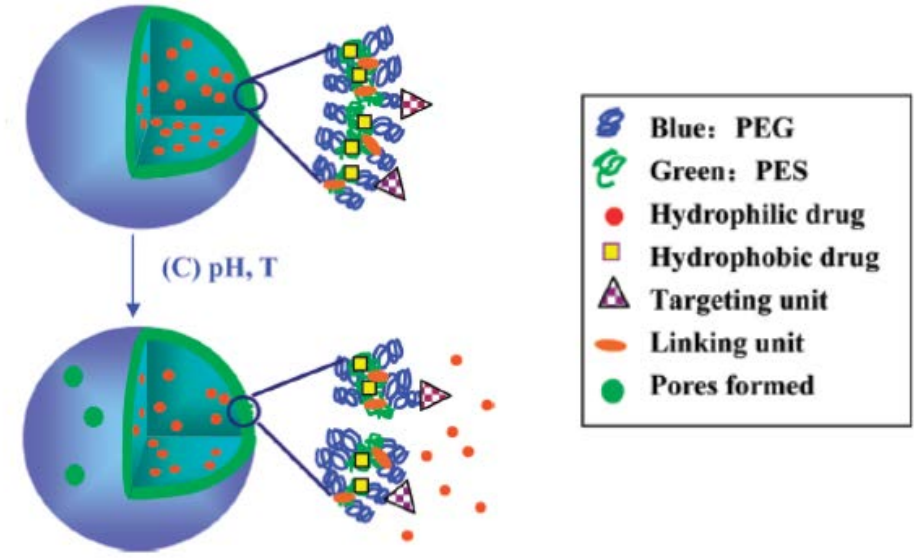

Figure 5: Schematically dipiction for the dissotiation of stimuli responsive polymersomes adopted from Ref[B45].

This makes it possible to attach target structures on the polymersome surface. This enables a target oriented adressing of particles on specific cells or organells. Here the particles can accumulate localy in a higher extend and so increase the amounf of relased encapsulated compound. Thus momentous side effects in chemo therapeutics are reduced on a minimum as there is a lower systemic strain on the whole treated organism. Due to this outstanding property polymer based drug delivery systems are gaining more and more importance in actual research especially in the area of biomedical.[B41]

Properties and mechanism of vesicles

Polymer vesicle are categorized analoug to lipid vesicles in sizes. Depending on the diameter there are small (small unilamellar vesicles, SUV), large (large unilamellar vesicles, LUV) and giant vesicles (giant unilamellar vesicles, GUV). Besides that there are multilamellar vesicles (MLV) and so called multivesicular vesicles in which multiple seperate vesicles are closed inside in the membrane of another vesicle.

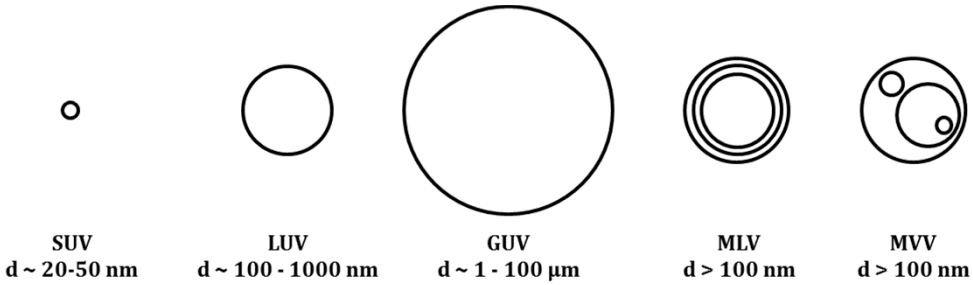

Figure 6: Categorisation of vesicles adopted from Ref[B0].

The hydrophilic weight fraction f of the polymer chains can used as a parameter to estimate the expected aggregat structure in aqueos solvents. As rule of thumb the self assembly to vesicles occur when with a value for f of[B46,B47]

$$f = (35 \pm 10)\ \% \qquad \{2\}$$

This value is similar to the ratio often found in phospholipids. As there is a broad variety of block materials this value hast o consider as an approximate value. The found structure of a certain polymer depends strongly from the experimental conditions. Furthermore there is an inherent dispersity for the synthetic obtained blockcopolymers. The used aliquot of the polymer containd molecules with different degree of polymerisation resulting in different hydrophilic weight fractions. That is the reason why in most cases istead of a single aggregat form mixtures of different superstructures are obtained. The mechanism of formation for the aggregates is not clearly elucidated. There are existing at this stage of time two theoretic studies which describe the formation of aggregtaes in regard to the individuel clock copolymers. They distinguished from each other singnificantly in their encapsulation efficiency (EE) for hydrophilic compounds. Both starting from the initial and very fast formation of small spherical micells as depicted in the following figure.

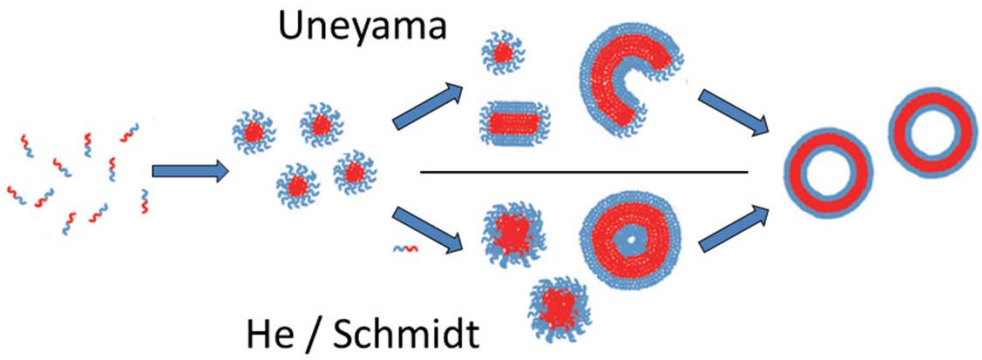

Figure 7: Mechanism for the vesicle formation after Uneyama (upper row) and He / Schmidt (lower row). Modified after adopted from Ref[B48].

After Uneyama the spherical micelles are merged to anisotropic small rods and disciodic micelles and they become that big that their flexibility makes a curvature possible.[B49] To minimize the surface energy of the system the planar aggregat closes to a vesicle.[B50] During this process the hydrophilic compound can be encapsulated which are solved in the aqueos interior. He and Schmid propose a mechanism in which the spherical micelles are growing to clusters of low order by intake of further polymer chains. Through small internal rearrangement processes and swelling of the internal hydrophillic domains over the absorbed solvent they become to vesicles.[B51] But over this process no big aqueous compartiment is encapsulated and the EE of hydrophilic compounds is low. Even it is difficult to verify the very small short living interstages there are for both proposed mechanism experimental proved evidence.[B52-B54]

At this stage of investigation it can be assumed that there are various pathways possible for the formation of vesicles.[B55] The progress is dependent of concrete experimental conditions. The often used polymer type is AB. Triblock copolymers of type ABA, BAB and ABC are also possible where C also stands for an hydrophilic unit as can be seen in the following figure.

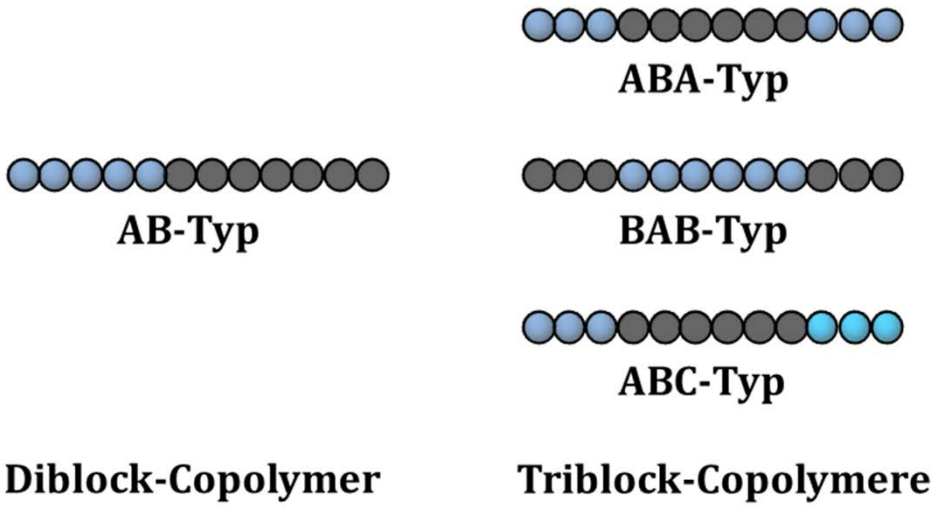

Figure 8: Types of ampiphilic block copolymers for the formation of polymersomes adopted from Ref[B0].

Figure 9 shows the possible arrangement of different types in the membrane. It can be seen that only for the types AB and ABA a double layer can be formed analogue to the membrane of lipid vesicles. Triblock copolymers ABA orientate themselves in an U form in which the opposite B clocks are formind the hydrophobic part. Per polymer molecule two water solouble blocks A are formed the hydrophilic corona. Furthermore ABA block copolymers can arrange themselves in an I form not resulting in a bilayer structure butin a spehrical closed mono layer. This happens when one of the both A blocks is statistically significantly shorter than the other or when in the ABC type the hydrophilic matierial is different. In both cases the shorter block has by trend a higher ration at the hydrophilic domain pointing into the inner vesicle due to the curvature of the membrane.[B56]

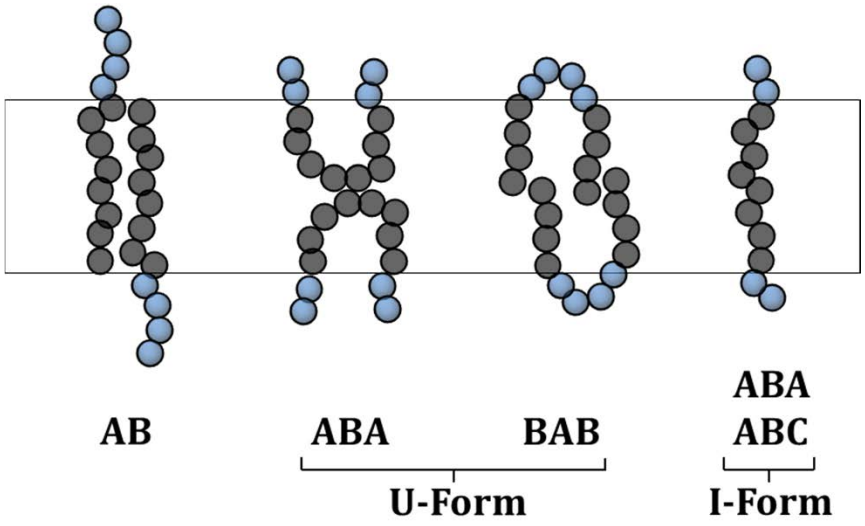

Figure 9: Arrangement of blockcopolymers forming vesicle in the membrane adopted from Ref[B0].

Diblock copolymers form more compact membranes due to the better overlap and entanglement. They are due to the double layer structure more inflexible and less permeable compared to triblock copolymers.[B57] the entaglement increase with molecular weight. Therefore the molecular weight is crucial for the membrane thickness and for the stability of the polymersomes.[B58,B59] Currently there are polymer vesicles formed of amphiphilic block copolymers up to a molecular weight of 100 kDa known.[B60] The magnitude of order ist wo times higher than that for natural lipids which do not excess in general 1 kDa. For polymersomes the resulting mebrane thicknesses are in the range of 10-50 nm [B58] 57 compared to 3-5 nm for lipid vesicles.[B46,B61,B62] Through the high membrane thickness and the narrow entanglement of the polymer chains the polymersomes are less permeable for neutral low molecular compounds. The permeability for water molecules through lipid membranes is 15 – 150 µm/s while for the polymersomes it is only 0,7 - 10 µm/s.[B63] The high molecular weight of block copolymers compared to lipids has big influence on the CMC. After

$$c_{CMC} \sim \exp\left(-\frac{n\varepsilon_h}{k_B T}\right) \qquad \{3\}$$

The CMC is dependent on the number of repeating units n and so the molecular weight of the hydrophobic block. Amphiphilic blockcopolymers lean to aggregation at low concentration compared to lipids. The CMC is depending on material and block length 10-6 – 10-7 mol/L.[B63,B64,B65] Furthermore the exchange rate of single molecules between aggregates is proportional to CMC which menas it is also small. The high membrane thickness in combination with the low diffusion ability of the polymer molecules as well as the inherent sterical stabilisation makes the polymersomes to remarkable stable aggregtaes. They are compared to virale capsids even they are similar in their structure to lipids. Capsids exhibit similar molecular weights of their building blocks as well as similar in the robustness and low permeability.[B46,B66-B68]

Preparation methods for polymersomes

As polymersomes are an analogue to liposomes their preparation method is not much different to the later one. There exist different techniques for the preparation of vesicles. Besides the duale centrifugation method which is used in this work to obtain vesicles there are conventional preparation methods like the solvent switch or film rehydratisation.

The preparation over solvent switch is conducted by the slow switch of a solvent in which both polymer blocks are soluble to a good solvent for only the hydrophilic compratment.[B69] Through repulsion of the hydrophobic non soluble polymer compartment with the good solvent particular superstructures are formed. Hereby the total removal of the remaining organic solvent is often not possible. Due to the potential cytotoxic effect of the used organic solvent and future attempt and desired use in biomedical application this method was not used, besides the fact that the encapsulation efficacy for hydrophilic compounds is much lower than that for the duale centrifugation.

The film rehydratisation does not use any solvent. Hereby a thin polymer film is immersed into the aqueos phase. Due to the concentration gradient between the pure polymer film and the aqueous phase there a diffusion exchange happening.[B70] As

shown in the following figure lyotrope lamellar phases (a) are formed followed by constriction to vesicles (b).[B71] To accelerate the process one can put into the system energy from extern e.g. temperature increase.

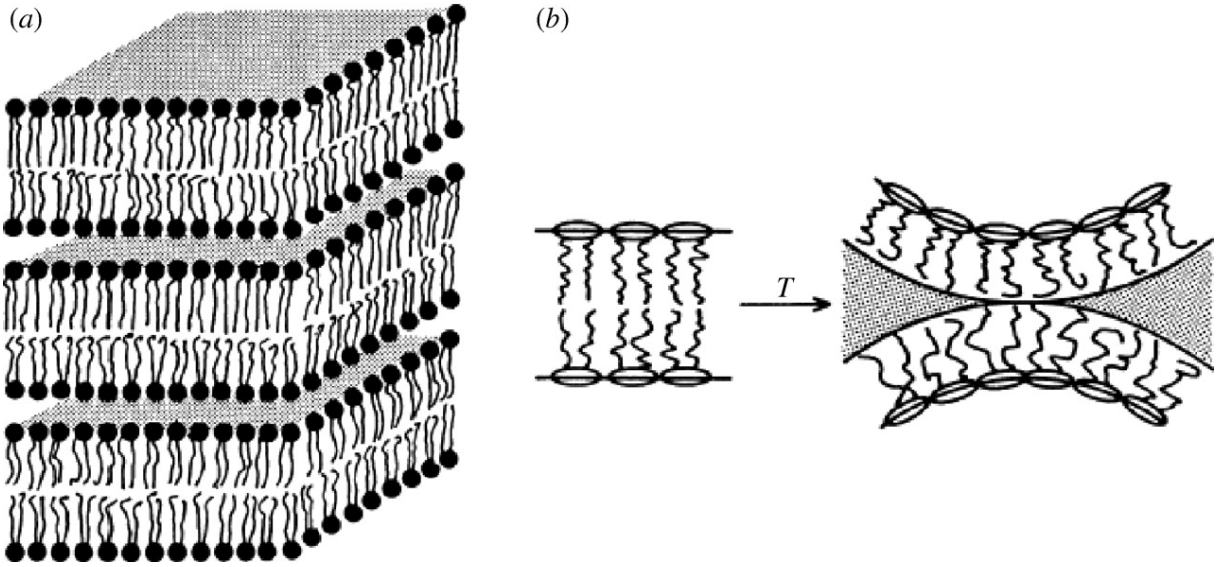

Figure 10: Schematically depiction of lamellar phases and formation of vesicles adopted from Ref[B72].

With this method vesicles are obtained which are often big and multilamellar. They can be homogenized by extrusion to unilamellar versicles.[B73] This technique was not used for the vesicles prepared in this work as the subsequent extrusion step of the polymersomes and fragmentation of bigger vesicles would result in a high concentration loss of the encapsulated drug.

The duale centrifugation technique can be seen as a new method for the formulation of polymersomes. For the lipid based particles it is already an etablated technique.[B74] [S11] This reveals an extingish advantage. Hereby no potential toxic organic solvent is needed. Furthermore the preparation is not time consuming and it can be achieved moderate encapsulation efficiancy.[B74]

As shown in the following figure the sample is rotated around the x axis as well as y axis. Hereby the sample is pushed in contrary to the common centrifugation not to the outer side but to the inner side to the middle of the sample tube.

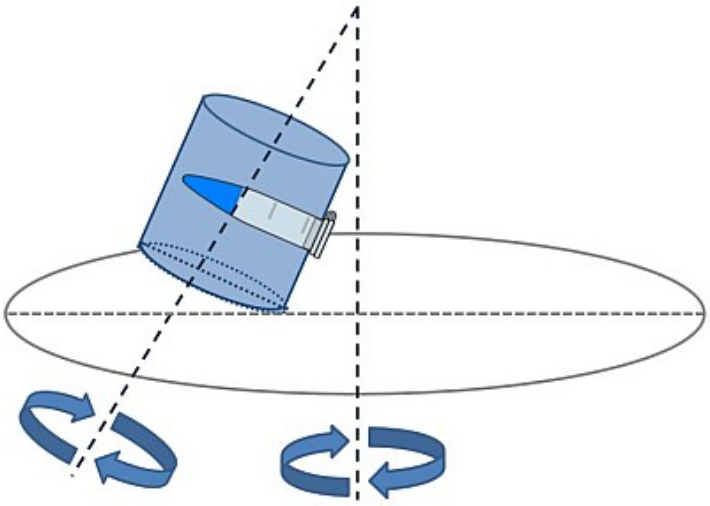

Figure 11: Principal of the duale centrifugation technique adopted from Ref.[B1].

This leads to an efficient stirred sample under simultaneous formation of vesicles. For the formation of liposomes it was able from *Hirsch et. al.*[B75] to obtain encapsulation efficiancy of 40-80 % with a main size distribution of 70 - 120 nm.[B76]

Polymeric Therapeutics

In the beginning of 20th century Paul Ehrlich recognized that for pharmacologic active compounds it is very important that they reach the desired place to develop their effect.[B77] The fundament for the practical efficient use was developed by Helmut Ringsdorf in the mid of 70th with his model of pharmacoloic active polymers.

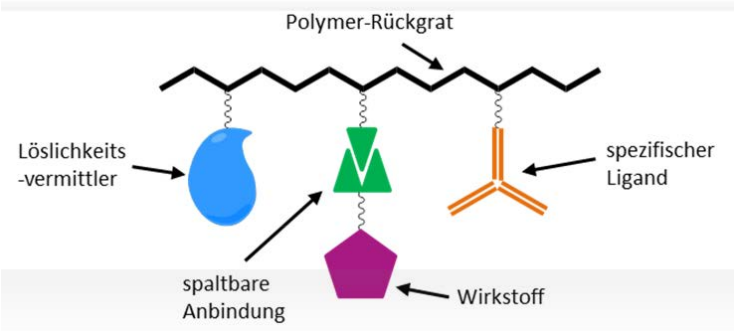

Figure 12: Pharmakologic active polymers after the Ringsdorf model adopted from Ref.[B78]

There is a reversible juction of a drug to a water soluble non toxic polymer. Furthermore over an additional ligand which can bind specific to suitable target structure and enhanced the cell uptake. When linking a hydrophobic drug to a hydrophilic polymer the water solubility can be increased and the pharmacological availability can be enhanced in an extensive manner. Furthermore the drug is protected from degradation influences. Also due to a higher molecular weight the polymer drug conjugate or polymer based nanoparticle can not be easily eliminate over the kidneys. Cause to the pore size of the kidney endothel of 3-5 nm bigger particles can not be filtered off.[B79] This means dependent to the properties of a concrete polymer a molecular weight of 30-50 kDa. [B80] Polymer particles which are over this value do have an enhanced circulation time. [B81-B83] Started with Ringsdorf in the last 40 years a broad research are in regard to polymeric therapeutics has been developed. After Duncan it includes polymeric drug [B84]123, polymer-drug [B85] 124 and polymer protein conjugates[B86,B87] as well as polymeric micelles[B88] and polyplexes.[B89]

Polymeric Therapeutics in the anti tumor therapy

Polymeric therapeutics are gaining more in importance and are a promising alternative for the application in the are of biomedical as well as potential therapeutic in the tomur therapy.[B90,B91]

Major point for an effective impact is the accumulation of particles and release of drugs at the desired local inflammatory area in the organism. Therefore it was developed a concept referred to active targeting where polymeric drug delivery systems are modified in that way that they could adress selective specific cells.[B90] This exclude and minimize undesired side effects as when treat in a systemic way the whole organism. Furthermore the efficiancy of drug delivery is enhanced. Besides the active targeting there is possibility of an indirect targeting referred to passive targeting through the EPR effect which can be used in application with particular systems. [B92]

The EPR effect (*enhanced permeability and retention)* decribes the enhanced permeability and retention of macromolecules in the tumor tissue. Due to the fast angiogenese of the tumor the tumor endothel layer can only form in a defective manner its vascular structure. The endothel cells of the capillary vessel of the tumor are strong fenestrated as shown in the following figure.

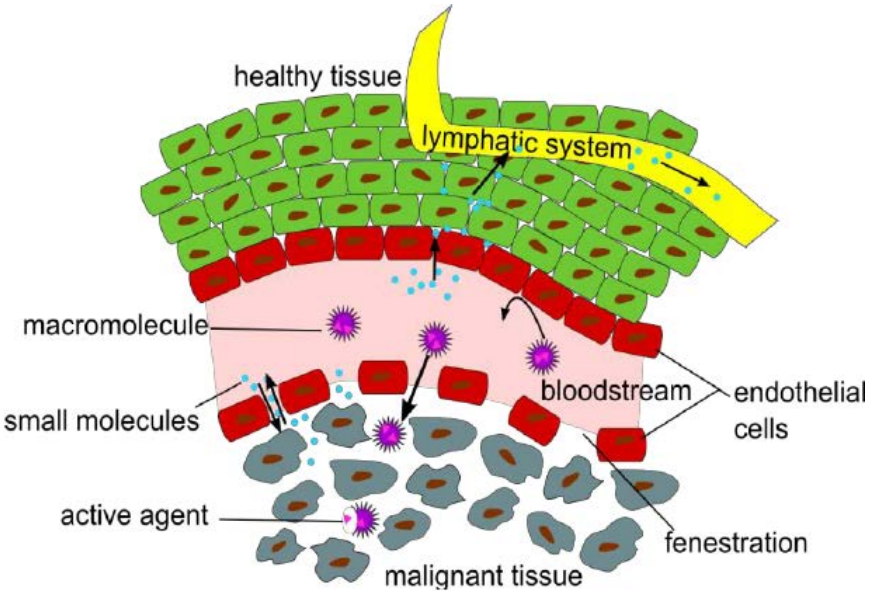

Figure 13: Illustration for the EPR effect of macromolecules as drug delivery systems in malignant tissue adopted from Ref**[B96].**

The have a much bigger porous holes as healthy endothel tissue.[B93] The permeability for macromolecules is higher and they diffuse into the malignant tissue. Hereby the defective lymph drainage of tumor tissue plays a crucial role leads to retention of the macromolecules and accumulation in that environment.[B94] The EPR effect can be detected for macromolecules with a molecur mass bigger that 50 kDa and a long plasma half life starting from a circulation time of 6 hours. Macro molecules under this molecular mass are segregate over renale filtration.[B95,B96] Through better comrehension and intensive research of the immune system and the formation of tumor the research focus in the last time was set extensive on the immune therapy. [B9749] As immune therapy every therapy can be named which uses the immune system to cure a infammatory herd. For tumor patients the immune system should recognize the tumor cells and destroy them. As drugs it is used molecules which can provoke an inflammatory herd in combination with an antigen leading to an selective

immune response for the tumor. Hereby antibodies, siRNA, DANN and cytokine as the tumor necrose factor α (TNF-α) are used.[B98] For application of the polymersomes as drug delivery systems for the tumor therapy the anti tumoral effect of TNF-α is used. *Carswell et. al.* reported 1975 for the first time that certain host cells are released a serum factor by contact with endotoxine which leads to necrosis of murine and humane tumors and referred to TNF-α.[B99] It is a strong inflammatoric cytokine. It is mainly produced by activated macrophages, T-lymphocytes and natural killer (NK) cells as a 25 kDa membrane bounded pro-TNF.[B100] It contains an intracellular N-Terminus and is classified as a type II transmembraneproteine. [B10153] Over proteolytic decomposition of the extra cellular domains (*Ectodomain-shedding*) through the enzyme TACE (*TNF-a converting Enzyme*) it becomes soluble and 17 kDa in ist weight.[B102]

In his active form it embeds into a non covalent counded hetero trimer. [B10355] The bio activity of the cytokine is mainly regulated through the soluble form.[B104] For TNF-α there are existing two kinds of receptors (TNF-R1 and TNF-R2) which exhibits different affinities.[B105] TNF-R1 is constitutive expressed on all cells while TNF-R2 can only be found on immune cells and bound the membrane bounded TNF-α as a ligand. The receptor signalizes through activation of transcription factor NF-κB the cell viability, the cell proliferation and triggers the further production of inflammatoric cytokines. TNF-R1 contains a death domain (DD) and triggers through ist activation the cell death.[B105]

TNF-α induced tumor necrosis

TNF-α as drug in the tumor therapy has its advantage as the receptor TNF-R1 is enhanced experessed on the surface on the tumor endothel cells.[B104] When TNF-α is released localy at the tumor side its cytotoxic effect can developed through the junction. As shown in the following figure the endothel layer dies off thorugh the TNF-α induced apoptose.

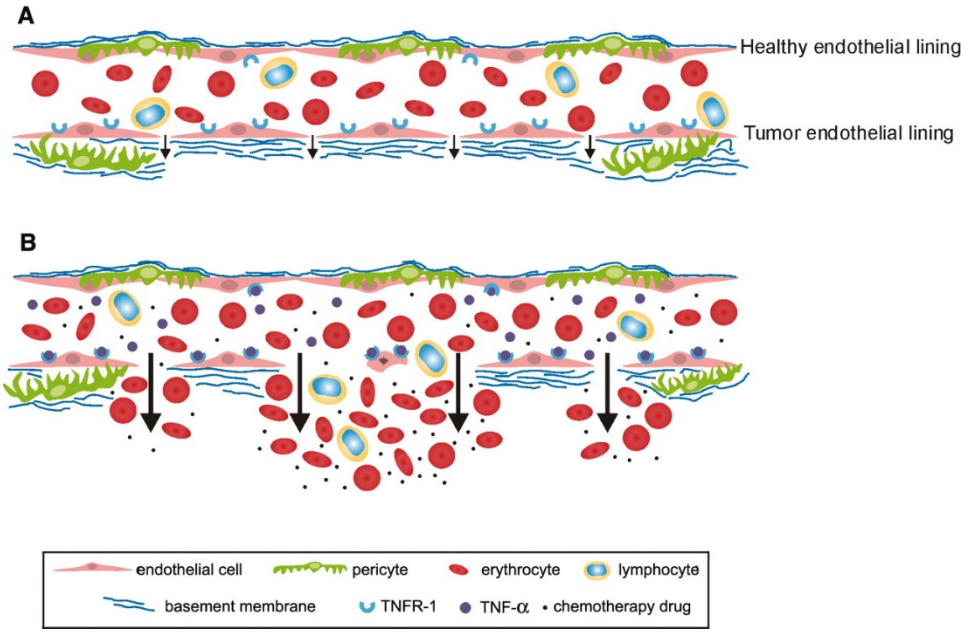

Figure 14: (A) Differences between healthy and tumor endothel lyer. (B) Effects after TNF-α treatment adopted from Ref**[B104]**.

This has a strong effect for the further penetration of nanoparticles into the tumor. As the EPR effect is to that a relative slow process it becomes strongly enhanced by destroyed endothel membrane. This leads to an extensive extravasation of the blood components into the tumour tissue.[B104] This makes it possible for a deeper penetration of polymersomes. When TNF-α is released in deeper layers it leads to a necrotic death of the tumor cells. At same time there is an activation of the immune cells happening like the macrophages through the TNF-α and cell fragments of dying cells which can now also penetrate depper. This leads in the sum to an inflammatory reaction against the tumor while further TNF-α is released leading in the end to necrosis of the tumor.

Strain promoted Azide Alkyne Cycloaddiction (SPAAC)

An attractive method to obtain polymer bioconjugates, the most important starting materials for biomedical applications, is the concept of click chemistry developed from Sharpless et al. in 2001.[B105,B106] Under the term click chemistry are summarized reactions which proceed under mild reaction conditions with excellent efficiancy and selectivity for the formation of one single reaction product and a high tolerance for a plurality of functional groups and reaction conditions. [B106-B108]67-69 To stress out from the known reactions is the cupper(I) mediated 1,3 diploare-Cycloaddition between azides and terminal alkynes which were developed almost at the same time from Sharpless[B106] and Medlad[B109] in 2001 and which turned out to be the parade exemplar of click chemistry.[B105,B110]

In contrast to classic 1,3 diploare-Cycloaddition, showed by Huisgen in 1950, which have to conduct at high temperature and pressure, the Cu mediated azide-alkyne Cycloaddition (CUAAC) is happen even at mild reaction conditions to allow regioselective synthesis of stable 1,4 disubstituated 1,2,3-triazole (reaction B in figure).[B111,B112]

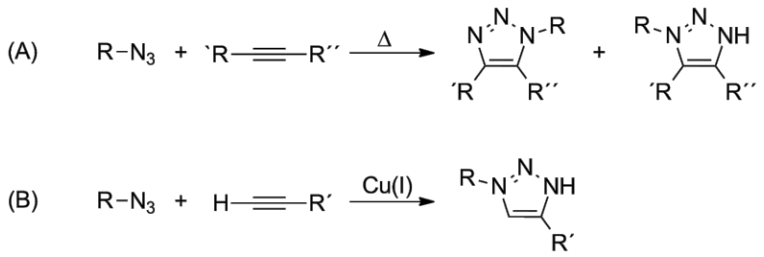

Figure 15: (A) Huisgen-1,3-dipolare Cycloadditon, (B) cupper catalysed azide alkyne cycloaddition adopted from Ref[B113].

A further advantage of CuAAC is the distinct bioorthogonality of the used azide and alkyne groups. These groups have small sizes, dispose a high intrinsic energy, are practically not to find in biological systems and do not have a natural reaction partner.[B107]

This is the reason why CuAAC, besides other reactions, is count to the group of bioorthogonal ligation, which are characterized that they not access in biological processes, conduct with a high rate under physiologic conditions and are inert in regard in vivo arised functionality.[B112]

This high synthetic potential allows functionalisation and ligation of biological systems where the sythesis of polymer bioconjugates and functionalisation of polymer nanoparticles under the use of azide- or alkyne functionalized initiatiors is possible, respectively.[B105,B114]

Despite this outstanding properties an application in living organism is not possible as the oligated cupper catalysts are high toxic. To achieve a better biocompatibility, Bertozzi et al. in 2004 achieve an activation of the alkynes due to ring tension.[B107]
In this so called ring tension mediated azide-alkyne-cycloaddition (SPAAC) there is a massive bond angle deformation in the cyclooctyne which leads to a destabilization of the ground state in regard to the transition state resulting in a distinct speedup of the reaction.[B111]

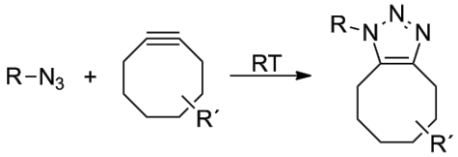

Figure 16: Strain promoted azide alkyne cycloaddition (SPAAC) adopted from Ref[B113].

Already acquired in first trials there could be shown the successful reaction of the bioconjugation between cyclooctyne derivates (figure OCT) and azide functionaled cell surface glykanen under physiologic conditions without addition of adjuvants. Zytotoxic side reactions in cells could not be observed. However the reaction speed of the first generation of ring tension mediated cycloaddition was clearly lower in regard to CuAAC, but showed typically click properties as they turned out to be chemoselective and accomplishable under physiologic conditions.[B112,B114] In contrast to cupper mediated the ring tension mediated AAC is not regioselective.[B112] To achieve a higher reaction speed it was synthesized certain molecules with electron

drawing fluor atoms at the propargyl position.[B115] With the difluorinated cyclooctyne derivate (figure DIFO) it could be achieve a similar reaction rate as in the case of CuAAC why the reaction between DIFO and azides form the term of cupper free click chemistry.[B112]

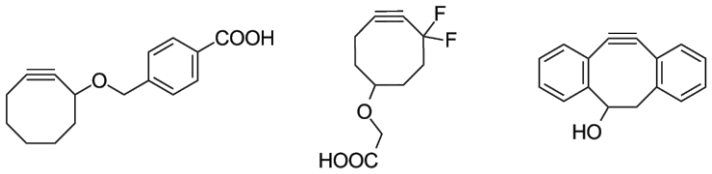

Figure 17: Synthesized cyclooctyne for the cupper free click reaction in living systems adopted from Ref[B113].

Developments were done very fast in which the pharmakokinetic and the properties of water soloubility turned better.[B112] Boons et el al. could synthesize in 2008 the synthesis of 4-Dibenzocyclooctinole (fig. DIBO) which has a higher ring tension due to the aromatic rings and leads to a higher reactivity for azides. Furthermore the hydrogen atoms in ortho position lead to a shielding against nucleophil attack and so care for a stabilisation of the molecule. The hydroxyl group in 4-position offers an additional position for modifications.[B117] The work done by Bertozzi, Boon and co workers create new possibilities for the selective functionalisation and ligation biological species. Cyclooctyne ligations own a high potential in the area of chemist biology and are despite the lack of regioselectivity a promising biocompatible tool in click chemistry.[B114]

Synthesis of functional block copolymers

The requirements of medicine for polymer based drug delivery systems as polymersomes include an extensive control about the properties of the polymers. Besides the low or non toxicity and immunogenicity of the materials the degree of polymerization, dispersity, relative size of each block and architecture of the polymers is important. A very good control about these parameters can be achieved over anionic polymersation but has a high requirement for the synthetic procedure

like an absolute water free condition and furthermore incompatibility of many functional groups. Free radical polymerization in contrary is compatible with many monomers but do have only a restricted reaction control. Synthesized polymers over this procedure show in general a broad molecular weight distribution and different end groups. The free radical polymerisation method is therefore not suitable to obtain defined block structures which is used for polymer vesicle and other nanocarriers. Therefore controlled radical polymerisation techniques referred to *controlled reversible-deactivation radical polymerization* (RDRP 170)[B118] are used in general like Atom Transfer Radical Polymerization (ATRP),[B119,B120] Reversible Addition-Fragmentation Chain Transfer (RAFT)[B121] and Nitroxide-Mediated Polymerization (NMP).[B122] The clue is get a control the polymerisation in the kinetic and to suppress chain termination. The rate $v_{W/A}$ of chain propargation and termination is given below, respectively.

$$v_W = k_W[P\cdot][M] \qquad \{4\}$$

$$v_A = 2k_A[P\cdot]^2 \qquad \{5\}$$

$k_{W/A}$ stands fot the certain rate, $[P\cdot]$ For the concentration and $[M]$ for the monomer concentration. As $[P\cdot]$ has a square dependancy while v_W is first order as to the concentration of active species, the termination reactions are suppressed and one can obtain a narrow molecular weight distribution. This occurs over the interplay of active and sleeping species.

The RAFT process

For synthesis of polymers used for biomedical applications the RAFT process, first reported in 1998 from Moad, Rozzardo and Thang is suitable.[B121] On the one hand the process is compatible with a brad range of monomers Monomertypen (like (meth-)acrylate und –amide, styrol derivates, vinyl esters) and solvents. Also on the

other hand there is no need of transition metals, like in ATRP, which besides the toxicity it is hard to remove from the products.

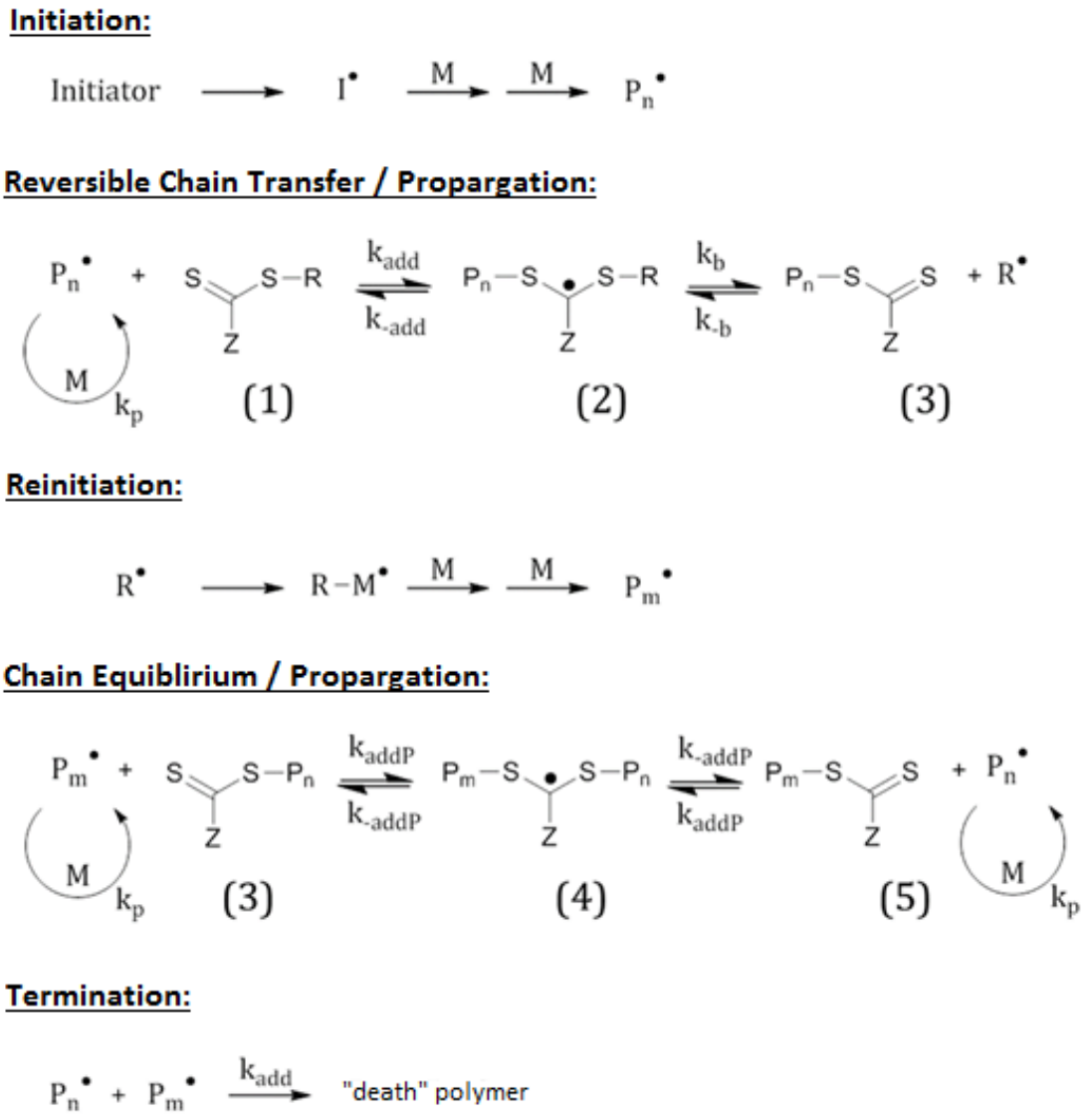

Figure 18: Mechanism of RAFT polymerisation. Adopted and modified from Ref[B123].

The postulated mechanism starts like in the case of free radical polymersiation with the formation of starting radicals from a suitable initiator molecule. They initiate the chain building through addition of monomers. Crucial for the kinetic control of the polymerization is a sequence of additions- and fragmentations equilibrium caused through addition of a suitable thiocarbonyl compound. On this chain transfer agent (1) (CTA) the propargated radical Pn • is added which leads to formation of the intermediate species (2). Its decomposition leads to the release of a radical R • which

can forms with monomer molecules new propargating chains Pm•. This results over the transition state (4) to a fast equilibrium of propargating species Pn• and Pm• and so to a similar growth propability for all chains. For the sequencially process in this order the reactivity of the CTA is crucial. The bond S-R should be split homolytic easy and R• has to be efficient in initiating new chains. The substituent Z should be strong enough to activate the C=S bond for a effectual reactivity of species (1), (3) and (5) and at the same time to stabilize the species (2).[B124] The stabilized radicals (2) can not reinitiate and so decrease the number of active chain ends whereby chain breakup reactions are pushed back. In combination with similar rate of growth the chains lead to a narrow dispersity regarding the molecular weight. For the Z substituents it can be used aryl- or thioalkyl-ligands whereas for *R* it is often used nitrile substituated isobutyl groups.[B125] Species (3) and (5) which are not propargated are referred to the „sleeping" one. When interrupt a RAFT polymerization most of the chains are ending like this.[B123] They can be isolated as stable compounds and used as a macro CTA. This makes the RAFT process to an attractive synthesis method for block architectures whereas it is not possible to obtain in free radical polymerization.

Furthermore the RAFT polymerization has a big advantage as the degree of polymerization (X_n) can be estimated over the ration of the amount of substance.[B126] Hereby the following assumption for X_n of a RAFT polymer is given:

$$X_N = \frac{p' \cdot [M]0}{p'' \cdot [CTA]0 + 2 \cdot f \cdot p''' \cdot [I]0} \qquad \{6\}$$

$[M]_0$, $[CTA]_0$ and $[I]_0$ describe the initial concentrations of monomer, chain transfer agent and initiator, with p', p'', und p''' the conversion, respectively. During the decomposition of the initiator there are two radicals formed the decay rate *f* is supplement wit a factor of 2. The chain transfer agent is used in a high excess relative to the initiator. This makes it possible for the following assumption:

$$p'' \cdot [CTA]_0 \gg 2 \cdot f \cdot p''' \cdot [I]_0 \qquad \{7\}$$

The X_n can then be written:

$$X_n = \frac{p' \cdot [M]_0}{p'' \cdot [CTA]0} \rightarrow X_{N=p} \cdot \frac{M]_0}{[CTA]0} \qquad \{8\}$$

p is here the total efficiancy for the conversion of the RAFT polymerization. Over this the desired molecular weight can be determined:

$$M_{theor.} = X_n \cdot M_{Monomer} + M_{Kettenende} \qquad \{9\}$$

$$\rightarrow M_{theor.} = p \cdot \frac{[M]0}{[CTA]0} \cdot M_{Monomer} + M_{CTA} \qquad \{10\}$$

$M_{Monomer}$ and M_{CTA} are the molecular weights of monomer and CTA.

Reactive ester polymers and their polymer analogues conversion

The subsequently modification of polymers under preservation of its degree of polymerization (polymer analouges reaction) to obtain selective properties is known for a long time. In 1840 Hancock and Ludersdorf observed the change of mechanical properties of kautschuk by treatment with sulfur.[B127] The scope of suitable chemical reactions for polymer analogues modifications was for a long time limited due to the lack of polymerisation techniques for many functional groups.[B128] This changed with the intrduction of RDRP procedure. The most important one in the synthesis of functional polymers for application as therapeutika are the so called active ester. Primary used in the synthesis of peptides, [B129-B132] the concept was adopted from Ringsdorf[B133] and Ferruti[B134] for the polymer chemistry. By using electron withdrawing groups the active ester can react fast, efficient and with a high yield in nucleophilic reactions. Hereby amines are usually used which have a high nucleophilic manner and so can be converted very selective. This conversion gives

the possibility for a manifold functionalisation possibility e.g. the conversion with fluorecence marker or targeting structures. [B135]

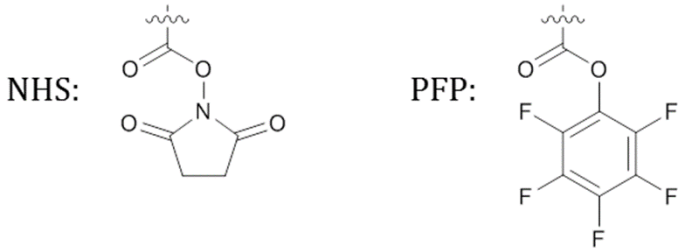

Figure 19: Chemical sturucture of active ester repeating units NHS and PFP adopted from Ref[B0].

As described by Theato and Kakuchi a broad range of suitable compounds are available.[B136,B137] Besides monomers the collection also include active ester modified chain transfer agents which allows a selective end group modification.[B138]

Pentafluorphenyl-acrylat und -methacrylat (PFPMA)[B139] is gaining in importance in the polymerisation to the alternative *N*-Hydroxysuccinimid derivates (NHS). Poly-PFPMA has the advantage in contrary to NHS based Poly-NAS and Poly-NMAS that it is soluble in various organic solvents and has a high reactivity.[B140] For the first time Barz described in 2008 the polymer analogues conversion of PFPMA active ester polymers with 2-Hydroxypropylamin (HPA) to the hydrophilic polymer Poly-HPMA.

Since then there was made manifold approaches for the synthesis of functional and bio compatible polymers and nanoparticles via PFPMA active ester approach.[B141] Hereby also micellar structures for the drug delivery over the blood brain barrier counting in as well as ^{18}F marked polymers for PET inverstigations, p(HPMA)-p(Lys), p(HPMA)-antibody conjugates[B142,B143] and polymeric tensides. This broad scope for functionalisations with good bio compatiblity makes the combination of these two concepts active ester chemistry and RAFT polymerization to a promising approach in the development of future polymeric therapeutics.

Bibliography

[B0] Scherer, M.; Dissertation, Mainz, **2016**

[B1] Letchford, K.; Burt, H. A Review of the Formation and Classification ofAmphiphilic Block Copolymer Nanoparticulate Structures: Micelles, Nanospheres, Nanocapsules and Polymersomes. *Eur. J. Pharm. Biopharm.* **2007**, *65* (3), 259–269.

[B2] Products, N.; For, A.; Or, U. S. E. NANOMEDICINE PRODUCTS APPROVED FOR USE OR IN. **2015**, *9* (1), 1–14.

[B3] Talelli, M.; Barz, M.; Rijcken, C. J.; Kiessling, F.; Wim, E. *Europe PMC Funders Group Core-Crosslinked Polymeric Micelles : Principles , Preparation , Biomedical Applications and Clinical Translation*; 2015; Vol. 10.

[B4] Discher, B. M.; Bermudez, H.; Hammer, D. A.; Discher, D. E.; Won, Y.; Bates, F. S. Cross-Linked Polymersome Membranes : Vesicles with Broadly Adjustable Properties. **2002**, 2848–2854.

[B5] Stoddart, J. F.; Tseng, H. Chemical Synthesis Gets a Fillip from Molecular Recognition and Self-Assembly Processes. **2002**, *99* (8), 4797–4800.

[B6] Lehrbuch, E. Grenzflächen Und Kolloid-Disperse Systeme Wird Sehr Aktuell Benötigt , Da Das Gebiet Der Kolloidchemie Gerade. **2002**, *49* (0), 91022.

[B7] Baldwin, R. L. Temperature Dependence of the Hydrophobic Interaction in Protein Folding. **1986**, *83* (November), 8069–8072.

[B8] Hartley, G. S.; Lindman, B. lMicelles in Aqueous Solution. **1973**, 25–42.

[B9] Tanford, C. The Hydrophobic Effect and the Organization of Living Matter. **1978**, *200* (June).

[B10] Nagarajan, R. Amphiphilic Surfactants and Amphiphilic Polymers : Principles of Molecular Assembly. **2011**, 1–22.

[B11] Schürer, S; Diploma Work, Mainz, **2016**

[B12] Adams, M. L.; Lavasanifar, A.; Kwon, G. S. *J. Pharm. Sci.* **2003**, *92* (7), 1343–1355.

[B13] Torchilin, V. P. *Pharm. Res.* **2007**, *24* (1), 1–16.

[B14] Letchford, K.; Burt, H. *Eur. J. Pharm. Biopharm.* **2007**, *65* (3), 259–269.

[B15] Smart, T.; Lomas, H.; Massignani, M.; Flores-Merino, M. V; Perez, L. R.; Battaglia, G. **2008**, *3* (3), 38–46.

[B16] Blanazs, A.; Armes, S. P.; Ryan, A. J. *Macromol. Rapid Commun.* **2009**, *30* (4-5), 267–277.

[B17] Alexandridis, P.; Lindman, B. *Amphiphilic Block Copolymers: Self-Assembly and Applications*; Elsevier: Amsterdam, 2000.

[B18] Mai, Y.; Eisenberg, A. *Chem. Soc. Rev.* **2012**, *41* (18), 5969.

[B19] Riess, G. *Prog. Polym. Sci.* **2003**, *28* (7), 1107–1170.

[B20] Zhang, P.; Xu, X.; Zhang, M.; Wang, J.; Bai, G.; Yan, H. *Langmuir* **2015**, 150219095049004.

[B21] Jiang, W.; Zhou, Y.; Yan, D. *Chem. Soc. Rev.* **2015**, *44*, 3874–3889.

[B22] Matsen, M. W.; Schick, M. *Curr. Opin. Colloid Interface Sci.* **1996**, *1* (3), 329–336.

[B23] Hajduk, D.; Kossuth, M. B.; Hillmyer, M.; Bates, F. S. *J. Phys. Chem. B* **1998**, *5647* (97), 4269–4276.

[B24] Zhang, L.; Eisenberg, A. *Science (80-.).* **1995**, *268*, 1728–1731.

[B25] Cameron, N. S.; Corbierre, M. K.; Eisenberg, A. *Can. J. Chem.* **1999**, *77*, 1311–1326.

[B26] Zhang, L.; Eisenberg, A. *J. Am. Chem. Soc.* **1996**, *118* (13), 3168–3181.

[B27] Bangham, A. D.; Horne, R. W. *J. Mol. Biol.* **1964**, *8* (5), 660–IN10.

[B28] Torchilin, V. P. *Nat. Rev. Drug Discov.* **2005**, *4* (2), 145–160.

[B29] Drummond, D. C.; Meyer, O.; Hong, K.; Kirpotin, D. B.; Papahadjopoulos, D. *Pharmacol. Rev.* **1999**, *51* (4), 691–744.

[B30] Moghimi, S. M.; Hunter, A. C.; Murray, J. C. *Pharmacol. Rev.* **2001**, *53* (2), 283–318.

[B31] Cho, K.; Wang, X.; Nie, S.; Chen, Z.; Shin, D. M. *Clin. Cancer Res.* **2008**, *14* (5), 1310–1316.

[B32] Senior, J. H. *Crit. Rev. Ther. Drug Carr. Syst.* **1987**, *3*, 123–193.

[B33] Regen, S. L.; Bronislaw, C.; Singh, A. *J. Am. Chem. Soc.* **1980**, *102*, 6638–6640.

[B34] Cho, I.; Chung, K.-C. *Macromolecules* **1984**, *17*, 2935–2937.

[B35] Woodle, M. C.; Lasic, D. D. *Biochim. Biophys. Acta* **1992**, *1113*, 171–199.

[B36] Woodle, M. C. *Adv. Drug Deliv. Rev.* **1998**, *32* (1-2), 139–152.

[B37] Parr, M. J.; Ansell, S. M.; Choi, L. S.; Cullis, P. R. *Biochim. Biophys. Acta* **1994**, *1195*, 21–30.

[B38] Kenworthy, A. K.; Simon, S. A.; McIntosh, T. J. *Biophys. J.* **1995**, *68*, 1903–1920.

[B39] van Hest, J. C.; Delnoye, D.; Baars, M. W.; van Genderen, M. H.; Meijer, E. W. *Science* **1995**, *268* (5217), 1592–1595.

[B40] Zhang, L.; Yu, K.; Eisenberg, A. *Science (80-.).* **1996**, *272* (5269), 1777–1779.

[B41] LoPresti, C.; Lomas, H.; Massignani, M.; Smart, T.; Battaglia, G. Polymersomes: Nature Inspired Nanometer Sized Compartments. *J. Mater. Chem.* **2009**, *19* (22), 3576.

[B42] Georgieva, J. V; Brinkhuis, R. P.; Stojanov, K.; Weijers, C. A. G. M.; Zuilhof, H.; Rutjes, F. P. J. T.; Hoekstra, D.; Hest, J. C. M. Van; Zuhorn, I. S. Peptide-Mediated Blood – Brain Barrier Transport of Polymersomes ** Angewandte. **2012**, 8339–8342.

[B43] Chen, W.; Meng, F.; Cheng, R.; Zhong, Z. pH-Sensitive Degradable Polymersomes for Triggered Release of Anticancer Drugs: A Comparative Study with Micelles. *J. Control. Release* **2010**, *142* (1), 40–46.

[B44] Liu, G.-Y.; Lv, L.-P.; Chen, C.-J.; Liu, X.-S.; Hu, X.-F.; Ji, J. Biocompatible and Biodegradable Polymersomes for pH-Triggered Drug Release. *Soft Matter* **2011**, *7* (14), 6629.

[B45] Meng, F.; Zhong, Z.; Feijen, J. Stimuli-Responsive Polymersomes for Programmed Drug.pdf. **2009**, *10* (2).

[B46] Aranda-Espinoza, H.; Bermudez, H.; Bates, F. S.; Discher, D. E. *Phys. Rev. Lett.* **2001**, *87* (20), 208301.

[B47] Discher, D. E.; Eisenberg, A. *Science* **2002**, *297* (5583), 967–973.

[B48] Thiermann, R. **2014**.

[B49] Uneyama, T. *J. Chem. Phys.* **2007**, *126* (11), 114902–114917.

[B50] Antonietti, M.; Forster, S. *Adv. Mater.* **2003**, *15* (16), 1323–1333.

[B51] He, X.; Schmid, F. *Macromolecules* **2006**, *39* (7), 2654–2662.

[B52] Chen, L.; Shen, H.; Eisenberg, A. *J. Phys. Chem. B* **1999**, *103* (44), 9488–9497.

[B53] Du, J.; Chen, Y. *Macromolecules* **2004**, *37* (15), 5710–5716.

[B54] Adams, D. J.; Adams, S.; Atkins, D.; Butler, M. F.; Furzeland, S. *J. Control. Release* **2008**, *128* (2), 165–170.

[B55] Brinkhuis, R. P. Polymeric Vesicles for drug delivery over the blood-brain barrier and in vivo imaging, Radboud Universiteit Nijmegen, 2012.

[B56] Luo, L.; Eisenberg, A. *Langmuir* **2001**, *17* (22), 6804–6811.

[B57] Rodriguez-Garcia, R.; Mell, M.; Lopez-Montero, I.; Netzel, J.; Hellweg, T.; Monroy, F. *Soft Matter* **2011**, *7* (4), 1532.

[B58] Bermudez, H.; Brannan, A. K.; Hammer, D. A.; Bates, F. S.; Discher, D. E. *Macromolecules* **2002**, *35*, 8203–8208.

[B59] Opsteen, J. A.; Cornelissen, J. J. L. M.; Hest, J. C. M. Van. *Pure Appl. Chem.* **2004**, *76*, 1309–1319.

[B60] Chang, H.; Sheng, Y.; Tsao, H. *Soft Matter* **2014**, *10*, 6373–6381.

[B61] Lee, J. C. M.; Santore, M.; Bates, F. S.; Discher, D. E. *Macromolecules* **2002**, *35* (2), 323–326.

[B62] Dimova, R.; Seifert, U.; Pouligny, B.; Forster, S.; Dobereiner, H.-G. *Eur. Phys. J. E* **2002**, *250*, 241–250.

[B63] Lorenceau, E.; Utada, A. S.; Link, D. R.; Cristobal, G.; Joanicot, M.; Weitz, D. A. *Langmuir* **2005**, *21* (20), 9183–9186.

[B64] Napoli, A.; Valentini, M.; Tirelli, N.; MUller, M.; Hubbell, J. A. *Nat. Mater.* **2004**, *3*, 183–189.

[B65] Checot, F.; Brulet, A.; Oberdisse, J.; Gnanou, Y.; Mondain-Monval, O.; Lecommandoux, S. *Langmuir* **2005**, *21* (10), 4308–4315.

[B66] Ahmed, F.; Photos, P. J.; Discher, D. E. *Drug Dev. Res.* **2006**, *67*, 4–14.

[B67] Discher, D. E.; Ahmed, F. *Annu. Rev. Biomed. Eng.* **2006**, *8*, 323–341.

[B68] Le Meins, J.-F.; Sandre, O.; Lecommandoux, S. *Eur. Phys. J. E. Soft Matter* **2011**, *34* (2), 1–17.

[B69] Zhang, L.; Eisenberg, A. Multiple Morphologies and Characteristics of " Crew-Cut " Micelle-like Aggregates of Polystyrene- B -Poly (Acrylic Acid) Diblock Copolymers in Aqueous Solutions. **1996**, No. 24, 3168–3181.

[B70] Battaglia, G.; Ryan, A. J.; Tomas, S.; February, R. V; Final, I.; April, F. Polymeric

Vesicle Permeability : A Facile Chemical Assay. **2006**, No. 13, 4910–4913.

[B71] Battaglia, G.; Ryan, A. J.; Building, D.; Uni, T.; Hill, B.; Sheffield, S. Pathways of Polymeric Vesicle Formation. **2006**, 10272–10279.

[B72] Sw, L. Pressure-Jump X-Ray Studies of Liquid Crystal Transitions in Lipids. **2006**, No. August, 2635–2655.

[B73] Biochimica 1979.9.pdf.

[B74] Massing, U.; Cicko, S.; Ziroli, V. Dual Asymmetric Centrifugation (DAC)-A New Technique for Liposome Preparation. *J. Control. Release* **2008**, *125* (1), 16–24.

[B75] Hirsch, M.; Ziroli, V.; Helm, M.; Massing, U. Preparation of Small Amounts of Sterile siRNA-Liposomes with High Entrapping Ef Fi Ciency by Dual Asymmetric Centrifugation (DAC). *J. Control. Release* **2009**, *135* (1), 80–88.

[B76] Huang, Z.; Li, X.; Zhang, T.; Song, Y.; She, Z.; Li, J. ScienceDirect Progress Involving New Techniques for Liposome Preparation. *Asian J. Pharm. Sci.* **2014**, *9* (4), 176–182.

[B77] Ehrlich, P. *Int. Wochenschrift fur Wissenschaft, Kunst und Tech.* **1907**, *1*, 125–132.

[B78] Ringsdorf, H. *J. Polym. Sci. Polym. Symp.* **1975**, *51* (1), 135–153.

[B79] Nakaoka, R.; Tabata, Y.; Yamaoka, T.; Ikada, Y. *J. Control. Release* **1997**, *46* (3), 253–261.

[B80] Fox, M. E.; Szoka, F. C.; Frechet, J. M. J. *Acc. Chem. Res.* **2009**, *42* (8), 1141–1151.

[B81] Duncan, R. *Adv. Polym. Sci.* **1984**, *57*, 51–101.

[B82] Duncan, R.; Dimitrijevic, S.; Evagorou, E. G. *STP Pharma Sci.* **1996**, *6*, 237–263.

[B83] Duncan, R. *Nat. Rev. Drug Discov.* **2003**, *2* (5), 347–360.

[B84] Donaruma, L. G. *Prog. Polym. Sci.* **1974**, *4*, 1–25.

[B85] *Handbook of Anticancer Drug Development*; Budman, D. R., Calvert, A. H., Rowinsky, E. K., Eds.; Lippincott Williams and Wilkins: Philadelphia, 2003.

[B86] Veronese, F. M.; Harris, J. M. *Adv. Drug Del. Syst.* **2002**, *54*, 453–609.

[B87] Harris, J. M.; R.B., C. *Nat. Rev. Drug Discov.* **2003**, *2*, 214–221.

[B88] Masayuki, Y.; Mizue, M.; Noriko, Y.; Teruo, O.; Yasuhisa, S.; Kazunori, K.; Shohei, I. *J. Control. Release* **1990**, *11* (1-3), 269–278.

[B89] Kabanov, A. V.; Felgner, P. L.; Seymour, L. W. *Self-assembling Complexes for Gene Delivery. From Laboratory to Clinical Trial*; Wiley: Chichester, 1998.

[B90] Duncan, R. Polymer Conjugates for Tumour Targeting and Intracytoplasmic Delivery. The EPR Effect as a Common Gateway? *Pharmaceutical Science and Technology Today*. 1999, pp 441–449.

[B91] Thambi, T.; Park, J. H.; Lee, D. S. Biomaterials Science Cancer Therapy. **2016**, 55–69.

[B92] Haag, R.; Kratz, F. Polymere Therapeutika: Konzepte Und Anwendungen. *Angew. Chem.* **2006**, *118* (8), 1218–1237.

[B93] Maeda, H. The Enhanced Permeability and Retention (EPR) Effect in Tumor Vasculature: The Key Role of Tumor-Selective Macromolecular Drug Targeting. *Adv. Enzyme Regul.* **2001**, *41* (00), 189–207.

[B94] Maeda, H.; Wu, J.; Sawa, T.; Matsumura, Y.; Hori, K. Tumor Vascular Permeability and the EPR Effect in Macromolecular Therapeutics: A Review. *J. Control. Release* **2000**, *65* (1-2), 271–284.

[B95] Maeda, H. Enhanced Permeability and Retention (EPR) Effect: Basis for Drug Targeting to Tumors. In *Biomedical aspects of drug targeting*; 2003; pp 211–228.

[B96] Gallium-68 Radiotracers for Alzheimer ' S Plaque Imaging Gallium-68 Radio Tracers for Alzheimer ' S Plaque I Maging. **2015**, No. August 2016.

[B97] Focus, N. Cancer Immunotherapy. **2013**, *342* (December), 1432–1434.

[B98] Yang, Y. Cancer Immunotherapy : Harnessing the Immune System to Battle Cancer. **2015**, *125* (9), 3335–3337.

[B99] Carswell, E. A.; Old, L. J.; Kassel, R. L.; Green, S. An Endotoxin-Induced Serum Factor That Causes Necrosis of Tumors Immunology : **1975**, *72* (9), 3666–3670.

[B100] Cai, W.; Kerner, Z. J.; Hong, H.; Sun, J. Targeted Cancer Therapy with Tumor Necrosis Factor-Alpha. *Biochem. Insights* **2008**, *2008*, 15–21.

[B101] Sidhu, R. S.; Bollon, A. P. Tumor Necrosis Factor Activities and Cancer Therapy - A Perspective. *Pharmacol. Ther.* **1993**, *57* (1), 79–128.

[B102] Black, R. A. Tumor Necrosis Factor-α Converting Enzyme. *Int. J. Biochem. Cell Biol.* **2002**, *34* (1), 1–5.

[B103] Balkwill, F. Tumour Necrosis Factor and Cancer. *Nat. Rev. Cancer* **2009**, *9* (5), 361–371.

[B104] van Horssen, R.; Ten Hagen, T. L.; Eggermont, A. M. TNF-Alpha in Cancer Treatment: Molecular Insights, Antitumor Effects, and Clinical Utility. *Oncologist* **2006**, *11* (4), 397–408.

[B105] Lutz, J.-F. *Angew. Chem. Int. Ed. Engl.* **2007**, *46*, 1018–1025.

[B106] Lutz, J.-F.; Börner, H. G.; Weichenhan, K. *Macromolecules* **2006**, *39*, 6376–6383.

[B107] Kolb, H. C.; Finn, M. G.; Sharpless, K. B. *Angew. Chemie Int. Ed.* **2001**, *40*, 2004–2021.

[B108] King, M.; Wagner, A. *Bioconjug. Chem.* **2014**, *25*, 825–839.

[B109] Hawker, C. J.; Fokin, V. V.; Finn, M. G.; Sharpless, K. B. *Aust. J. Chem.* **2007**, *60*, 381.

[B110] Tornøe, C. W.; Christensen, C.; Meldal, M. *J. Org. Chem.* **2002**, *67*, 3057–3064.

[B111] Baskin, J. M.; Prescher, J. A.; Laughlin, S. T.; Agard, N. J.; Chang, P. V; Miller, I. A.; Lo, A.; Codelli, J. A.; Bertozzi, C. R. *Proc. Natl. Acad. Sci. U. S. A.* **2007**, *104*, 16793–16797.

[B112] Agard, N. J.; Prescher, J. A.; Bertozzi, C. R. *J. Am. Chem. Soc.* **2004**, *126*, 15046–15047.

[B113] Sletten, E. M.; Bertozzi, C. R. *Angew. Chemie* **2009**, *121*, 7108–7133.

[B114] Sletten, E. M.; Bertozzi, C. R. *Acc. Chem. Res.* **2011**, *44*, 666–676.

[B115] Lutz, J.-F. *Angew. Chemie* **2008**, *120*, 2212–2214.

[B116] Mbua, N. E.; Guo, J.; Wolfert, M. A.; Steet, R.; Boons, G.-J. *Chembiochem* **2011**, *12*, 1912–1921.

[B117] Ning, X.; Guo, J.; Wolfert, M. A.; Boons, G.-J. *Angew. Chem. Int. Ed. Engl.* **2008**, *47*, 2253–2255.

[B118] Jenkins, A. D.; Jones, R. G.; Moad, G. *Pure Appl. Chem.* **2009**, *82* (2), 483–491.

[B119] Kato, M.; Kamigaito, M.; Sawamoto, M.; Higashimuras, T. *Macromolecules* **1995**, *28*, 1721–1723.

[B120] Wang, J.-S.; Matyjaszewski, K. *Macromolecules* **1995**, *28* (23), 7901–7910.

[B121] Chiefari, J.; Chong, Y. K. B.; Ercole, F.; Krstina, J.; Jeffery, J.; Le, T. P. T.; Mayadunne, R. T. A.; Meijs, G. F.; Moad, C. L.; Moad, G.; Rizzardo, E.; Thang, S.H.; South, C. *Macromolecules* **1998**, *31*, 5559–5562.

[B122] Salomon, D. H.; Rizzardo, E.; Cacioli, P.; 1985; Polymerization process and

polymers produced thereby. US Patent 4,581,429, 1985.

[B123] Moad, G.; Rizzardo, E.; Thang, S. H. *Aust. J. Chem.* **2012**, *65*, 985–1076.

[B124] Moad, G.; Barner-Kowollik, C. In *Handbook of RAFT Polymerization*; Barner-Kowollik, C., Ed.; Wiley-VCH: Weinheim, 2008.

[B125] Moad, G.; Rizzardo, A. E.; A, S. H. T. *Aust. J. Chem.* **2006**, 669–692.

[B126] Moad, G.; Chong, Y. K.; Postma, A.; Rizzardo, E.; Thang, S. H.; *Polymer (Guildf).* **2005**, *46* (19 SPEC. ISS.), 8458–8468.

[B127] Cunningham, W. a. *J. Chem. Educ.* **1935**, *12* (3), 120–124.

[B128] Gunay, K. A.; Theato, P.; Klok, H.-A. In *Functional Polymers by Post-Polymerization Modification*; Theato, P., Klok, H.-A., Eds.; Wiley-VCH; Weinheim, 2013.

[B129] Wieland, T.; Schafer, W.; Bokelmann, E. *Ann. der Chemie* **1951**, *7*, 99–104.

[B130] Schwyzer, R.; Iselin, B.; Feurer, M. *Helv. Chim. Acta* **1954**, *1* (7), 69–79.

[B131] Farrington, J. A.; Hextall, P. J.; Kenner, G. W.; Turner, J. M. *J. Chem. Soc.* **1957**, 1407–1413.

[B132] Anderson, G. W.; Zimmerman, J. E.; Callahan, F. M. *J. Am. Chem. Soc.* **1964**, *86* (9), 1839–1842.

[B133] Batz, H. G.; Franzmann, G.; Ringsdorf, H. *Angew. Chem. Int. Ed. Engl.* **1972**, *11* (12), 1103–1104.

[B134] Ferruti, P.; Bettelli, A.; Fere, A. *Polymer (Guildf).* **1972**, *13*, 462–464.

[B135] Gauthier, M. A.; Gibson, M. I.; Klok, H.-A. *Angew. Chemie* **2009**, *121* (1), 50–60.

[B136] Theato, P. *J. Polym. Sci. Part A-Polymer Chem.* **2008**, *46* (3), 6677–6687.

[B137] Kakuchi, R.; Theato, P. In *Functional Polymers by Post-Polymerization Modification*; Theato, P., Klok, H.-A., Eds.; Wiley-VCH: Weinheim, 2013.

[B138] Roth, P. J.; Jochum, F. D.; Zentel, R.; Theato, P. *Biomacromolecules* **2010**, *11*, 238–244.

[B139] Eberhardt, M.; Theato, P. *Macromol. Rapid Commun.* **2005**, *26* (18), 1488–1493.

[B140] Eberhardt, M.; Mruk, R.; Zentel, R.; Theato, P. *Eur. Polym. J.* **2005**, *41* (7), 1569–1575.

[B141] Barz, M.; Tarantola, M.; Fischer, K.; Schmidt, M.; Luxenhofer, R.; Janshoff, A.; Theato, P.; Zentel, R. *Biomacromolecules* **2008**, *9* (11), 3114–3118.

[B142] Tappertzhofen, K.; Bednarczyk, M.; Koynov, K.; Bros, M.; Grabbe, S.; Zentel, R.
Macromol. Biosci. **2014**, *14* (10), 1444–1457.
[B143] Tappertzhofen, K.; Weiser, F.; Montermann, E.; Reske-Kunz, A.; Bros, M.; Zentel, R. *Macromol. Biosci.* **2015**

Chapter 4: Stimuli responsive (smart) Polymersomes

It was shown in a previous research work the possibility to degrade polymersomes after 48 h formed by amphiphilic blockcopolymers at pH 4,5 through the introduction of 30 % of pH sensitive units, 4-(2-Hydroxyethyl)-2,2-dimethyl-1,3-dioxolan (DDEMA), regarding the LMA ratio.[A0]

The goal in this chapter is to generate a new synthetic procedure to modify the pH labile amphiphilic blockcopolymers with a higher ratio of DDEMA (40 %) to enhance the pH response. Furthermore a second monomer was statistically copolymerized, namely hydrody-hexylmethacrylate (HHMA), which facilitate the hydrolysis and makes it possible to obtain degradable particles at a pH of 5 as confirmed by DLS kinetic measurements.

Furthermore a new synthetic procedure for the introduction of redox sensitive units is presented in which the particles can be reductive degraded with a GSH solution. The redox responsive units were incorporated into the hydrophobic as well as in the hydrophilic domains of the amphiphilic blockcopolymer.

Generating smart polymersomes with pH responsive polymers

Polymersomes formed by amphiphilic blockcopolymers p(DHPA)-*b*-p(LMA) have a robust structure and are more stable than liposomes regarding the incorporation of hydrophilic cargos into the inner aqueos interior.[B0] Due to their high molecular weight the possibility to aggregate with other vesicles or cell compartments is

strongly restricted. To facilitate the release of the cargo different approaches were developed over time in which the polymersomes could be destabilized referred in this work to smart polymersomes.

For the amphiphilic polymer systems used in this work it is difficult and limited to generate redox sensitive units as the procedure steps of the synthesis go through RAFT and subsequently polymer analogoues reaction. So for these systems a pH indicated response of the vesicles is generated and due to hydrolysis the polarity of the certain repeating unit increases. Hereby, the hydrophobicity of the total water unsoluble block is reduced strongly leading to decomposition of the double layered membrane and the vesicle degrade as shown in figure 4.1.

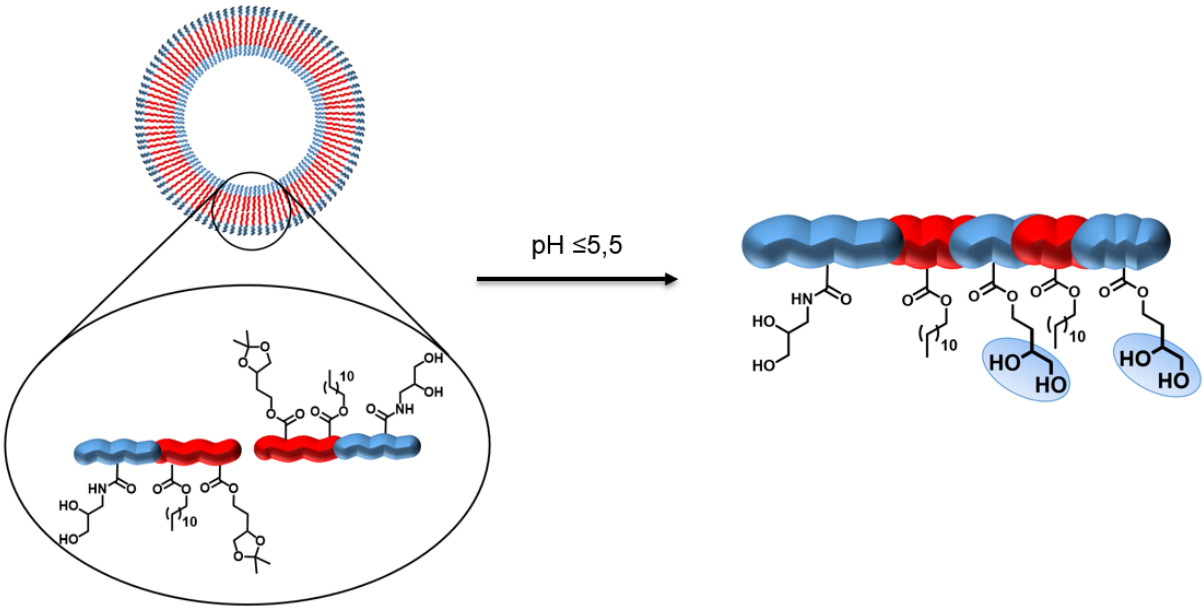

Figure 4.1: pH responsive decomposition of double layered membrane.

For this purpose monomers like (2,2-Dimethyl-1,3-dioxolan-4-yl)methylmethacrylate (Solketal-Methacrylate, DMDMA) are suitable. The polymerization and hydrolysis was first reported by Beinert et al. The protection group acetone is released and the deprotected hydroxy groups increase strongly the water solubility. This mechanism for acid induced degradation of micelles was used by Zhang and Louage which contained the acrylate as analogous.[C1,C2]

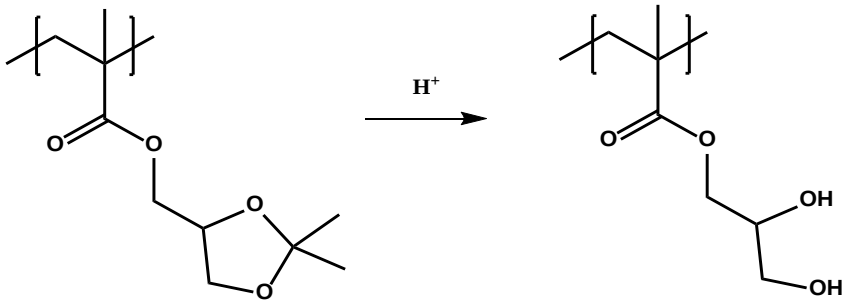

Figure 4.2: Hydrolysis of Solketal-Metacrylate.

The ester group of DMDMA is due to the stronger electronegative oxygen atom in the periphery to the α carbon atom a weak active ester. Therefore the side reaction in the aminolysis process can happen with the DMDMA repating unit. To eliminate this problem it was extend with one methylen group in the case of the solketal monomer.

In this work, the synthesis of 4-(2-Hydroxyethyl)-2,2-dimethyl-1,3-dioxolan (DDEMA) was done over a 2 step reaction starting from protection of 1,2,4-butanetriol followed by addition of methacryloylchloride with use of triethylamine as helping base and dry diethylether.

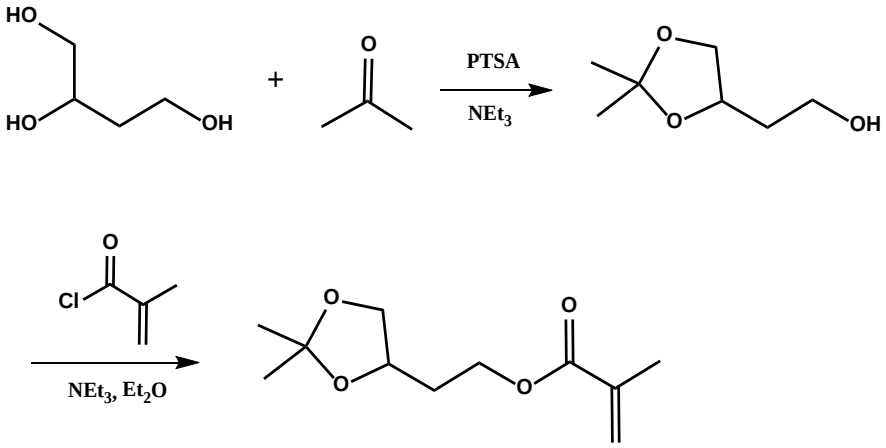

Figure 4.3: Synthesis of 4-(2-Hydroxyethyl)-2,2-dimethyl-1,3-dioxolane (DDEMA).

After precipitation and purification over a column chromatography (Cyclohexan/Ethylacetate (8/1)) the product was obtained as a colorless oil in 65 % yield. The revealed ^{1}H-NMR spectrum shows that DDEMA could be isolate in good purity. Also traces of solvents are in the spectrum which are important as the monomer in total dry state tend to an extreme fast polymerization.

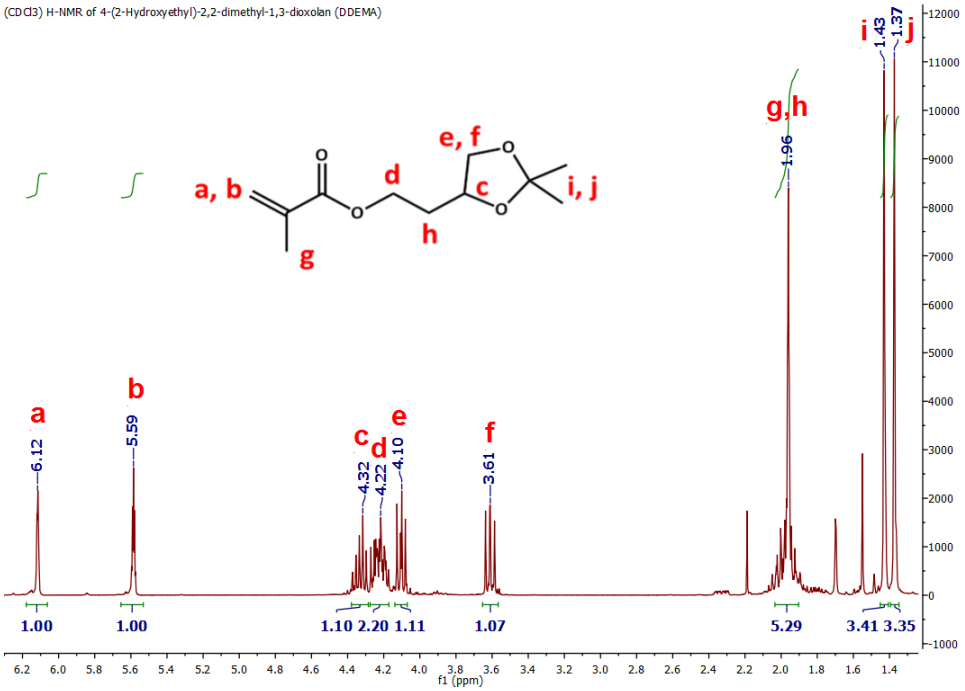

Figure 4.4: ^{1}H-NMR of DDEMA.

Previous work (30 % of pH labile units)

Dr. Martin Scherer synthesized the polymer p(LMA$_{16}$-stat-DDEMA$_{6}$)-*b*-p(PFPMA)$_{21}$ in a ratio for the educt monomers LMA/DDEMA of 7/3 with a molecular weight of 10.7 kDa and a PDI of 1,11.[A1] The ^{1}H-NMR spectra is given in the following figure.

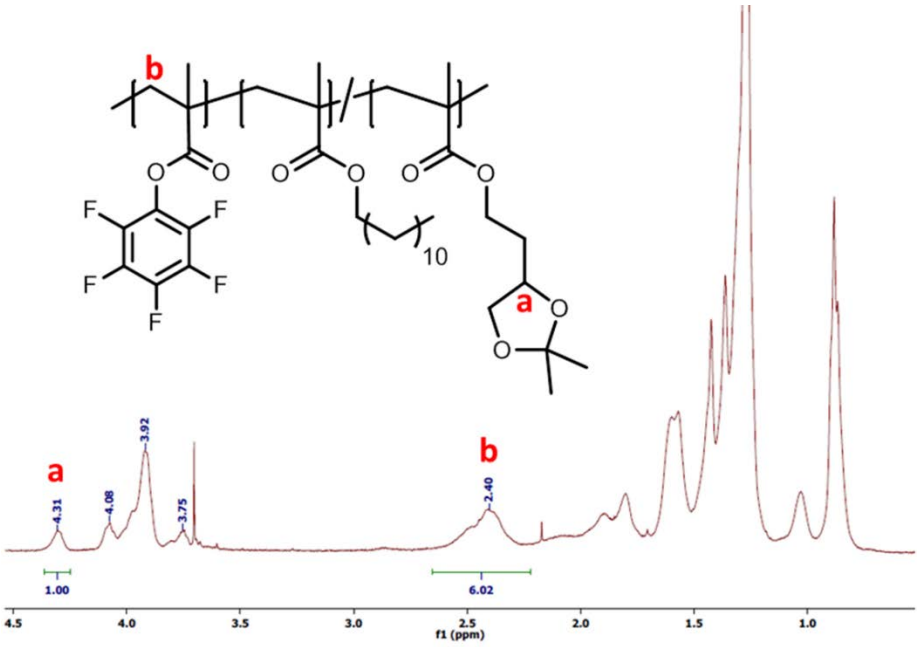

Figure 4.5: ^{1}H-NMR of statistically copolymerized DDEMA adopted from Ref[B0].

After CTA end group removal and aminolysis with DHPA the obtained amphiphilic blockcopolymer p(LMA_{16}-*stat*-$DDEMA_6$)-*b*-p$(DHPA)_{21}$ synthesized by Dr. Martin Scherer[B0] with a molecular weight of 8.8 kDa and a PDI of 1,27 was used for pH degradation studies after 48 h of incubation time. Herefore the polymersomes were formed over a phase inversion technique in a 5 mM NaCl solution and extruded to an unitary hydrodynamic radius of R_h = 100 nm. In comparison analogue prepared polymersomes without the pH sensitive group with a similar molecular weight of 8.9 kDa were performed. The vesicle dispersions were aliquoted and acidified with HCl on a pH of 6,5/6,0/5,5/4,5/3,0. The final polymer concentrations were 10 mg/L. After 48 h of incubation time the particles were investigated over dynamic light scattering at a scattering angle of 90°.

As it can be seen that in the case of the particles without a pH sensitive group the stability is still given at pH 6 and pH 4,5. There is no degradation occuring as it is possible to measure a sensible correlation function.

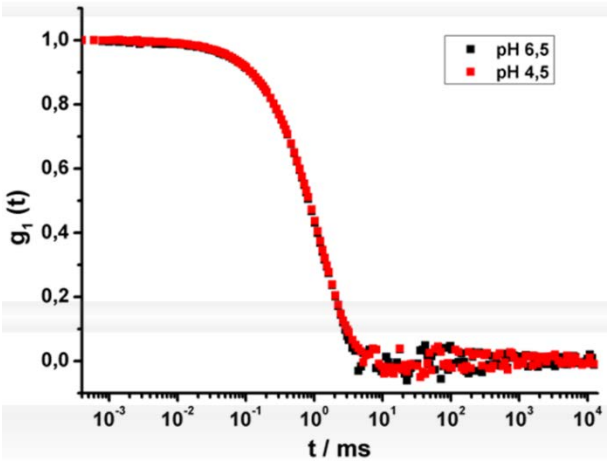

Figure 4.6: DLS measurements of non pH labile blockcopolymers preincubated at pH 6,5 and 4,5 adopted from Ref[B0].

However the particles containing the pH sensitive groups remain stable at pH 6,5 but degrade at pH 4,5 as there is no correlation function measurable.

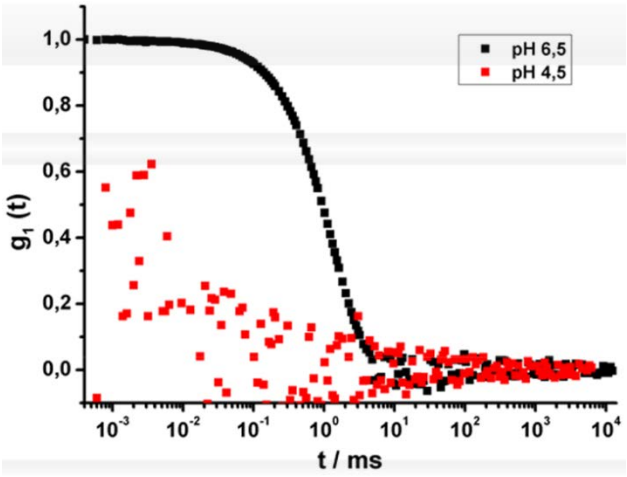

Figure 4.7: DLS measurements of pH labile blockcopolymers preincubated at pH 6,5 and 4,5 adopted from Ref[B0].

New synthetic procedure to obtain enhanced pH responsive polymers

pH of 4,5 is too strongly acidic as for applications in the biomedical field a degradation at a higher pH around 5 - 5,5 is desired as the milieu and environment of cancer cells are in this range. The question here to be solved is to make it possible that the hydrolysis happening at higher pH values and the H^+ atoms can reach the pH sensitive ester units leading to degradation of the vesicle.

For this purpose it was synthesized in this chapter a new polymer with a higher amount of pH sensitive groups in a ratio for the educt monomers of LMA/DDEMA of 6/4 to yield the resulting final amphiphilic blockcopolymer p(LMA-stat-DDEMA)-*b*-(DHPA) which is referred to **SC**.

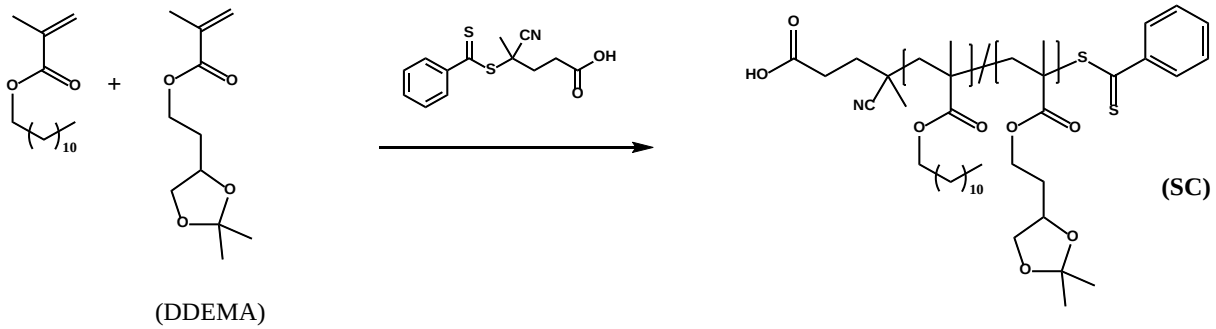

Figure 4.8: Copolymerisation with pH labile units over RAFT (DDEMA).

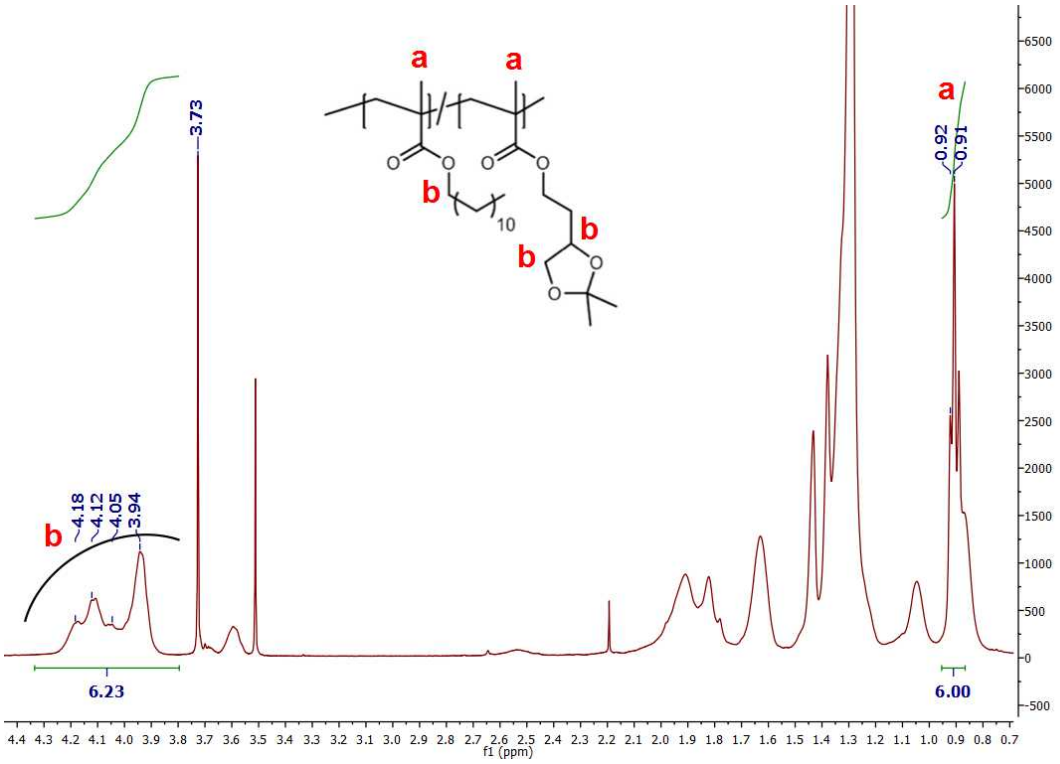

Figure 4.9: ^{1}H-NMR of statistically copolymerized DDEMA with LMA.

The analysis for the composition of **SC** was done via ^{1}H-NMR with the signals in the area of δ = 4,28 – 3,81 ppm. It was normed on the methyl groups of each polymer unit in the area of δ = 0,81 – 0,96 ppm. The integral **b** (I=6,23) is given by the two methylen groups H_b of the dioxalan ring, the α methylengroup of the dodecylester as well as the single hydrogen group in the dioxalan ring. Due to the normation on methyl groups of the polymer units the ratio of H_b protons is $I(H_b)=3$ and it remains $I(\alpha\text{-}CH_2)=3{,}23$. So the number for the repeating units of LMA per DDEMA unit is given in the following equation:

$$\frac{3{,}23}{2} = 1{,}62 \qquad \{4.1\}$$

This results for the amount of substance

$$1 - \left(\frac{1{,}62}{1{,}62 + 1}\right) = 38{,}2\ \% \quad \{4.2\}$$

For the used ratio of n(LMA)/n(DDEMA) of 6/4 it could be obtained the desired ratio to 95,5 %. So the composition of the statistically polymer **SC** is p(LMA_{10}-stat-$DDEMA)_6$.

Table 4.1: Analysis of p(LMA-stat-DDEMA) **SC**.

Polymer	Composition [a]	M_n/g*mol^{-1} [b]	PDI [b]
SC	p(LMA_{10}-stat-$DDEMA_6$)	4000	1,11

[a] obtained over H-NMR and THF-GPC, [b] obtained over THF-GPC

Using polymer **SC** as a macro CTA a blockcopolymer p(LMA-stat-DDEMA)-*b*-p(PFPMA) (**BS**) was synthesized for conversion via aminolysis with DHPA to the amphiphilic blockcopolymer p(LMA-stat-DDEMA)-*b*-p(DHPA) (**BS**).

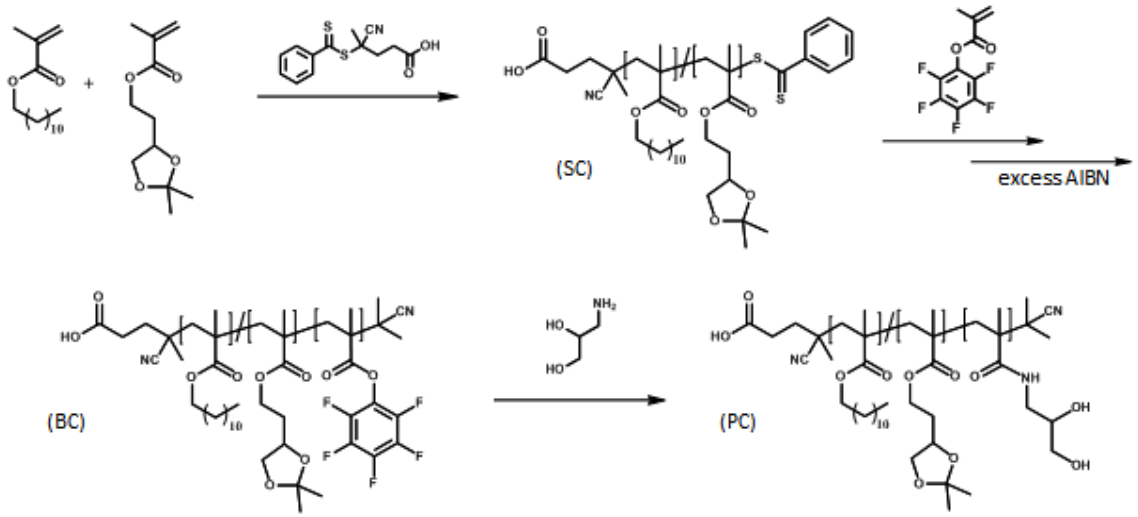

Figure 4.10: Blockcopolymerisation with PFPMA **(BC)**, end group removal and conversion to amphiphilic blockcopolymer **(PC)**.

Table 4.2: Analysis of p(LMA_{10}-stat-$DDEMA_6$)-*b*-$p(PFPMA)_{20}$ **BC**.

Polymer	Composition [a]	M_n/g*mol^{-1} [a]	PDI [a]
BC	p(LMA_{10}-stat-$DDEMA_6$)-*b*-$(PFPMA)_{20}$	9200	1,15

[a] obtained over THF-GPC

After removal of the CTA end group with AIBN and polymer analogous conversion with DHPA it was able to obtain the amphiphilic blockcopolymer p(LMA_{10}-stat-$DDEMA_6$)-*b*-$(DHPA)_{20}$ (**PC**).

Table 4.3: Analysis of p(LMA_{10}-stat-$DDEMA_6$)-*b*-$(DHPA)_{20}$ (**PS**).

Polymer	Composition [a)]	M_n/g*mol^{-1} [a)]	PDI [a)]
PC	p(LMA_{10}-stat-$DDEMA_6$)-*b*-$(DHPA)_{20}$	5100	1,36

[a)] obtained over HFIP-GPC

Table 4.4 summarizes the polymers synthesized with pH labile units.

Table 4.4: Analysis of polymers with DDEMA.

Polymer	Composition [a)]	M_n/g*mol^{-1}	PDI
SC	p(LMA_{10}-stat-$DDEMA_6$)	4000 [a)]	1,11 [a)]
BC	p(LMA_{10}-stat-$DDEMA_6$)-*b*-$(PFPMA)_{20}$	9200 [a)]	1,15 [a)]
PC	p(LMA_{10}-stat-$DDEMA_6$)-*b*-$(DHPA)_{20}$	5100 [b)]	1,36 [b)]

[a)] obtained over H-NMR and THF-GPC, [b)] obtained over HFIP-GPC

(40 % of pH labile units with HHMA)

Furthermore a co-monomer was statistically copolymerized namely hydrody-hexylmethacrylate referred to „HHMA“ in a ratio of 10 % of n(DDEMA).

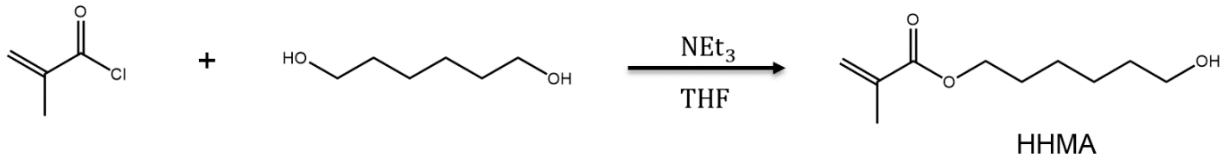

Figure 4.11: Synthesis of Hydrodyhexylmethacrylate (HHMA).

This monomer has a longer alkyl chain and one hydroxy group at the end which can be used to facilitate the desired hydrolysis at certain pH values when it is in the periphery of the pH labile ester. It was used an hexyl derivate as one has to keep in mind not to change to strong the hydrophilic weight fraction which is very important for the formation of polymersomes. Furthermore its incorporation into the hydrophobic domain hast o be consider as it posses a certain hydrophilic character through its hydroxy group. The synthetic procedere is given in the figure 4.11. Here, DDEMA and HHMA were mixed together and polymerized statistically with LMA as the first block to yield p(LMA-*stat*-DDEMA-*stat*-HHMA) (**SH**).

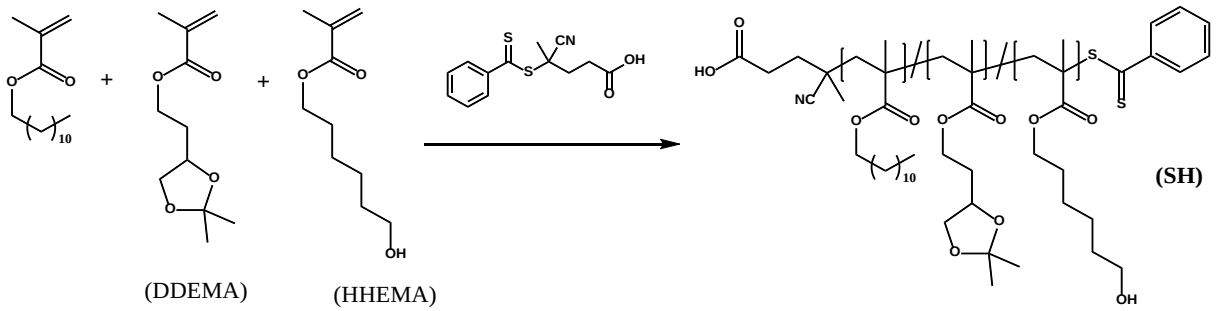

Figure 4.12: Statistically copolymerization of DDEMA and HHMA with LMA.

The composition of the polymer was determined over inverse gated (ig) ^{13}C-NMR spectroscopy as over ^{1}H-NMR the significant signals of each monomers are overlapping which makes it difficult to distinguish. But over ig ^{13}C-NMR due to the suppression of the Core-Overhauser-Effect the spectra could be analysed in a quantitative manner.

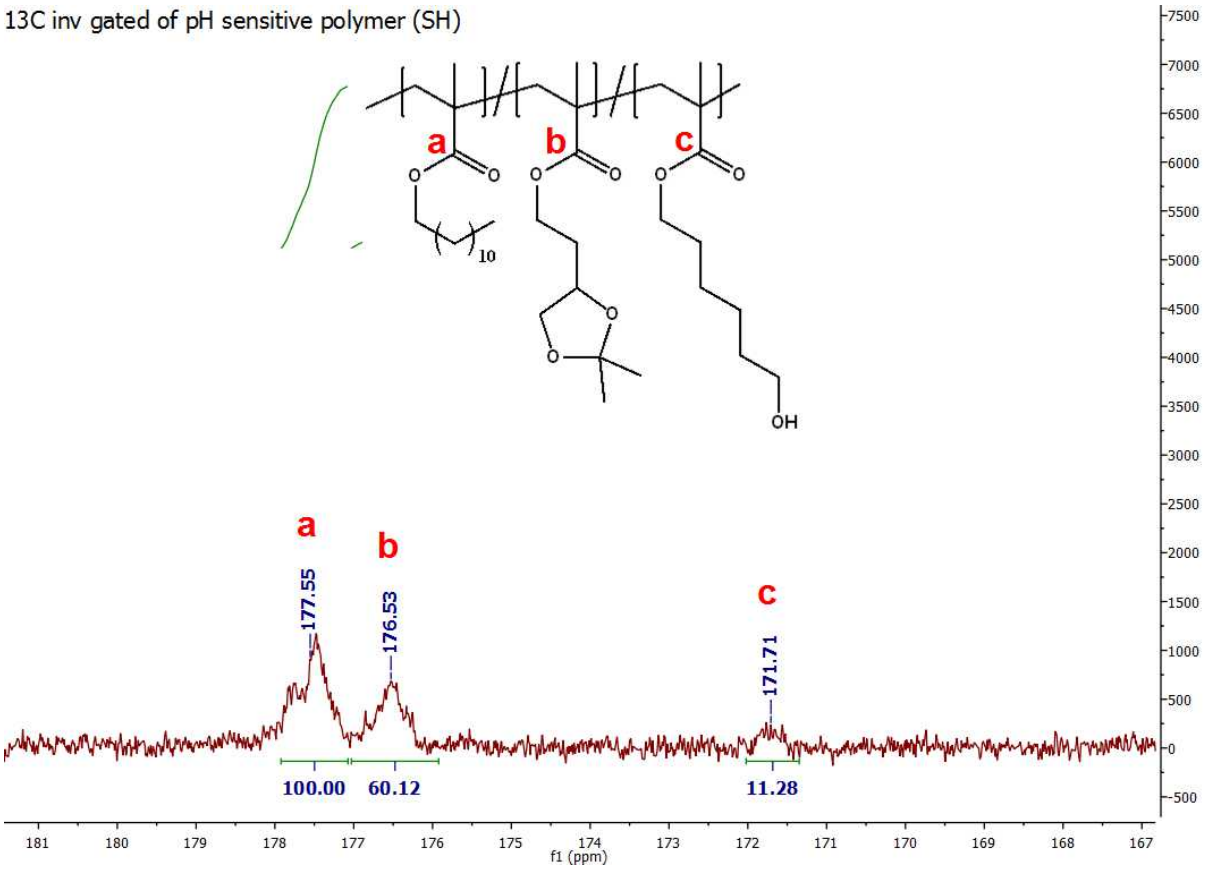

Figure 4.13: $^{13}C_{invgated}$ NMR of statistically copolymerized DDEMA and HHMA with LMA.

The integral of the carbonyl atom for laurylmethacrylate (a) (δ = 177.55 ppm) was set in proportion to the integral of the carbonyl atom of DDEMA (δ = 176.53 ppm) and HHEMA (δ = 171.71 ppm). The desired ratio of 40 % for the DDEMA could be reached as revealed from the spectra. HHEMA has a low ratio as it was kept in mind not to change to strong the total hydrophilic weight fraction due to the existing hydroxy group in the hydrophobic domain. The polymer **SC** was used as a macro CTA to synthezise the second block of the blockcopolymer p(LMA_{13}-stat-$DDEMA_9$-stat-$HHMA_{1,3}$)-*b*-p$(PFPMA)_{20}$ (**BH**) followed by conversion with DHPA to the amphiphilic blockcopolymer p(LMA-stat-DDEMA-stat-HHMA)-*b*-p(DHPA) (**PH**).

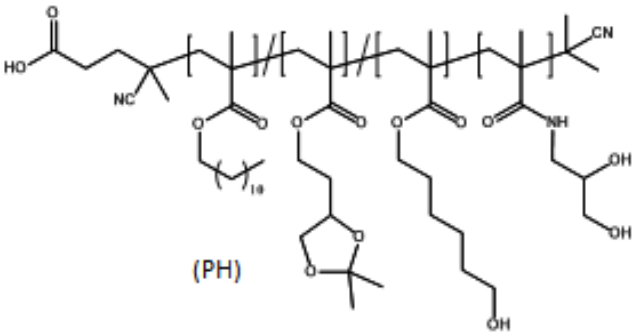

Figure 4.14: Resulting pH responsive amphiphilic blockcopolymer PH.

Table 4.5: Analysis of polymers with DDEMA and HHMA.

Polymer	Composition [a)]	M_n/ g*mol^{-1} [a)]	PDI [a)]
SH	p(LMA$_{13}$-stat-DDEMA$_9$-stat-HHMA$_{1,3}$)	5600 [a)]	1,13 [a)]
BH	p(LMA$_{13}$-stat-DDEMA$_9$-stat-HHMA$_{1,3}$)-*b*-(PFPMA)$_{20}$	12000 [a)]	1,24 [a)]
PH	p(LMA$_{13}$-stat-DDEMA$_9$-stat-HHMA$_{1,3}$)-*b*-(DHPA)$_{20}$	5600 [b)]	1,41 [b)]

[a)] obtained over H-NMR and THF-GPC, [b)] obtained over HFIP-GPC

With both polymers, p(LMA$_{10}$-*stat*-DDEMA$_6$)-*b*-(DHPA)$_{20}$ **(PC)** (5.1 kDa, PDI = 1,3) and p(LMA$_{13}$-*stat*-DDEMA$_9$-*stat*-HHMA$_{1,3}$)-*b*-(DHPA)$_{20}$ **(PH)** (5.6 kDa, PDI = 1,4) particles were formed over the duale centrifugation method, were extruded to an uniform size and were then investigated regarding the pH sensitive degradation over dynamic light scattering in a higher sensitive measurement setup by Dr. Martin Scherer (scattering angle 30°). Both polymers have similar molecular weights and PDIs to make them comparable. By the use of the blockcopolymer containing only DDEMA the particles remain almost stable at pH 6,5. At pH 5,0 there is a slight degradation happening over 200 h (red curve left) and at pH 4,5 the degradation of the vesicles is very strong as expected at this high acidic environment (black curve left). But when copolymerize the monomer HHMA the degradation at pH 5.0 is occuring in a stronger manner, as it was desired to see a degradation at this pH value. Again as expected at pH 4,5 the strongest degradation happens and at pH 6,5 the particles remain almost stable.

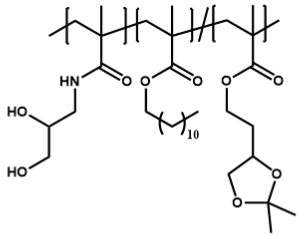

p(LMA$_{10}$-stat-DDEMA$_6$)-*b*-(DHPA)$_{20}$

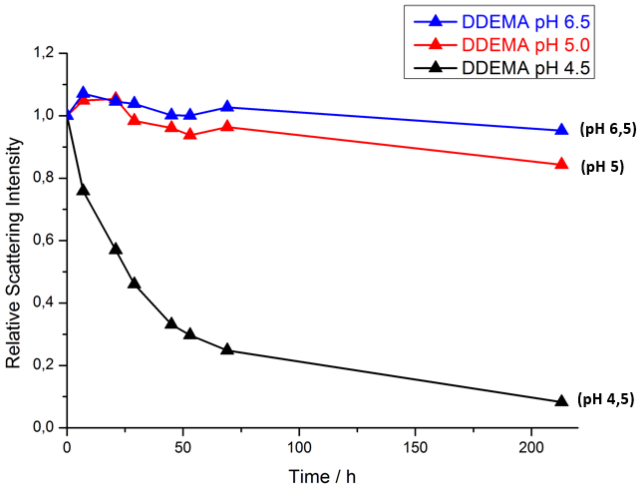

(a)

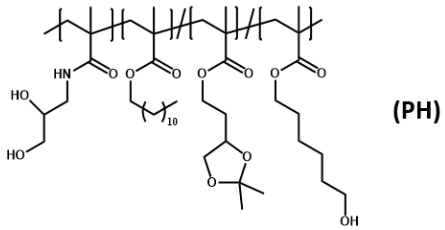

p(LMA$_{13}$-stat-DDEMA$_9$-stat-HHMA$_{1,3}$)-*b*-(DHPA)$_{20}$

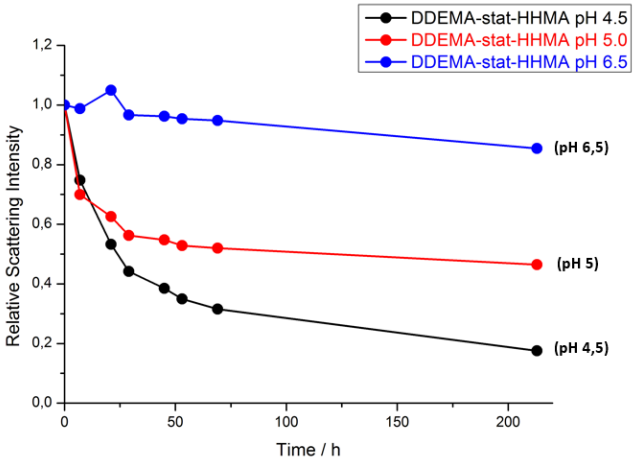

(b)

Figure 4.15: pH degradation studies at different pH values for particles formed by the amphiphilic blockcopolymers **PC** (a) and **PH** (b).

With the DLS kinetic measurements within the framework of pH degradation studies it could be confirmed the facilitated hydrolysis due to the copolymerized monomer HHMA. This helps to trap acidic protons in the periphery of the ketal to finally deprotect and changing the whole hydrophilic weight fraction of the polymer and internal hydrophilic/hydrophobic interplay and ratio of the blockcopolymer leading to its degradation.

New synthetic procedure to obtain redox resposive polymers

Direct polymerization of disulfide containing precursors

As mentioned above the synthetic polymerisation pathway does not allow an introduction of redox sensitive units as over RAFT the electronrich disulfide bond would act as a radical scavenger leading to byproducts and destroying of the main blockcopolymer. So it should be used a polymerizable monomer containing an electronpoor disulfide. Here, one can think about dipyridyldisulfide as a suitable monomer with a methacrylate group. The coupound pyridyldisulfildemethacrylate is referred to PDSMA and was synthesized over 2 steps.

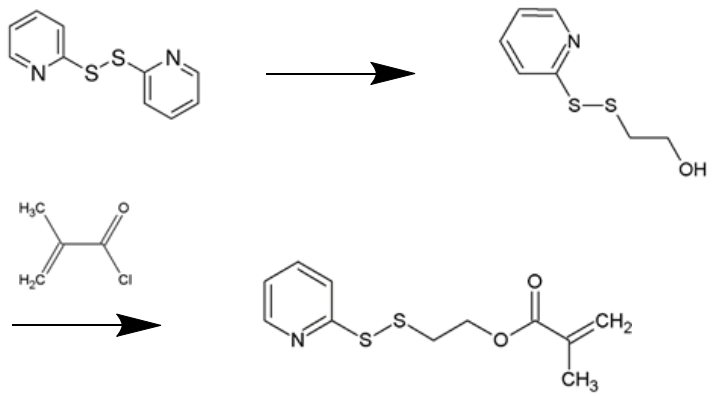

Figure 4.16: Synthesis of Pyridyldisulfildemethacrylate.

The idea behind is now to copolymerize this monomer statistically into the hydrophobic compartment with LMA starting from the homopolymer PFPMA.

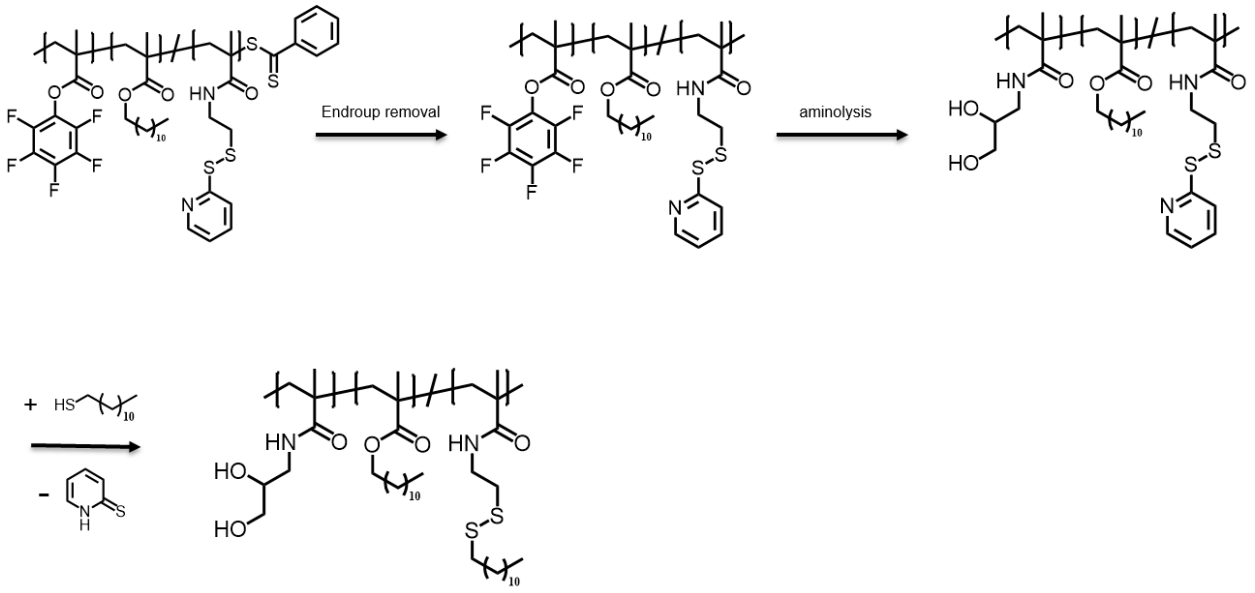

Figure 4.17: Synthetic procedure for introduction of disulfide bonds into the amphiphilic blockcopolymer over RAFT.

Proof of concept:

After end group removal of the CTA and aminolysis with DHPA leading to the amphiphilic blockcopolymer the thiol exchange reaction can be conducted at the end to yield the blockcopolymer with a redox sensitive group in the hydrophobic compartment. Hereby for the thiol exchange reaction it was used a thiol with a similar chain length as LMA to avoid a change in the hydrophobicity ratio.

However, before aminolysis and conversion of the PFPMA block the CTA end group has to be removed to eliminate side reactions and toxicity. It has to be tested before if the polymerized pyridyldisulfid methacrylate survives the end group removal with an excess of AIBN at a certain temperature. A prestep was to generate a homopolymer with this monomer. For this it was used a monomer based on pyridyldisulfide with an hexyl alkyl chain polymerized with AIBN in DMF at 70 °C.

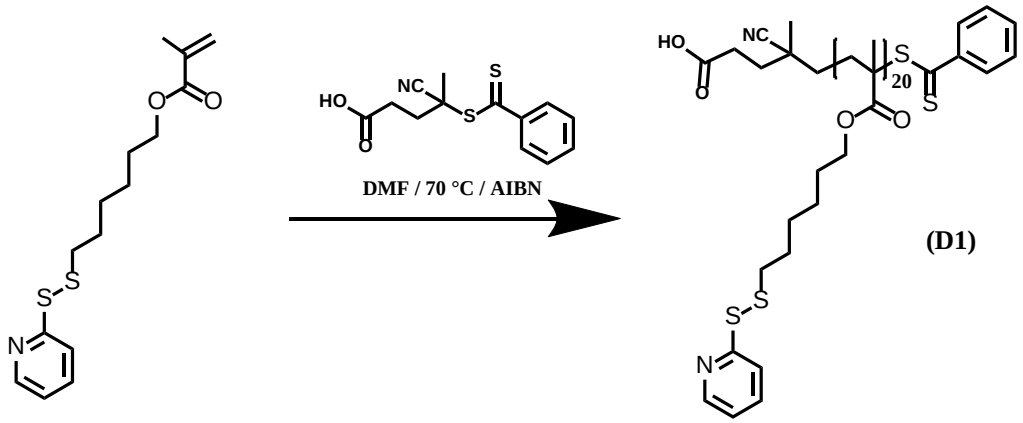

Figure 4.18: Synthesis of Hexyl-PDSMA

The THF-GPC showed a bimodal distribution with a molecular weight of 5.9 kDa, a degree of polymerization of 20 and a PDI of 1,25. CTA end group removal with 30 eq excess of AIBN destroyed the homopolymer resulting in very high PDI and lower molecular weigth.

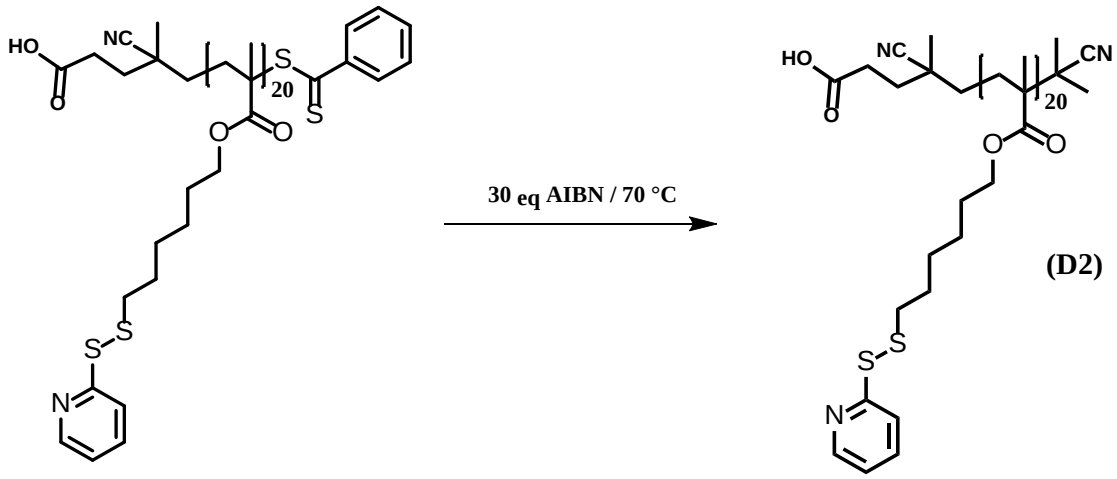

Figure 4.19: End group removal of disulfide containing polymer.

Table 4.6: Analysis of disulfide containing polymer prior and after eng group removal.

Polymer	M_n / kDa	PDI
D1	5.9 [a)]	1,25 [a)]
D2	4.6 [a)]	1,72 [a)]

[a)] Determined over THF- GPC

This synthetic idea has intrinsic problems needed to be solved as the aminolysis has to be done by low temperature and a longer reaction time. Furthermore the end group removal of the CTA is a critical point.

Redox responsive units in the hydrophobic domain

To introduce stimuli resposive units based on a redox system it was developed a new synthetic stragety from the bottom up to obtain amphiphilic blockcopolymers containing a disulfide bond and eliminate the above mentioned problems through the synthesis. Starting from an hydrophobic protected diol *N*-[(2,2-dimethyl-1,3-dioxolan-4-yl)methyl]-2-methylpropen-2-amid (DDMMA) which has the same structure after deprotection like DHPA it is possible to copolymerize with PFPMA as the whole resulting blockcopolymer remains still hydrophobic. And then aminolyis can be conducted with a disulfide containing long alkyl chain compound, 2-(Dodecyldisulfanyl)ethylamine (DDSEA), over reactive ester chemistry. This makes it possible to introduce the redox compound over aminolysis as in the end the converted PFPMA block builds the hydrophobic part and after deprotection of the acetal group this part becomes hydrophilic.

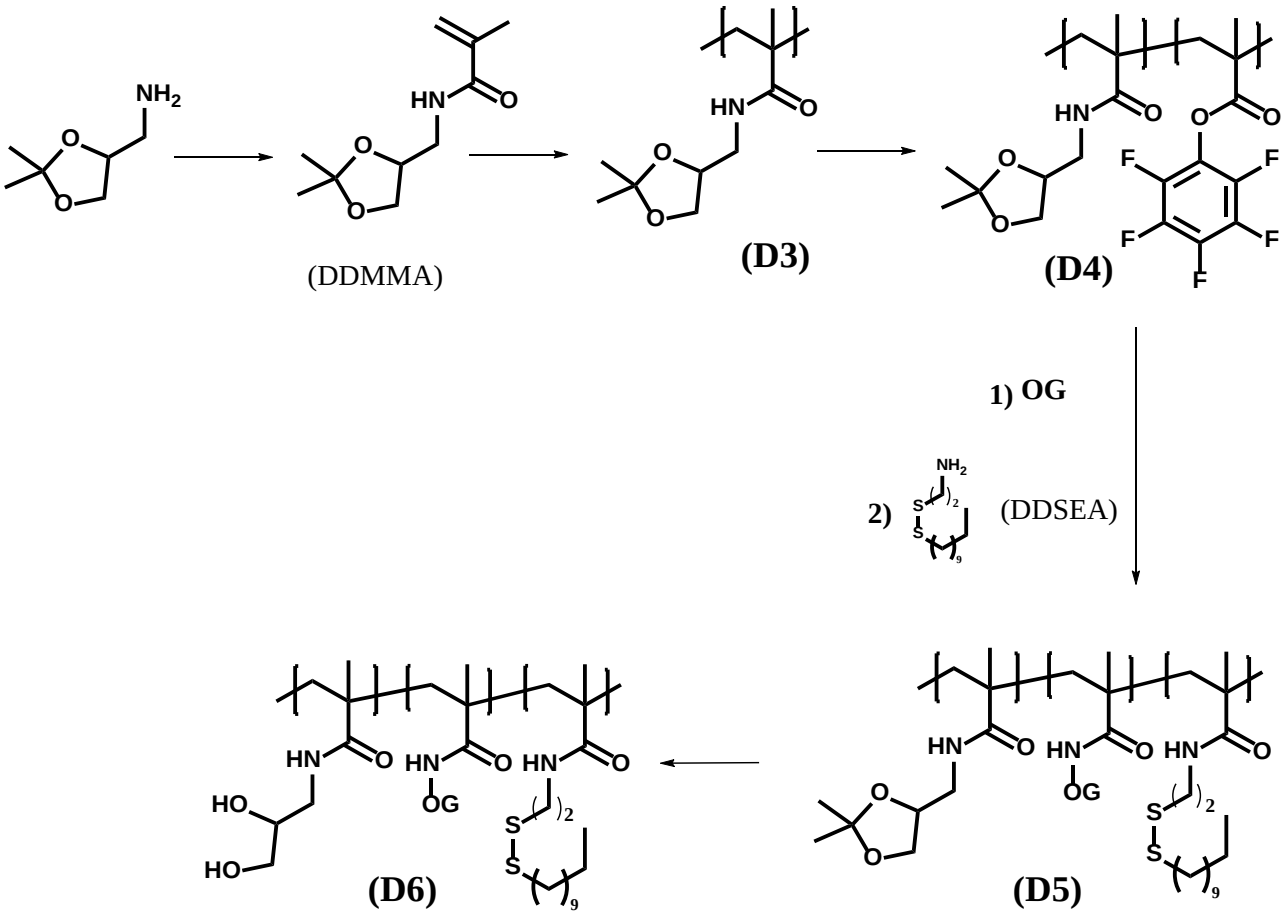

Figure 4.20: New synthetic procedure to obtain redox resposive blockcopolymers over RAFT.

Table 4.7: GPC data precursor polymers and redox resposinve one.

Polymer	Composition	M_n / kDa	PDI	Dye
D3	p(DDMMA)$_{18}$	3.6 [a)]	1,25 [a)]	/
D4	p(DDMMA)$_{18}$-*b*-(PFPMA)$_{20}$	8.6 [a)]	1,41 [a)]	/
D5	p(DDMMA)$_{18}$-*b*-(DDSEA$_{20}$-*stat*-OG)	11.8 [a)]	1,47 [a)]	OG 488
D6	p(DDMMA)$_{18}$-*b*-(DHPA$_{20}$-*stat*-OG)	11.7 [b)]	1,36 [b)]	OG 488

[a)] Determined over THF-GPC [b)] Determined over HFIP-GPC

So the main difference here is that after aminolysis and conversion of the PFPMA reactive ester it still remains hydrophobic and not hydrophilic as the polymers

synthesized before. Formation of polymersomes via duale centrifugation method containing the disulfide bond in the hydrophobic part can then be used for degradation studies by reduction agents like glutathione (GHS). In cellular level cells express on the cell surface GHS, in the intercellular in a concentration of 10 µM and in the intracellular level in a concentration of 100 mM. This can be used to degrade these particles in the process of cell uptake. In the following figure there is given the ^{1}H-NMR spectrum of the protected in total hydrophobic blockcopolymer in DMSO.

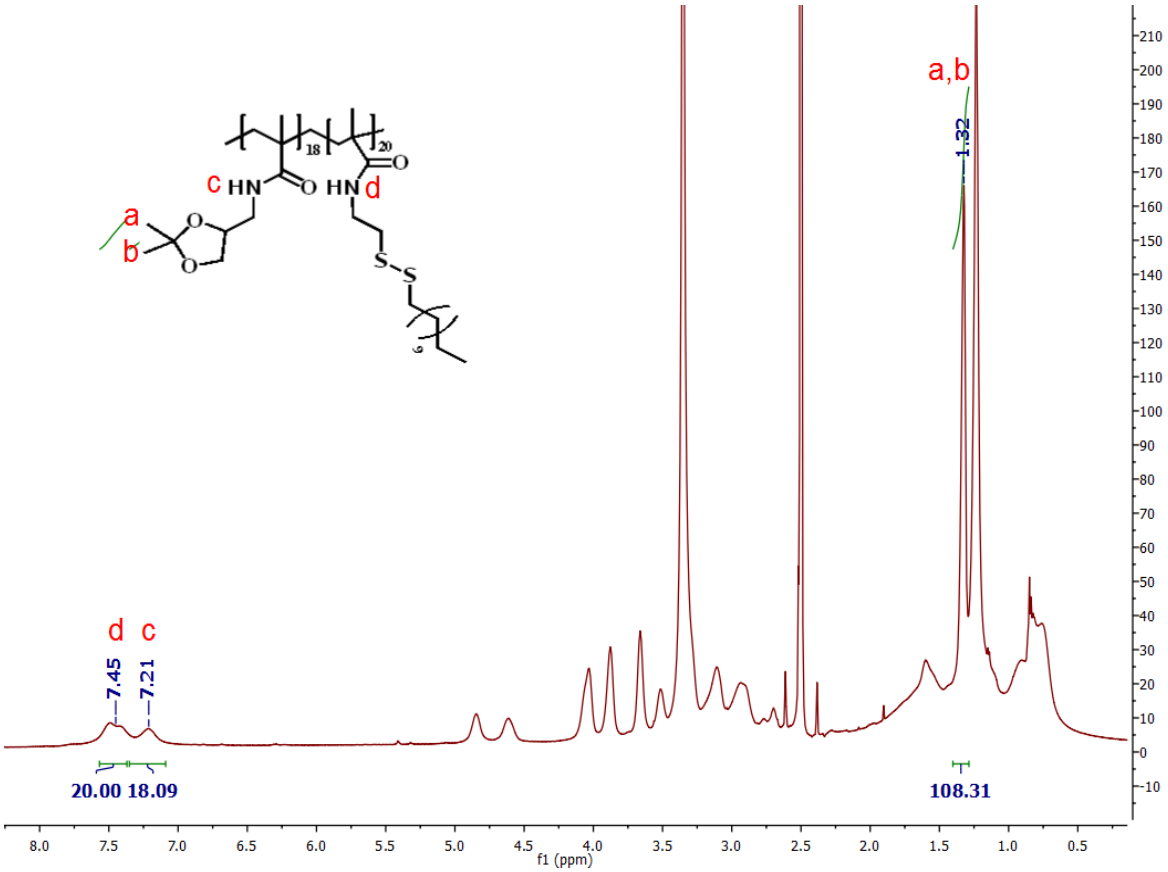

Figure 4.21: ^{1}H-NMR of disulfide containing blockcopolymer **D5**.

The integrals for each amide groups are conform with the one revealed from GPC data. The methyl groups of the acetale can be seen at 1.32 ppm. The integral here is 108,31. When devided with 18 as degree of polymerization it results 6 which are the H atoms of these two methyl groups. The next step is now to deprotect the diol and to obtain the desired amphiphilic blockcopolymer. For this purpose it was carried out kinetic ^{1}H-NMR measurements. Every 10 min it was measured an ^{1}H-NMR over a time frame of 16 h. The ^{1}H-NMR sample was acidified with HCl to a pH of 2. The time frame between acidification and the first ^{1}H-NMR measurement was 15 min. It

can be seen in the whole measurement spectra that the peak for the acetale at 1,28 ppm is disappeared as time goes on. The deprotection of the acetale leads to the release of acetone which can be tracked in the ^{1}H-NMR at 2,05 ppm. The signal become enhanced as time goes on.

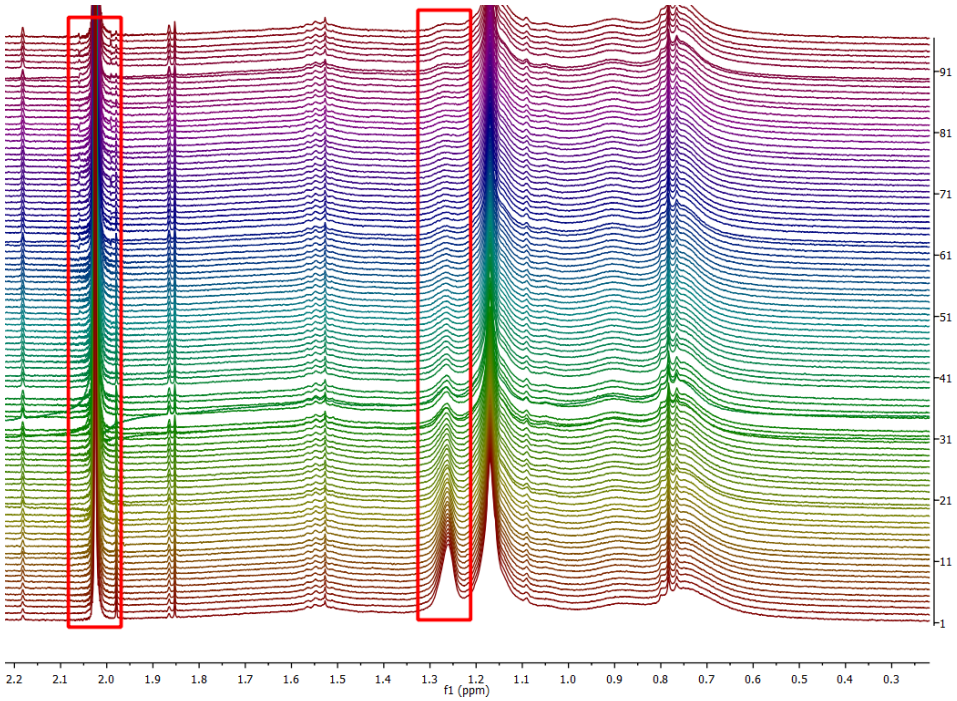

Figure 4.22: ^{1}H-NMR kinetic of acidified blockcopolymer.

For a better overview it was compared only the first measurements, the one after 8 h and the last one after 16 h. Here, the decrease in intensity of the peak for the protected diol group can be observed clearly.

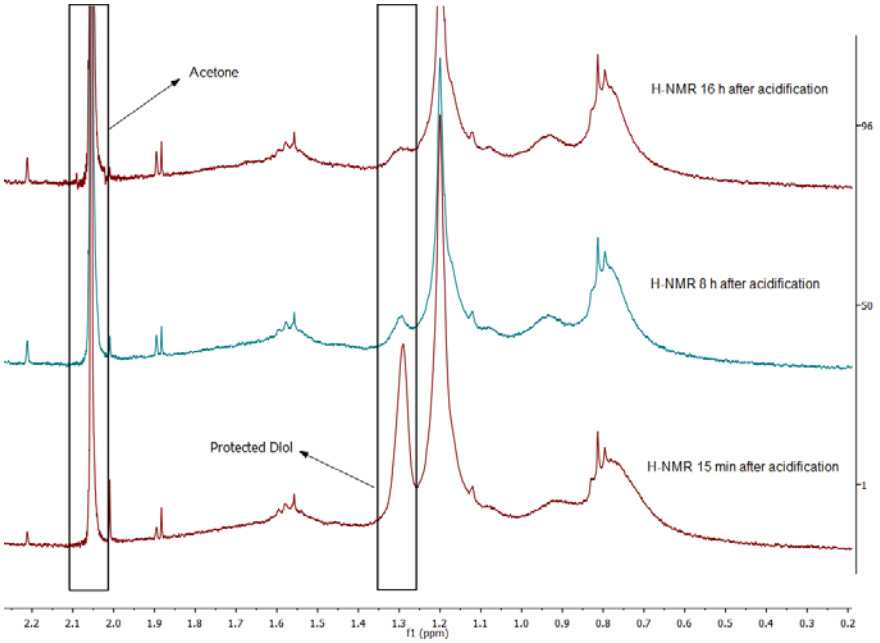

Figure 4.23: ^{1}H-NMR kinetic of acidified blockcopolymer in higher resolution. When one goes to low magfinaction the increase in intensity of the released acetone can be clearly observed.

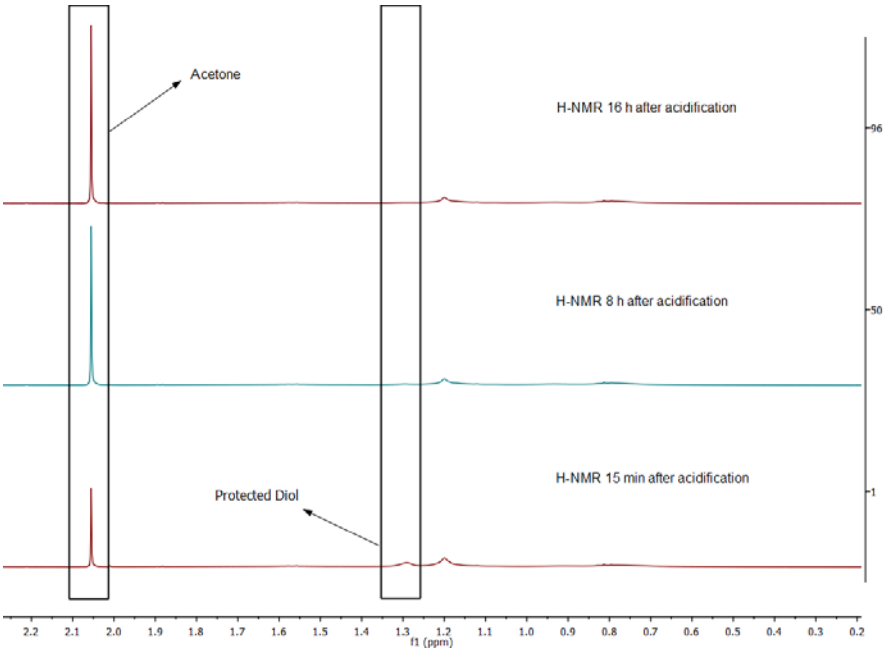

Figure 4.24: ^{1}H-NMR kinetic of acidified blockcopolymer - overview.

With this new synthetic procedure it was able to synthesize redox responsive amphiphilic blockcopolymers using the reactive ester approach. The deprotection of the acetale group could be confirmed with ^{1}H-NMR over time. After deprotection of **(C)** it was formed particles with resulting redox sensitive amphiphilic blockcopolymer **(D)**. Hereby, AF 647 as hydrophilic cargo was encapsulated and the encapsulation efficiency was determined by UV-vis. 20 µL of a 100 µM AF 647 solution in PBS was incubated with 5 mg of the amphiphilic blockcopolymer **(D)** for 5 h. Then 75 mg of ceramic beads were added and the samples were centrifugated over the duale centrifugation method. The obtained particles were purified over sephadex CL-2B. After eluation and isolation of the vesicles the column was washed with PBS and the supernatant was measured over UV-vis spectroscopy as well as the stock solution with the used amount for the encapsulation process. The absorption maximum wavelength of AF 647 is 650 nm.

Table 4.8: Determination of encapsulation efficiency for redox sensitive amphiphilic blockcopolymer by UV-vis spectroscopy.

Polymer	Cargo	Initial Absorption^{max} (a. u.)	Supernatant Absorption^{max} (a. u.)
D6	AF 647	2.10603	1.54235

The concentrations can be calculated over the Labert-Beer equation. The extinction coefficient for the dye AF 647 is 270.000 $\frac{\mathrm{L}}{\mathrm{mol}*\varepsilon}$ while the thickness of the used cuvette was 0,001 cm.

AF 647 as hydrophilic cargo in redox sensitive blockcopolymer (D6)

$$c_{initial} = \frac{2.10603}{270.000\frac{\mathrm{L}}{\mathrm{mol}*\varepsilon} * 0{,}001\ \mathrm{cm}} = 7{,}8 * 10^{-3}\frac{\mathrm{mol}}{\mathrm{L}} \qquad \{4.3\}$$

$$c_{supernatant} = \frac{1.54235}{270.000\frac{\mathrm{L}}{\mathrm{mol}*\varepsilon} * 0{,}001\ \mathrm{cm}} = 5{,}71 * 10^{-3}\frac{\mathrm{mol}}{\mathrm{L}} \qquad \{4.4\}$$

The encapsulation efficiency can be calculated as followed:

$$EE = \left(1 - \frac{\text{amount of free dye}}{\text{total amount}}\right) * 100\ \% = 27\% \qquad \{4.5\}$$

So 27% of the AF 647 could be encapsulated in the particles into the aqueous interior.

Redox responsive units in the hydrophilic domain

It is also possible to introduce a redox containing stimuli responsive unit into the hydrophilic part of the amphiphilic polymer. For this purpose it was synthesized a similar compound like DHPA with the difference, that it contains a disulfide bond (DHPA-SS). The synthetic pathway is given below:

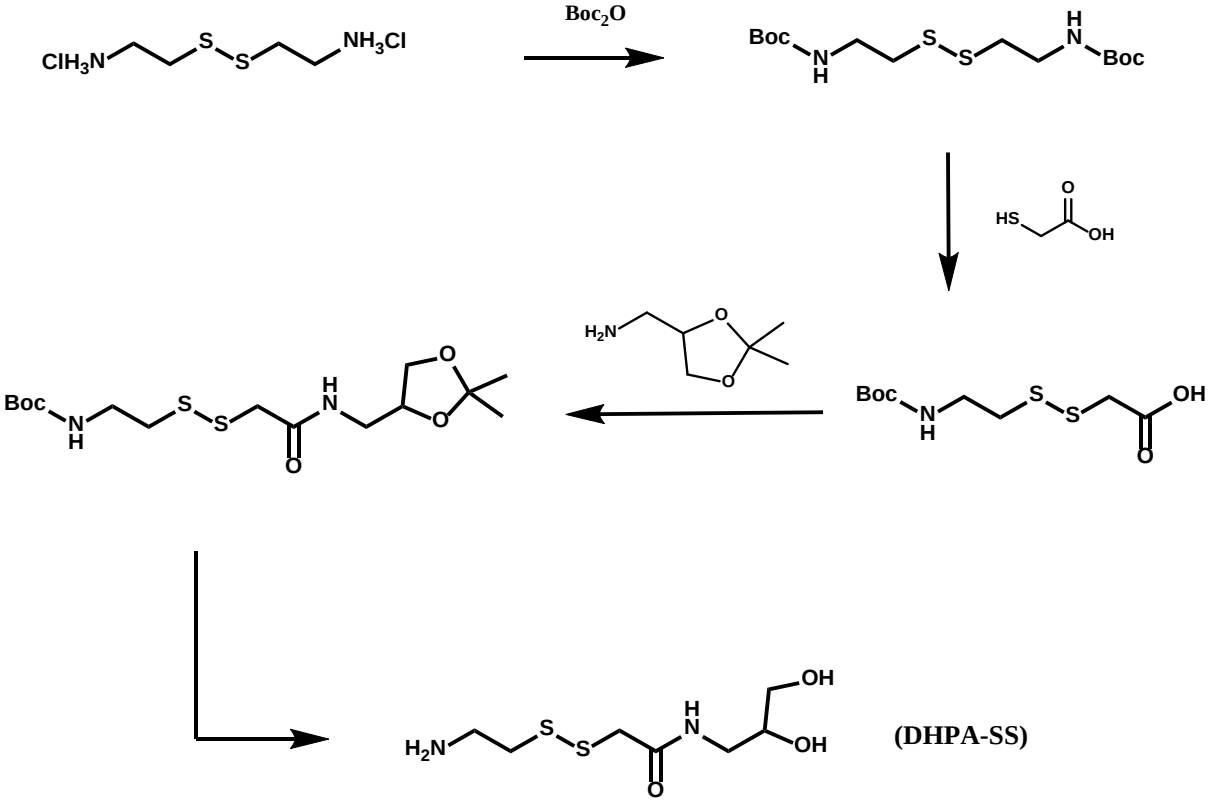

Figure 4.25: Synthetic procedure of DHPA-SS.

When using DHPA-SS / DHPA in a ratio of 1:1 in the conversion step it can be attached covalently to the blockcopolymer in the same synthetic procedure as described and used before in the case of DHPA. The resulting amphiphilic blockcopolymer is depicted in the following figure.

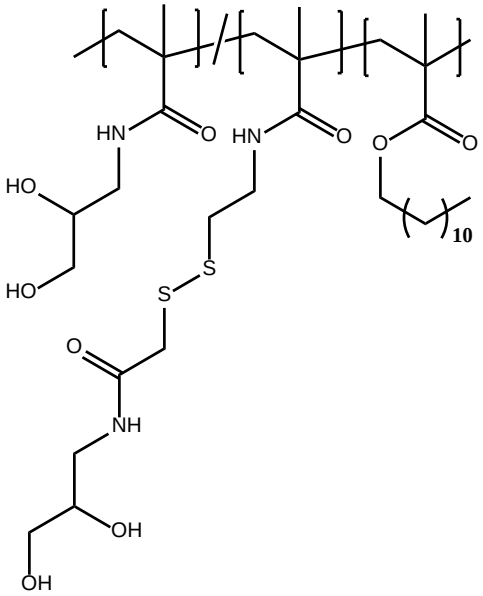

Figure 4.26: Amphiphilic blockcopolymer with redox senstitive units in the hydrophilic domain.

Particles were made with this amphiphilic blockcopolymer and were investigated over DLS within a zetaziser setup. It was prepared a solution of GSH of 10 mmol/L and it was added to the polymersome dispersion. As it can be seen in the following carried out measurements the polymersomes measured direct after the duale centrifugation method (filtered over 200 nm) exhibit an average diameter of around 90 nm.

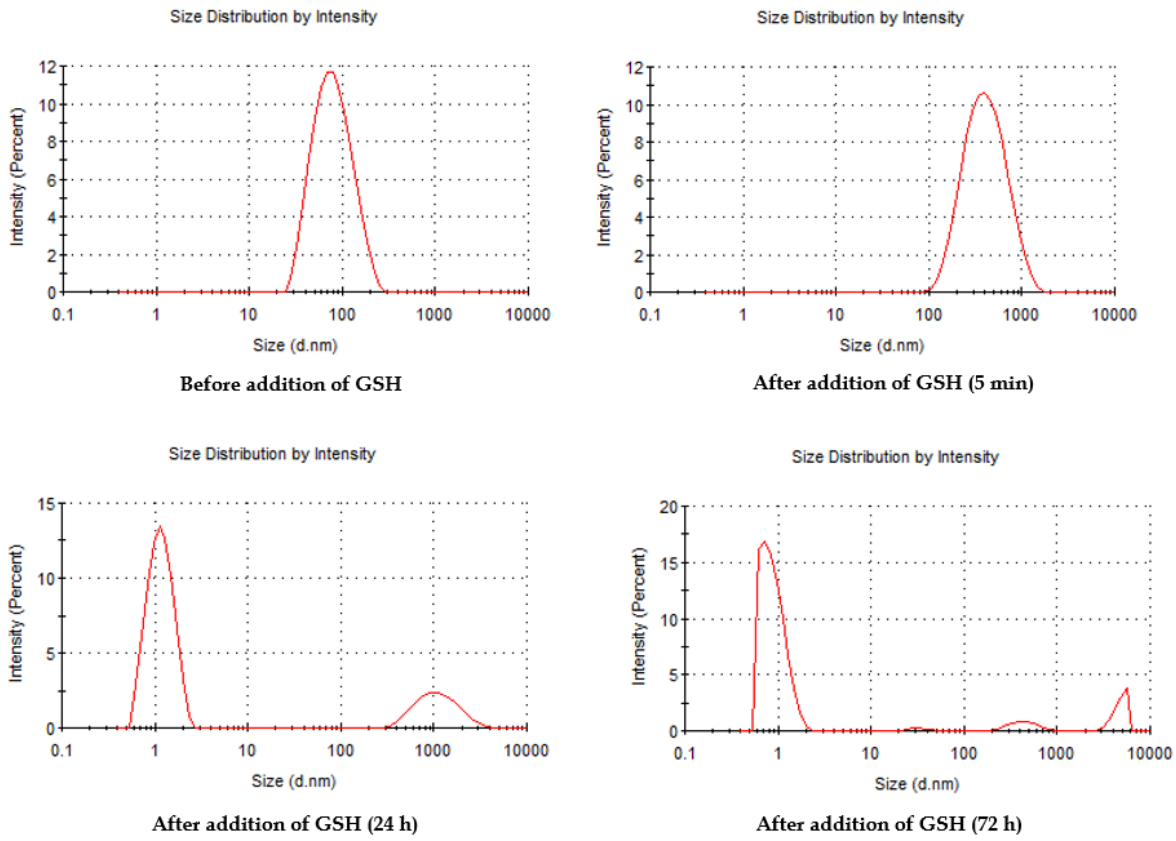

Figure 4.23: Reduction with GHS of particles formed by amphiphilic blockcopolymer containing redox resposive units in the hydrophilic domain.

5 min after GHS addition the particles seem to get bigger in diameter of around 500 nm pointing out in the direction of aggregates. 24 h after addtion of GHS there are larger aggregates of around 1000 nm in diameter and also a high detected intensity of a species around 1 nm in diameter revealed to the free polymer chains (unimers). GHS reduces the disulfide bonds in the polar domains of the blockcopolymer and it becomes stronger less polar. This leads to disaggregation of the vesicles due to the drastic change in the hydrophilic weight fraction. After 72 h the intensity increases for the free polymer chains and the larger aggregated becomes lower leading to the assumption that also the aggregated formed are reduced from the excess of GHS in the solution. As after 5 min the particles in diameter become larger one can assumes that at first the disulfide bonds get reduced to thiols which can also segregate and interact between each other of minimum two independent vesicles. As time goes on most of the existing disulfide bonds get reduced and the intensity detected for the free polymer chains increase as expected.

Conclusion

In this chapter stimuli responsive (smart) polymersomes were synthesized and characterized. Hereby, pH as well as redox sensitive units were introduced into the polymer domains both, in hydrophilic and hydrophobic parts. In the case of pH sensitive blockcopolymers it was possible to generate vesicles which can be degraded in contrast to those without pH sensitive units in a desired pH value of 5 as this level is the revealed conditions in the environment of cancer cells and inflammatory herds.

With the approach presented here in this chapter the statistically copolymerization of a further monomer HHMA with DDEMA (40 %) makes it possible to degrade the particles at a higher pH value of 5 as the hydroxy group in HHMA facilitate the hydrolyis of DDEMA leading to total decomposition of the aggregates as shown and confirmed in the DLS kinetic measurements.

Furthermore it was synthesized blockcopolymers obtaining disulfide bonds for the reductive decomposition of vesicles. The redox sensitive units were incorporated into the hydrophobic as well as in the hydrophilic domains of the amphiphilic blockcopolymers. In total contrast to the general methods the reactive ester approach was used here to generate after the conversion in the aminolysis process the resulting hydrophobic domain of the amphiphilic blockcopolymer. In the first case the total hydrophobic blockcopolymer with protected diol groups as acetale could be deprotected in acid conditions (release of acetone) to obtain the amphiphilic blockcopolymer consisiting of redox senstitive units in the hydrophobic domains as tracked over ^{1}H-NMR technique. The encapsulation efficiency was determined here to 27% for the hydrophilic cargo AF 647.For the amphiphilic blockcopolymers having their redox responsive units in the hydrophilic part it could be shown over DLS measurements that over time in a GHS solution the particles (ø 90 nm) degrade into the unimers (ø 1 nm).

Bibliography

[C1] Zhang, D.; Zhang, H.; Nie, J.; Yang, J. *Polym. Int.* **2010**, *59* (7), 967–974.

[C2] Louage, B.; Zhang, Q.; Vanparijs, N.; Voorhaar, L.; Casteele, S. Vande; Hennink, W. E.; Bocxlaer, J. Van; Hoogenboom, R.; Geest, B. G. De. *Biomacromolecules,* **2014**.

Chapter 5: Targeting

In this chapter the synthesized amphiphilic blockcopolymers were decorated with target structures. Here it was used folic acid as a hydrophobic and mannose as a hydrohphilic one. For the folic acid possesing a hydrophobic nature a polymer was synthesized with azide groups in the hydrophilic domains and particles were formed over duale centrifugation technique. The particles exhibit azide groups on their surface which can be used to bound the target structure over cupper free click chemistry. The target structure was modified prior click reaction to equip the folic acid with certain and suitable alkyne group under ring tension.

In the case of mannose, the target structure of hydrophilic nature, it was introduced over the aminolysis process in the hydrophilic domain and the amount per PFP repeating unit was determined over ^{13}C inverse gated spectroscopy.

Folic acid as target structure on amphiphilic blockcopolymers

To functionalize drug delivery systems with target structures on the surface of the used polymersomes like folic acid one needs first the target structure with a suitable group for modification after preparation of vesicles obtained from the dual centrifugation method. This was accomplished by an amphiphilic polymer containing azide groups in the hydrophilic compartment. The scheme in figure 5.1 represents the synthetic procedure. Starting from the monomer pentafluorophenylmethacrylate it was synthesized the PFPMA homopolymer $p(PFPMA)_{30}$ via RAFT and copolymerized with LMA to yield the blockcopolymer $p(PFPMA)_{30}$-b-$p(LMA)_{42}$.

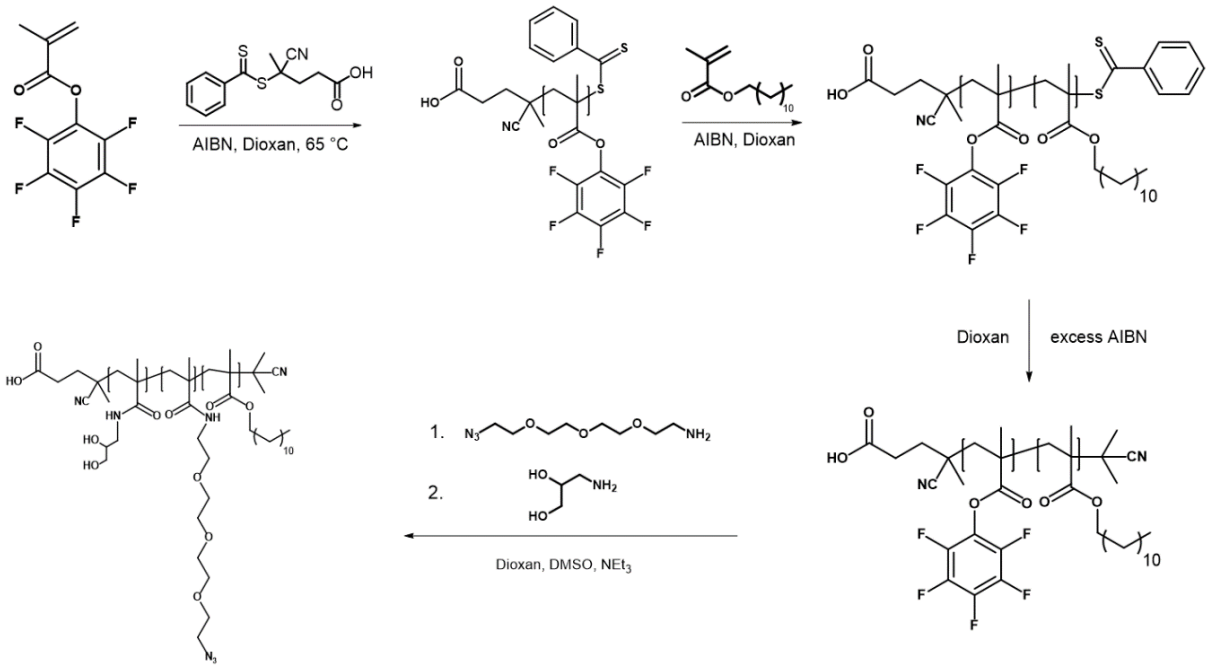

Figure 5.1: Synthesis pathway of azide functionalized amphiphilic blockcopolymers **(R5)**.

After removal of the CTA end group with an excess of AIBN (30 eq), 200 mg of the blockcopolymer was used in a conversion with OG 488 (0.01 mol per PFPMA repeating unit). The azide functionality was introduced over aminolysis (0,08 eq per PFPMA unit) into the blockcopolymer p(PFPMA$_{30}$-*stat*-OG)-*b*-p(LMA)$_{42}$ **(R2)** followed by DHPA (2 eq per PFPMA unit). After dialysis (MWCO = 6.5 kDa) and lyophilisation the azide functionalized polymer p(DHPA$_{30}$-*stat*-OG-*stat*-(NH$_2$-PEG-N$_3$))-*b*-p(LMA)$_{42}$ **(R5)** could be obtained as slight yellow colored powder.

After purification over dialysis and lyophylisation the polymer was measured over FTIR spectroscopy to detect the azide group which appears at a wavenumber of 2100 cm^{-1} as shown in the following figure.

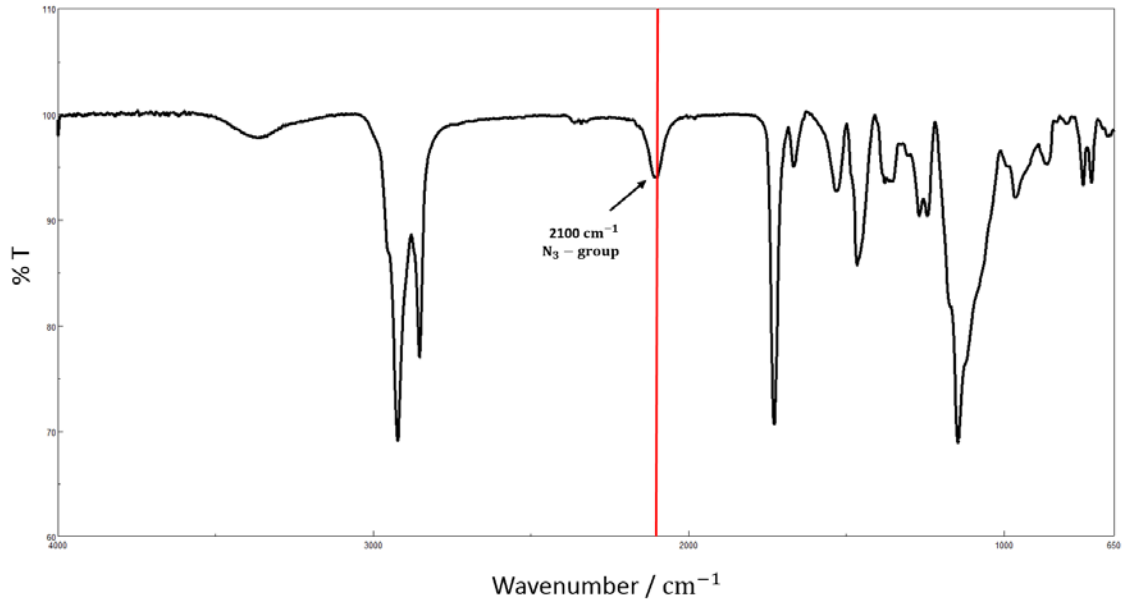

Figure 5.2: FTIR of azide functionalized blockcopolymer **(R5)**.

The polymer was used to generate particles equipped with azide groups on their surface to make it possible for their use in cupper free azide click chemistry to decorate the surface with folic acid as a target structure. Hereby, the target structure folic acid should be equipped with an alkyne group under ring tension. For this purpose it was first synthesized a compound which has on the one side the desired alkyne group and on the other side a moiety for modification with amine functionalized folic acid starting from cycloheptadiene.

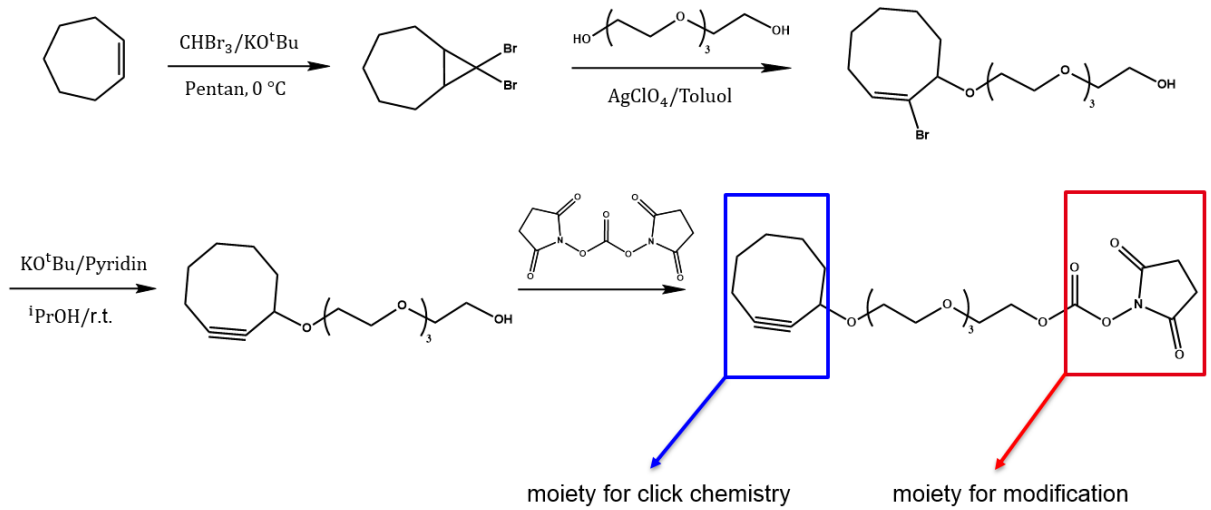

Figure 5.3: Synthesis of COT

Folic acid was modified with *N*-Boc protected diamine to result in the end to a free amine group which can be used to generate an alkyne group over aminolysis with pre synthezides COT.

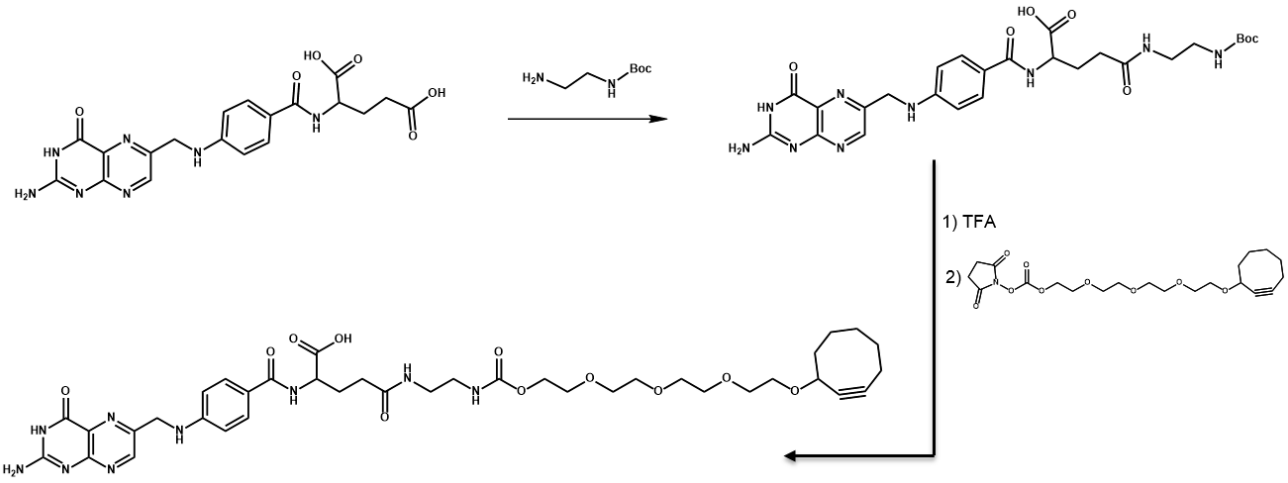

Figure 5.4: Synthesis of folic acid equipped with alkyne end group for the use in cupper free azide alkyne click reaction.

DOSY spectra revealed that there is only one diffusion component besides traces of solvents and in ESI there could be found the mass of the generated compound.

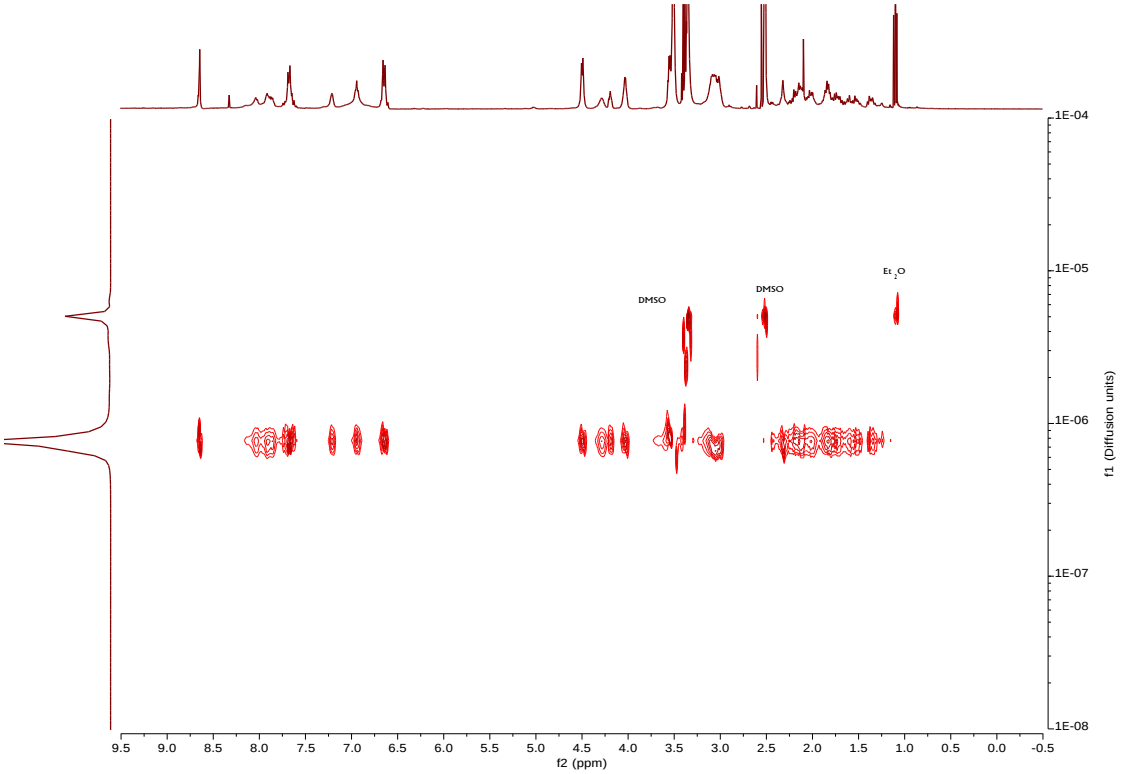

Figure 5.5: DOSY of FA-COT.

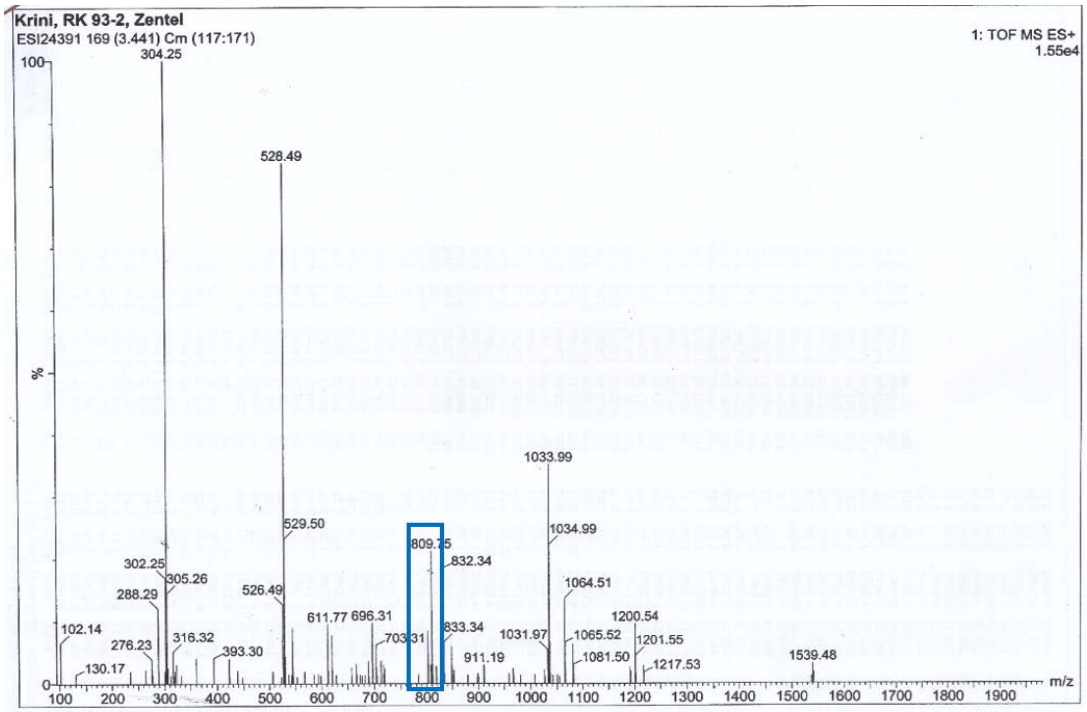

Figure 5.6: ESI of FA-COT.

Polymersomes equipped with azide groups on their surface were introduced via a cupper free click reaction with the folic acid modified compound. For this purpose azide functionalized particles (5 mg; 20 µL PBS, 70 mg ceramic beads – amount and condition are the same as described in appendix for the general procedure of particle formation) were formed over the duale centrifugation method. After purification over sephadex the particles dispersed in PBS (400 µL in total) were added to a solution of 5 mg FA-COT in 1 mL of dry DMSO and it was stirred at 30 °C for 48 h. The reaction mixture was then dialysed (MWCO = 6 kDa), filtered off from unsoluble compounds and lyophilised (yield = 2 mg).

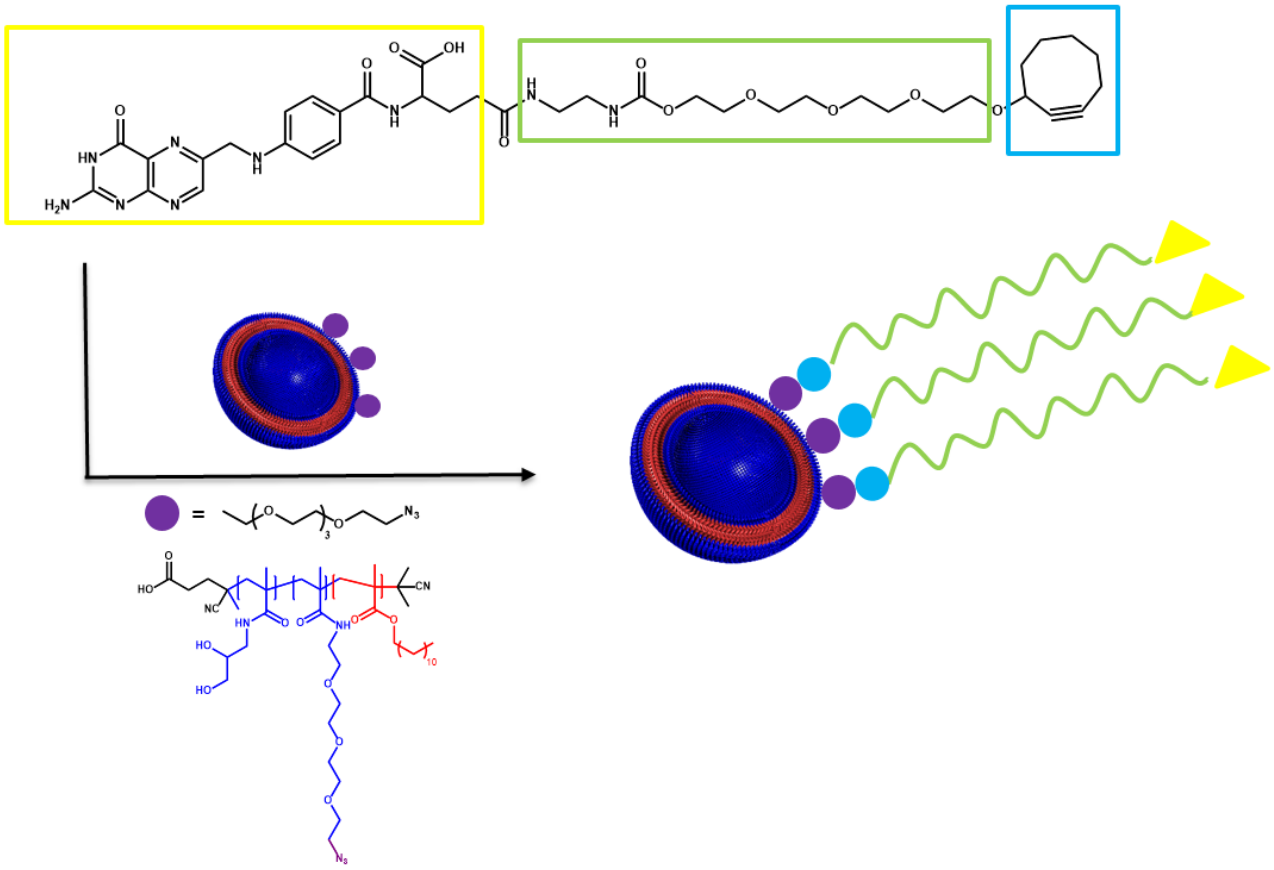

Figure 5.7: Cupper free azide alkyne click reaction of azide decorated particles with FA-COT.

After purification the obtained functionalized particles did not show the characteristic peak for the azide groups in FTIR spectroscopy indicating the successful click of azide and alkyne after 48 h reaction time. The following figure shows an overlay of the lyophylised polymers prior and after the conducted cupper free click reaction.

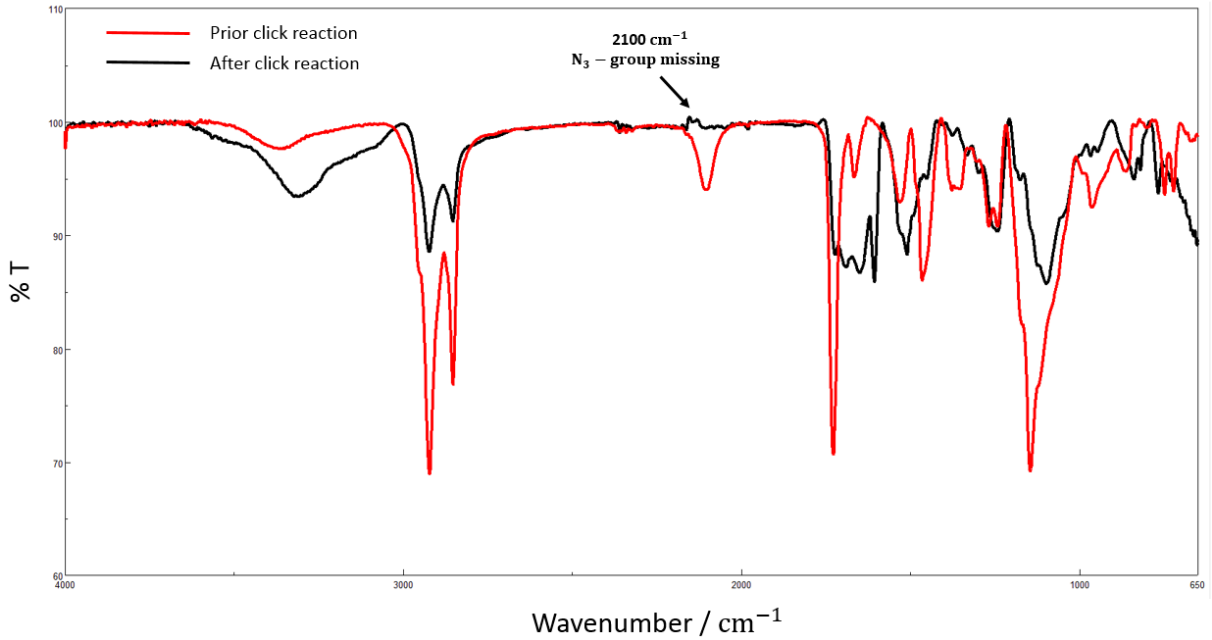

Figure 5.8: FTIR of FA functionalized particles after 48 h reaction time.

Nevertheless, it could not be proved *in vitro* the effect of folic acid on the particles. The lyophilised polymer obtained over click chemistry and decorated with folic acid p(DHPA$_{30}$-*stat*-OG-*stat*-(NH$_2$-PEG-N$_3$))-*b*-p(LMA)$_{42}$-FA could not be resolved in PBS leading to the assumption that the particles become to strong hydrophobic as the folic acid introduced over click chemistry on its surface is of a more hydrophobic nature. Here one has to consider the amount of folic acid on the surface and determine the optimal decoration density where the particles still can be formed and the amount of folic acid is high enough to obtain an enhanced cell uptake.

Mannose as target structure on pH labile blockcopolymers

Via receptor mediated endocytose the cell uptake of particles can be strongly enhanced. For the uptake in dentritic cells or macrophages as cells of the immune system, the mannose receptor is one of the most important carbohydrat recognizing protein structures.[B0] It belongs to the calcium dependant lectines and owns eight detection domains for mannosylated carbohydrate structures. To enhance the uptake through dendritic cells and macrophages the mannose sturcture was bounded into the hydrophilic domain of the amphiphilic blockcopolymer p((DHPA-*stat*-mannose)-*b*-p(LMA). The mannose linker derived from Dipl. Chem. Nadine Leber is given in the following figure.

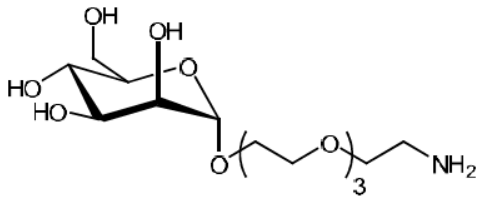

Figure 5.9: Amine terminated mannose linker.

It is a mannose derivate which is bounded over C_1 atom to an hydrophilic oligoethylenglycol spacer with an amine function. The approach to generate amphiphilic polymers over polymer analogues conversion with the certain pentafluorophenyl ester prepolymer do have synergetic sense. The mannose linker can be bonded selectively over the conversion into the hydrophilic DHPA block without any side reactions with the free hydroxy groups of the sugar. Furthermore this approach enables the multiple presentation of the sugar structure in regard to the receptor.

The goal was to synthesize enhanced pH labile polymers with mannose as target structure with its M_n=11.8 kDa and PDI of 1,5. Due to the labile units and as it shown in the chapter before they can degrade already at a pH of 5. This makes them attractive in the use for biomedial applications and with mannosylation the particles would be enhaced in cell uptake.

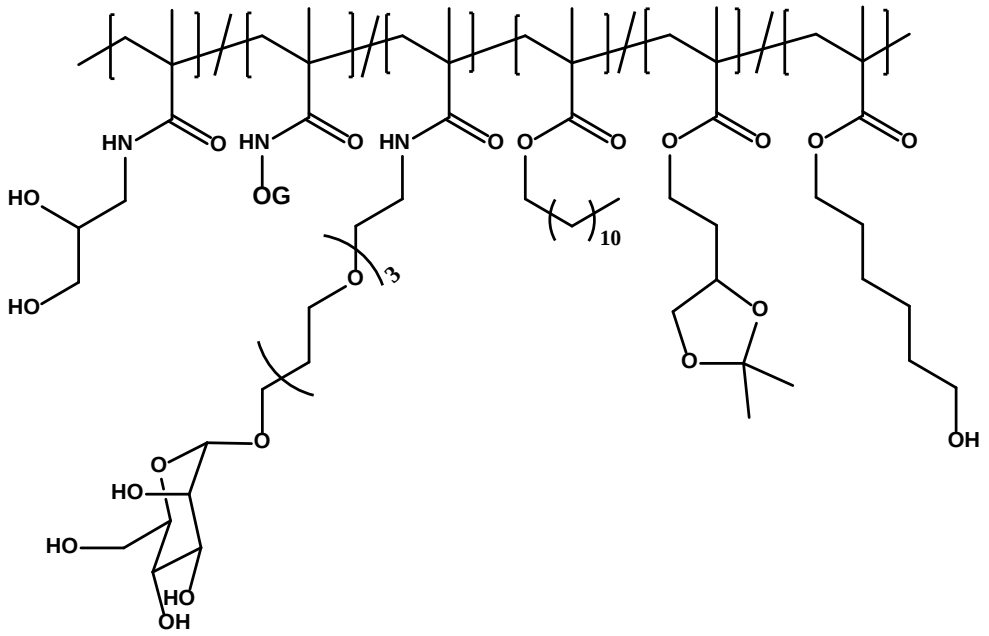

Figure 5.10: Structure of mannoslylated amphiphilic blockcopolymer.

Mannosylated pH labile p(DHPA-*stat*-mannose)-*b*-p(LMA-*stat*-DDEMA-*stat*-HHMA) blockcopolymer was obtained over polymer analogues conversion, respectively. The reaction temperature was set to 55 °C. Furthermore, for quantification in the cell uptake studies the polymers were labeled with OG 488 cadaverine. The mannose linker was used in 8 mol % of the PFP ester groups. As the reaction of PFPMA repeating units with the used amines is a statistically process, the low amount of mannose linker and OG 488 were given at first. The mixture was stirred for several hours before the high amount of DHPA (2 eq per PFPMA repeating unit) was introduced. After purification over dialysis against Milli-Q water the determination of mannose content was done over inverse gated (ig) ^{13}C-NMR spectroscopy. Due to the suppression of the Core-Overhauser-Effect the spectra could be analysed in a quantitative manner. The integral of the mannose-C_1-atom (δ = 100,2 ppm) was set in proportion to the total integral (δ = 179,0 – 176,5 ppm).

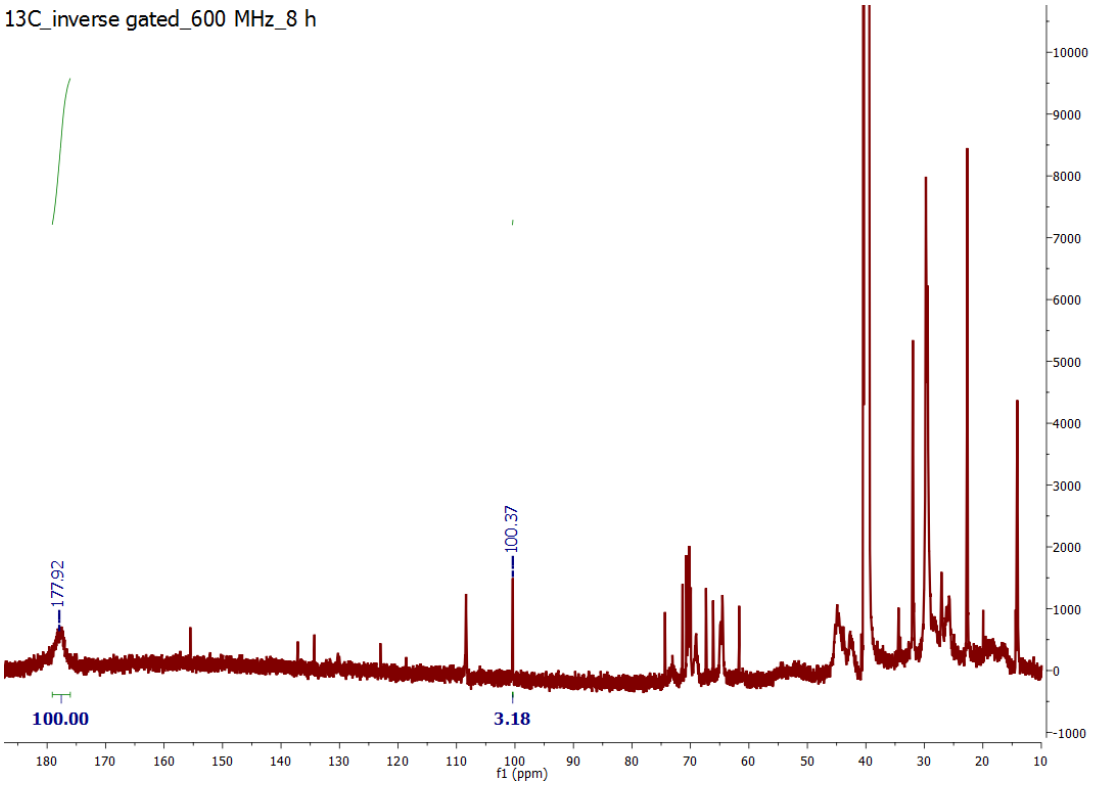

Figure 5.11: $^{13}C_{invgated}$ of mannose functionalized amphiphilic block copolymer.

When DHPA was given 24 h after mannose addition it could be shown that the mannose linker could be quantitative bounded into the hydrophilic part of the amphiphilic polymer[B0]. Here, the mannose per repeating unit is 3,2 %. As shown before by Dr. Martin Scherer[B0] the amount of mannose per repeating unit should be over 2 % to see its effect of upregulated cell uptake in cells.

Conclusion

In this chapter it is presented the decoration of particles obtained from amphiphilic blockcopolymers with target structures over aminolysis and incorporation into the polymer backbone and over post modification with cupper free azide alkyne click chemistry. Hereby target structures based on mannose as the hydrophilic one and folic acid as the hydrophobic one were used.

For the folic acid functionalized particles it could be shown the successfull synthesis of folic acid (FA-COT) conjugates equipped with an alkyne group for the use into the

strain promoted reaction procedure. The azide groups of the amphiphilic blockcopolymer dissapear in the FTIR measurement after successful clickable reaction of the certain azide and alkyne group of FA-COT, respectively. After decorating the particles with folic acid and lyophilisation they could not be redissolved in PBS leading to the assumption that the particles become stronger hydrophobic as the folic acid introduced over click chemistry on its surface is of a more hydrophobic nature. The lyophylisation process was crucial as the control particles without folic acid on their surface should have the similar concentration to compare the resulting effect in enhanced cellular uptake regarding the target structure.

pH labile amphiphilic blockcopolmers were synthesized and decorated with mannose as target structure into the hydrophilic domain. The amount of mannose was determined over ^{13}C inverse gated spectroscopy to 3,1 % per PFP repeating unit sufficient for enhanced cell uptake. As shown in the previous chapter particles formed by the pH labile polymers can be degraded at pH 5. So encapsulation of drugs together with the enhanced cell uptake and facilitate release makes this polymer to a promising candidate for a synergetic drug delivery system.

Chapter 6: In vitro experiments

In this chapter amphiphilic blockcopolymers were synthesized labled with different dyes suitable for *in vitro* application. The attempt here was the encapsulation of hydrophilic as well as hydrophobic cargos in the aqueos interior or in the hydrophobic membrane, respectively. Hereby it was used as the hydrophilic cargo AF 647 and as hyrophobic one PMI in regard as a model compound for biological active drugs. The encapsulation efficiency for both cargos were determined over UV-vis spectroscopy. The polymers were labled with dyes which do not overlap in their emission wavelength makes it possible for colocalisation of polymer and cargo in CLSM measurements. Also FACS measurements were conducted to show a good interaction/uptake of the encapsulated cargos with the cells.
Furthermore, TNF-α loaded polymersomes were formed and investigated over a MTT kinetic to prove the safe encapsulation of this high cytotoxic drug compared with pure TNF-α. The amount of encapsulated drug was determined over ELISA. Besides that DC-TC proliferation tests with the encapsulated TNF-α were conducted.

Encapsulation efficiency of hydrophilic and hydrophobic compounds

A crucial important information is how much of hydrophilic or hydrophobic drug can be encapsulated in the aqueos interior or in the hydrophobic membrane of the vesicles, respectively. For this prupose AF 647 as model compound for hydrophilic was encapsulated in the aqueous interior and PMI as model compound for hydrophobic drugs were used for incorporation in the hydrophobic membrane and the encapsulation efficiency was determined over UV-vis spectrometry.

20 µL of a 100 µM AF 647 (PMI) solution in PBS (THF) was incubated with 5 mg of the unlabled amphiphilic blockcopolymer **R1** overnight. For the sample containing polymer PMI it was added in addition 20 µL of PBS in the next morning. Then 70 mg of ceramic beads were added and the samples were centrifugated over the duale centrifugation method. The obtained particles were purified over sephadex CL-2B.

After eluation and isolation of the vesicles the column was washed with PBS (THF) and the supernatants were measured over UV-vis spectroscopy as well as the stock solution with the used amount for the encapsulation process. The absorption maximum wavelength of AF 647 is 650 nm and PMI is 488 nm.

Table 6.1: Determination of encapsulation efficiency by UV-vis spectroscopy.

Sample	Polymer	Cargo	Initial Absorption^{max} (a. u.)	Supernatant Absorption^{max} (a. u.)
1	R1	AF 647	0.9884	0.4936
2	R1	PMI	0.5239	0.0647

The concentrations can be calculated over the Labert-Beer equation. The extinction coefficient for the dye AF 647 is 270.000 $\frac{L}{mol*\varepsilon}$ and for PMI 44.000 $\frac{L}{mol*\varepsilon}$ while the thickness of the used cuvette was 0,01 cm.

AF 647 as hydrophilic cargo

$$c_{initial} = \frac{0.9884}{270.000\frac{L}{mol*\varepsilon} * 0{,}01\ cm} = 3{,}66 * 10^{-4}\frac{mol}{L} \qquad \{6.1\}$$

$$c_{supernatant} = \frac{0.4936}{270.000\frac{L}{mol*\varepsilon} * 0{,}01\ cm} = 1{,}82 * 10^{-4}\frac{mol}{L} \qquad \{6.2\}$$

The encapsulation efficiency can be calculated as followed:

$$EE = \left(1 - \frac{\text{amount of free dye}}{\text{total amount}}\right) * 100\ \% = 49\ \% \qquad \{4.5\}$$

So 49 % of the AF 647 could be encapsulated in the particles into the aqueous interior.

PMI as hydrophobic cargo

$$c_{initial} = \frac{0.5239}{270.000 \frac{L}{mol * \varepsilon} * 0{,}01\ cm} = 1{,}94 * 10^{-6} \frac{mol}{L} \qquad \{6.4\}$$

$$c_{supernatant} = \frac{0.0647}{270.000 \frac{L}{mol * \varepsilon} * 0{,}01\ cm} = 2{,}39 * 10^{-7} \frac{mol}{L} \qquad \{6.5\}$$

The encapsulation efficiency for PMI is:

$$EE = \left(1 - \frac{\text{amount of free dye}}{\text{total amount}}\right) * 100\ \% = 89\ \% \qquad \{6.6\}$$

So 89 % of the PMI could be encapsulated into the particles in the hydrophobic membrane.

Table 6.2: Encapsulation efficiency for AF 647 and PMI.

Sample	Polymer	Cargo	Polarity	EE
1	R0	AF 647	hydrophilic	49 %
2	R0	PMI	hydrophobic	89 %

The high encapsulation efficiency for PMI can be explained due to its hydrophobic nature as there is only the possibility to incorporate into the hydrophobic membrane of the particles through the experimental procedure.

Polymersomes loaded with hydrophilic / hydrophobic cargo – *in vitro*

For visualization the cell uptake of vesicles by endocytosis the polymers were labeled with Oregon green 488 (OG 488) and texas red (TR), p(DHPA$_{30}$-*stat*-OG)-*b*-p(LMA)$_{42}$ **(R2)** and p(DHPA$_{30}$-*stat*-TR)-*b*-p(LMA)$_{42}$ **(R3)**.

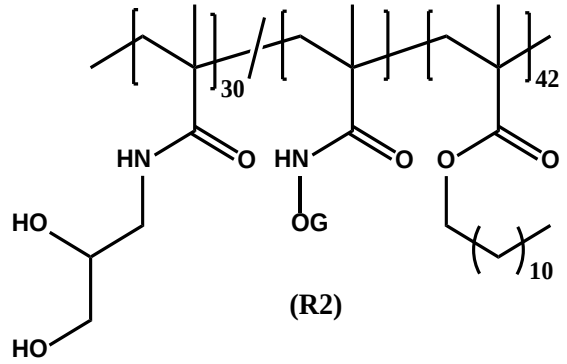

(R2)

(a)

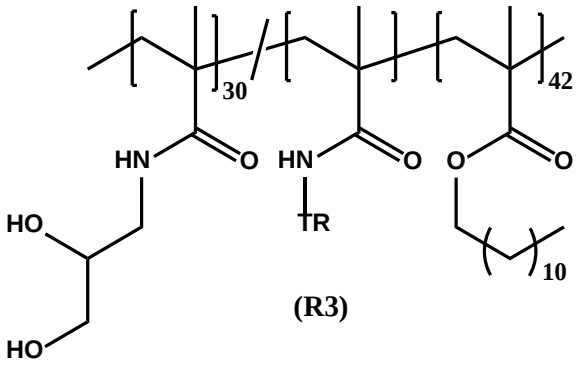

(R3)

(b)

Figure 6.1: OG 488 (a) and Texas Red (b) labled amphiphilic blockcopolymers for encapsulation studies of hydrophilic and hydrophobic cargos.

Table: 6.3: Analysis of OG 488 and Texas Red labled amphiphilic blockcopolymers.

Polymer	Composition	M_n	PDI	Dye
R2	p(DHPA$_{30}$-*stat*-OG)-*b*-p(LMA)$_{42}$	8.1 [a)]	1,46 [a)]	OG 488
R3	p(DHPA$_{30}$-*stat*-TR)-*b*-p(LMA)$_{42}$	10.5 [a)]	1,53 [a)]	TR

[a)] Determined by HFIP-GPC

The covalent dye labeling of polymers makes it possible to locate and track the polymers on the cellular level. For the synthesis 0.01 equivalent of the dye was added prior addition of DHPA and stirred for 5 h at same temperature. To track colocalization of cargo and polymer it was used as hydrophilic cargo Alexa Fluor 647 (AF) in the case of OG 488 labeled polymers encapsulated into the aqueos interior. In the case of TR labeled polymer it was used as cargo a highly hydrophobic dye, namely perylenmonoimid (PMI) – derived from BASF and MPIP - which incorporated in the hydrophobic membrane of formed polymersomes. The encapsulation efficiency of encapsulated hydrophilic cargo, AF 647, was determined to 49 % over the ratio of absorbance in UV-vis spectroscopy of the supernatant in regard to the stock solution after eluation and isolating the particles over sephadex. Here the eluent was PBS. For the hydrophobic dye, PMI, the encapsulation efficiency was determined to 89 % whereas the eluent was DMSO. The absorption maxima of the fluorescence dyes are different which enables its independent as well as simultaneous detection.

Table 6.4: Absorption maxima of fluorescent dyes in used combination

Fluorescence dye (Polymer / Cargo)	Absorption maxima / nm
Particle (a) OG 488 / AF 647	488 / 633
Particle (b) Texas Red / PMI	561 / 488

Prior uptake of confocal laser scanning microscope (CLSM) FACS measurements were conducted by [redacted] With this it could be detected if there is an interaction between cells and the particles. For this purpose bone marrow derived dendritic cells (BM-DCs) were incubated for 24 h with the particles and afterwards stained with anti-CD11c^{+}-antibodies as marker for dendritic cells. The FACS analysis was carried out from [redacted] at the certain specific wavelengths to detect on the one hand the polymer and on the other hand the encapsulated or incorporated cargo. The untreated culture in which no particles were added was used as negative control. The unstained culture was used as the control group.

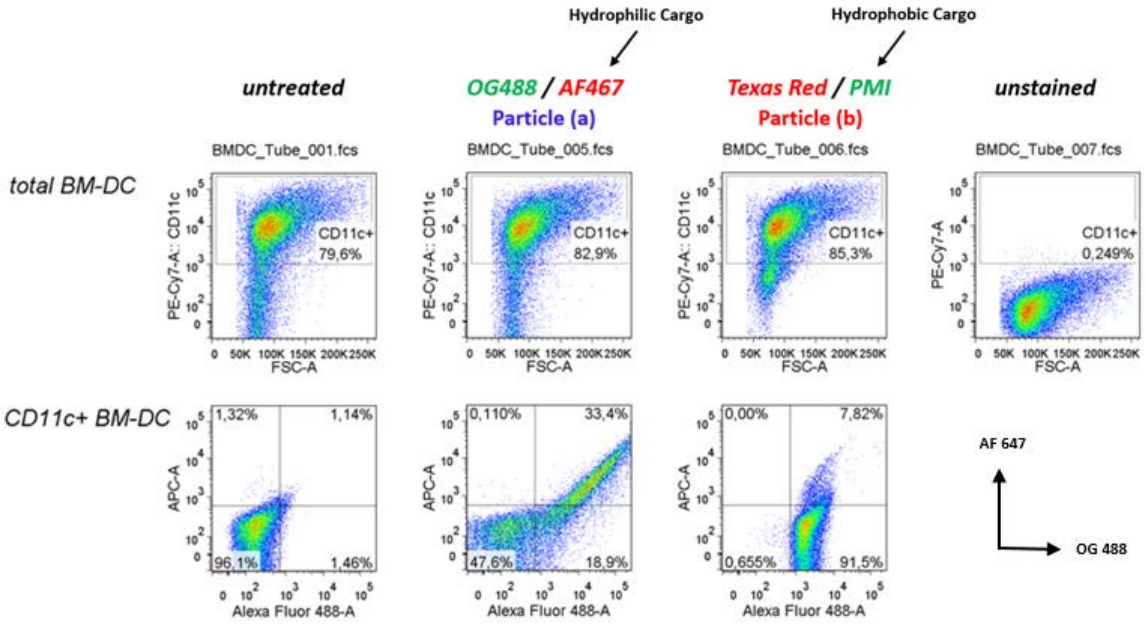

Figure 6.2: FACS analysis with untreated one as negative control, Particle (a): OG labeled polymer and AF 647 as a hydrophilic cargo, Particle (b): detection only hydrophobic cargo PMI (detection of TR not shown), and as control unstained BM-DC culture.

In the upper row it was determined the number of CD11c+-DCs from the macro culture of BM-DCs. As it can be seen the cultures contain around 80 % of CD11c+-DCs. The unstained sample serves as control group and shows as desired no CD11c+-DCs. In the lower row for the CD11c+ fraction is shown how much percentage of the DCs are positive for the fluorescence labeled polymer and the encapsulated or incorporated cargo. The x axis in the dot plot shows the detection of OG or PMI (channel: Alexa- Fluor 488-A). The y axis shows the detection of AF 647 (channel: APC-A). In comparison to negative control (the untreated one) after incubation with sample (a) (OG/AF) 33,4 % were positive for AF 647 and 18,9 % positive for OG. As for sample (b) (TR/PMI) the detection of TR is not able with this setup only the detection of PMI could be achieved. All DCs were positive for the hydrophobic cargo dye (PMI). It is known that hydrophobic drugs can be uptaken even without the particles through leakage. So here no conclusion can be done about the uptake of the particles incorporated with the dye as ensemble.

CLSM meausrements were carried out by [redacted] to track the particles and the cargo after cell uptake. As it can be seen for the polymer system encapsulated the hydrophilic cargo AF 647 there can be seen the successful uptake into the cells. Furthermore colocalisation of polymer (green) and cargo (red) can be found which appears yellow-orange. The DC membrane is stained in blue with CD11c in figure 6.12.

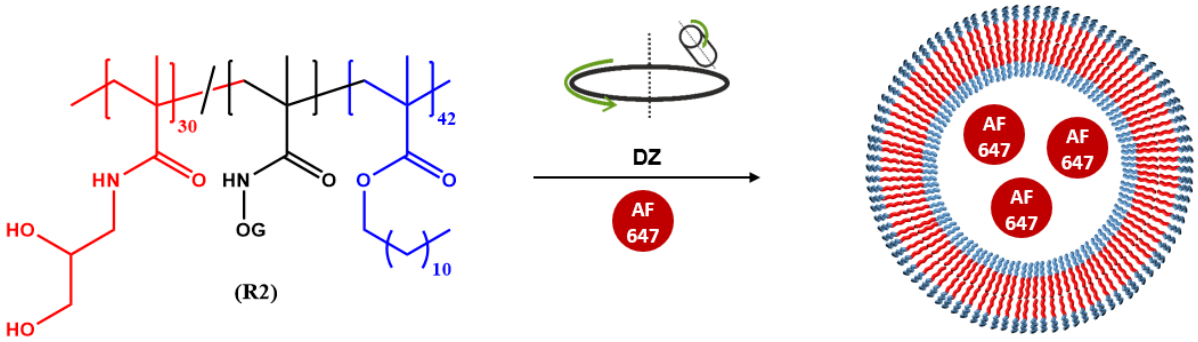

Figure 6.3: Encapsulation of hydrophilic cargo (AF 647) into amphiphilic blockcopolymer **(R2)** labled with OG 488 – particle (a).

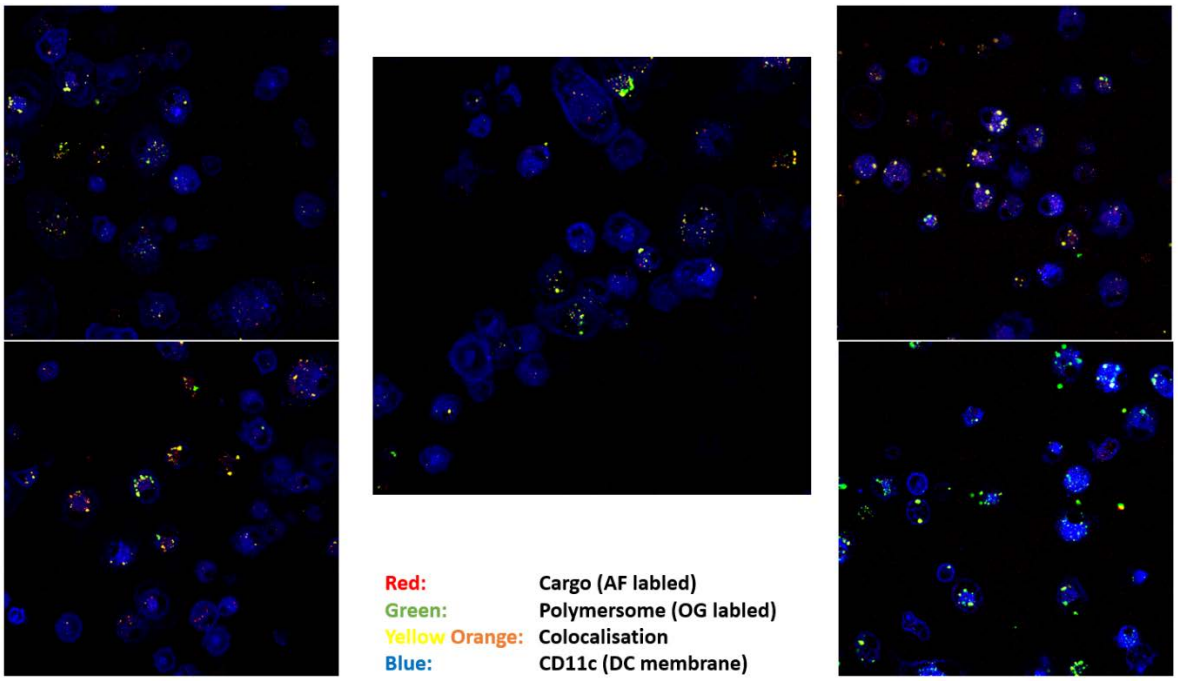

Figure 6.4: CLSM of encapsulated hydrophilic cargo (AF 647).

In the case of the polymer system incorporated with a hydrophobic compound, a highly hydrophobic dye (PMI), there can be seen a high density of the particles. While the polymer appears red (TR) and the cargo green (PMI) the colocalisation appears yellow orange.

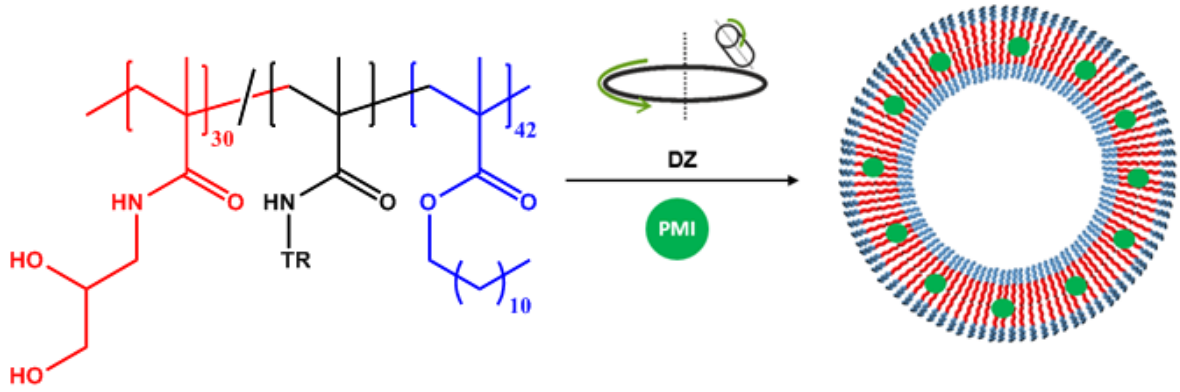

Figure 6.5: Encapsulation of hydrophobic cargo (PMI) into amphiphilic blockcopolymer **(R3)** labled with Texas Red – particle (b).

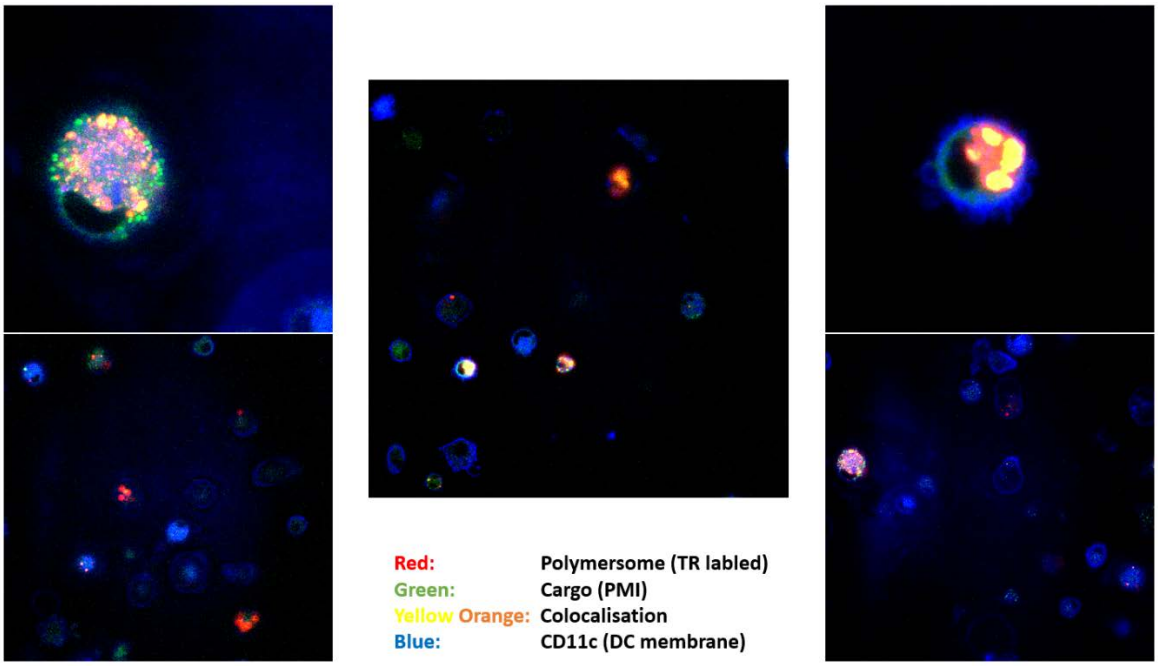

Figure 6.6: CLSM of incorporated hydrophobic cargo (PMI).

With these systems of polymers it was able to incorporate both – hydrophilic and hydrophobic – cargos. This makes such Polymersomes very attractive as a codelivery of different cargos and drugs can be accomplished at the same time with one polymeric system in a synergetic manner.

TNF-α loaded polymersomes (MTT-Kinetic)

Cell viability of TNF-α and PBS encapsulated polymersomes after uptake were investigated with a MTT assay in cooperation with [redacted] and [redacted] To get an estimation of the used polymersomes concentration the vesicles were lyophilised and the mass was determined for which it was found to lie between 300-400 µg. This means that for the used volume of 75 µL the particle concentration was 4-5 µg/µL. In the MTT experiments it was possible to encapsulate the high cytotoxic TNF-α temporally over a period of 6 h while after 24 h cytotoxity was obtained due to leakage of the drug out of the vesicles while the PBS loaded polymersomes remain still non toxic.

Conclusion

In this chapter it is presented that the polymersomes can be loaded efficiently with drugs without acting toxic and the possibility to encapsulate hydrophilic as well as hydrophobic drugs. Proved colocalisation of carrier system and drug makes them as promising candidates for codelivery in a synergetic manner.

Carrier systems based on the amphiphilic blockcopolymer p(DHPA$_{30}$-*stat*-OG)-*b*-p(LMA)$_{42}$ **(R2)**, labeled with OG 488 and encapsulated with the hydrophilic cargo Alexa Fluor 647 and ones p(DHPA$_{30}$-*stat*-TR)-*b*-p(LMA)$_{42}$ **(R2)** labeled with Texas Red and incorporated with the hydrophobic dye PMI as a model for a hydrophobic drug were in FACS with BCDMs and cell uptake could be proved. The encapsulation efficiency was determined to 48 % for the hydrophilic cargo and for the hydrophobic one 89 %. The high encapsulation efficiency for PMI can be explained due to its hydrophobic nature as there is only the possibility to incorporate into the hydrophobic membrane of the particles. Furthermore it could be shown in the CLSM after cell uptake the colocalisation of cargo and polymer as well as free released cargo. In the case of encapsulating high cytotoxic drug like TNF-α the polymersomes encapsulate over a time frame up to 24 h safe and secure without acting significantly toxic compared to pure TNF-α which already start to act toxic after 3 h. Also dentritic cells which matured with TNF-α loaded polymersomes were able to activate T cells which proliferate strongly.

Chapter 7: In vivo experiments

Particles formed by synthesized amphiphilic blockcopolymers were used for *in vivo* studies. Hereby, unlabeled particles were encapsulated with labeled Cy5-siRNA as the hydrohphilic drug and injected retroorbital in which it was found an accumulation primarly in the liver. Also the extend in uptake by liver macrophages was determined.
Furthermore particles were formed from amphiphilic blockcopolymers labeled with NIR 800 RS dye and injected subcutaneous as well as systemic and the upcoming differences are discussed.

Determination of encapsulation efficiency of Cy5-siRNA

It was conducted *in vivo* experiments for the Polymersomes obtained from p(DHPA)$_{30}$-*b*-p(LMA)$_{42}$ **(R1)** p(DHPA$_{30}$-*stat*-NIR-RS-800)-*b*-p(LMA)$_{42}$ **(R4)** loaded with various drugs, like siRNA. Here an important information is how much of hydrophilic drug can be encapsulated in the aqueos interior of the vesicles. For this prupose Cy5 labled siRNA was encapsulated into particles and the encapsulation efficiency was determined over UV-vis spectrometry. 20 µL of a 100 µM Cy5-siRNA solution was incubated with 5,35 mg of the amphiphilic blockcopolymer **R1** overnight. Then 72 mg of ceramic beads were added and the sample was centrifugated over the duale centrifugation method. The obtained particles were purified over sephadex CL-2B. After eluation and isolation of the vesicles the column was washed with PBS and the supernatant (total volume of 2,6 mL) – referred to sample 2 – was measured over UV-vis spectroscopy. Here, sample 1 is set as reference of the used stock solution (20 µL of a 100 µM Cy5-siRNA).

Table 7.1: Determination of encapsulation efficiancy over spectroscopy.

Sample	Absorption (a. u.)
1	0,12
2	0,05

The concentrations can be calculated over the Labert-Beer equation. The extinction coefficient for the dye Cy5 is 250.000 $\frac{\mathrm{L}}{\mathrm{mol}*\varepsilon}$ and the thickness of the used cuvette is 0,01 cm. For samples 1 and 2 it follows for the concentrations:

$$c_1 = \frac{0{,}12}{250.000\,\frac{\mathrm{L}}{\mathrm{mol}*\varepsilon} * 0{,}01\ \mathrm{cm}} = 4{,}5 * 10^{-5}\,\frac{\mathrm{mol}}{\mathrm{L}} \qquad \{7.1\}$$

$$c_2 = \frac{0{,}05}{250.000\,\frac{\mathrm{L}}{\mathrm{mol}*\varepsilon} * 0{,}01\ \mathrm{cm}} = 2 * 10^{-5}\,\frac{\mathrm{mol}}{\mathrm{L}} \qquad \{7.2\}$$

The encapsulation efficiency can be calculated as follows:

$$\mathrm{EE} = \left(1 - \frac{\text{amount of free dye}}{\text{total amount}}\right) * 100\ \% = 30\ \% \qquad \{4.5\}$$

Therefore 30 % of the Cy5 labled siRNA could be encapsulated into the particles into the aqueous interior. The schematic depiction is given below.

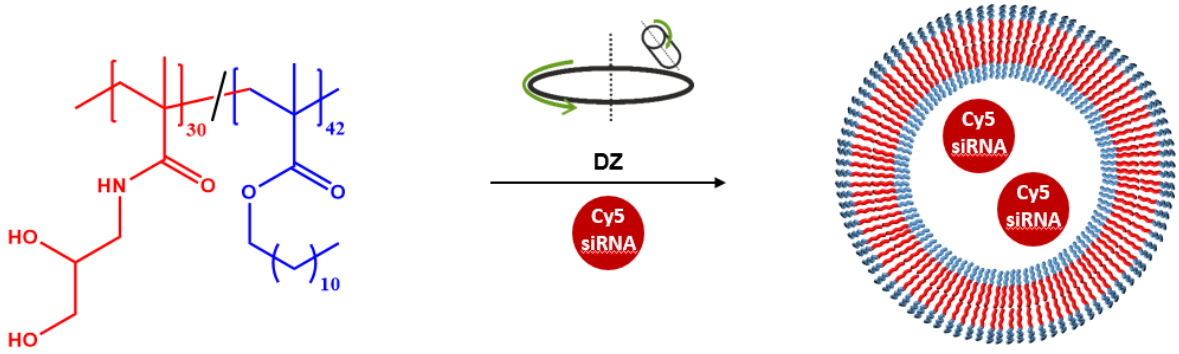

Figure 7.1: Encapsulation of Cy5 lables siRNA.

Retroorbital application of Cy5-siRNA loaded particles

For *in vivo* application (carried out by [redacted] and detection of the Cy5 a minimum amount of 50 µg (2 mg/kg) of Cy5 labeled siRNA is needed per injection (retroorbital) and mouse (Balb/c type) as revealed from experience. In this experiment 65 µg of Cy5-siRNA per injection is used. The total number of mices was 4 while one was used as reference and treated only with PBS.

The *ex vivo* analysis is more sensitive in detection of the fluorescence dye as it has not to penetrate the body to the detector. Therefore the organs of the mices were examined after 24 h of the injection. As it can be seen the particles tend to accumulate primarly in the liver.

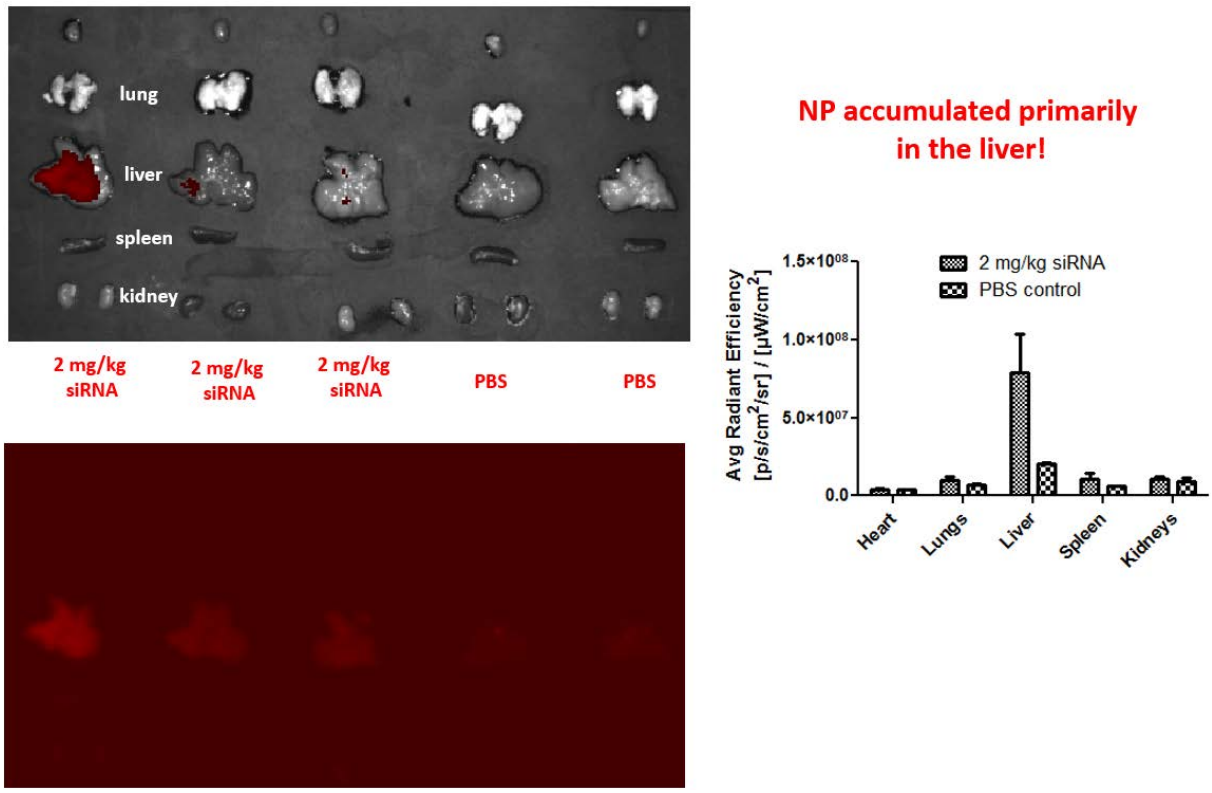

Figure 7.2: *Ex vivo* analysis of retroorbital injected particles encapsulated with Cy5-siRNA after 24h.

Furthermore in FACS data analysis the cell uptake of NPs in liver macrophages (F4/80+ cells) were taken up moderately up to 10 %.

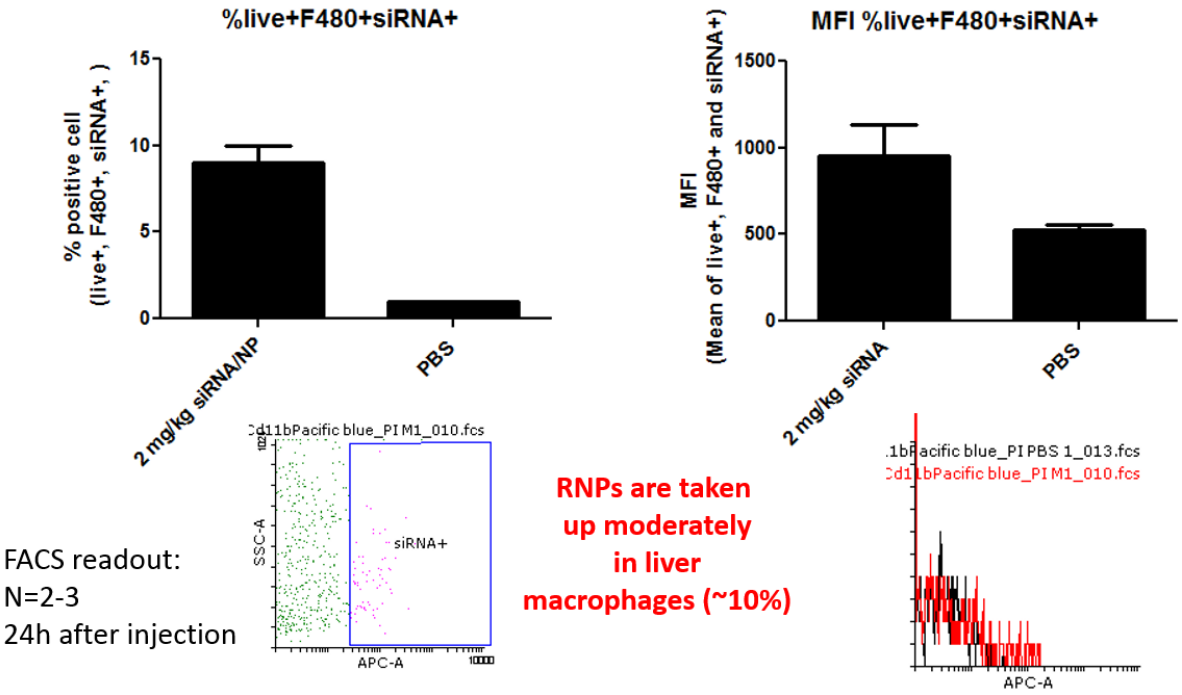

Figure 7.3: FACS analysis of injected particles and control.

Subcutaneous application of NIR-RS-800 labled particles

As another high potential drug for *in vivo* use is TNF-α. Here, the procedure for the formation of the particles was done over duale centrifugation technique as described before. The particles were stored on ice to maintain the bioactivity of the drug. The amphiphilic blockcopolymer used was p(DHPA$_{30}$-*stat*-NIR-RS-800)-*b*-p(LMA)$_{42}$ **(R4)** labled with the dye NIR 800 RS for detection of the particles and encapsulated with PBS.

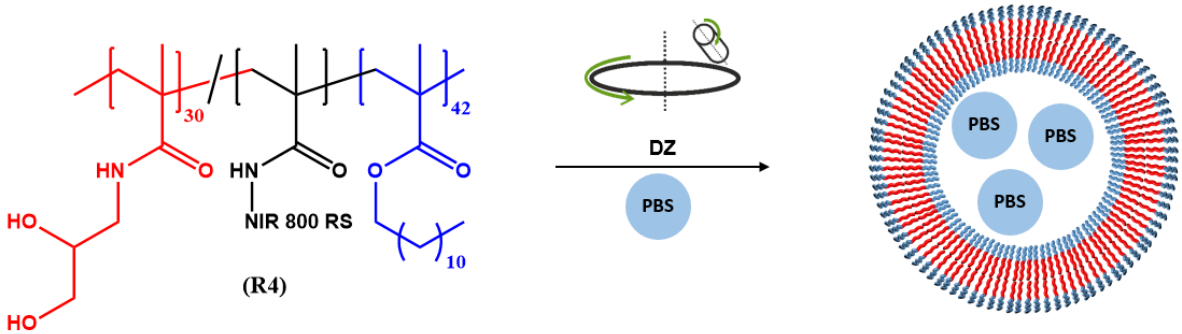

Figure 7.4: PBS encapsulated particles labled with NIR dye.

The size distribution of the obtained particles were measured over DLS (Zetasizer) and is shown in the following figure:

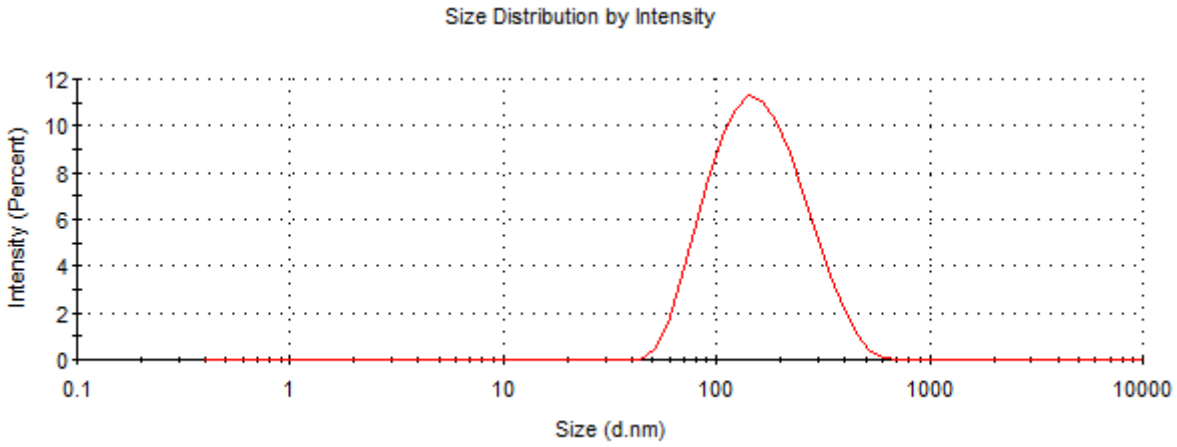

Figure 7.5: Size distribution of PBS encapsulated particles labled with NIR dye.

The particles were injected localy subcutaneous by [redacted]n the back (the pelt was removed) and the fluorescence was measured after different time points up to 72 h carried out by [redacted]. It was used in total 7 mices (NOD/*scid*tgHLA-A2.1), one as a control mice C (untreated), mices 1 and 2 were investigated after 24 h, mices 3 and 4 after 48 h and mices 5 and 6 after 72 h *ex vivo*.

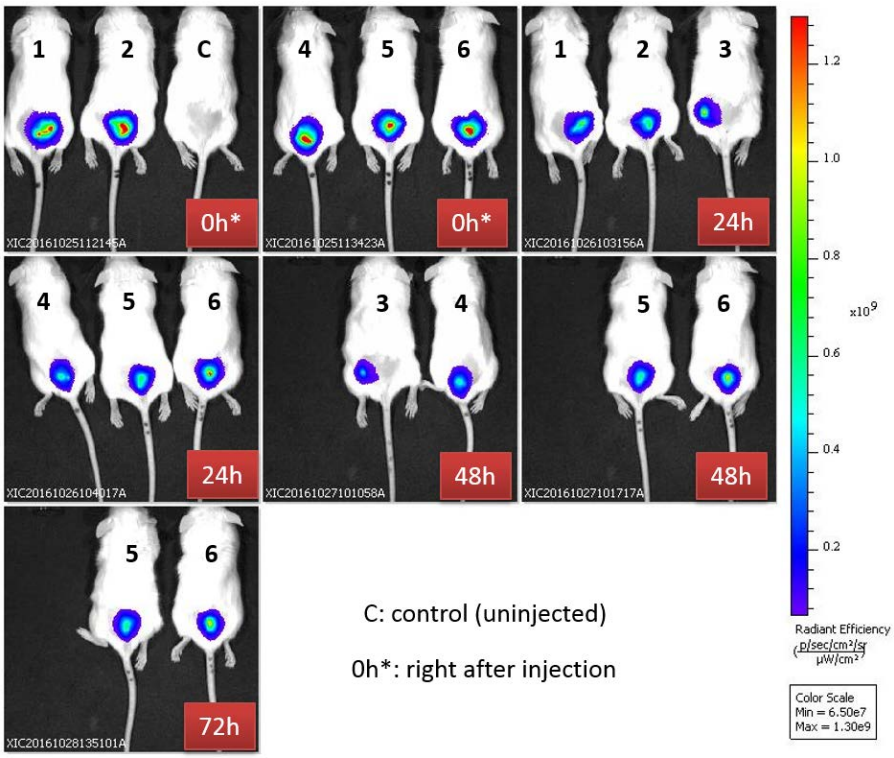

Figure 7.6: Subcutaneous application of NIR RS 800 labled particles into mices.

Mices 1, 2, 4, 5, 6 and the control mice C were measured direct after injection. After 24 h mices 1, 2, 3 whereas mices 1 and 2 were then examined *ex vivo*. It can be seen a local depot effect of the particles at the injected side over a timeframe of 72 h without significantly loss of fluorescence and so particle concentration.

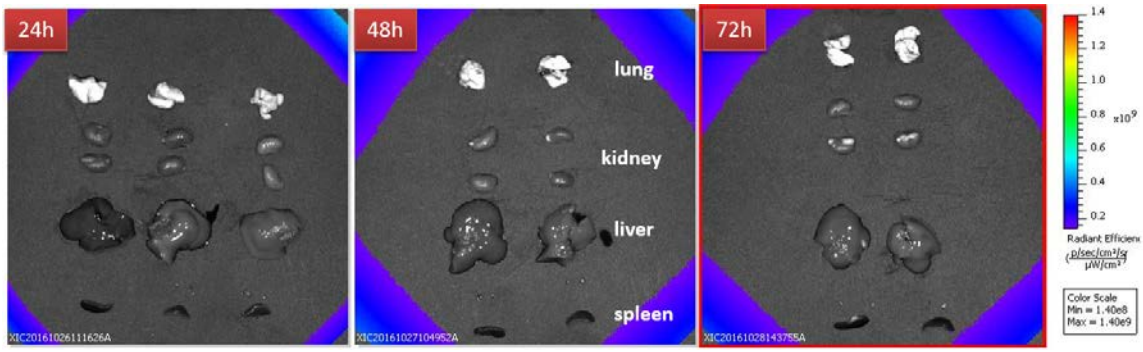

Figure 7.7: *Ex vivo* analysis of subtaneous injected particles after different time points.

The *ex vivo* experiment showed for the different time points of 24 h, 48 h and 72 h no detectable signal leading to the conclusion that there is no systemic redistribution which confirms the local stable depot effect of the particles over 72 h. The next step would be now to load these particles with TNF-α and injection at the tumor side of the mices, to investigate the regression of the tumor and to see an effect regarding the time dependant release of the high cytotoxic drug from the particles.

Systemic application of NIR-RS-800 labeled particles

Furthermore, same particles (unloaded) were used for the *in vivo* application in a systemic manner. The total mice number was three while 2 were treated and one was the used as control mice. The particles were injected in the tail and it was imaged after 30 and 90 min after injection. Then after 24 h and 48 h before examination over *ex vivo*.

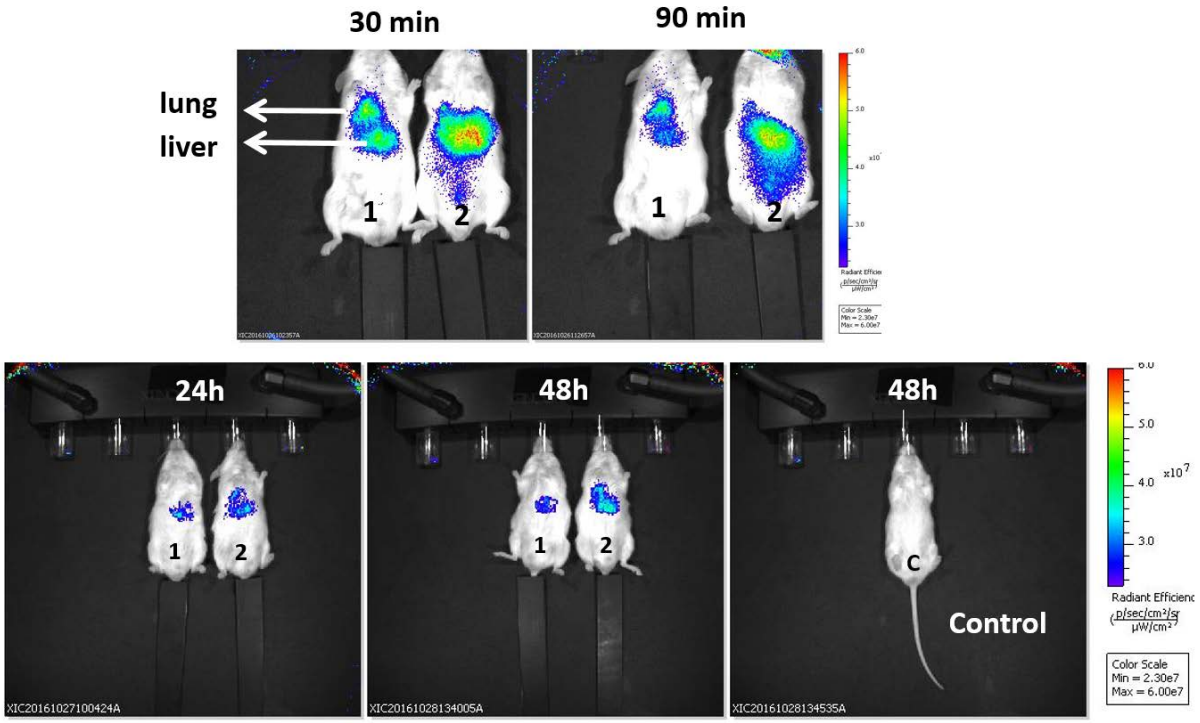

Figure 7.8: Systemic application of NIR RS 800 labled particles into mices.

As it can be seen after 30 min there are strong signals in the lungs and livers which is decreasing with time after 90 min, 24 h and 48 h. All three mices were imaged ex vivo to detect the amount of accumulated dye labled particles in the different organs.

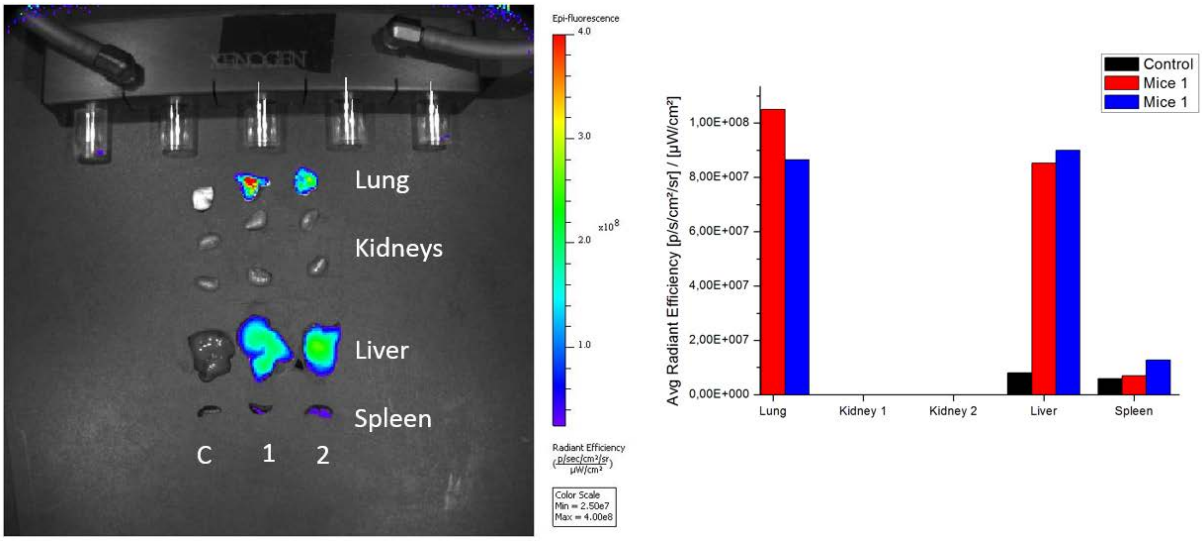

Figure 7.9: *Ex vivo* analysis of systemic injected particles after 48 h.

The analysis revealed that the main accumulation is happening in the lungs and liver and a slight signal in the spleen. Even the distribution of the accumulated particles in

the lungs is of a high density the mices did not choke and take up the particles without outside visible healthy restrictions. Nevertheless a study should be carried out to investigate the biodistribution in dependence with the particle sizes.

Conclusion

In this chapter the synthesized polymers and formed particles over duale centrifugation technique were used for *in vivo / ex vivo* studies. It was able to encapsulate Cy5 labled siRNA into the particles in the aqueous interior. It was reached an encapsulation efficiency of 30%. Then particles were formed and injected into mices whereas the total amount of injected Cy5 labled siRNA was 2 mg/kg. The *in vivo* and *ex vivo* imaging showed that the particles primarly accumulated in the liver leading to a further prove that the siRNA is encapsulated in the particles as there is no indication of a rapid clearance of siRNA by the kidneys.

Nevertheless for the *in vivo* imaging the Cy5-siRNA was not sufficient for optimal detection. As the *ex vivo* is more sensitive it was used for the determination of the biodistribution. FACS dot plots show the tracking of siRNA in the liver macrophages and an uptake of up to 10% which is moderate to good value for macrophage targeting.

Furthermore the particles were decorated with NIR-RS 800 dye for *in vivo* imaging in a subcutaneous and systemic application. In the case of the subcutaneous application the particles stay stable over 72 h at the injection point without significant loss in intensity leading to the assumption that there is a stable local depot effect which is high desirably when loading the particles with drugs and injected in the near of a tumor. In a systemic application the particles accumulate in liver and lungs almost in the same manner even the mices did not choke and taken up the particles without outside visible side effects.

Appendix II:

Synthesis of Dithiobenzoeacid

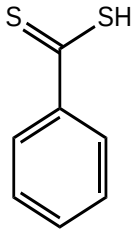

In a 250 mL two neck round reaction vessel equipped with a magnetic stirring bar it was given under Ar atmosphere 56,25 mL of a 0,8 M Phenylmagnesiumchlorid solution in THF (45,0 mmol). Then it was further diluted with 40 mL of dried THF (destilled over sodium). Then it was carefully and slowly added 2,72 mL CS_2 (45,0 mmol; 1,0 eq.) to the Grignard solution and kept at weak boiling and after complete addition it was stirred further for 1 h before the mixture was given on 30 g ice. After acidifying with conc. HCl on pH 1 it was extracted with 40 mL diethylether 3 times. The extracs were given together and the solvent removed under reduced pressure. The obtained red violet, viscosy solution was directly used in the next step.

Synthesis of Dithiobenzoyldisulfite

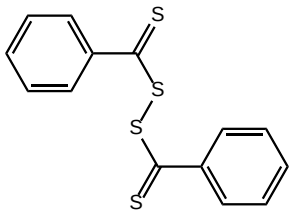

3,36 g KI (21,0 mmol) and 5,14 g I_2 (21,0 mmol) were solved overnight with stirring in 175 mL water. Then it was added to the crude product from the prestep and diluted with 90 mL diethylether. The mixture was extracted in a seperating funnel until the aqueos phase remained slightly yellow which was seperate and the organic layer was washed with 80 mL water for 3 times and dried over $MagSO_4$. Solvent was removed and the viscous crude product was washed with a mixture of 50 mL acetonitril and 50 mL water. It was obtained a violet solid which was isolated and dried in vacuum at 40 °C.

Yield: m = 12,85 g (41.9 mmol; 93,1 % of Theory)

Synthesis of 4-Cyano-4-((thiobenzoyl)sulfanyl)pentanoicacid

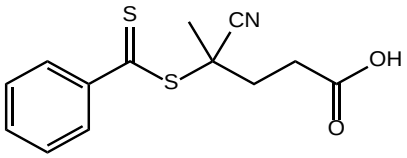

The crude product of the prestep was given in a 250 mL schlenk vessel and solved in 150 mL ethylacetate with 18,81 g ACVA (67,1 mmol; 1,6 eq.). The mixture was freezed in liquid nitrogen and precesses 3 Freeze-Pump-Thaw-Cyclen. After the third cycle a reflux condenser in nitrogen reverse flow was fixed and the mixture was kept boiling for overnight. Then the solvent was removed and the redviolet crude product was purified over column chromatography ($CHCl_3$/ EtOH, 20:1 v/v). The end product was obtained as a red-violet, amorphous solid.

Yield: m = 6,67 g (23,8 mmol; 56,8 % of Theory).

^{1}H-NMR (400 MHz, CDCl3): δ [ppm] = 7,92 (d, 8,4 Hz, 2H, *o*-Ar*H*); 7,57 (t, 7,4 Hz, 1H, *p*-Ar*H*); 7,40 (t, 7,7 Hz, 2H, *m*-Ar*H*); 2,82-2,41 (m, 4H, - C*H*2-C*H*2-); 1,95 (s, 3H, -C*H*3)

^{13}C-NMR (100 MHz, CDCl3): δ [ppm] = 222,28 (-*C*SS); 177,30 (-*C*OOH); 144,61 (CSS-Ar*C*); 133,24 (*p*-Ar*C*); 128,73 (*m*-Ar*C*); 126,82 (*o*-Ar*C*); 118,52 (-*C*N); 45,73 (-*C*-CH3); 33,14 (-*C*H2-COOH); 29,68 (-*C*H2- CH2-COOH); 24,32 (- C*H*3)

Synthesis of Pentafluorphenylmethacrylat (PFPMA)

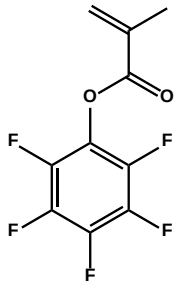

In 1 L two necked round bottom flask under inert gas athmosphere 30 g (0.16 mmol; 1 eq) of pentafluorophenol in 300 mL of dichloromethane were solved and cooled in a ice water bath to 0 °C. After addition of 18,10 g (178.9 mmol; 1,10 eq.) triethylamine 17,47 mL of methacryloyl chloride were added dropweise under stirring and further cooling. After complete addition it was stirred for 15 min in ice water bath and then for 12 h at room temperature. The resulting colorless precipitate was filtered and the

reaction mixture was washed with 150 mL water for three times. The organic layer was seperated and dried over $MgSO_4$. Then the solvent was removed under reduced pressure and the resulting yellow crude product was purified over fractionated vacuum destilation ($2x10^{-2}$ mbar, 36 °C) in which the product was obtained as colorless liquid.

Yield: m = 29,78 g (118.1 mmol; 72,5 % of Theory)

^{1}H-NMR (400 MHz, $CDCl_3$): δ [ppm] = 6,45 (s, 1H, C=C*H*2-cis); 5,91 (s, 1H, C=C*H*2-trans); 2,09 (m, 3H, -C*H*3)

^{13}C-NMR (CDCl3, 75 MHz): δ [*ppm*] = 163,22 (-*C*O2); 142,79-142,54 (*o*-Ar*C*); 141,00-140,65 (*p*-Ar*C*); 140,29-140,04 (*o*-Ar*C*); 139,47-139,11 (*m*-Ar*C*); 138,45-138,18 (*p*-Ar*C*); 136,96-136,01 (*m*-Ar*C*); 133,83 (*C*=CH2); 130,14 (C=*C*H2); 125,49 (Ar*C*-CO2-); 18,43 (-*C*H3).

^{19}F-NMR (377 MHz, CDCl3): δ [ppm] = -153,95 (d, J = 18,0 Hz, 2F, *o*-Ar*F*); -159,9 (t, J = 21,7 Hz, 1F, *p*-Ar*F*); -163,65 (t, J = 26,0 Hz, 2F, *m*-Ar*F*)

Synthesis of 2,2-Dimehtyl-1,3-dioxolan-4-ethyl-alcohol

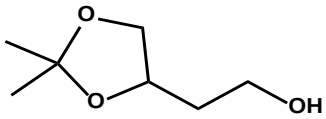

1,2,4-Butanetriol (1.64 mL, 18.9 mmol) was added to a stirred solution of PTSA (93 mg, 0.49 mmol) in acetone (13.3 mL, 181 mmol) and the mixture stirred at room temp. for 20 h. Triethylamine (0.30 mL, 1.9 mmol) was added, and the volatiles were removed under reduced pressure (80 mbar) to give the crude product as a yellow oil. The crude product was purified by flash column chromatography (silica gel; dichloromethane/diethyl ether, 4:1 as eluent) to give the desired product as a pale yellow oil.

Yield: m = 2,43 g (16.6 mmol; 87 % of theory)

^{1}H-NMR (500 MHz, $CDCl_3$): δ [ppm] = δ = 4.30–4.25 (m, 1 H), 4.09 (dd, J = 6.1,

8.0 Hz, 1 H), 3.82–3.79 (m, 2 H), 3.60 (t, J = 7.6 Hz, 1 H), 2.21–2.18 (m, 1 H), 1.85–1.81 (m, 2 H), 1.43 (s, 3 H), 1.37 (s, 3 H)

^{13}C-NMR (125 MHz, $CDCl_3$): δ [ppm] = 109.1, 75.1, 69.4, 60.6, 35.6, 26.9, 25.7

Synthesis of 2-(2,2-Dimethyl-1,3-dioxolan-4-yl)ethylmethacrylat (DDEMA)

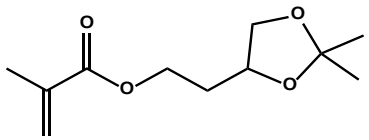

4-(2-Hydroxyethyl)-2,2-dimethyl-1,3-dioxolan (5 g; 34.2 mmol) was solved in 80 mL diethylether and 4,15 g (41.0 mmol; 1.2 eq) triethylamin was added. 3,65 mL Methacryloyl chloride (37.6 mmol, 1.1 eq) was added slowly dropwise. The mixture was stirred at 0 °C under Argon-Atmosphare. The solvent was removed and the crude product was purified over column chromatography with the eluent cyclohexane/ethyl acetate (8/1). The desired product was obtained after dolvent removal and drying in vacuum.

Yield: m = 4,79 g (22,3 mmol; 65 % of Theory)

R_f = 0,63

^{1}H-NMR (400 MHz, $CDCl_3$): δ [ppm] = 6,12 (s, 1H, C=CH_2-cis); 5,59 (s, 1H, C=CH_2-trans); 4,32 (m, 1H, -O-C*H*-CH_2-); 4,22 (m, 2H, -COO-CH_2-); 4,10 (dd, J_1 = 7,0 Hz; J_2 = 1,1 Hz, 1H, -O-CH_2-CH-); 3,62 (dd, J_1 = 7,0 Hz; J2 = 1,1 Hz, 1H, -O-C*H*2-CH-); 2,06-1,89 (m, 2H, -COO-CH_2-CH_2-); 1,97 (s, 3H, CH_3-C(CH2)-); 1,43 (s, 3H, C*H*3-C(CH3)-O-); 1,38 (s, 3H, CH_3-C(CH_3)-O-).

Synthesis of 8,8-Dibromobicyclo[5.1.0]octan

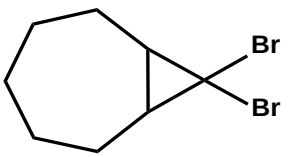

In a 500 mL three necked round bottom vessel with magnetic stirring bar and dropping funnel was solved a mixture of *cis*-Cycloheptene (2,22 g; 23,08 mmol; 1,00 eq) and Potassium-tert-butanolate (2,98 g; 26.54 mmol; 1.15 eq) in 150 mL of dried *n*-

pentane. The mixture was cooled in a ice bath to 0 °C and then a solution of bromoforme in 150 mL of dried n-pentane was slowly added over the dropping funnel. After complete addition the reaction mixture was warmed up to room temperature and stirred overnight. As the reaction control via DC showed the entire conversion it was extracted with 400 mL water and the aqueos pahse was treated 6 times with 50 mL of n-pentane. The combined organic layers were washed wirh saturated NaCl solution and dried over sodium sulfate. The remaining yellow liquid was exempt from solvent to isolate the product as yellow oil.

Yield: m = 2,27 g (8,47 mmol; 37 % of theory)

$\mathbf{R_f}$ = 0,80 (cHex, UV-Lampe)

^{1}H-NMR ($CDCl_3$, 400 MHz): δ [*ppm*] = 2,29-2,22 (dt, 2H, *J* = 14,3 und 5,4 Hz, H^2 und H^6); 1,92-1,80 (m, 3H, H^3, H^4 und H^5); 1,75-1,67 (m, 2H, H^1 und H^7); 1,42-1,32 (m, 2H, H^3 und H^5); 1,25-1,11 (m, 3H, H^2, H^4 und H^6).

Synthesis of 2-Bromcyclooct-2-en-1-tetraethylenglykol

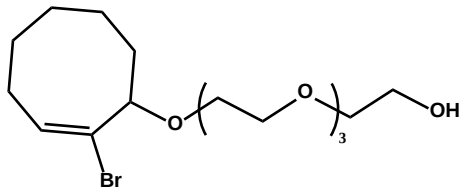

Tetraethylenglykole (43,9 mL; 254,10 mmol; 30 eq) und silver perchlorate (5,27 g; 25,41 mmol; 3 eq) were solved in 11 mL of dried toluol under inertgas and added to a solution of 8,8-Dibrombicyclo[5.1.0]octane (2,27 g; 8,47 mmol; 1 eq), pyridine (6,1 mL; 74,96 mmol; 9 eq) and 5 mL of dried toluene. The reaction mixture was refluxed overnight under exclusion of light and the next day the solvent was removed under reduced pressure. After addition of 120 mL of saturated NaCl solution the hardly soluble silver salts were filtered and the filter residue were washed with 150 mL diethylether. The aqueos filtrat was extracted ten times eith 50 mL diethylether before the combined organic layers were dried over sodium sulfate. After removing

solvent under reduced pressure the desired product was obtained as a yellow-brown oil.

Yield: m = 2,11 g (7.20 mmol; 85 % of theory)

$\mathbf{R_f}$ = 0,34 (EtOAc, UV-Tisch)

^{1}H-NMR (CDCl3, 400 MHz): δ [*ppm*] = 6,19-6,15 (dd, 1H, *J* = 11,7 und 4,2 Hz, -C*H*=CBr-); 3,93-3,89 (dd, 1H, *J* = 10,4 und 5,0 Hz, -CH=CBr-C*H*OR-CH2-); 3,72-3,58 (m, 17H, -O-(C*H*2-C*H*2-O)4-*H*); 2,77-2,66 (qd, 1H, *J* = 11,9 und 5,4 Hz, -C*H*H-CH=CBr-); 2,30-2,24 (m, 1H, -C*H*H-CH=CBr-); 2,04-1,82 (m, 4H, -CHOR-C*H2*-, -CHOR-CH2-C*H*H- und –CHOR-(CH2)3-C*H*H-); 1,72-1,64 (m, 1H, -CHOR-(CH2)2-C*H*H-); 1,52-1,42 (m, 1H, -CHOR-(CH2)3-C*H*H-); 1,31-1,22 (m, 1H, -CHOR-(CH2)2-C*H*H-); 0,82-0,73 (m, 1H, -CHOR-(CH2-C*H*H-).

Synthesis of Cyclooct-2-in-1-tetraethylenglykol

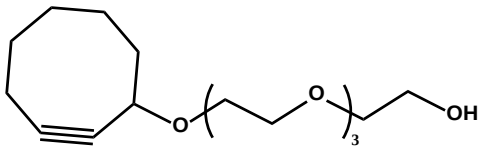

In a three necked round bottom vessel with magnetic stirring bar were solved 2-Bromcyclooct-2-en-1-tetraethylenglykol (2,04 g; 5,35 mmol; 1,0 eq) and Pyridin (7,4 mL; 91,68 mmol; 17,1 eq) in 46 mL isopropanol. After addition of sodium-*tert*-butanolat (1,50 g; 13,38 mmol; 2,5 eq) the reaction mixture was stirred for 64 h at room temperature and neutralize with HCl solution (5%). Afterward it was added 100 mL of water and 150 mL of dichloromethane. The orange colored organic phase was seperated from the yellow aqueos phase and the aqueos phase was extracted ten times with 50 mL diethylether until it turned colorless. The combined organic layers were dried and then the solvent was removed under reduced pressure. The resulting brown-yellow oily crude priduct (1,35 g) was purified over silica column chromatography (EtOAc/cHex 1:1) and the product could be isolated as a yellow oil.

Yield: m = 0,75 g (2.50 mmol; 47 % of theory)

$\mathbf{R_f}$ = 0,29 (EtOAc, UV-Tisch)

^{1}H-NMR ($CDCl_3$, 400 MHz): δ [*ppm*] = 4,23-4,19 (ddt, 1H, J = 7,3 und 5,0 und 2,2 Hz, -C≡C-C*H*OR-CH2-); 3,74-3,47 (m, 16H, -O-(C*H2*-C*H2*-O)4-H); 2,60 (s, 1H, -O*H*); 2,28-2,20 (m, 3H, -C≡C-CHOR-C*H*H- und –C≡C-CHOR-CH2-C*H2*-); 2,03-1,54 (m, 6H, -C≡C-CHOR-C*H*H-, -C≡C-CHOR-(CH2)2-C*H2*-), -C≡C-CHOR-(CH2)3-C*H*H- und –C≡C-CHOR-(CH2)4-C*H2*-); 1,46-1,38 (m, 1H, -C≡C-CHOR-(CH2)3-C*H*H-).

^{13}C-NMR ($CDCl_3$, 400 MHz): δ [*ppm*] = 100,17 (-*C*≡C-CHOR-); 92,92 (-C≡*C*-CHOR-); 72,89 (-C≡C-*C*HOR-); 72,68 (-*C*H2-CH2-OH); 70,77 (-*C*H2-O-CH2-CH2-OH); 70,71 (-*C*H2-CH2-O-CH2-CH2-OH); 70,66 (-*C*H2-(O-CH2-CH2)2-OH); 70,54 (-*C*H2-CH2-(O-CH2-CH2)2-OH); 70,49 (-*C*H2-(O-CH2-CH2)3-OH); 68,61 (-*C*H2-CH2-(O-CH2-CH2)2-OH); 61,90 (-*C*H2-OH); 42,38 (-C≡C-CHOR-*C*H2-); 34,42 (-C≡C-CHOR-(CH2)2-*C*H2-); 29,87 (-C≡C-CHOR-(CH2)4-*C*H2-); 26,50 (-C≡C-CHOR-(CH2)3-*C*H2-); 20,83 (-C≡C-CHOR-CH2-*C*H2-).

ESI-MS (Acetonitril): m/z (%) = 323,53 g/mol (100,00) [M+Na]+; 339,17 g/mol (12,00) [M+K]+; 301,22 g/mol (5,20) [M+H]+; C16H28O5 (berechnet: 300,19 g/mol).

Synthesis of COT

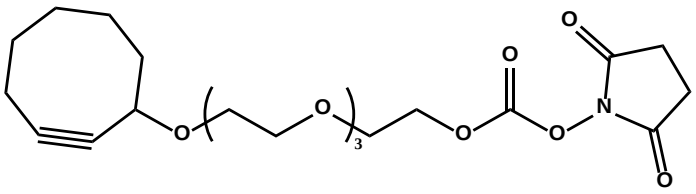

N,N´-Disuccinimidylcarbonat (1,89 g; 7,39 mmol; 3 eq) was dissolved in a 100 mL three necked round bottom vessel under Ar athmosphere. Cyclooct-2-in-1-tetraethylenglykol (0,74 g; 2,46 mmol; 1 eq) was dissolved in 15 mL of acetonitrile and was added over a septum to the reaction mixture together with triethylamine (1,0 mL; 7,39 mmol; 3 eq). The yellow mixture was stirred at room temperature for 18 h before unsolved *N,N´*-Disuccinimidylcarbonate was filtered and the solvent removed under reduced pressure. The reamaining brown-yellow oil was solved in 2 mL of acetonitrile and given on silica gel. After silica column chromatography (

cyclohexane/ethylacetate 1:1, then pure ethylacetate) the product could be succesful purified and isolated as colorless oil.

Yield: m = 0,91 g (2.06 mmol; 84 % of theory)

$\mathbf{R_f}$ = 0,69 (EtOAc)

^{1}H-NMR (CDCl3, 400 MHz, COSY, HSQC): δ [*ppm*] = 4,47-4,44 (m, 2H, -CH2-CH2-O-CO-O-); 4,24-4,20 (m, 1H, -C≡C-C*H*OR-CH2-); 3,79-3,77 (m, 2H, -O-C*H2*-CH2-O-CO-O-); 3,74-3,69 (m, 1H, -O-C*H*H-CH2-O-(CH2-CH2-O)3-CO-O-); 3,66-3,63 (m, 10H, -O-CH2-C*H2*-O-(C*H2*-C*H2*-O)2-O-CH2-CH2-O-CO-O-); 3,53-3,48 (m, 1H, -O-C*H*H-CH2-O-(CH2-CH2-O)3-CO-O-); 2,83 (s, 4H, -CO-C*H2*-C*H2*-CO-); 2,28-2,20 (m, 1H, -C≡C-CHOR-CH2-C*H*H-); 2,18-2,08 (m, 2H, -C≡C-CHOR-C*H*H- und –C≡C-CHOR-CH2-C*H*H-); 2,00-1,88 (m, 2H, -C≡C-CHOR-C*H*H- und –C≡C-CHOR-(CH2)2-C*H*H-); 1,85-1,78 (m, 2H, -C≡C-CHOR-(CH2)2-C*H*H- und –C≡C-CHOR-(CH2)3-C*H*H); 1,72-1,55 (m, 2H, C≡C-CHOR-(CH2)4-C*H2*-); 1,46-1,38 (m, 1H, C≡C-CHOR-(CH2)3-C*H*H-).

^{13}C-NMR (CDCl3, 100 MHz, HSQC): δ [*ppm*] = 168,68 (-*C*O-CH2-); 151,76 (-O-*C*O-O-); 100,12 (-*C*≡C-CHOR-); 92,97 (-C≡*C*-CHOR-); 72,88 (-C≡C-*C*HOR-); 70,99 (-*C*H2-CH2-O-(CH2-CH2-O)2-CO-O-); 70,78 (-*C*H2-O-(CH2-CH2-O)2-CO-O-); 70,73 (-*C*H2-CH2-O-CH2-CH2-O-CO-O-); 70,67 (-*C*H2-O-CH2-CH2-O-CO-O-); 70,52 (-*C*H2-O-(CH2-CH2-O)3-CO-O-); 70,40 (-CH2-*C*H2-O-CO-O-); 68,62 (-O-*C*H2-CH2-O-(CH2-CH2-O)3-CO-O-); 68,47 (-O-*C*H2-CH2-O-CO-O-); 42,40 (-C≡C-CHOR-*C*H2-); 34,43 (-C≡C-CHOR-(CH2)2-*C*H2-); 29,88 (-C≡C-CHOR-(CH2)4-*C*H2-); 26,52 (-C≡C-CHOR-(CH2)3-*C*H2-); 25,60 (-CO-*C*H2-*C*H2-CO-); 20,84 (-C≡C-CHOR-CH2-*C*H2-).

ESI-MS (Acetonitril): m/z (%) = 464,14 g/mol (100,00) [M+Na]+; 459, 21 g/mol (50,36) [M+NH4]+; 480,15 g/mol (33,53) [M+K]+; C21H31NO9 berechnet: 441,20 g/mol.

<u>Synthesis of *N*-BOC ethylenediamine</u>

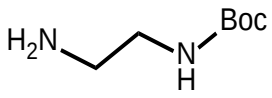

In a round-bottomed flask was dissolved 4 ml (60 mmol, 10 eq) of ethylene diamine in 40 ml of drydichloromethane and stirred at 0ºC. Then, it was added drop-by-drop a solution of Boc anhydride (1,31g, 6 mmol, 1 eq) in 20 ml of dichloromethane. After the addition was finished the reaction mixture was stirred for 24 hours at room temperature, before the solvent was removed under low pressure to yield a viscous oil. It was redissolved in a solution of 2M $NaCO_3$ (60 ml) and extracted twice with 60 ml of dichloromethane. The organic phase was dried with NaSO4, evaporated to dryness. N-Boc ethylenediaminewas isolated as an uncolored oil with enough purity to be used in subsequent reactions.

Yield: m = 1,05 g (6.55 mmol; 91 % of Theory)

^{1}H NMR (400 MHz, $CDCl_3$): δ [*ppm*] = 4.94 (bs, 1H), 3.17-3.11 (q, 2H), 2.79-2.72 (t, 2H), 1.42 (s, 9H), 1.16 (bs, 2 H)

Synthesis of *N*-BOC ethylenediamine-folate

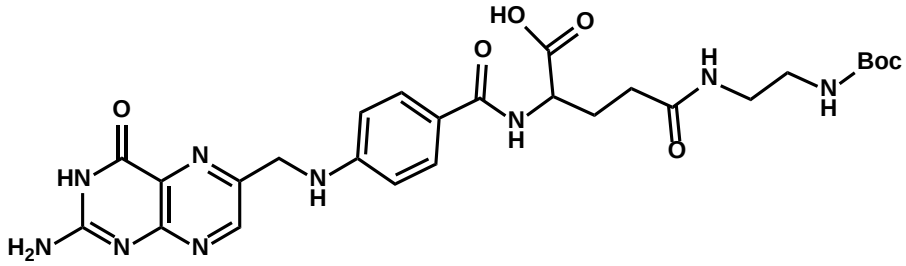

In a round-bottomed flask was dissolved 1 g of folic acid (2.11 mmol, 1 eq. dehydrated powder) in 40 ml of DMSO. After the dissolution was complete (about 30 minutes with mild heating), 482 mg (2 eq) of N-hydroxysuccinimide and 863 mg (2 eq) of DCC were added successively. The reaction mixture was stirred for 16 h at room temperature, after which the urea precipitate was filtered off. Then, it was added 0.59 ml (2 eq) of triethylamine followed by 683 mg (2 eq) of *N*-Boc-ethylene diamine dissolved in 5 ml of DMSO. The mixture was again stirred overnight, before it was added to a mixture of 20% acetone in diethylether. The thin yellow precipitated was carefully centrifuged and washed four times with acetone and two with diethyl ether and dried under vacuum. The folic acid was conjugated with N-Bocethylene diamine almost exclusively in the terminal carboxylic acid as confirmed

by RP-HPLC (injection of sample dissolved in DMSO, 1 ml/min, 0 to 5.5min 100% water, linear gradient from 5.5 min at 100% water to 15.5min at 100% acetonitrile, Gemini 5u 18 110A, 5umx4.6x250mm, Phenomenex column) and ^{1}H-NMR.

Yield: m = 987 g (1.69 mmol; 72 % of Theory)

^{1}H NMR (400 MHz, DMSO): δ [*ppm*] = 8.64 (s, 1H, pterin), 8.04-7.86 (m, 2H), 7.68-7.62 (m, 2H, aromatic), 7.10-6.82 (m, 3H), 6.65-6.63 (d, 2H, aromatic), 4.48 (bs, 2H, benzylic), 4.27 (m, 1H, αH), 3.43 (bs, water) 3.06- 2.88 (m, 4H, ethylenediamine), 2.28-1.85 (m,4H, glutamic moiety), 1.35(s, 9H, Boc).

^{13}C NMR (100 MHz, DMSO) δ 172.38, 166.60, 161.64, 156.07, 154.46, 151.23, 151.19, 149.00, 129.53, 129.32, 128.44, 122.01, 111.72, 78.07, 52.84, 46.43, 46.12, 40.94, 39.27, 32.50, 31.51, 28.68, 10.14.

Synthesis of Ethylenediamine-folate

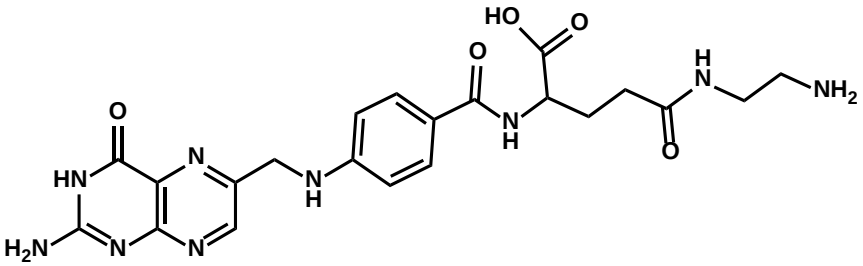

300 mg *N*-Boc-ethylenediamine folate (0.51 mmol) was dissolved in 2 ml of trifluoroacetic acid and stirred during two hours. The solvent was removed under pressure with aid of dichloromethane and the red-dark residue was dissolved in the minimal amount of dry DMF. The addition of triethylamine resulted in the precipitation of a yellow powder which was washed and centrifuged four times with acetone and two times with diethyl ether.

Yield: m = 0,21 g (0.43 mmol; 84 % of Theory)

^{1}H NMR (400 MHz, DMSO): δ [*ppm*] = 8.64 (s, 1H, pterin), 8.19-7.96 (m, 1H), 7.66-7.58 (m, 2H, aromatic), 7.18-6.91 (m, 3H), 6.66-6.63 (m, 2H, aromatic), 4.47 (bs, 2H,

benzylic), 4.31-4.07 (m, 1H), 3.52 (water), 3.32-3.19 (m, ethylene diamine), 2.86-2.80 (m, 2H, ethylene diamine), 2.24-1.93 (m, 4H, glutamic moiety).

Synthesis of COT-Ethylenediamine-folate

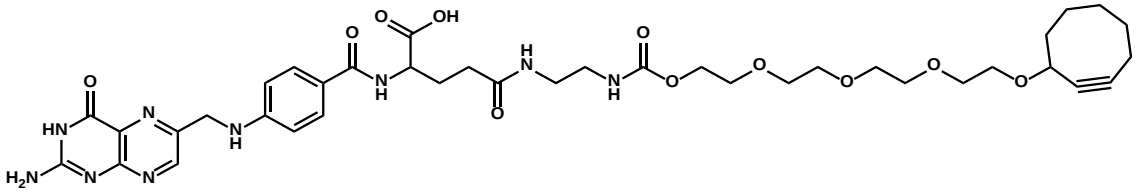

To a solution of ethylenediamine-folate (54 mg, 0.11 mmol, 1 eq) in a total volume of 5 mL of dry DMSO was added diisopropylethyl amine (75 µL, 4 eq) and COT (60 mg, 0.14 mmol, 1.4 eq) and stirred until a clear solution is obtained (about 1 h). The reaction mixture was poured into a mixture of 20% acetone in diethylether. The thin yellow precipitated was carefully centrifuged and washed two times with acetone and two times with diethyl ether and dried under vacuum.

Yield: m = 50 mg (0.06 mmol, 56 % of Theory)

^{1}H NMR (400 MHz, DMSO): δ [*ppm*] = 8.63 (s, 1H, pterin), 8.19-7.96 (m, 1H), 7.66-7.58 (m, 2H, aromatic), 7.18-6.91 (m, 3H), 6.66-6.63 (m, 2H, aromatic), 4.47 (bs, 2H, benzylic), 4.31-4.07 (m, 1H), 3.32-3.19 (m, ethylene diamine), 2.86-2.80 (m, 2H, ethylene diamine), 2.24-1.93 (m, 4H, glutamic moiety) 4,47-4,44 (m, 2H, -CH2-CH2-O-CO-O-); 4,24-4,20 (m, 1H, -C≡C-C*H*OR-CH2-); 3,79-3,77 (m, 2H, -O-C*H2*-CH2-O-CO-O-); 3,74-3,69 (m, 1H, -O-C*H*H-CH2-O-(CH2-CH2-O)3-CO-O-); 3,66-3,63 (m, 10H, -O-CH2-C*H2*-O-(C*H2*-C*H2*-O)2-O-CH2-CH2-O-CO-O-); 3,53-3,48 (m, 1H, -O-C*H*H-CH2-O-(CH2-CH2-O)3-CO-O-); 2,83 (s, 4H, -CO-C*H2*-C*H2*-CO-); 2,28-2,20 (m, 1H, -C≡C-CHOR-CH2-C*H*H-); 2,18-2,08 (m, 2H); 2,00-1,88 (m, 2H); 1,85- 1,78 (m, 2H); 1,72-1,55 (m, 2H); 1,46-1,38 (m, 1H).

Synthesis of 6-(Hydroxyhexyl) methacrylate (HHMA)

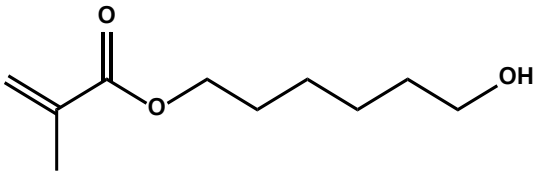

1,6-hexane-diol (73,6 g, 623 mmol, 10 equivalents) was dissolved in THF (200 mL) with stirring and heat. The respective solutions were then cooled to below 10 °C using an ice bath before triethylamine (9 mL) was added. Using a pressure equalizing dropping funnel, methacryloyl chloride (6 mL, 1 molar equivalent) was added drop-wise with stirring, over 30 min. The precipitated solid (trimethylamine hydrochloride and unreacted 1,6-hexane-diol) was removed by filtration. Solvent was removed from the filtrate under reduced pressure and the remaining colorless oil was resuspended in chloroform and washed sequentially with dilute HCl and deionized water. The organic layer was dried over anhydrous magnesium sulfate, filtered, and the solvent removed under reduced pressure to yield a clear, colorless oil.

Yield: m = 6,95 g (37 mmol; 60 % of Theory)

^{1}H NMR (400 MHz, DMSO): δ [*ppm*] = 6.1 (s, 1H); 5.5 (s, 1H); 4.1 (t, 2H); 3.6 (t, 2H); 1.9 (s, 3H); 1.6 (d, 4H); 1.39 (s, 4H).

Synthesis of Pentafluorophenyl lipoic acid

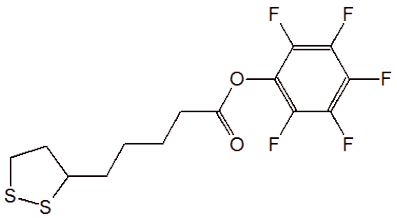

Variation A

To a solution of lipoic acid (4.31 g, 20.88 mmol) in 50 mL dichloromethane was added unter stirring slowly in portions *N,N*-Dicyclohexylcarbodiimid (4.31 g, 20.88 mmol, 1 eq.). After complete addition the resulting mixture was stirred for further 15 min at room temperature. Then a solution of pentafluorophenol (4.13 g, 22.42 mmol, 1 eq.) in 10 mL dichloromethane was added via a syringe and septum and the mixture was stirren for overnight followed by addition of 80 mL destilles water. The solution was filtered and extracted with dichloromethane twice (50 mL). The combined organic layers were washed with saturated NaCl solution, dried over Na_2SO_4 and solvent

was removed under reduced pressure. The resulting crude product was obtained as a yellow oil. Purification was carried out over column chromatography (2:1 Cyclohexan/Essigsäureethylester) to yield the product as a colorless solid.

Variation B

To a solution of lipoic acid (1.34 g, 6.5 mmol) and triethylamine (1.27 g, 1.74 mL, 12.58 mmol, 2 eq.) in 50 mL of dry *N,N*-Dimethylformamid (p.a) was added via a syringe and septum pentafluorophenyltrifluoracetate (3.49 g, 2.14 mL, 12.45 mmol, 2 eq.) and the mixture was stirred overnight. Then 50 mL dichloromethane was added and the mixture was washed three times with destilles water (50 mL). The aqueos phase were extracted with with 50 mL dichloromethane and the combined organic layers were dried ober $MgSO_4$ followed by solvent evaporation under reduced pressure. The crude product was obtained as a gold yellow oil. Purification was conducted over column chromatography (2:1 Cyclohexan/Essigsäureethylester) to yield the desired product as colorless solid.

Yield: 3,44 g (9.24 mmol, 44% for variation A); 1,92 g (5.16 mmol, 79% for variation B).

R_f: 0.84 (2:1 cyclohexane/ethyl acetate).

^{1}H-NMR (400 MHz, $CDCl_3$): δ [*ppm*] = 3.61–3.57 (m, 1H); 3.25–3.06 (m, 2H); 2.69 (t, *J*=7.4 Hz, 2H); 2.52–2.44 (m, 1H); 1.97–1.85 (m, 1H); 1.86–1.70 (m, 4H); 1.67–1.49 (m 2H)

^{19}F-NMR (300 MHz, CDCl3) *δ* = -153.88 – -154.12 (m, 2F); -159.26 (t, *J*=21.7 Hz, 1F); -163.53 (t, *J*=21.6, 2F)

Synthesis of 2-(Pyridyldithio)-ethylamine (PDA)

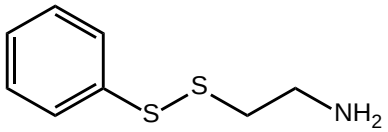

2-mercaptoethylamine hydrochloride (2,29 g, 20 mmol) was dissolved in 17.5 mL of methanol and added dropwise to a stirred solution of 2,2´-dipyridyl disulfide (8.815 g, 40 mmol) dissolved in 41.6 mL of methanol containing 1.6 mL of glacial acetic acid. The reaction was kept under an argon atmosphere to minimize free thiol oxidation. After 48 h, the mixture was concentrated under reduced pressure to give approximately 10-15 mL of yellow oil. The product was precipitated by the addition of 100 mL cold ether and purified by redissolving in 20 mL methanol and precipitating with 100 mL cold ether six times to give a colorless powder.

Yield: 2,75 g (12.35 mmol, 62 % of Theory)

^{1}H NMR (400 MHz, D_2O): δ [*ppm*] = 3.1 (t, *J*) 6.26 Hz, 2H), 3.3 (t, *J*) 6.26 Hz, 2H), 7.3 (m, 1H), 7.7 (m, 1H), 7.8 (m, 1H), 8.4 (m, 1H).

Synthesis of 2-(Pyridyldithio)-dodecane (PDD)

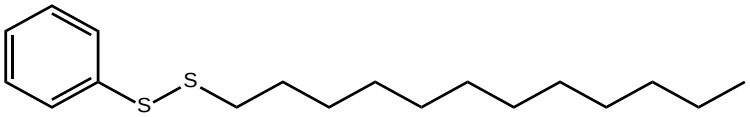

8 g (0.0728 mol) of 2,2' pyridine disulfide (aldrithiol) was dissolved in 50 mL of methanol and was added with 0.536 mL of glacial acetic acid. To this mixture, a solution of dodecanethiol (4 mL, 0.0182 mol) in 20 mL dichloromethane was added dropwise from an addition funnel. Once the addition was over the reaction mixture was stirred at room temperature for additional 3 h. The stirring was stopped, solvent was evaporated in the rotary evaporator and the crude product was purified by column chromatography using silica gel as stationary phase and mixture of ethyl acetate and hexane (1:9 v/v ratio) as eluent. 3.76 g pure product was obtained as light greenish oil in 67 % yield.

Yield: 1,61 g (5.2 mmol, 57 % of Theory)

^{1}H-NMR ($CDCl_3$): δ [*ppm*] = 8.46 (d, 1H), 7.72 (m, 1H), 7.63 (m, 1H), 7.00 (m, 1H), 2.8 (t, 2H), 1.7 (m, 2H), 1.40-1.19 (m, 16 H), 0.9 (t, 3H)

^{13}C-NMR ($CDCl_3$): δ [*ppm*] = 160.7, 149.4, 136.8, 120.3, 119.4, 39.0, 31.9, 29.58-28.5, 22.6, 14.1

Synthesis of 2-(Dodecyldisulfanyl)ethylamin hydrochloride

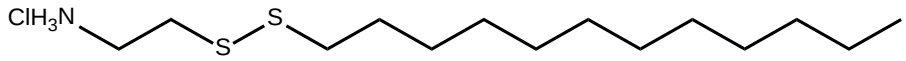

2-(Pyridyldithio)-ethylamine (PDA) (1,75 g; 7.9 mmol, 1 eq) was dissolved in 15 mL methanol and it was added 235 µL of glacial acetic acid. Then dodecanthiol (1,59 g; 7.9 mmol, 1 eq) dissolved in 9 mL dichloromethane was added to the mixture dropwise and it was stirred at room temperature for 2d. the mixture was concentrated under reduced pressure to give approximately 10-15 mL of yellow oil. The product was precipitated by the addition of 50 mL cold ether and purified by redissolving in 10 mL methanol and precipitating with 50 mL cold ether three times. The precipitate was isolated and dried in vacuum to yield the product as a colorless powder.

Yield: 1,45 g (5.22 mmol; 66% of theory)

^{1}H-NMR (MeOD): δ [*ppm*] = 3.1 (t, *J* = 6.26 Hz, 2H), 3.3 (t, *J* = 6.26 Hz, 2H), 7.3 (m, 1H), 7.7 (m, 1H), 7.8 (m, 1H), 8.4 (m, 1H).

Synthesis of 2-(Dodecyldisulfanyl)ethylaminemethacrylate

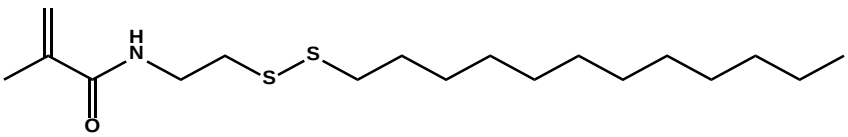

2-(Pyridyldithio)-ethylamine (PDA) (1,45 g; 4.56 mmol) and triethylamine (0.64 mL) were dissolved in 4 mL of anhydrous dichloromethane. Then a mixture of methacryloylchloride (0,51 mL; 5.02 mmol) and triethylamine (0,682 mL; 5.31 mmol) in 2 mL anhydrous dichloromethane were added slowly and dropwise to the reaction mixture. After complete addition it was stirred overnight. Then it was added

20 mL of satureated sodium hydrogen carbonate and it was extracted with ethyl acetate (3 x 25 mL). The combined organic layer were washed with 10 % hydrochloride acid followed twice with detilles water (2 x 50 mL). Solvent was removed under reduced pressure and the obtained crude product was purified over colomn chromatography with a mixture of ethyl acetate and hexane (2:1) as eluent to obtain the colorless desired product.

Yield: 0,835 g (2.41 mmol; 53 % of theory)

R_f = 0,92 (n-hexane/ethyl acetate 2/1)

^{1}H-NMR ($CDCl_3$): δ [*ppm*] = 0.9 (t, 3H), 1.2-1.35 (d, 18H), 1.65 (m, 2H), 1.9 (s, 3H), 2.67 (t, 2H), 2.85 (t, 2H), 3.70 (m, 2H), 5.34 (s, 1H), 5.72 (s, 1H), 6.26 (s, 1H).

Synthesis of *N,N'*-di-(tert-butoxycarbonyl)-cystamine

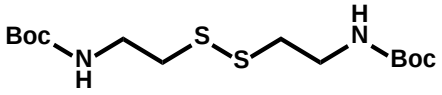

In a round bottom flask equipped with a stir bar cystamine dihydrochloride (6.90 g; 30.64 mmol) was dissolved in a mixture of dioxane (25 mL) and water (25 mL) together with triethylamine (8.5 mL; 61.15 mmol). Then di(tert-butyl) pyrocarbonate (14,70 g; 67.35 mmol) was added portion wise and the reaction mixture was stirred for 3 h at room temperature, before it was diluted with dichloromethane (150 mL). The organic layer was washed with saturated $NaHCO_3$ solution (3x 50 mL), dried over $MgSO_4$ and concentrated by rotary evaporation. The obtained residue was crystallized from dichloromethane affording *N,N'*-di-(tert-butoxycarbonyl)-cystamine as colorless crystals.

Yield: 10,1 g; 28.65 mmol (94 % of theory)

^{1}H-NMR (400 MHz, $CDCl_3$): δ [*ppm*] = 5.02 (br, 2H, -CO-N*H*-); 3.44 (q, 4H, *J* = 5.9 Hz,-CO-N*H*-C*H2*-); 2.79 (t, 4H, -C*H2*-S-S-C*H2*-); 1.44 (s, 18H, -C*H3*)

Synthesis of 2-((2-((tert-butoxycarbonyl)amino)ethyl)disulfanyl)acetic acid

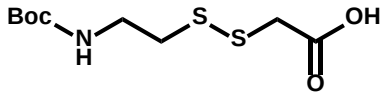

In a round bottom flask equipped with a stir bar *N,N'*-di-(tert-butoxycarbonly)-cystamine (2,65 g; 7.6 mmol) was dissolved in chloroform (40 mL) with triethylamine (6,4 mL; 45,6 mmol). Thioglycolic acid (0,56 mL; 8.36 mmol) was added slowly and drop wise via syringe while stirring vigorously. After further stirring for 2 h at room temperature, the reaction mixture was extracted with 0.5 M $KHSO_4$ (3 x 70 mL). The organic layer was dried over $MgSO_4$ and concentrated by rotary evaporation. The obtained residue was dissolved in diethyl ether (300 mL) and extracted with saturated $NaHCO_3$ solution (5 x 100 mL). The combined aqueous layers were washed with diethyl ether (70 mL) and acidified portion wise with $KHSO_4$ to pH 3. A precipitate was formed that could be extracted with chloroform (5 x 100 mL). All chloroform layers were combined, dried over $MgSO_4$ and concentrated in vacuo affording 2-((2-((tertbutoxycarbonyl) amino)ethyl)disulfanyl)acetic acid as colorless oil.

Yield: 451 mg; 1.03 mmol (22,5 % of theory)

^{1}H NMR (400 MHz, $CDCl_3$): δ [*ppm*] = 6.88 (br, 1H, -COO*H*); 5.06 (br, 1H, -CO-N*H*-); 3.50 (s, 2H, -S-C*H2*-COOH); 3.45 (m, 2H, -CO-NH-C*H2*-); 2.89 (t, 4H, -CO-NH-CH2-C*H2*-S-); 1.45 (s, 9H, -C*H3*)

Synthesis of *N*-BOC-ethyl-disulfide-dimethyloxolan

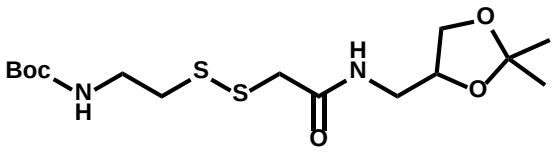

In a round bottom flask 2-((2-((tert-butoxycarbonyl)amino)ethyl)disulfanyl)acetic acid (380 mg; 1.42 mmol; 1.2 eq) and *N*-[(2,2-dimethyl-1,3-dioxolan-4-yl)methyl]-2-methylpropen-2-amid (155 mg; 1.18 mmol; 3 eq) were solved in 8 mL of dry dichloromethane and it was added EDC (340,6 mg; 1.78 mmol; 1.5 eq) and HOBT (240 mg; 1.78 mmol; 1.5 eq) and stirred under Ar atmosphere for 24 h under light

exclusion. The reaction mixture was transferred into a seperating funnel, diluted with DCM p.a. and ectracted with 5 % citric acid. The isolated organic phase was then washed with a saturated $NaHCO_3$ solution followed by saturated NaCl solution. The organic phase was dried over $MgSO_4$, filtered and the solvent was removed. Then it was purified over column chromatography cyclohexane and ethyl acetate (8/2) to yield the desired product as clear viscose liquid.

Yield: 230 mg; 0.61 mmol (51 % of theory)

^{1}H-NMR (400 MHz, DMSO): δ [*ppm*] = 8.23 (s, 1H); 6.98 (s, 1H); 4.10-3.93 (m, 2H); 3.58 (m, 1H); 3.43 (s, 2H); 3.20 (m, 4H); 2.76 (t, 2H); 1.37 (s, 9H); 1.33 (s, 3H); 1.25 (s, 3H).

<u>Synthesis of 2-[(2-amino-ethyl)-disulfanyl]-*N*-(2,3-dihydroxypropyl)acetamid (DHPA-SS)</u>

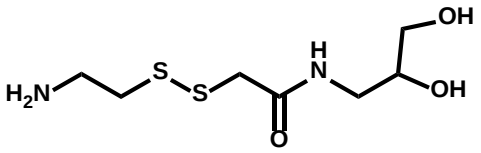

N-BOC-ethyl-disulfide-dimethyloxolan (150 mg; 0.39 mmol) was dissolved in 1.5 mL of dichloromethane and it was added under stirring and cooling 3 mL of Milli-Q water. Then 3 mL trifluoroacetic acid was added over syringe dropwise to the cooled solution. After 3 h the same amount of toluol was added and concentrated in vacuum. Then it was codestilled three times with toluol followed three times with DCM to remove the remaining toluol. The crude product as slightly brown oil was dried in vacuum for 1 h. The it was lyophylised from Milli-Q water. The unsoluble part was filtered over a GHP 0,45 µm.

Yield: 105,8 mg; 0.44 mmol (73 % of theory)

^{1}H NMR (400 MHz, D_2O): δ [*ppm*] = 3.84-3.79 (m, 1H), 3.63-3.59 (dd, 1H), 3.54-3.34 (m, 3H), 3.29-3.24 (q, 1H), 3.00-2.79 (t, 2H).

Synthesis of N-[(2,2-dimethyl-1,3-dioxolan-4-yl)methyl]-2-methylpropen-2-amid (DDMMA)

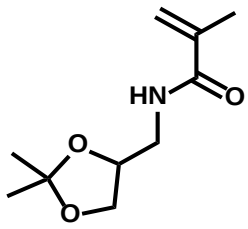

2,2-Dimehtyl-1,3-dioxolan-4-methylamine (2,5 g; 19.06 mmol) was dissolved in 80 mL of anhydrous diethylether and the reaction mixture was cooled to 0 °C with an ice bath. Methacryloyl chloride dissolved in 20 mL of anhydrous diethyl ether was added dropwise at this temperature and a white solid precipitate. After complete addition the mixture was diluted until stirring is starting again. The ice bath was removed and it was stirred at room temperature for further 1 h. The precipitated solid was filtered and purified over column chromatography with a mixture of cyclohexane and ethyl acetate (2:1) as eluent to yield the desired pure product.

Yield: 2,75 g (72 % of theory)

$\mathbf{R_f}$ = 0,17 (cyclohexane/ethyl acetate in 2/1)

^{1}H-NMR ($CDCl_3$): δ [*ppm*] = 1.34 (t, 3H), 1.43 (t, 3H), 1.97 (t, 3H), 3.36-3.45 (m, 1H), 3.53-3.66 (m, 2H), 4.04 (m, 1H), 4.28 (m, 1H), 5.35 (s, 1H), 5.72 (s, 1H), 6.16 (s, 1H).

Synthesis of p(*N*-[(2,2-dimethyl-1,3-dioxolan-4-yl)methyl]-2-methylpropen-2-amid) (p(DDMMA))

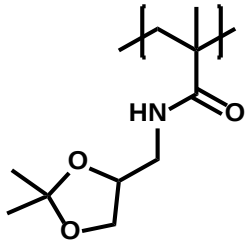

N-[(2,2-dimethyl-1,3-dioxolan-4-yl)methyl]-2-methylpropen-2-amid (DDMMA) (478 mg; 2.4 mmol; 70 eq) was dissolved in 0,7 mL of dried dioxane in a schlenk tube under Ar atmosphere. Then 10 mg of 4-Cyano-4-(phenylcarboothioylthio)pentansäure (10 mg, 0.034 mmol, 1 eq) were added. 2,2´-

Azobis(4-methoxy-2,4-dimethylvaleronitril) (2,1 mg; 6,9*10^{-6} mol; 0.2 eq) as the initator was dissolved seperately in low amount of dried dioxane and was added via a syringe. Then it was immediatly freezed in liquid nitrogen and it was conducted three freeze-pump-thaw cycles. After the last cycle the tube was left under vacuum and it was stirred overnight at 35 °C. The polymer was precipitated in cold hexane (3 x 40 mL) and redissolved in 2 mL of dried dioxane, respectively. The polymer was dried under vacuum for 4 h to obtain the product as pink solid.

Yield: 324 mg (67 % of theory)
M_n (THF-GPC) = 3,6 kDa
PDI (THF-GPC) = 1,25
X_n = 18

^{1}H-NMR (dioxane): δ [*ppm*] = 0.97 (s, 3H), 1.33 (t, 3H), 1.42 (t, 3H), 3.37 (m, 1H), 4.02 (m, 1H), 4.22 (m, 1H), 6.73 (s, 1H).

Synthesis of p(DDMMA)$_{18}$-b-(PFPMA)$_{20}$

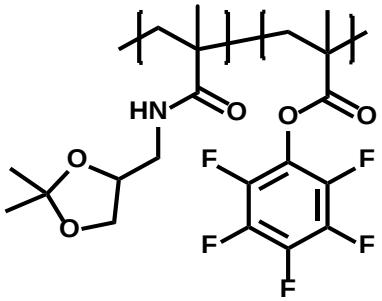

P(DDMMA) (103 mg; 28.6 µmol; 1 eq) was dissolved in 0,5 mL of dried dioxane in a schlenk tube under Ar atmosphere. Then 2,2´-Azobis(4-methoxy-2,4-dimethylvaleronitril) (AMDVN) (4,4 mg; 143 mmol; 0.01 eq of PFPMA) as the initator was dissolved seperately in low amount of dried dioxane and was added via a syringe. The monomer PFPMA (361 mg; 1,43 mmol; 50 eq) was given into the reaction vessel and it was immediatly freezed in liquid nitrogen. It was conducted three freeze-pump-thaw cycles. After the last cycle the tube was left under vacuum and it was stirred 5 d at 35 °C under light exclusion. The clear pink solution was precipitated in cold n-hexane (3 x 40 mL) and redissolved in 2 mL of dried dioxane,

respectively. The polymer was dried under vacuum for several hours to obtain the product as pink solid.

Yield: 334 mg

M_n (THF-GPC) = 8.6 kDa

PDI (THF-GPC) = 1,41

^{1}H-NMR ($CDCl_3$): δ [*ppm*] = 0.97 (s, 3H), 1.33 (t, 3H), 1.42 (t, 3H), 3.37 (m, 1H), 4.02 (m, 1H), 4.22 (m, 1H), 6.73 (s, 1H).

^{19}F-NMR (300 MHz, $CDCl_3$) δ = -153.88 – -154.12 (m, 2F); -159.26 (t, *J*=21.7 Hz, 1F); -163.53 (t, *J*=21.6, 2F)

Synthesis of p(DDMMA)$_{18}$-b-(DDSEA)$_{20}$

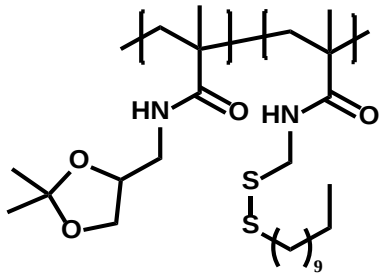

After endgroup removal with an excess of AMDVN (30 eq) at 35 °C the resulting precipitated and dried polymer p(DDMMA)$_{18}$-b-(PFPMA)$_{30}$ (150 mg; 0.33 mmol, 1eq) was dissolved in dioxane and 3 drops of NEt_3 were added under nitrogen atmosphere. Then OG 488 (1,6 mg; 3.34 µmol, 0.01 eq) dissolved in dry DMSO was added over a septum with a syringe. The resulting orange suspension was stirred under N_2 atmosphere at 55 °C under light exclusion. After 2,5 h the first charge of 2-(Dodecyldisulfanyl)ethylamine (DDSEA) (186 mg; 0.67 mmol, 2 eq) dissolved in 2 mL dry DMSO and 260 µl NEt_3 was added and stirred for 18 h. Then the second charge (containing same ratio as first charge) was added to the mixture and further stirred for 1 d. With cold n-hexane a slight yellow precipitate was formed which was centrifuged and dried in vacuum.

Yield: 90 mg

M_n (THF-GPC) = 11.8 kDa

PDI = 1.47

Synthesis of redox labile polymer in the hydrophilic domain

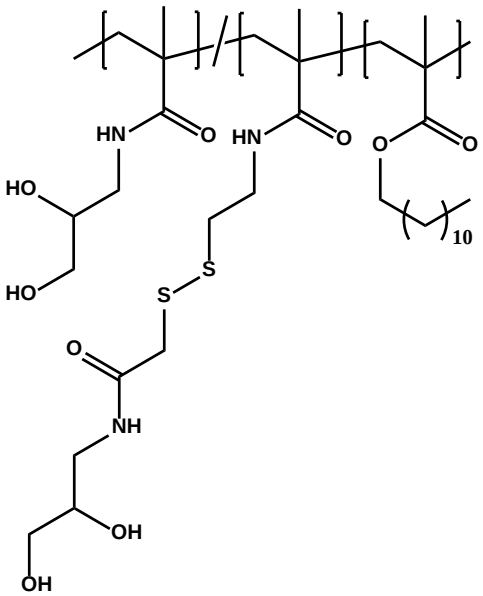

The blockcopolymer p(PFPMA)$_{30}$-*b*-p(LMA)$_{42}$ (200 mg; 10.26 µmol) with removed CTA end group was dissolved in 3 mL of dry dioxane and heated up to 50 °C. Then OG 488 (1,5 mg; 3.07 µmol) was added together with 5 drops of NEt_3 and it was stirred at 55°C for 5 h. Then a mixture of 2-[(2-amino-ethyl)-disulfanyl]-*N*-(2,3-dihydroxypropyl)acetamid (107 mg; 0.45 mmol) and NEt_3 (150 µL) dissolved in 1 mL of DMSO and 1 mL of dioxane were added slowly. The reaction mixture was stirred for 19 h at 55 °C. Then a second charge of a mixture containing DHPA (56 mg; 0.62 mmol) and NEt_3 (170 µL) dissolved in DMSO/Dioxane was added and it was stirred for further 24 h at 55 °C. The complete conversion could be monitored by ^{19}F-NMR by tracking the released pentafluorophenol. It was dialysed for 3 days against Milli-Q water (MWCO = 9 kDa) and then lyophylised. The redox labile amphiphilic blockcopolymer was obtained as a yellowish, voluminous solid.

Yield: 63 mg (mol)

M_n (HFIP-GPC) = kDa

PDI (HFIP-GPC) =

Synthesis of pH labile polymer SC

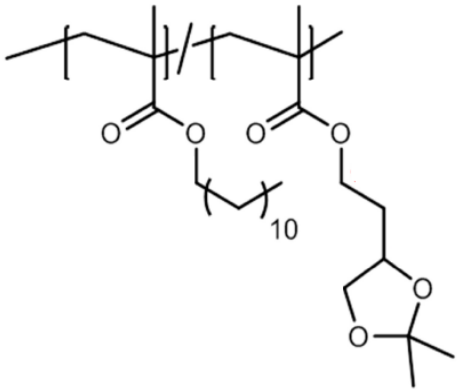

Laurylmethacrylate (1 g; 3.93 mmol) was given in a schlenk tube together with DDEMA (561 mg; 2.62 mmol) and dissolved under stirring in dried dioxane (freshly destilled over Na). As chain transfer agent 4-Cyano-4-((thiobenzoyl)sulfanyl)pentanoicacid (46 mg; 0.17 mmol) was added to the solution. After addition of the initiator AIBN (4,5 mg; 0.028 mmol) dissolved in small amount of dried dioxane) the mixture was conducted with the freeze-pump-thaw technique for three cycles and was stirred overnight at 70 °C to initiate the polymerisation. The total volume of dioxane was 5,5 mL. Purification was done over precipitation with cold methanol (3 times) and sequentially dried in vaccum overnight. The desired statistically polymer was obtained as a pink solid.

Yield: 550 mg (0.14 mmol)
M_n (THF-GPC) = 4 kDa
PDI (THF-GPC) = 1,11

^{1}H-NMR (400 MHz, $CDCl_3$): δ [ppm] = 4,18 – 3,91 (br, -O-C*H*-CH_2, -COO-CH_2- LMA, -O-CH_2-CH-, -COO-CH_2- DDEMA); 2,65 – 0,82 (br,-C(C$H3)_2$, -CH_2 (LMA side chain), -COO-CH_2-CH_2- (DDEMA), -CH_2- (backbone DDEMA/LMA), -CH_3 (backbone DDEMA/LMA), -CH_3 (LMA)).

Synthesis of pH labile blockcopolymer BC

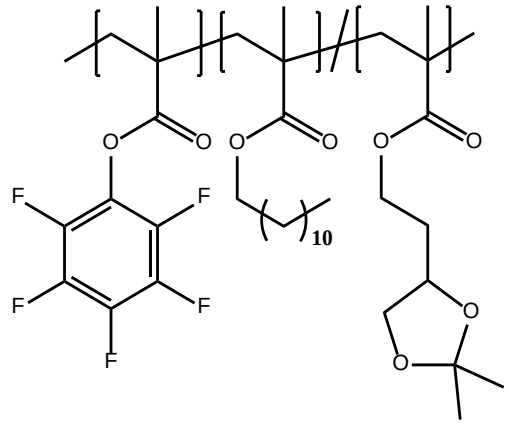

Polymer **SC** (111 mg; 0.028 mmol) was used as a macro CTA which was dissolved in dried dioxane. PFPMA (153 mg; 0.61 mmol) and AIBN (1,2 mg; 0.0061 mmol) were dissolved in dioxane seperately and added over a septum to the solution of the macro CTA. The total amount of dioxane was 4 mL per gram polymer. The reaction mixture was degassed over freeze-pump-thaw technique over three cycles. Then it was stirred for 71 h at 65 °C to initiate the polymerisation. It was precipitated with cold ethanol (3 times) and dried under vacuum overnight. The blockcopolymers were obtained as a pink solid with high viscosity.

Yield: 30 mg (3.26 µmol)
$\mathbf{M_n}$ (THF-GPC) = 9.2 kDa
PDI (THF-GPC) = 1,15

^{1}H-NMR (400 MHz, $CDCl_3$): δ [ppm] = 4,18 – 3,91 (br, -O-C*H*-CH_2, -COO-C*H*$_2$- LMA, -O-C*H*$_2$-CH-, -COO-C*H*$_2$- DDEMA), 2,65 – 0,82 (br,-C(C*H*$_3$)$_2$, -C*H*$_2$ (LMA side chain), -COO-CH_2-C*H*$_2$- (DDEMA), -C*H*$_2$- (backbone DDEMA/LMA/PFPMA), -C*H*$_3$ (backbone DDEMA/LMA/PFPMA), -C*H*$_3$ (LMA))

^{19}F-NMR (300 MHz, CDCl3) *δ* = -153.88 – -154.12 (m, 2F); -159.26 (t, *J*=21.7 Hz, 1F); -163.53 (t, *J*=21.6, 2F)

Synthesis of pH labile blockcopolymer PC

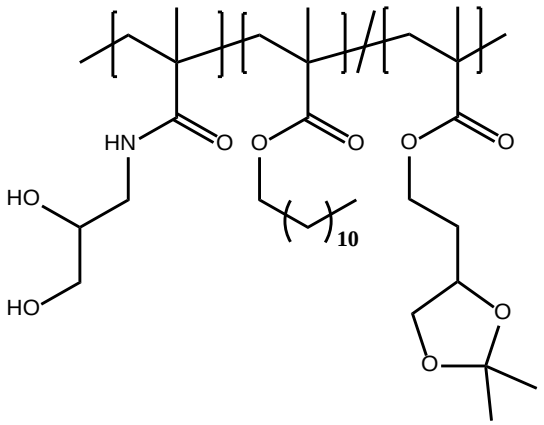

The blockcopolymer **BC** (124,2 mg; 0.014 mmol) with removed CTA end group was dissolved in 3 mL of dry dioxane and heated up to 50 °C. Then OG 488 (0,47 mg; 0.95 µmol) was added together with 3 drops of NEt_3 and it was stirred at 55°C for 5 h. A mixture of dihydroxypropylamine (40 mg; 0.44 mmol) and triethylamine (90 mg; 0.88 mmol) dissolved in 1 mL of DMSO and 1 mL of dioxane were added slowly. The reaction mixture was stirred for 19 h at 55 °C. Then a second charge of a mixture DHPA/triethylamine dissolved in DMSO/Dioxane was added and it was stirred for further 24 h at 55 °C. The complete conversion could be monitored by ^{19}F-NMR by tracking the released pentafluorophenol. It was dialysed for 3 days agains milli-Q water (MWCO = 3.5 kDa) and then lyophylised. The pH labile amphiphilic blockcopolymer was obtained as a colorless, voluminous solid.

Yield: 13,5 mg (2.65 µmol)
M_n (HFIP-GPC) = 5.1 kDa
PDI (HFIP-GPC) = 1,36

^{1}H-NMR (400 MHz, DMSO-d_6): δ [ppm] = 4,95 – 4,72 (br, -C*H*OH-); 4,67 – 4,40 (br, -C*H*$_2$OH); 3,90 – 3,45 (br, -COO-C*H*$_2$- LMA, -COO-C*H*$_2$- DDEMA, -NH-C*H*$_2$-); 2,95 – 0,27 (br, -C(C*H*$_3$)$_2$, -C*H*$_2$ (LMA side chain), -COO-CH$_2$-C*H*$_2$- (DDEMA), -C*H*$_2$- (backbone DDEMA/LMA/DHPMA), -C*H*3 (backbone DDEMA/LMA/DHPMA), -C*H*3 (LMA)).

Synthesis of pH labile polymer SH

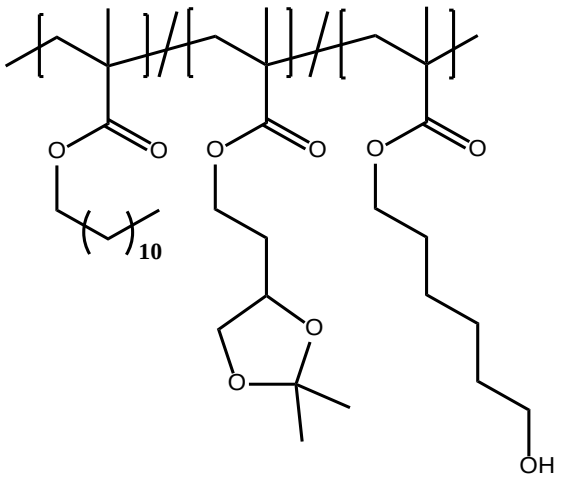

Laurylmethacrylate (1 g; 3.93 mmol) was given in a schlenk tube together with DDEMA (564 mg; 2.64 mmol), HHMA (50 mg; 0.26 mmol) and dissolved under stirring in dried dioxane (freshly destilled over Na). As chain transfer agent 4-Cyano-4-((thiobenzoyl)sulfanyl)pentanoicacid (46 mg; 0.17 mmol) was added to the solution. After addition of the initiator AIBN (4,5 mg; 0.028 mmol) dissolved in small amount of dried dioxane) the mixture was conducted with the freeze-pump-thaw technique for three cycles and was stirred overnight at 70 °C to initiate the polymerisation. The total volume of dioxane was 5,5 mL. Purification was done over precipitation with cold methanol (3 times) and sequentially dried in vaccum overnight. The desired statistically polymer was obtained as a pink solid.

Yield: 560 mg (0.1 mmol)
M_n (THF-GPC) = 5.6 kDa
PDI (THF-GPC) = 1,13

^{1}H-NMR (400 MHz, $CDCl_3$): δ [ppm] = 4,18 – 3,91 (br, -O-C*H*-CH_2, -COO-CH_2- LMA, -O-CH_2-CH-, -COO-CH_2- DDEMA); 2,65 – 0,82 (br,-C(C$H3)_2$, -CH_2 (LMA side chain), -COO-CH_2-CH_2- (DDEMA), -CH_2- (backbone DDEMA/LMA), -CH_3 (backbone DDEMA/LMA), -CH_3 (LMA)).

Synthesis of pH labile polymer BH

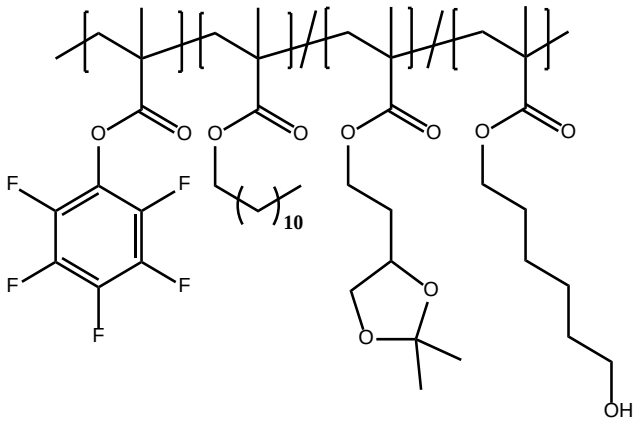

Polymer **SH** (314 mg; 0.056 mmol) was used as a macro CTA which was dissolved in dried dioxane. PFPMA (153 mg; 1.22 mmol) and AIBN (1,2 mg; 0.0061 mmol) were dissolved in dioxane seperately and added over a septum to the solution of the macro CTA. The total amount of dioxane was 4 mL per gram polymer. The reaction mixture was degassed over freeze-pump-thaw technique over three cycles. Then it was stirred for 73 h at 65 °C to initiate the polymerisation. It was precipitated with cold ethanol (3 times) and dried under vacuum overnight. The blockcopolymers were obtained as a pink solid with high viscosity.

Yield: 180 mg (15 µmol)

M_n (THF-GPC) = 12 kDa

PDI (THF-GPC) = 1,25

^{1}H-NMR (400 MHz, $CDCl_3$): δ [ppm] = 4,18 – 3,91 (br, -O-C*H*-CH_2, -COO-CH_2- LMA, -O-CH_2-CH-, -COO-CH_2- DDEMA), 2,65 – 0,82 (br,-C(CH_3)$_2$, -CH_2 (LMA side chain), -COO-CH_2-CH_2- (DDEMA), -CH_2- (backbone DDEMA/LMA/PFPMA), -CH_3 (backbone DDEMA/LMA/PFPMA), -CH_3 (LMA))

^{19}F-NMR (300 MHz, CDCl3) *δ* = -153.88 – -154.12 (m, 2F); -159.26 (t, *J*=21.7 Hz, 1F); -163.53 (t, *J*=21.6, 2F)

Synthesis of pH labile polymer PH

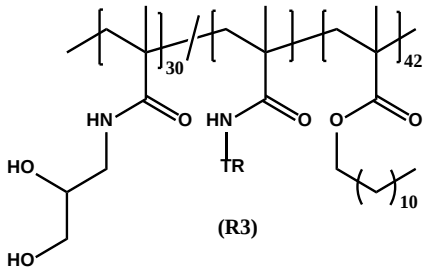

(R3)

The blockcopolymer **BH** (113 mg; 0.0094 mmol) with removed CTA end group was dissolved in 3 mL of dry dioxane and heated up to 50 °C. Then OG 488 (1,16 mg; 2.35 µmol) was added together with 3 drops of NEt_3 and it was stirred at 55°C for 5 h. A mixture of dihydroxypropylamine (42 mg; 0.44 mmol) and triethylamine (64 mg; 0.62 mmol) dissolved in 1 mL of DMSO and 1 mL of dioxane were added slowly. The reaction mixture was stirred for 19 h at 55 °C. Then a second charge of a mixture DHPA/triethylamine dissolved in DMSO/Dioxane was added and it was stirred for further 24 h at 55 °C. The complete conversion could be monitored by ^{19}F-NMR by tracking the released pentafluorophenol. It was dialysed for 3 days against Milli-Q water (MWCO = 3.5 kDa) and then lyophylised. The pH labile amphiphilic blockcopolymer was obtained as a orange, voluminous solid.

Yield: 99 mg (17.67 µmol)
M_n (HFIP-GPC) = 5.6 kDa
PDI (HFIP-GPC) = 1,41

^{1}H-NMR (400 MHz, DMSO-d_6): δ [ppm] = 4,95 – 4,72 (br, -C*H*OH-); 4,67 – 4,40 (br, -CH_2OH); 3,90 – 3,45 (br, -COO-CH_2- LMA, -COO-CH_2- DDEMA, -NH-CH_2-); 2,95 – 0,27 (br, -C(CH_3)$_2$, -CH_2 (LMA side chain), -COO-CH$_2$-CH_2- (DDEMA), -CH_2- (backbone DDEMA/LMA/DHPMA), -C*H*3 (backbone DDEMA/LMA/DHPMA), -C*H*3 (LMA)).

Synthesis of p(PFPMA) homopolymer

p(PFPMA) homopolymers were synthesized in cooperation with [redacted]

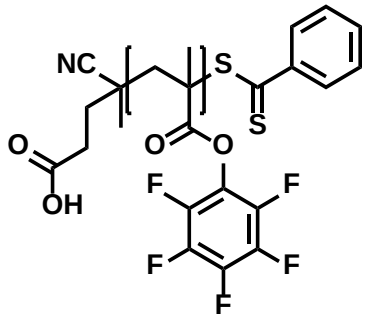

Pentafluorophenol was given in a schlenk tube and dissolved under stirring in dried dioxane (freshly destilled over Na). As chain transfer agent 4-Cyano-4-((thiobenzoyl)sulfanyl)pentanoicacid was added to the solution. After addition of the initiator AIBN (dissolved in small amound of dried dioxane) the mixture was conducted with the freeze-pump-thaw technique for three cycles and was stirred over night at 70 °C to initiate the polymerisation. Purification was done over precipitation with cold hexane (3 times) and sequentially dried in vaccum overnight. The desired homopolymer was obtained as a pink solid.

Table: Used ratios for synthesis of p(PFPMA) homopolymers.

Polymer	Monomer / mol	CTA / mmol	AIBN / mmol	Yield / g
P1	0,018	0,745	0,071	3,15
P2	0,017	0,736	0,064	3,1
P3	0,017	0,736	0,064	3,1
P4	0,018	0,736	0,064	3,6

^{1}H-NMR (400 MHz, $CDCl_3$): δ [ppm] = 2,55 – 1,90 (br, 2H, -CH_2-); 1,65 – 1,18 (br, 3H, -CH_3).

^{19}F-NMR (377 MHz, $CDCl_3$): δ [ppm] = -151,30 – -153,50 (br, *o*-Ar*F*); -157,60 – -158,60 (br, *p*-Ar*F*); -162,65 – -163,70 (br, *m*-Ar*F*).

Synthesis of p(PFPMA)-*b*-p(LMA) blockcopolymer

p(PFPMA)-*b*-p(LMA) blockcopolymer were synthesized in cooperation with [redacted]

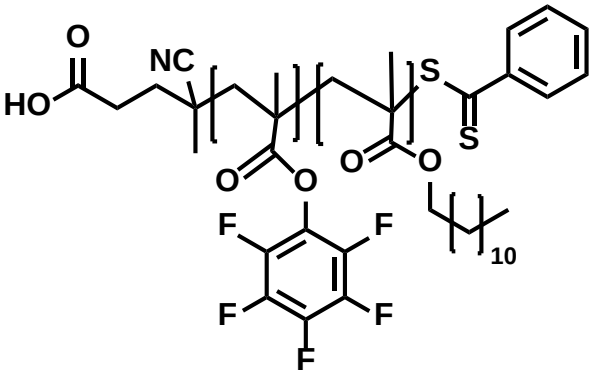

p(PFPMA) was used as a macro CTA which was dissolved in dried dioxane. LMA and AIBN were dissolved in dioxane seperately and added over a septum to the solution of hte macro CTA. The total amount of dioxane was 4 mL per gram polymer. The reaction mixture was degassed over freeze-pump-thaw technique over three cycles. Then it was stirred for 72 h at 65 °C to initiate the polymerisation. It was precipitated with cold methanol (3 times) and dried under vacuum overnight. The blockcopolymers were obtained as a pink solid with high viscosity.

Table: Used ratios for synthesis of p(PFPMA)-*b*-p(LMA) blockcopolymers.

Polymer	Homopolymer	Macro CTA / mol	LMA / mol	AIBN / mol	Yield / g
B1	HP2	$1{,}1 \cdot 10^{-4}$	$6{,}05 \cdot 10^{-3}$	$1{,}1 \cdot 10^{-6}$	1,2
B2	HP3	$6{,}8 \cdot 10^{-5}$	$3{,}4 \cdot 10^{-3}$	$6{,}1 \cdot 10^{-6}$	0,11
B3	HP3	$5{,}1 \cdot 10^{-5}$	$2{,}8 \cdot 10^{-3}$	$5{,}1 \cdot 10^{-6}$	0,65
B4	HP3	$2{,}2 \cdot 10^{-5}$	$1{,}1 \cdot 10^{-3}$	$6{,}1 \cdot 10^{-6}$	0,360
B5	HP4	$6{,}6 \cdot 10^{-5}$	$2{,}9 \cdot 10^{-3}$	$6{,}1 \cdot 10^{-6}$	0,57
B6	HP4	$6{,}5 \cdot 10^{-5}$	$2{,}9 \cdot 10^{-3}$	$6{,}1 \cdot 10^{-6}$	0,67

^{1}H-NMR (400 MHz, $CDCl_3$): δ [ppm] = 3,96 – 3,68 (br, -O-CH_2-CH_2-); 2,70 – 0,78 (br, -CH_2- (backbone PFPMA/LMA), -CH_3 (Rückgrat PFPMA/LMA), -CH_2- (LMA side chain), -CH_3 (backbone PFPMA/LMA))

^{19}F-NMR (400 MHz, $CDCl_3$): δ [ppm] = -151,30 – -153,50 (br, *o*-Ar*F*); -157,60 – -158,60 (br, *p*-Ar*F*); -162,65 – -163,70 (br, *m*-Ar*F*).

General procedure for substitution of the Dithiobenzoat group with AIBN/AMDVN

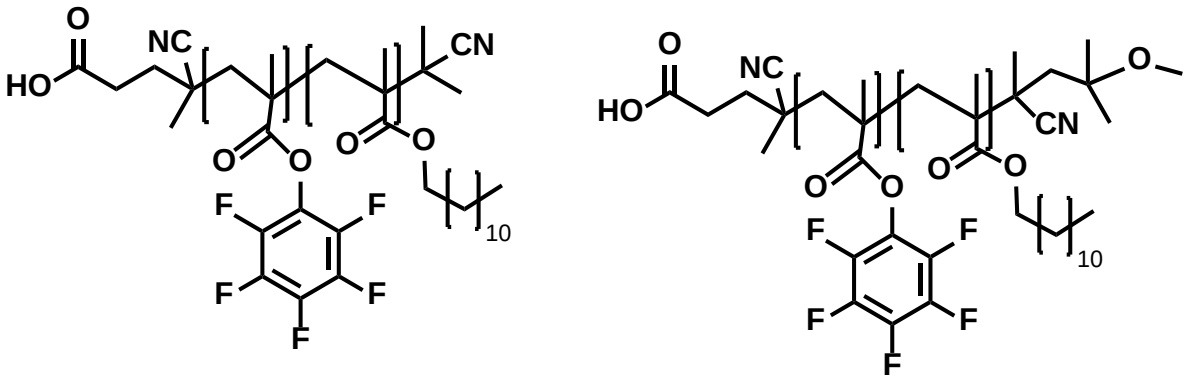

The blockcopolymer (1 eq) was dissolved in dry dioxane and AIBN /AMDVN (30 eq) was added. The reaction mixture was stirred overnight at 70 °C. Hereby, the polymer becomes colorless. Then it was precipitated in cold methanol (3 times) and dried in vacuum overnight. The resulting blockcopolymer becomes colorless due to the removal of the colored dibenzoate group.

Amphiphilic blockcolymers formed from p(PFPMA)$_{30}$-*b*-p(LMA)$_{42}$

p(PFPMA)$_{30}$-*b*-p(LMA)$_{42}$ with M_n = 18.5 kDa and PDI = 1.19

Polymer	Composition	Mn / kDa	PDI	Dye
R1	p(DHPA)$_{30}$-*b*-p(LMA)$_{42}$	12.5 [a)]	1,27 [a)]	/
R2	p(DHPA$_{30}$-*stat*-OG)-*b*-p(LMA)$_{42}$	8.1 [a)]	1,46 [a)]	OG 488
R3	p(DHPA$_{30}$-*stat*-TR)-*b*-p(LMA)$_{42}$	10.5 [a)]	1,53 [a)]	TR
R4	p(DHPA$_{30}$-*stat*-NIR-RS-800)-*b*-p(LMA)$_{42}$	11.9 [a)]	1,37 [a)]	NIR
R5	p(DHPA$_{30}$-*stat*-OG-*stat*-(NH_2-PEG-N_3))-*b*-p(LMA)$_{42}$	11.8 [a)]	1,5 [a)]	OG 488

[a)] Determined over HFIP-GPC

General procedure for the polymer analogues conversion with DHPA

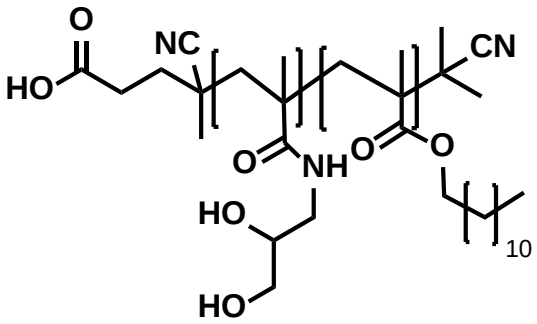

The blockcopolymer with removed CTA end group was dissolved in 3 mL of dry dioxane and heated up to 50 °C. A mixture of dihydroxypropylamine and triethylamine dissolved in 1 mL of DMSO and 1 mL of dioxane were added slowly. The reaction mixture was stirred for 19 h at 55 °C. The a second charge of a mixture DHPA/triethylamine dissolved in DMSO/Dioxane was added and it was stirred for further 24 h at 55 °C. The complete conversion could be monitored by ^{19}F-NMR by tracking the released pentafluorophenol. It was dialysed for 3 days agains milli-Q water (MWCO = 7 kDa) and then lyophylised. The amphiphilic blockcopolymer was obtained as a colorless, voluminous solid.

^{1}H-NMR (400 MHz, $CDCl_3$/MeOH-d_4): δ [ppm] = 3,95 – 3,68 (br, -O-C*H*$_2$-CH$_2$-); 3,35 – 3,05 (br, O=CNH-C*H*$_2$-); 2,96 – 2,66 (br, -C*H*OH-CH$_3$); 2,59 – 0,51 (br, -C*H*$_2$- (backbone DHPA/LMA), -C*H*$_3$ (backbone DHPA/LMA), -C*H*$_2$- (LMA side chain)).

^{13}C-NMR (100 MHz, $CDCl_3$/MeOH-d_4): δ [ppm] = 177,99 (-*C*ON-); 177,68 (-*C*OO-); 77,43 (-NH-CH$_2$-*C*OH-); 65,14 (HO-*C*H$_2$-); 64,32 (COO-*C*H$_2$-); 54,32 (-*C*H$_2$- Backbone); 54,16 (-*C*H$_2$- backbone); 45,14 (-NH-*C*H$_2$-); 44,90 (C qart backbone); 44,75 (C qart backbone); 31,93 (COO-CH$_2$-*C*H$_2$-); 29,63/29,60/29,53/ 29,33/28,21/28,10 (-*C*H$_2$-side chain); 26,06 (CH$_3$-CH$_2$-*C*H$_2$-); 22,68 (CH$_3$-*C*H$_2$-); 18,38 (*C*H$_3$ backbone); 16,45 (*C*H$_3$ backbone); 14,01 (*C*H$_3$-CH$_2$-).

Genereal procedure for the polymer analogues conversion with fluorescent dyes (OG 488 / NIR-RS 800 / Cy5 / Texas Red)

The polymer analogues conversion with a certain fluorescent dye (0.01 eq) proceed analogue to the general conversion with DHPA. It was given 2 drops of triethylamine to the dissolved polymer (1 eq) and then the dye, dissolved in 1 mL of DMSO, was added dropwise and slowly. It was stirred for 5 h at 55 °C before continue with the general procedure of conversion with DHPA.

Genereal procedure for the polymer analogues conversion with target structures (mannose)

The mannose functionalized polymers were conducted as follows: The precursor polymer was solved in dry DMSO and 0.08 eq of the mannose linker per PFPMA repeating unit was added as well as a drop of triethylamine. The mixture was stirred under argon at 55 °C for 8 h (conversion 75 %) up to 24 h (conversion 100 %) before for the further procedure oregon green 488 cadaverin and DHPA as described above was added.

^{13}C-NMR (100 MHz, *inverse gated*, $CDCl_3$): δ [ppm] = 179,2 – 176,2 (m, O=CNH); 100,4 – 100,0 (m, C_1-Mannose)

General techniques and used instrumentations

Sample and particle preparation

The amphiphilic polymers were weighted into 0,2 mL PCR tubes and were incubated with the desired drug which should be encapsulated for at least 5 h on ice. Then ceramic beads (ø 0,3-0,4mm) were added and centrifugated at a rotaional speed of 2500 min^{-1} for 16 min. The samples were then changed in 180° in the sample holder and it was centrifuged again at a speed of 2500 rpm for 16 min. It was added PBS and it was centrifuged again for 2 min at a speed of 2500 rpm. The samples were turned again in 180° and centrifugated again at for 2 min at 2500 rpm. The samples were kept on ice until further processing and purification.

Purification of particles

Polymersomes obtained via duale centrifugation were purified over sepharose CL-2B in a steril hood. The column was diluted and washed in a prestep with 10 mL PBS and the compound was transfered on the column and eluate with PBS. As the eluated drops turned turbid which is the indication for polymersomes the drops were collected. The total volume was 400 µL. After each purification the column was washed with 10 mL of PBS and stored under 20 % of ethanol mixture.

MTT-Assay

MTT tests were done over the *Cell Titer 96 Non-Radioactive Cell Proliferation Assay* (MTT) kits (*Promega*) after protocol of manufacturer. Therefore cells were sowed in the cavities of a 96 well culture plate and incubated with the certain amount of polymer, dissolved in 50 µL of sterile PBS buffer and a total volume of 100 µL for 24 h at 37 °C.

This test was done as threefold determination for each sample. The next day 10 µL of the MTT substrate solution was added to each preparation and the cells were incubated for further 4 h. Then 100 µL of the solubilisation-/stop misxture were added. After at least 5 h the absorption was measured at a wavelength of λ = 570 nm.

Sowing of WeHi-164 cells

The first day WeHi-164 were sowed as indicator cell line per 2 x 10^4 Zellen per well in a 96 well with flat top in 50 µL medium (equates 4 x 10^5 Zellen/mL). Hereby the medium was filtered under vacuum followed by addition of 3-4 mL of Trypsin EDTA and incubated at 37 °C for 5 min in the incubator. Then the cells were collected in 10 mL medium (DMEM + 10 % FCS) and transfered in a 15 mL grainer tube. The cell number was determined in a Neubauer counting chamber. 50 µL of the cell suspension were diluted with 50 µL of Trypan blue. Then 50 µL were given to the counting chamber and the living blue dyed cells (X) were counted.

$$Cell\ number\ (pro\ mL) = X\ (cells) * 2\ (diluting) * 10^4\ (chamber\ factor)$$

The needed cell concentration of $4*10^5$ per mL were set with the needed total volume. For this purpose the cells were centrifugated in the grainer tube at 250-300 g for 5 min. The supernatant was removed and the cell pellet was taken into the medium for the desired needed concentration. The cells were subsequently sowed and incubated in a 96 well plate with 50 µL per well overnight at 37 °C and 5 % CO_2 in the incubator.

Titration and addition of sample

At the second day to a 96 well plate were added 75 µL of test substance per well in a threefold determination experiment, respectively. Then the plate was titrated out with a dilution of 1:5. Then 50 µL of test substance were added to the sowed cells, respectively. The total volume per well was 100 µL. For the living control 50 µL of medium and for the death control 50 µL of DMSO were added. It was incubated at 37 °C and 5 % CO_2 in the incubator for 24 h.

Addition of MTT- and Stop solution

10 µL of MTT solution per well were added followed by incubation at 37 °C and 5 % CO_2 in incubator for 4 h, respectively. Then 100 µL of stop solution were added per well and incubated overnight or at least for 5 h in the incubator followed by measurement at the MTT reader at a wavelength of 560 nm.

Sowing of HELA cells and incubation with particles for 24 h

First, cells were sowed on a 24 well plate. For the fluorescence microscope recording HELA cell as cell line were used with a final concentration of $4*10^4$/mL. The cells were incubated with 50 µg polymersomes for 24 h, respectively.

Sample preparation (*in vitro*)

For sample preparation the medium was filtered under vacuum. Then it was washed with PBS and again filtered under vacuum. The bottom of the well plate was covered with trypsin and incubated for 5 min at 37 °C. Then 1 – 2 mL mediumper well was added and resuspended, respectively. The cell suspension was transfered into a greiner tube and was filled with medium followed by centrifugation for 5 min at 250

– 300 g and the suoernantand was removed. 100 µL cell suspension were transfered inti the cytospin reservoir and centrifugated for 5 min. The round shaped film on the object plate was marked with a pen and fixed with 4 % of paraformaldehyde for 20 min. The object plate was carefully tapped on a tissue and washed twice with TBS-T buffer. After tapping of the object plate one drop of medium was given on the marked place and dried.

Sandwich ELISA

Determination of concentration for TNF-α was done over ELISA MAX™ standard set (*BioLegend*). To coat the plate 100 µL of the capture antibody solution per well was added and incubated overnight at 2 °C - 8 °C in the refrigerator. The next day it is washed 4 - 5 times with 300 µL of washing buffer followed by the addition of 200 µL blocking buffer per well. It was incubated under shaking (500 rpm) for 1 h. During the incubation the standard dilution row and samples were prepared. The first standard concentration of TNF-α was set to 1000 pg/mL. Hereby 10 µL of the stock solution with the concentration of 10 µg/mL were taken and diluted with 990 µL assay diluent. Starting from the first standard value further six 1:2 standard dilution were prepared. The particles suspension were diluted with assay diluent to 1:10000. After incubation in the intended time the plate was washed 4 times with washing buffer followed by a further washing step with PBS. Then 100 µL standard/sample were deposit per well. For the negative control 100 µL of assay diluent were used. The plate was closed and incubated at room temperature on the shaker (500 rpm) for 2 h. It was washed twice with PBS and three times with washing buffer. It was added 100 µL of detection antibody solution per well. The plate was closed and incubated for 1 h at room temperature on the shaker (500 rpm). It was washed 5 times with washing buffer. Then 100 µL of the Avidin-HRP solution per well were added. The plate was closed and incubated for 30 min at room temperature on the shaker (500 rpm) and then washed 5 times with washing buffer. Hereby for each washing step it was soaked for 0,5 - 1 min after adding of the washing buffer. Then 100 µL of the substrate solution was added per well and incubated for 10 - 30 min under light

exclusion. Then 100 µL of the stop solution was added and the absorption was measured in a timeframe of 15 min at a wavelength of 450 nm and 570 nm.

Duale Centrifugation (DC)

The vesicle manufacture procedure and encapsulations experiments were done over a duale centrifugation technique *Rotanta 400* (prototype, *Andreas Hettich*). Hereby 0,2 mL PCR vials from *Kisker Biotech* and *Sigmund Lindner Silibeads ZY* (ø = 0.3- 0.4 mm) were used. The subsequent purification occured by *Mobicol "F" columns* (*MoBiTec*) which was filled with speharose *Sephadex CL-2B* (*Sigma Aldrich*).

Fluorescence activated cell scanning (FACS)

Flow cytometric measurements were conducte with a *FACS Canto II* flow cytometric (*BD Bioscience*). For evaluation the software programs *BD FACS Diva* (*BD Bioscience*) and *FlowJo* (*FLOWJO*) were used.

Gelpermeationschromatographie (GPC)

The size determination of the polymers were obtained over a GPC from the company *Jasco*. It persists of an HPLC pump of type *PU 1850*, a sample donator *AS 1555* and the detectors *UV 1575* (UV detection, λ = 254 nm) and *RI 1530* (refractive index detection).

The gel permetaion column (*MZ analyse technique*) was filled with crosslinked styrol-divinylbenzole copolymers with pore sizes of 102 A, 104 A and 106 A. For calibration polystyrol standards of the company *PSS Polymer Standards Service* (Mainz) were used. The sample conventration was set to 2 mg/mL. Tolouene (*Acros Organics*) was added as internal standard to an amount of 0,2 %.

Nuclear Resonance Spectroscopy (NMR)

Recording of nuclear resonance spectra were conducted with *Avance II 400* (400 MHz ^{1}H-NMR; 100 MHz ^{13}CNMR; 377 MHz ^{19}F-NMR) of the company *Bruker*. The measurements were done at room temperature. The chemical shifts δ were donated

in ppm relative to the standard tetramethylsilane. The evaluation of the spectra were done with the help of the software *MestReNova 9.0.0*.

Dynamic Light Scattering over Zetasizer

Dynamic light scattering for size determination of particles were done with the help of *Zetasizer Nano ZS* (*Malvern Instruments*) at an angle of 173° and a wavelength of 532 nm at 25 °C. The data evaluation was carried out with *Zetasizer Software Version 7.11*.

For measurements using dynamic light scattering methods the samples were filtered in a dust free flow box through *Millex LCR/GHP* filter with a pore size of 0,45/0,20 µm into zylindric measurement cuvettes (*Suprasil* 20 mm, *Hellma*, Muhlheim) which were washed before with freshly destilled acetone. DLS measurements were conducted under use of an *Uniphase* He/Ne lasers (λ = 632,8 nm, 25 mW), an *ALV-SP125* goniometers, an *ALV/High QE APD* Avalanche photodiode with fiber optical detection, an *ALV 5000/E/PCI* correlator and a *Lauda RC-6* thermostate at 20 °C. Angle dependent measurements were done in an area of 30°-150° in steps of 15°. The experimental obtained intensity correlation functions were transfered via Siegert relation into amplitudes correlation functions to take into account the negative values after baseline correction. The amplitude correlation functions were obtained with $g_1(t)$ = SIGN ($G_2(t)$) · SQRT(ABS($G_2(t)$-A)/A) in which A is the measured baseline and $G_2(t)$ the experimental obtained intensity correlation function. The field correlation functions were fitted with the sum of two exponential functions $g_1(t) = a \cdot \exp(-t/b) + c \cdot \exp(-t/d)$ to include polydispersity of the samples. The average apparent diffusion coefficients D_{app} were determined after $q_2 \cdot Dapp = (a \cdot b\text{-}1 + c \cdot d\text{-}1)/(a+c)$ from which the correspondent angle dependent diffusion coefficents and reciprocal hydrodynamic radii $\langle 1/R_h \rangle_{app}$ could be calculated, respectively. The *z* average of the hydrodynamic radii R_h were determined from extrapolation of angle dependent $\langle 1/R_h \rangle_{app}$ to q = 0. The normalized second cumulant μ_2 were calculated with a cumulant fit at 90°. Static light measurements were done with an He/Ne Lasers (λ = 632,8 nm, 25 mW), an *ALV-SP86* goniometers, an *ALV-3000* correlators and an ALV/High QE APD Avalanche photodiode with fiber optical detection.

Angle dependent reciprocal static scattering intensity were evaluated with Zimm- or Berry method. Due to non linear deviations of hte reciprocal form factor in combination with intrinsic moderate dispersity of the samples the Berry method was used to take into account the size dependent upward curvature. Both methods afford the *z* averaged mean radius of gyration IQ _ s⟨IQ(⟩v.

Static Light Scattering (SLS)

The static light scattering measurements were conducted with an uniphase He/Ne Lasers (λ = 632,8 nm, 25 mW), an *ALV-SP86* goniometer, an *ALV-3000* correlator and an ALV/High QE APD Avalanche Photodiode with fiber optical detection from Dr. Karl Fischer. The angle dependant reciprocal static scattering intensities were evaluated over the Zimm of Berry procedure. The procedure after Berry was used to take into account the size dependant upwards curvature due to non linear deviation of the reciprocal form factors in combination with the intrinsic moedrate dispersity. Both procedures revealed the z averaged radius of gyration $R_{g.}$

Lyophilisation

The obtained amphiphilic blockcopolymers over polymer analogous conversion were lyophylised after purification via dialysis. Herein, the certain dispersion in MilliQ water was devided in aliquots with a maximal volume of 20 mL and freezed in liquid nitrogen and lyophylized at a lysophylizer of *VirTis Benchtop Pro* (*SP Scientific*) for three days to yield the compound as dried solid.

UV-vis spectroscopy

UV-vis spectra and absorption-/transmission values were obtained with a spectrometer of type *V-630* (*Jasco*). It was used quarz glas cuvettes (*Hellma Analytics*) with a layer thickness of radiographed solution of d = 10 mm. The spectrometer was tempered with the help of eines *Jasco ETC-717* Peltier Elementes on T = 20 °C.

Reflected light- and fluorescencemicroscopy

For optic microscopy the model *BX53* (*Olympus*) was used. It was equipped with a lamp *Olympus U-LH100L* for the conventional reflected light microscopy as well as a

mercury discharge lamp *Olympus U-LH100HG* for fluorescence microscopic picturing. For the wavelength selective detection HC filter sets *DAPI/GFP/TRITC* (*AF analyse technique*) were used.

Cryo-Transmissionselektronenmicroscopy

CryoTEM measurements were conducted with *Zeiss Libra 120* and *FEI Tecnai 12*. The accelerating voltage was U = 120 kV. As sample holder it was used *Quantifoil R2/1* cupper net (round holes, 200 Mesh, *Plano*) and prior use hydrophylised with oxygen plasma. The samples were fritted with the help of the plunger *Leica EM GP* and *Gatan Cp3* in $N_{2,(l)}$ cooled liquid ethane. The image acquisition was done over CCD cameras *Gatan UltraScan 1000XP, Olympus Megaview* and *TVIPS TemCam F416*.

Extrusion

The subsequent influence of the prepared vesicle size and size distribution the particles were extruded after vesicle preparation with a desired pore size through a polycarbonate membrane. Hereby the *Mini-Extruder* (*Avanti Polar Lipids*) with *Whatman Nuclepore Track-Etched Membranes* with a pore size of 400 nm / 200 nm / 100 nm was used including the *Filter Supports* (*Avanti Polar Lipids*). The dispersions were extruded through the membrane 21 times to reach a high homogeneity as possible und to leave behind eventual present precipitates in the origin syringe.

Cell culture and Cryo-TEM sample preparation

For TEM experiments, HeLa cells were seeded at a concentration of 30,000 cells /cm−2 and cultivated for 24 h before nanoparticles were added. In order to use high pressure freezing (HPF) as the fixation technique for TEM, cells were seeded on 3 mm plasma-sterilized sapphire discs[Z1] that had been covered with a 20 nm carbon layer before usage. The culture medium of HeLa cells consisted of Dulbecco's Modified Eagle's Medium (DMEM) (Life Technologies, U.S.A.) supplemented with 10% fetal calf serum (FCS) (Invitrogen, Karlsruhe, Germany), 100 units penicillin and 100 µg·mL−1 medium streptomycin (Life Technologies) and 1 mM pyruvate (Life Technologies). On the second day of cultivation the cells were incubated with 300 µg/ml sample dispersion for 20 min before HPF fixation using a high-pressure

freezer Compact[Z1] (Wohlwend GmbH, Switzerland). Subsequently, freeze-substitution was conducted using a Leica EM AFS 2 device (Leica Microsystems, Germany). Here, the substitution/staining medium (acetone p.a., 0.2% osmium tetroxide, 0.1% uranylacetate and 5% water) was pre-cooled to −90 °C before samples were added. Finally, the samples were embedded in EPON 812 and sectioned at room temperature using a diamond knife. Examination of the thin sections was conducted with a FEI Tecnai F20 transmission electron microscope (FEI, USA) operated at an acceleration voltage of 200 kV. Conventional bright field micrographs were acquired using a Gatan US1000 slow scan CCD camera (Gatan Inc., USA).

[Z1] Messerschmidt, C.; Hofmann, D.; Kroeger, A., et al.; *Beilstein Journal of Nanotechnology* 2016, 7, 1296-1311.

Fluoreszenzspectroscopy

Fluoreszenzemissionsspectra were obtained over a *Varian Cary Eclipse* spectrometer (*Agilent Technologies*). Hereby a fluorescence cuvette with a thickness of 10x10 mm (*Hellma Analytics*) was used.

Gelpermeationschromatography

The size determination of PFPMA based polymers were obtained with a GPC of the company *Jasco*. It has an HPLC pump from type *PU 1850*, a sample injecter *AS 1555* and detectors *UV 1575* (UV detection, λ = 254 nm) and *RI 1530* (refractive index detektion). The gel permeation coloumn (*MZ-Analysentechnik*) was filled with crosslinked styrol divinylbenzole copolymers of opre size 102, 104 und 106 A. For calibration it was used polystyrol standards of the company *PSS Polymer Standards Service* (Mainz). As eluent it was used tetahydrofurane (purity p.a.) from *Sigma Aldrich*.

The polymer concentration was 2 mg/mL. As an internal standard toluol (*Acros Organics*) of a percentage of 0,2 % was added to the samples. The flow rate was 1 mL/min. For the amphiphilic blockcopolymers p(DHPA)-*b*-p(LMA) it was used a second GPC of the company *Jasco*. It has an HPLC pump of type *PU 2080+*, a sample injecter *AS 1555* and the detectors *UV 2075+* (UV detektion, λ = 254 nm) und *RI*

2080+ (refractive index detektion). The gel permeation coloumn (*MZ analyse technique*) was filled with modified silica gel (PFG) with pore sizes of 102 and 103 A. The particle size was 7 µm. For calibration it was used PMMA standards of the company *PSS Polymer Standards Service* (Mainz). As eluent it was used hexafluoroisopropanol with an addition of 3 g/L potassium trifluoro acetic acid. The sample concentration was 2 mg/mL. As an internal standard toloul (*Acros Organics*) was added to a percentage of 0,2 %. The was tempered on T = 40 °C and the flow rate was 0,8 mL/min.

Infrared spectroscopy

Measurements of infrared spectra were conducted with an ATR-FT-IR spectrometer *Spectrum 100 FT-IR* (*Perkin Elmer*). Hereby 0,5 mg of each sample were given directly on the measurement crystal. If the sample was a liquid then a drop was used.

LAL tests for determination of endotoxine

Before further going to cell experimets the vesicles were tested on contamination due to bacterial endotoxine. The samples were investigated with the Limulus-Amobozyten-Lysat (LAL) test. Hereby the *Pierce LAL Chromogenic Endotoxin Quantitation Kit* (*ThermoFisher Scientific*) was used and the tests were conducted after protocol procedure. Hereby the samples were incubated together with LAL and the chromogene substrate Ac-Ile-Glu-Ala-Arg-pNA. In the case of present endotoxine they activate the LAL factor C which release the chromophore *p*-Nitroanilin (pNA) from the peptidic substrate. Under the use of endotoxine standards for a calibration curve the amount of endotoxine in the certain sample could be determined. The investigated samples did not show the presence of endotoxines which means that during the vesicle preparation over duale centrifugation and the sequential purification steps there was no contamination.

pH determination

pH values were determined with a pH meter *S230 SevenCompact* (*Mettler Toledo*). The pH meter was calibrated over a three point calibration pH 3,0/8,0/11,0) method.

Ultrasonication

Ultrasonication mediated dispersion trials were conducted with *Sonopuls mini20* Sonotrode (*Bandelin*) under the use of a titanm icrospitze *MS 1.5* at an amplitude of 90 %.

Abbreviation

0 D	Zero dimensional
1 D	One Dimensional
2 D	Two Dimensional
3 D	Three Dimensional
a_B	Radius of the Hydrogen atom
ACF	Autocorrelationfunction
Ag	Silver
Au	Gold
Ar-	Aryl-
ATRP	Atom Transfer Radical Polymerization
-b-	Blockcopolymer
BMDC	Bone marrow-derived dendritic cell
br	Broad signal
c	Speed light or concentration
CB	Conduction band
CdO	Cadmium oxide
CdS	Cadmium sulfide
CdSe	Cadmium selenide
CFQDs	Cadmium free quantum dots
CL	Chain length
CM	Compound Micelle
CMC	Critical micelle concentration
cpp	Critical packing parameter
cryoTEM	Cryogene Transmissionselectron microscopy
CTA	Chain transfer agent
Cu	Cupper
d	Dublett
d	Diameter
D_a	Apparent diffusion coefficient
DC	Dendritic cell

D(E)	Density states
DDEMA	2-(2,2-Dimethyl-1,3-dioxolan-4-l)ethylmethacrylate
-dendr-	Dendritic polymer
PDI	Dispersity index
DHPA	2,3-Dihydroxypropylamine
DHPMA	2,3-Dihydroxypropyl-methacrylamide
DLS	Dynamic light scattering
DNA	Desoxyribonucleinacid
DZ	Duale centrifugation
e	Electron
e	Elementary electric charge
EDX	Energy dispersive X–ray spectroscopy
EE	encapsulation efficiency
$\mathbf{E_{gap}}$	Band gap
$\mathbf{E_{kin}}$	Kinetic energy
EPR	Enhanced permeability and retention
eq.	Equivalent
f	Hydrophilic weight fraction
FACS	Fluorescence activated Cell Sorting
FG	Functional group
fs	Femto second
FT-IR	Fourier transform infrared spectroscopy
FWHM	Full width at half maximum
GPC	Gelpermeationchromatographie
GUV	Giant unilamellar vesicle
h	Hole or plank constan
hh	Heavy hole
HPA	Hexylphosphonic acid
HPMA	2-Hydroxypropyl-methacrylamide
HOMO	Highest occupied molecular orbital
HR-TEM	High resolution-transmission electron microscope

IG	Igepal CO-520–(Polyethylene glycol nonylphenyl ether)
ig	Inverse gated
InGaAs	Indium gallium arsenide
InP	Indium phosphide
KAIST	Korean Advanced Institute of Science and Technology
kDa	Kilodalton
KRICT	Korean Research Institute of Chemical Technology
LAL	Limulus-Amobozyten-Lysat
LCM	Laser confocal microscopy
lh	Light hole
LMA	Laurylmethacrylate
LPR	Lipid to Protein ratio
LUMO	Lowest unoccupied molecular orbital
LUV	Large unilamellar vesicle
µm	Mikrometer
mol%	Precentaged amount of substance
m	Mass; or multiplet
m-	Meta-
min	Minute
nm	Nanometer
Mann	Mannose
mbar	Millibar
mg	Milligram
MHz	Megahertz
mL	Milliliter
MLV	Multilamellar vesicle
mM	Millimol
$\mathbf{M_n}$	Number average molar mass
MPS	Mononuclear phagozyt system
ms	Millisecond

MTT	3-(4,5-Dimethylthiazol-2-yl)-2,5-diphenyltetrazoliumbromid
MUD	11-mercapto-1-undecanol
n	Number
N_A	Avogadro constant
$N_{2,l}$	Liquid nitrogen
NHS	*N*-Hydroxysuccinimid
nm	Nanometer
NMP	Nitroxide-Mediated Polymerization
NMR	Nuclear magnet resonance
NW	Nanowire
o-	Ortho-
OA	Oleic acid
ODE	1-octadecene
OLEDs	Organic light emitting Diodes
OPA	One photon absorption
p-	para-
p.a.	For analysis
PEG	Polyethylenglycol
PFP	Pentafluorphenyl
PFPMA	Pentafluorphenylmethacrylate
PGMEA	Propylene glycol methyl ether acetate
pH	Negative common logarithm of Oxonium ion concentration
PoPR	Polymer to Protein ratio
p	Impulse
PL	Photoluminescence
PP	Particle plasmon
ppm	parts per million
PZT	Piezoelectric
q	quartett
QDs	Quantum dots

QSE	Quantum size effect
QY	Quantum yield
r	Radius
RAFT	Reversible Addition-Fragmentation Chain Transfer
RDRP	Reversible-deactivation radical polymerization
R_h	Hydrodynamic radius
R_H	Rydberg constant
Rg	Radius of gyration
RI	Refractive index
RNA	Ribonucleic acid
RGB	Red Green Blue
s	Second
s	Singulett
se	Selenium
SERS	Surface enhanced Raman spectroscopy
siRNA	Small interfering RNA
SLS	Static light scattering
SPR	Surface plasmon resonance
SPs	Surface plasmons
SR	Vibration relaxation
-stat-	Statistical copolymer
SUV	Small unilamellar vesicle
t	Time; or Triplet
T–1yl	Trimethoxy(7–octen–1–yl)silane
TEM	Transmission electron microscopy
TEOS	Tetraethylorthosilicate
TLR9	Toll-like-Receptor 9
TMS	Trimethoxy(octyl)silane
T–MMA	3–(trimethoxysilyl)propylmethacrylate
T–NCO	3–Isocyanatopropyltriethoxysilane
TOP	Trioctylphosphine
TOPO	Triooctylphosphinoxide

TPA	Two photon absorption
TPL	Two photon Lithography
UV	Ultraviolet
V	Volume
VB	Valence band
VP	Volume plasmon
Vis	Visible
XPS	X-ray photoelectron spectroscopy
Xn	Degree of polymerisation
ZnS	Zinc sulfide